Metabolism of the Doxorubicin Cardioprotective Agent Dexrazoxane and its One Ring-Opened Intermediates **B** and **C** to ADR-925

By

Patricia E. Schroeder

A Thesis Submitted to the Faculty of Graduate Studies in Partial Fulfillment
of the Requirements for the Degree of
Doctor of Philosophy

Faculty of Pharmacy
University of Manitoba
Winnipeg, Manitoba

May, 2005

THE UNIVERSITY OF MANITOBA

FACULTY OF GRADUATE STUDIES
*****
COPYRIGHT PERMISSION PAGE

Metabolism of the Doxorubicin Cardioprotective Agent Dexrazoxane and its

One Ring-Opened Intermediates **B** and **C** to ADR-925

BY

Patricia E. Schroeder

A Thesis/Practicum submitted to the Faculty of Graduate Studies of The University

of Manitoba in partial fulfillment of the requirements of the degree

of

DOCTOR OF PHILOSOPHY

PATRICIA E. SCHROEDER ©2005

Abstract

Doxorubicin is one of the most effective chemotherapeutic agents available and has gained widespread use in the treatment of numerous solid tumors and hematologic malignancies. The therapeutic potential and use of doxorubicin, however, is limited by its cumulative dose-dependent cardiotoxicity. There is a significant body of evidence indicating that anthracycline-induced cardiotoxicity may be mediated by iron-based oxygen free radical stress on the heart. Dexrazoxane attenuates anthracycline cardiotoxicity and likely acts as a cardioprotective agent by diffusing into the cell and hydrolyzing to its one-ring open intermediates **B** and **C**, and then to its fully rings-opened metal ion-chelating form ADR-925. The objective of this project was to examine the hydrolysis-activation of dexrazoxane, **B** and **C**, to ADR-925. In a rat model, ADR-925 was found to be rapidly formed in plasma following both a dexrazoxane and a **B/C** bolus, indicating that the hydrolysis of **B** and **C** were enzymatically-mediated. This result was also found in patients receiving dexrazoxane rescue from etoposide for cancer patients with brain cancer metastasis from primary small cell lung cancer where ADR-925 was formed rapidly after a dexrazoxane bolus. To further investigate the enzymatic role of **B** and **C** hydrolysis *in vitro*, a purified dihydroorotase enzyme kinetic model showed that both **B** and **C** were good substrates for dihydroorotase. To investigate the potential role of dihydroorotase-mediated hydrolysis of **B** and **C** *in vivo*, dihydroorotase inhibitors furosemide and 5-aminoorotic acid were used in a rat model where significant decreases in the formation of ADR-925 was observed. A suspension neonatal rat myocyte and adult rat hepatocyte model also indicated that hydrolysis of **C** in the heart and liver was dihydroorotase mediated. Dihydroorotase, in these cell models, was determined to be a

large contributor to the activation of **C** to ADR-925. Ultimately, dihydroorotase-mediated hydrolysis of **B** and **C** provides a mechanism by which dexrazoxane may exert its cardioprotective effects.

Acknowledgments

I have been fortunate to interact with many people who have influenced me greatly. One of the pleasures of finishing is this opportunity to thank them.

Firstly, I would like to thank my thesis advisor, Dr. Brian Hasinoff, for the advice, support and encouragement that made this study possible. His enthusiasm, dedication and enjoyment of the research is a true inspiration, and one I certainly did not take for granted. His encouragement of my attending and presenting at international conferences and participating in collaborations has truly enriched my program and developed my appreciation of the vastness of the scientific community. My advisory committee consisted of Dr. A. McIntosh, Dr. C. Briggs, Dr. D. Sitar, and Dr. H. Perreault who offered new insights to my work during our annual meetings of which I am also thankful. I would also like to express my gratitude to Dr. Sitar who helped me fully appreciate the complexities of pharmacokinetics through both course work and examination of my thesis.

I also benefited greatly from my fellow graduate students, post doctoral fellows, and visiting professors within our faculty. A special thank you to Dr. Rosemary Marusak who showed me great kindness and personal generosity of spirit during her year long stay in Winnipeg. Daywin Patel, Xing Wu, and Junzhi Yao were my sounding boards for new ideas and went out of their way to encourage me. In particular, Daywin Patel was consistently irreplaceable with an ability to fix anything, learn anything, and laugh at everything. I have also been fortunate to meet people who I now consider great friends, among them two truly special people, Kimi Guilbert and Debrah Keling.

I would also like to acknowledge the financial support of the Canadian Institute of Health Research (CIHR) and the Manitoba Health Research Council (MHRC).

Table of Contents

6.0 Chapter 6: Metabolism of dexrazoxane and its one-ring opened intermediates by the isolated neonatal rat myocytes and adult rat hepatocytes.....240

List of Figures

List of Tables

xix

Abbreviations

A, zero time intercept of alpha line (2-compartment model)

ATCase, aspartate transcarbamylase

B, zero time intercept of beta line (2-compartment model)

C_{max}, maximum concentration

CAD, trifunctional protein containing CPSase, ATCase, and DHOase

CPSase, carbamyl phosphate synthetase

DHOase, dihydroorotase

DHPase, dihydropyrimidine amidohydrolase or dihydropyrimidinase

ECOG, Electrocorticographic

EDTA, ethylenediaminetetraacetic acid

HPLC, high-pressure liquid chromatography

k_{10}, elimination rate constant

k_{α}, distribution rate constant (2-compartment model)

k_{β}, beta rate constant (2-compartment model)

K_f, equilibrium formation constant

K_m, Michaelis-Menten constant

λ_{ex}, excitation wavelength

λ_{em}, emission wavelength

LOD, limit of detection

LOQ, limit of quantitation

PBS, phosphate buffered saline

SE, standard error

t_r, retention time

$t_{1/2}$, half-time

V_{max}, maximum velocity

V_o, initial velocity

1.0   Chapter 1: Introduction

1.1   Anthracyclines in the treatment of cancer

1.1.1   The clinical use of doxorubicin

The anthracyclines, doxorubicin, epirubicin, and daunorubicin (Figure 1.1) are among the most effective chemotherapeutic agents available and have gained widespread use in the treatment of numerous solid tumors and hematologic malignancies (Comstock, 1995). Doxorubicin, first isolated over 30 years ago from *Streptomyces peucetius*, is the most successful anthracycline and has become the most utilized chemotherapeutic agent for the treatment of breast cancer.

Anthracycline use, however, is limited by dose-dependent acute and chronic cardiotoxicity (Bonadonna et al., 1969; Lefrak et al., 1973) which is thought to be independent from its mechanism of antitumor activity. Where acute toxicity, such as arrhythmias and hypotension, are typically clinically manageable, chronic toxicity can evolve into congestive heart failure and can manifest itself up to 20 years after completion of anthracycline treatment (Steinherz et al., 1991). Chronic toxicity occurs most frequently in patients who have received a cumulative doxorubicin dose of 550 mg/m^2 (maximum recommended cumulative dose for the 21-day schedule) or more (Keizer et al., 1990).
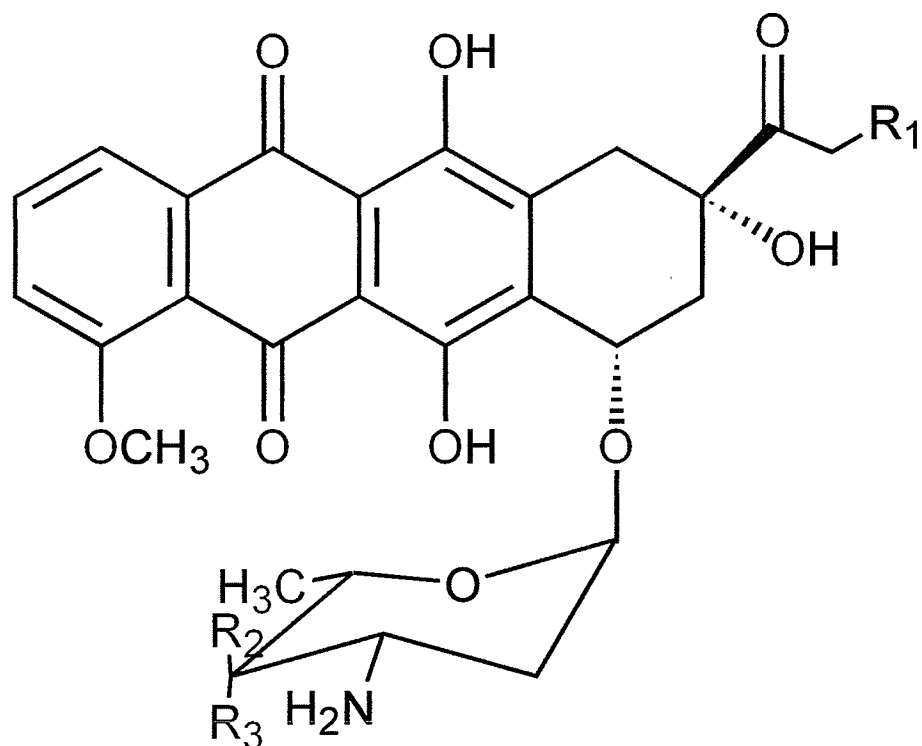
Anthracycline	R_1	R_2	R_3
Doxorubicin	OH	H	OH
Daunorubicin	H	H	OH
Epirubicin	OH	OH	H

Figure 1.1 Structures of chemotherapeutic anthracyclines doxorubicin, daunorubicin, and epirubicin.

1.1.2 Proposed mechanisms of anthracycline antitumor action

A number of different mechanisms have been proposed for the cytostatic and cytotoxic antineoplastic mechanism of action of anthracyclines. As reviewed by Gewirtz, these include a) DNA intercalation, b) free radical formation causing DNA damage and/or lipid peroxidation c) DNA binding and alkylation d) DNA cross-linking, e) interference with DNA unwinding or DNA strand separation and helicase activity, f) direct membrane effects, and g) topoisomerase II inhibition causing DNA damage (Gewirtz, 1999). The clinically significant antitumor mechanism, however, has yet to be completely resolved. After a bolus dose of doxorubicin (typically 60 mg/m^2) the initial doxorubicin plasma concentration (C_{max}) is approximately 11 μM (Hochster et al., 1992) followed by a rapid distribution phase (alpha $t_{1/2}$ 5.2 ± 2.3 min). This pharmacokinetic concentration-time profile suggests that *in vitro* cell culture work at doxorubicin concentrations exceeding 2 μM may not describe the clinical mechanism of doxorubicin cytotoxicity (Gewirtz, 1999). When examined in this context, topoisomerase II inhibition and DNA intercalation remain the primary mechanisms of anthracycline antitumor activity at clinically relevant concentrations (Gewirtz, 1999).

1.1.3 Anthracycline-induced cardiotoxicity in patients

The therapeutic potential of anthracyclines is limited by their cumulative dose-dependent cardiotoxicity. Cases of anthracycline-induced cardiomyopathy involving doxorubicin where the incidence of congestive heart failure has been found to range from 7 to 15 percent in patients receiving cumulative doxorubicin doses of greater than 450 to 500 mg/m^2 (Von Hoff et al., 1977; Von Hoff et al., 1979). Also, for patients who received a cumulative doxorubicin dose of greater than 500 mg/m^2, the incidence of

congestive heart failure increased to greater than 25% (Schwartz et al., 1987). While cumulative dose is the most important risk factor of anthracycline cardiotoxicity; age, prior irradiation, concomitant administration of other chemotherapeutics, and underlying heart disease are all considered risk factors for anthracycline cardiotoxicity (Schimmel et al., 2004).

1.1.4 Mechanism of anthracycline-induced cardiotoxicity: the role of iron

The exact mechanism of anthracycline-induced cardiotoxicity is not yet fully understood. However, there is an increasing body of evidence to support the view that an increase in oxidative stress, as evidenced by increase in free radical formation, lipid peroxidation, as well as decreases in antioxidants and sulfhydryl groups, play an important role in the pathogenesis of doxorubicin cardiotoxicity (Schimmel et al., 2004). The heart, more so than other organs, is particularly vulnerable to free radical damage because protective antioxidant enzymes such as superoxide dismutase and catalase are present at lower levels (Myers, 1998). Also, while doxorubicin has been shown to accumulate in the heart to a lesser extent relative to other organs (Terasaki et al., 1984), cardiomyocytes are rich in mitochondria (Page and McCallister, 1973) which are a target of anthracycline damage.

The increase in oxidative stress by doxorubicin is due to its chemical structure where the quinine ring can undergo redox cycling between quinone and semiquinone. Doxorubicin itself can be reduced by enzymes including cytochrome c reductase, xanthine oxidase, glutathione reductase, and NADPH cytochrome P450 reductase forming the semiquinone radical that can reduce molecular oxygen (reaction 1.1) and further participate in reactions 1.2 and 1.3.

$$DOX^{\cdot-} + O_2 \longrightarrow DOX + O_2^{\cdot-} \tag{1.1}$$
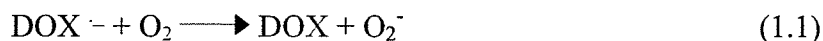
Superoxide dismutase catalyzes the dismutation reaction of superoxide to hydrogen peroxide (reaction 1.2), a reaction that can also be chemically catalyzed through the reduction of Fe^{3+} to Fe^{2+}.

$$2\, O_2^{\cdot-} + 2\, H^+ \longrightarrow H_2O_2 + O_2 \tag{1.2}$$

In the presence of Fe^{2+}, hydrogen peroxide is reduced in the Fenton reaction (reaction 1.3) producing the highly reactive hydroxyl radical ($OH^{\cdot}$).

$$Fe^{2+} + H_2O_2 \longrightarrow Fe^{3+} + OH^- + OH^{\cdot} \tag{1.3}$$
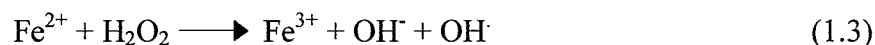
Doxorubicin is a powerful generator of oxygen radicals through the formation of an iron-anthracycline complex. The Fe^{3+}-doxorubicin complex, in tern, can be reduced to the Fe^{2+}-doxorubicin complex by superoxide (reaction 1.4). Upon which the Fe^{2+}-doxorubicin complex can reduce hydrogen peroxide to the highly reactive hydroxyl radical (Zweier et al., 1986) through the Fenton reaction (reaction 1.5).

$$Fe^{3+}\text{-(DOX)} + O_2^{\cdot-} \longrightarrow Fe^{2+}\text{-(DOX)} + O_2 \tag{1.4}$$

$$Fe^{2+}\text{-(DOX)} + H_2O_2 \longrightarrow Fe^{3+}\text{-(DOX)} + OH^- + OH^{\cdot} \tag{1.5}$$

It is during this process that generated electrons reduce oxidizing agents (such as molecular oxygen) thereby initiating a chain reaction leading to the generation of free radical species that anthracyclines are thought to exert their cardiotoxic effects as shown in Figure 1.2 (Thornalley and Dodd, 1985; Costa et al., 1988; Alegria et al., 1989).
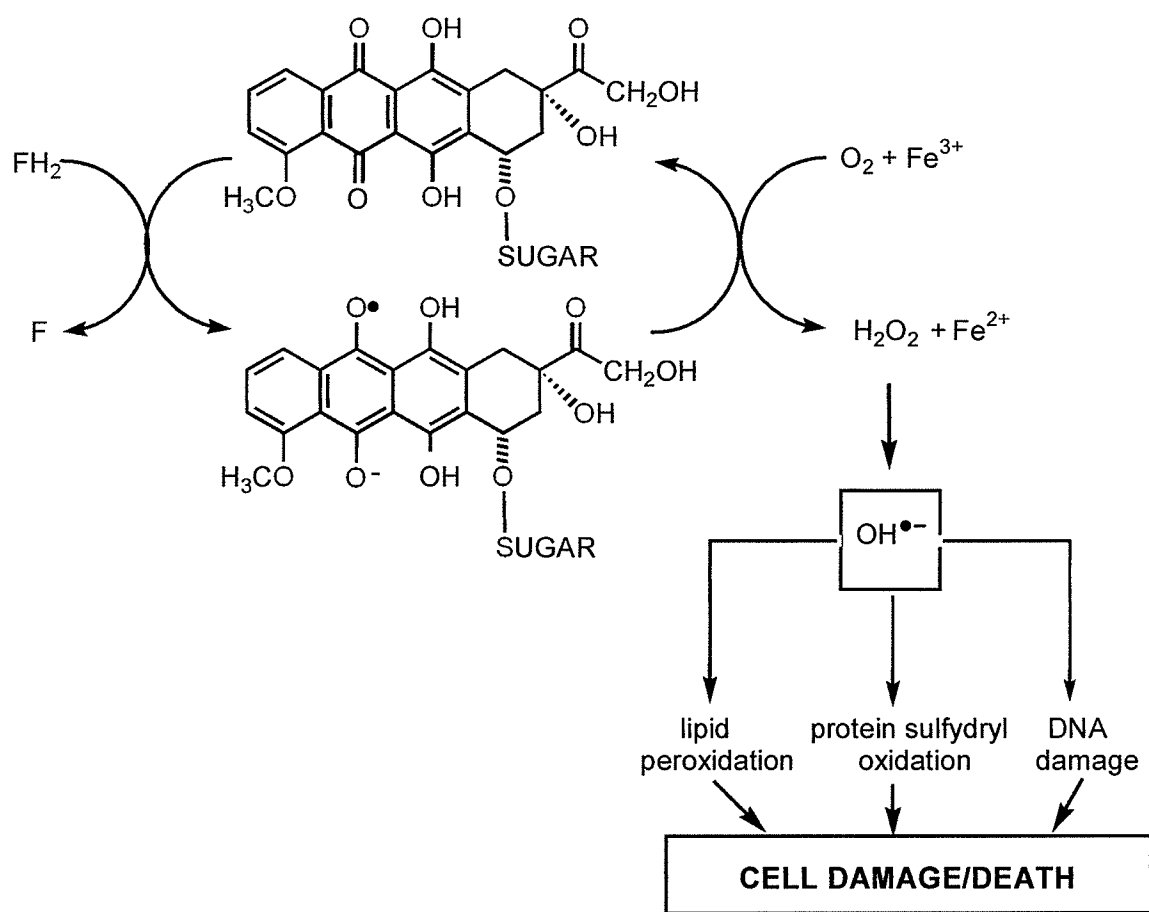
Figure 1.2 Generation of free radicals via iron mediated redox cycling between quinone and semiquinone form of doxorubicin. Where F/FH₂, oxidized/reduced flavoproteins (NADPH cytochrome P450 reductase).

1.2 Protection against anthracycline-induced cardiotoxicity by dexrazoxane

1.2.1 The synthesis and development of dexrazoxane

Razoxane (Figure 1.3), a racemic mixture of dexrazoxane (Zinecard®, ICRF-187) and levrazoxane (ICRF-186), is a bisdioxopiperazine synthesized in the late 1960s by Creighton as an antitumor agent (Creighton et al., 1969). Razoxane was found to have antitumor activity in animals (Creighton et al., 1969) and initial clinical trails showed razoxane antineoplastic activity in sold tumors and leukemia (Bakowski, 1976). However, upon further investigation, clinical trials have revealed that razoxane does not possess any clinically significant antineoplastic effects (Koeller et al., 1981; Liesmann et al., 1981; Vogel et al., 1987). Razoxane was, however, found to ameliorate the acute toxicity of daunorubicin in both Syrian golden hamsters and monkeys (Herman et al., 1974).

Dexrazoxane (Figure 1.3), the (+)-(S)-enantiomer of razoxane, was found to be significantly more water soluble (Repta et al., 1976), turning attention to its further development as a cardioprotective agent. Dexrazoxane undergoes stepwise hydrolysis (Figure 1.4) of the two piperazine rings to form one-ring open intermediates **B** and **C**; where the latter eventually hydrolyzes to give ADR-925, a diacid-diamide structural analog of EDTA, and chelates iron bound to low-molecular-weight cellular ligands or iron from the iron-anthracycline complex.

razoxane
(ICRF-159, racemic)

dexrazoxane
(+)-(S)-enantiomer of ICRF-159

levrazoxane
(-)-(R)-enantiomer of ICRF-159
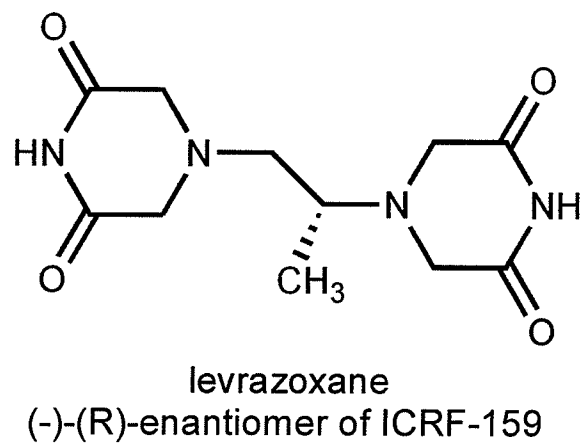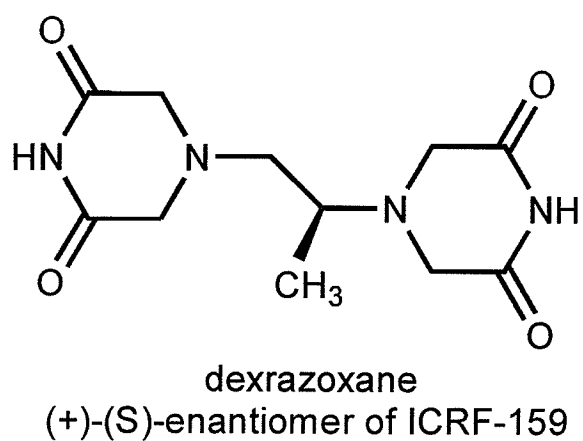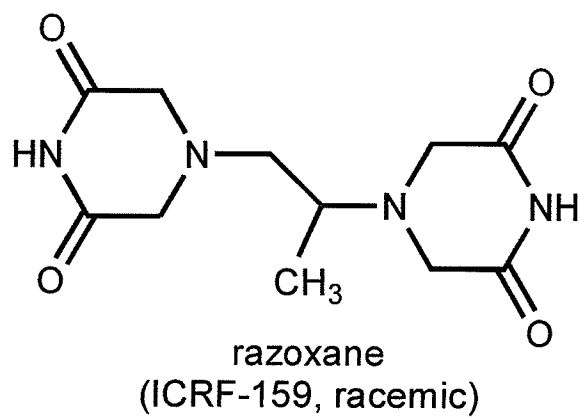
Figure 1.3 Chemical structures of razoxane (racemic), dexrazoxane, and levrazoxane.

1.2.2 Preclinical studies of dexrazoxane-mediated cardioprotection against anthracycline cardiotoxicity

Cardiotoxicity induced by the chronic exposure of anthracyclines is of greatest clinical relevance. The long term cardioprotective effects of dexrazoxane from anthracyclines have been examined in rabbits (Herman and Ferrans, 1986), dogs (Herman et al., 1985b; Herman and Ferrans, 1993), and miniature swine (Herman and Ferrans, 1983) where significant cardioprotection was realized when dexrazoxane was given prior to doxorubicin. Animal models have also been developed to test the effects of repeated exposure to anthracyclines and the protective role of dexrazoxane. In a rat model, dexrazoxane was most effective in reducing doxorubicin-induced cardiotoxicity when administered with the first dose of doxorubicin (Agen et al., 1992). The cardioprotective effects of dexrazoxane in the rat was also found to persist for over 6 months after the last doxorubicin dose (Della Torre et al., 1996). Herman *et al.* determined that in spontaneously hypertensive rats, sensitive to doxorubicin-induced cardiotoxicity (Herman et al., 1985a), dexrazoxane reduced doxorubicin-induced cardiotoxicity and nephrotoxicity (Herman et al., 1988).

Cardioprotective effects were also observed in a rat model with iron chelators such as desferrioxamine (Herman et al., 1994). While dexrazoxane provided superior cardioprotection, the differences in their *in vivo* protective effects were thought to be related to their cellular uptake and intracellular distribution and to the relative availability of different intracellular iron pools to these agents. In *in vitro* cardiac myocytes, dexrazoxane has been shown to prevent the acute effects of doxorubicin (Doroshow et al., 1990) and has been shown to protect against anthracycline-induced lethality in animals (Herman et al., 1979). The dexrazoxane dose-response curve which evaluates

the cardiomyopathy (mean total scores) as a function of dexrazoxane:doxorubicin ratio was determined to be a ratio of 10:1, with only a slight improvement in mean total scores above that ratio (Imondi et al., 1996). These preclinical animal studies helped form the basis for the initial evaluation for human use of dexrazoxane to prevent anthracycline-induced cardiotoxicity (Speyer et al., 1988).

1.2.3 The clinical use of dexrazoxane

Over the last 15 years, several clinical trials have demonstrated the cardioprotective effects of dexrazoxane in patients treated with doxorubicin (Speyer et al., 1988; Speyer et al., 1992; Swain et al., 1997a; Swain et al., 1997b; Swain, 1998), epirubicin (Venturini et al., 1996; Lopez et al., 1998), and doxorubicin in combination with paclitaxel (Sparano et al., 1999). As was the case in the animal models, dexrazoxane was found to be protective against doxorubicin-induced cardiotoxicity at both dexrazoxane:doxorubicin dose ratios of 10:1 (Swain et al., 1997b) and 20:1 (Speyer et al., 1988; Swain et al., 1997b). The dose ratio of dexrazoxane to doxorubicin to achieve cardioprotection while keeping dexrazoxane side effects tolerable is 10:1 with an exacerbation of myelotoxicity (usually in the form of grade 3 or 4 neutropenia) as the dose-limiting toxicity (Hochster et al., 1992). However, as clinical studies have indicated, while higher doses of dexrazoxane have been associated with a risk of developing neutropenia, the incidence of fever, infections, alopecia, nausea, vomiting, or therapy-related deaths is not increased when dexrazoxane is given with doxorubicin (Speyer et al., 1988; Speyer et al., 1992). It was also found that dexrazoxane provided significant cardioprotection when given in patients who had already received a cumulative doxorubicin dose of 300 mg/m^2 (Swain et al., 1997a).

In a clinical trial (Speyer et al., 1992) 50 % of patients with advanced breast cancer receiving fluorouracil/doxorubicin/cyclophosphamide (FDC) withdrew due to cardiotoxicity compared to only 8 % of patients receiving FDC and dexrazoxane. Also in a randomized, double-blind study described by Swain *et al* (Swain et al., 1997b) 31% of patients receiving FDC plus placebo reported cardiac events, relative to only 14 % in the FDC and dexrazoxane arm. Similar protective results were found in breast cancer patients (Venturini et al., 1996) and breast cancer or soft tissue sarcomas (Lopez et al., 1998) receiving a fluorouracil/epirubicin/cyclophosphamide protocol, where patients receiving dexrazoxane had significant cardioprotection versus patients receiving the control. Clinical studies in humans have also shown that dexrazoxane diminished the dose-dependent decrease in cardiac ejection fraction associated with anthracycline therapy (Green et al., 1990). In a randomized clinical trial of breast cancer patients, patients who received dexrazoxane prior to doxorubicin could be treated with more cycles and higher cumulative doses of doxorubicin (700-1000 mg/m^2 or more) than patients in the control intervention group (Speyer et al., 1992). Moreover, significant reduction in anthracycline-induced cardiotoxicity was observed in patients treated with dexrazoxane prior to doxorubicin relative to those treated with doxorubicin alone (Speyer et al., 1992).

1.2.4 Hydrolysis activation and chemistry of dexrazoxane

The hydrolysis of dexrazoxane has been followed over a wide pH range by HPLC (Hasinoff, 1994a) and spectrophotometrically (Hasinoff, 1990). The reaction was shown to undergo base-catalyzed hydrolysis, making the rate of dexrazoxane, **B**, and **C** hydrolysis highly pH dependant. Under physiological conditions (pH 7.4 at 37 °C), first

order rate constants for dexrazoxane hydrolysis to **B** and **C** are 0.05 h^{-1} and 0.024 h^{-1}, respectively and the hydrolysis of **B** and **C** to ADR-925 are 0.043 h^{-1} and 0.094 h^{-1}, respectively, and the half life of ADR-925 formation was found to be 23 h (Hasinoff, 1994b).

It was also found that the Fe^{3+}-doxorubicin complex facilitated the hydrolysis of dexrazoxane and its one-ring open intermediates **B** and **C** (Buss and Hasinoff, 1993). Both Fe^{3+} and Fe^{2+} were found to promote the ring-opening hydrolysis of **B** and **C** by 6000- and 18-fold, for Fe^{2+} and Fe^{3+} respectively (Buss and Hasinoff, 1995). The ferrous ion which reduces H_2O_2 (as shown in reaction 1.6) to the highly reactive hydroxyl radical strongly promotes the hydrolysis of **B** and **C** to ADR-925.

ADR-925 has been found to quickly ($t_{\frac{1}{2}}$ 1.8 min) remove iron from the Fe^{3+} doxorubicin complex (Buss and Hasinoff, 1993), indicating that ADR-925 is a stronger chelator then doxorubicin for Fe^{3+}. Dexrazoxane removes Fe^{3+} far more slowly ($t_{\frac{1}{2}}$ 315 min) than ADR-925 (Buss and Hasinoff, 1995), however **B** and **C** were also shown to rapidly ($t_{\frac{1}{2}}$ 2.2 min) displace Fe^{3+} from the Fe^{3+}-doxorubicin complex. These intermediates which are formed *in vivo* (through enzymatic or non enzymatic mechanisms) chelate iron away from the Fe-doxorubicin complex almost as rapidly as ADR-925, making the one ring-open hydrolysis products of dexrazoxane potentially pharmacologically active. Thus, **B**, **C**, or ADR-925 may act by chelating the Fe^{2+} ion from the Fe-doxorubicin complex and thereby reduce or limit the site specific hydroxyl radical damage to the cell.
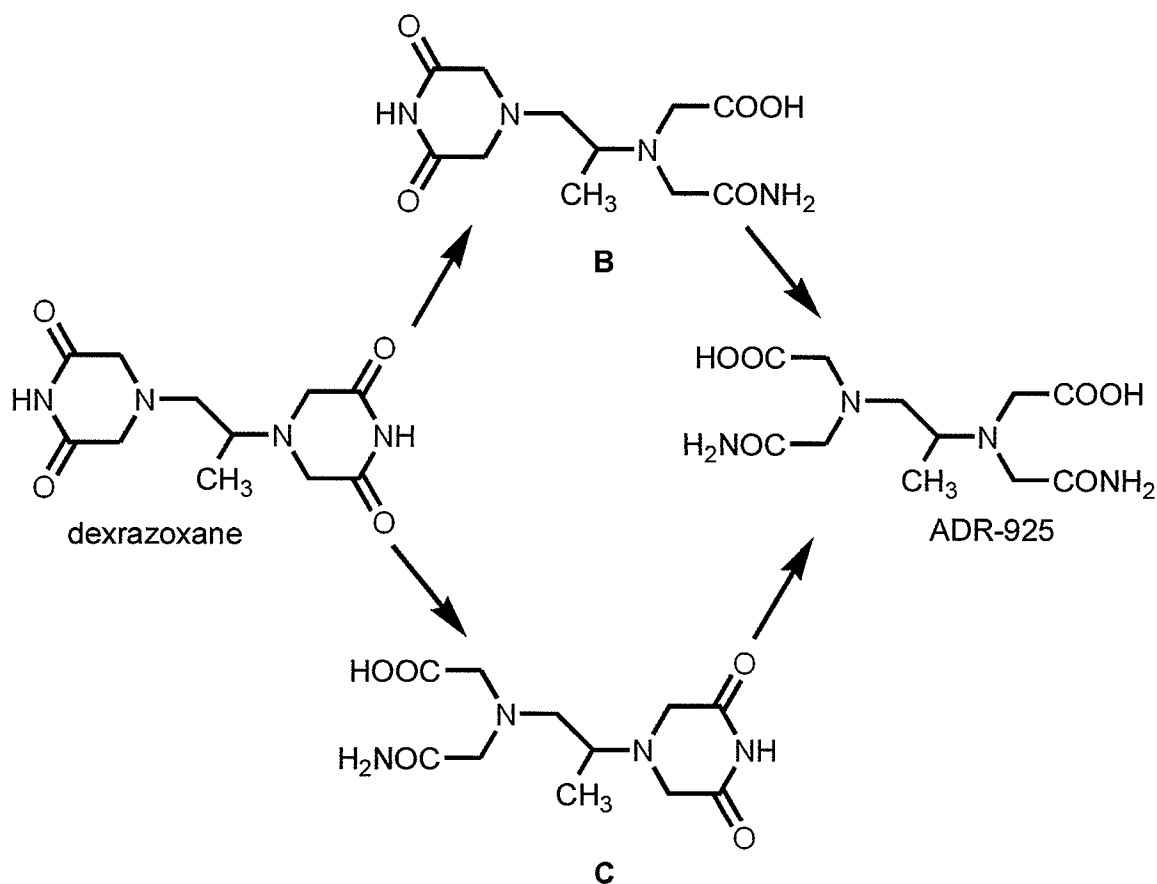
Figure 1.4 Reaction scheme for the hydrolysis of dexrazoxane.

1.2.5 Enzymatic activation of dexrazoxane

In vitro studies with adult heart myocytes in the presence of radio-labeled dexrazoxane indicate that dexrazoxane cellular uptake is rapid, approaching its maximum level within 1 min (Doroshow, 1995). Two brief reports by Doroshow *et al.* have indicated that dexrazoxane uptake into a primary culture of isolated adult rat myocytes is rapid and that dexrazoxane is also rapidly metabolized to ADR-925 (Doroshow et al., 1990, 1991). These studies, however, did not determine whether the hydrolysis of dexrazoxane, **B**, and **C** was enzymatically mediated. It has been previously shown that dexrazoxane hydrolysis was promoted in homogenate supernatants of porcine liver and kidney, but not the heart (Hasinoff et al., 1991). It was determined that the enzyme

primarily responsible for this hydrolysis was dihydropyrimidine amidohydrolase, EC 3.5.2.2, (DHPase) which, in a purified enzyme study, showed Michaelis-Menton saturation kinetics for dexrazoxane with a V_{max} exceeding that of its natural substrates dihydrouracil and dihydrothymine (Hasinoff et al., 1991). Primary isolations of adult rat hepatocytes also indicated that the hydrolysis of dexrazoxane and levrazoxane to **B** and **C** was DHPase-mediated (Hasinoff et al., 1994). DHPase, however, showed no activity toward the hydrolysis of **B** or **C** (Hasinoff et al., 1991; Hasinoff, 1993).

1.2.6 Mechanism of dexrazoxane-mediated cardioprotection: a case for iron chelation

There is significant evidence indicating that anthracycline-induced cardiotoxicity may be mediated by iron-based oxygen free radical stress on the heart. Cardiac cells are specifically more susceptible to oxidative stress due to lower levels of antioxidant enzymes (Doroshow et al., 1980). Also, studies in rat hearts indicate that doxorubicin is able to further reduce antioxidant enzymes in the heart (Li and Singal, 2000). ADR-925, like its structural analogue EDTA (Figure 1.5), is also a strong metal ion chelator and binds the biological metal ions Ca^{2+}, Fe^{2+} and, Mg^{2+} with formation constants of $10^{6.9}$ mol/l, 10^{10} mol/l, and $10^{5.1}$ mol/l, respectively (Huang et al., 1982). At physiological pH dexrazoxane is uncharged and is permeable to cells (Dawson, 1975). The dexrazoxane mechanism of protection may involve diffusing into the cell and hydrolyzing to its metal ion binding form, ADR-925, and chelating either free iron or iron bound to the iron-anthracycline complex.

A substantial body of evidence suggests that anthracycline-dependent free radical generation resulting in DNA or membrane damage is the most probable cause for

14

anthracycline-induced cardiotoxicity (Myers, 1998; Singal and Iliskovic, 1998). In an *in vitro* heart microsomal model, Fe^{3+}-mediated oxidative damage was significantly reduced by ADR-925 (Vile and Winterbourn, 1990) relative to dexrazoxane, suggesting that the hydrolysis of dexrazoxane to ADR-925 is necessary to limit the role of iron in doxorubicin-mediated free radical production (Vile and Winterbourn, 1990). Another study of neonatal rat myocytes showed that although dexrazoxane provided protection against mitoxantrone cadiotoxicity it did not protect against a nonchelating mitoxantrone analogue, further suggesting the dexrazoxane's mechanism of action is metal chelation (Shipp et al., 1993). Strong evidence exists from isolated primary adult and neo natal rat myocyte models that dexrazoxane's mechanism of protection involves inhibition of doxorubicin-dependant hydroxyl radical production (Rajagopalan et al., 1988) and inhibition of lipid peroxidation and thiol oxidation (Thomas et al., 1993). Thus while the Fe^{2+}-ADR-925 complex is able to produce hydroxyl radicals (Thomas et al., 1993; Malisza and Hasinoff, 1995), dexrazoxane's cardioprotective nature may be in complexing of iron away from the iron-doxorubicin complex and thereby preventing site-specific oxygen radical damage.

A study where spontaneously hypertensive rats were dosed with either the sulfhydryl agent amifostine (S-2-(3-aminopropylamino)ethylphosphorothioic acid; WR2721) or dexrazoxane prior to doxorubicin found that while both agents exerted cardioprotective effects relative to the doxorubicin control, dexrazoxane was found to be significantly more cardioprotective (Herman et al., 2000). This result ultimately concluded that the superior protection seen in animals dosed with dexrazoxane was due to dexrazoxane's ability to prevent oxygen radical generation through iron chelation as

15

opposed to amifostine's scavenging mechanism of protection (Herman et al., 2000). In a mouse model, mitochondrial damage and a disruption in myofibrillar organization was observed in the doxorubicin control group where a normal cardiac tissue morphology was observed in the dexrazoxane treated group (Alderton et al., 1990). Furthermore, there was no significant difference in antioxidant enzyme levels between the two groups, suggesting that dexrazoxane's cardioprotective nature was not related to the antioxidant enzymes in the heart (Alderton et al., 1990).

In vitro studies indicate that myocytes dosed with doxorubicin undergo apoptotic cell death (Arola et al., 2000). Anthracycline-induced apoptosis was attenuated by dexrazoxane in *in vitro* cardiomyocyte models using doxorubicin (Hasinoff et al., 2003a; Hasinoff et al., 2003b) and daunorubicin (Sawyer et al., 1999). However, an *in vivo* rat model found that while dexrazoxane attenuated doxorubicin-induced apoptosis in intestinal epithelial and renal cells from spontaneously hypertensive rats, it was not observed in cardiomyocytes (Zhang et al., 1996). This suggests that dexrazoxane cardioprotection against doxorubicin-induced cardiotoxicity is not mediated by the prevention of cardiac cell apoptosis but by other mechanisms such as prevention of iron mediated generation of oxygen radicals (Zhang et al., 1996). Additional studies are required to fully resolve the role of doxorubicin-induced apoptosis with the loss of myocardial function.
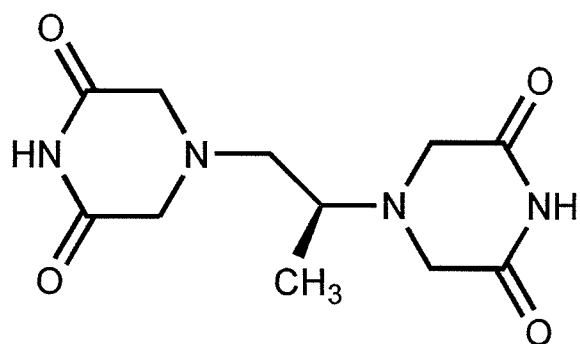
Dexrazoxane
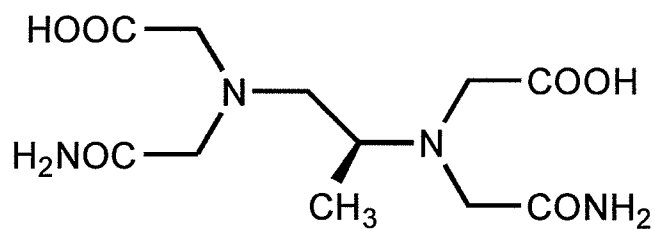
ADR-925
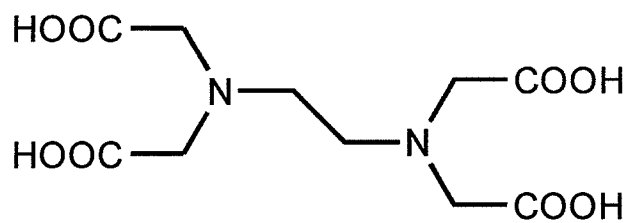
EDTA

Figure 1.5 Chemical structures of dexrazoxane, ADR-925, and EDTA.

17

1.2.7 The current and future status of dexrazoxane in preventing anthracycline-induced cardiotoxicity

An integral part of the preclinical development of dexrazoxane was the determination of whether dexrazoxane interferes with anthracycline antineoplastic activity. On a cellular level, dexrazoxane has shown to have no effect on doxorubicin cytotoxicity in a variety of tumor cell lines (Imondi, 1998). Also, dexrazoxane does not change the pharmacokinetics of doxorubicin in clinical trials (Hochster et al., 1992). An analysis of all randomized trials examining the possibility of dexrazoxane antagonism of tumor response to doxorubicin found that dexrazoxane does not alter the efficacy of the anthracycline chemotherapy protocols (Seymour et al., 1999). However, there is one trial that indicates that dexrazoxane may interfere with the antitumor activity of doxorubicin (Swain et al., 1997b) as the response rate to doxorubicin was significantly higher ($p = 0.007$) in the doxorubicin arm relative to the doxorubicin in combination with dexrazoxane arm. In this trial the placebo arm response rate to doxorubicin far exceeded the expected response, indicating that the anomaly most likely lies with the placebo arm. The report showing that dexrazoxane may reduce response rates in women receiving doxorubicin for treatment of advanced breast cancer (Swain et al., 1997b) is still controversial as it exists in only this clinical trial and the potential mechanisms of dexrazoxane antagonism of doxorubicin clinical activity have not be established. Mistaken dissemination of this result has slowed the use of dexrazoxane (Hellmann, 1999). Despite its promising protective cardiovascular effects, clinical use of dexrazoxane has been seriously limited because of the associated severe myelosuppression, which is potentiated by doxorubicin (Curran et al., 1991). In addition, it is not yet known whether any protection that dexrazoxane provides against early

doxorubicin-induced cardiotoxicity also extends to late cardiovascular effects. Additional clinical trials are required to fully appreciate these issues.

The conclusions of an expert panel review on use of anthracyclines stated that, in spite of their well-documented cardiotoxicity, anthracyclines are a valuable option in chemotherapy (Swain and Vici, 2004). Also, recent interest in combining anthracyclines with other chemotherapeutic agents indicates that anthracycline dose-dependant cardiotoxicity will continue to be a growing clinical concern. The panel concluded that there is overwhelming evidence that dexrazoxane does not interfere with doxorubicin anti-tumor activity and there is a great potential for its more widespread use (Swain and Vici, 2004). However, despite overwhelming preclinical and clinical evidence for the use of dexrazoxane prior to any anthracycline chemotherapy regimen, the guidelines for clinical use of dexrazoxane set by the *American Society of Clinical Oncology, Chemotherapy, and Radiotherapy Expert Panel* (Schuchter et al., 2002) are still quite conservative. According to the Expert Panel, the use of dexrazoxane is recommended in; patients who have received more than 300 mg/m^2 of doxorubicin for metastatic breast cancer and who may benefit from continued doxorubicin treatment; patients who have received more than 300 mg/m^2 doxorubicin for treatment of malignancies other than breast cancer; and patients who responded to previous anthracycline-based chemotherapy for advanced breast cancer and who may benefit from continued therapy with epirubicin.

1.3 Protection against anthracycline-induced cardiotoxicity by other agents

Most protective strategies to prevent anthracycline-induced cardiotoxicity involve protecting cardiomyocytes from anthracycline-induced free radical generation. Also, there is strong evidence that a free radical mechanism is not the primary mechanism of

doxorubicin-mediated antineoplastic activity, as *in vitro* studies have shown that the addition of various antioxidants such as vitamin C (Cervantes et al., 1988), N-acetylcysteine (Myers et al., 1983), glutathione (Yoda et al., 1986), superoxide dismutase (Cervantes et al., 1988), and catalase (Cervantes et al., 1988) did not compromise doxorubicin cytotoxicity in various tumor cell lines. *In vivo* murine models treated with vitamin E and thiol-containing rescue agents (N-acetylcysteine, glutathione, amifostine) showed positive results in the reduction of both acute and chronic anthracycline cardiotoxicity (Dorr, 1996). However, these antioxidants have shown disappointing results in dog models (Van Vleet et al., 1980; Herman et al., 1985b) as well as in clinical trials where vitamin E (Legha et al., 1982) and N-acetylcysteine (Myers et al., 1983) were given to patients to attenuate doxorubicin cardiotoxicity.

Probucol, a lipid-lowering drug, was found to possess strong antioxidant properties (Mao et al., 1991) and has been shown to prevent doxorubicin-induced cardiotoxicity in animal models (Siveski-Iliskovic et al., 1994; Siveski-Iliskovic et al., 1995) while not affecting doxorubicin antineoplastic activity. However, a more recent animal study revealed that probucol caused a rapid and significant increase in plasma doxorubicin clearance and a decrease in area under plasma doxorubicin concentration-time curve (50% reduction), in rats pretreated with probucol (El-Demerdash et al., 2003). Considering the evidence indicating that doxorubicin efficacy may be more dependent on the total area-under-plasma-doxorubicin-concentration-time-curve as opposed to initial plasma concentrations (Berrak et al., 2001), more rigorous preclinical animal studies on tumor response rates should be examined prior to application in a clinical context. Despite this one study, probucol has the unique ability to raise endogenous antioxidants

(Siveski-Iliskovic et al., 1995) while having no apparent effect on the antitumor efficacy of doxorubicin. This has lead to calls for clinical trials in cancer patients (Singal et al., 1997).

1.4   Dexrazoxane as a topoisomerase II inhibitor: a new clinical application

1.4.1   Topoisomerase II inhibition

Mammalian DNA topoisomerase II (EC 5.99.1.3) is a nuclear enzyme responsible for the changes in the topological conformation of DNA. Topoisomerase II alters DNA topology by catalyzing the passing of an intact DNA double helix through a transient double-stranded break made in the second helix (Corbett and Osheroff, 1993). In addition to the essential roles of topoisomerase in DNA metabolism, the enzyme is also a target for several anticancer agents. There are two classes of topoisomerase II inhibitors that interfere with the different aspects of the enzyme cycle. Topoisomerase II poisons, such as doxorubicin and etoposide act by stabilizing the enzyme-DNA cleavable complex that leads to irreversible DNA breaks and cell death (Corbett and Osheroff, 1993). Topoisomerase II catalytic inhibitors, such as the bisdioxopiperazines, inhibit topoisomerase II without the promotion of the cleavable complex formation (Ishida et al., 1991; Sehested et al., 1993). Thus, a topoisomerase II poison acts at a stage of the catalytic cycle of the enzyme where the gate DNA strand is open or cleaved, where as a catalytic inhibitor interacts with the enzyme at a stage where there are no DNA breaks (Burden and Osheroff, 1998).

1.4.2 Preventing systemic toxicity from topoisomerase II poisons with dexrazoxane

Etoposide has antitumor activity against a range of neoplasms including lung cancer, leukemias, neuroblastoma, germ-cell malignancies, non-Hodgkin's lymphomas, and soft-tissue sarcomas (Hande, 1998). Etoposide is thought to exert its cytotoxicity effects by inhibiting the resealing of the DNA breaks created by topoisomerase II. Catalytic inhibitors, such as dexrazoxane, are able to inhibit a topoisomerase II poison by interfering with the catalytic cycle in such a way as to reduce the amount of cleavable complex formation, or in other words, to decrease the available target of the poison (Roca et al., 1994; Ishida et al., 1995; Sehested and Jensen, 1996). The bisdioxopiperazines may lock topoisomerase II at its ATP binding site at the stage of the catalytic cycle where the homodimeric enzyme is thought to exist in the form of a closed clamp surround the DNA (Roca et al., 1994), a mechanism thought to be responsible for hindering the topoisomerase II poisons from their cytotoxicity. Dexrazoxane has been found to eliminate both DNA breaks and the cytotoxicity caused by etoposide (Sehested et al., 1993).

Where etoposide crosses the blood-brain barrier resulting in cytotoxic concentrations when administered at high doses (Postmus et al., 1984; Donelli et al., 1992), dexrazoxane most likely does not (von Hoff et al., 1980). Preclinical animal models where mice were inoculated with L1210 tumor cells resulted in a 3.6-fold escalation in etoposide dose (Holm et al., 1996) and a significant increase in life span (Holm et al., 1998) relative to mice dosed with etoposide alone, indicating that dexrazoxane was a promising lead compound for the development of schedules using high-dose topoisomerase II poisons in the treatment of brain tumors and metastases.

These preclinical cell and animal findings led to the proposal that dexrazoxane used in combination with etoposide could be used in a clinical setting to selectively limit systemic etoposide-mediated toxicity.

1.5 Questions addressed in this work

Previous spectrophotometric and HPLC studies (Hasinoff, 1994b; Hasinoff, 1994a) have shown that under physiological conditions dexrazoxane is only slowly hydrolyzed to **B** and **C** ($t_{1/2}$ of 9.3 hr at 37°C and pH 7.4), and the final hydrolysis product ADR-925 ($t_{1/2}$ of 23 h). Given the slow rate of the hydrolysis-activation *in vitro* it was unclear how sufficient amounts of ADR-925 could be present in heart tissue to chelate iron and prevent oxygen radical damage before dexrazoxane was eliminated (β $t_{1/2}$ of 4.2 ± 2.9 h in humans (Hochster et al., 1992)). ADR-925 is likely the pharmacologically active metabolite of dexrazoxane. Thus it was decided to determine whether the active metal ion binding form of dexrazoxane (ADR-925) was formed *in vivo* using a rat model as discussed in Chapter 2. The formation of ADR-925 after a dexrazoxane bolus was determined in both blood and tissue for rats dosed with dexrazoxane such that a greater understanding of the metabolism and cardioprotective effect of dexrazoxane could be obtained. The hydrolysis activation of dexrazoxane metabolite intermediates **B** and **C** to ADR-925 was also investigated in a rat model, as described in Chapter 2.

Prior to this work, there has been no published report concerning the pharmacokinetics of dexrazoxane metabolites in humans. Thus it was decided to measure the blood plasma levels of dexrazoxane, and dexrazoxane metabolites in a patient population receiving high dose etoposide with dexrazoxane rescue for the treatment of brain metastases from small cell lung cancer in order to obtain a greater

understanding of the metabolism and the mechanism of the protective effects of dexrazoxane. While the pharmacokinetics of etoposide and dexrazoxane (parent drug only) have been studied in detail, this study also examined whether the pharmacokinetics of etoposide and dexrazoxane differed significantly when the two drugs were co-administered. The *in vivo* hydrolysis activation of dexrazoxane to ADR-925 began to describe a pharmacodynamic explanation for dexrazoxane-mediated protection against anthracycline cardiotoxicity in humans.

The hydrolysis activation of dexrazoxane by metal ions (Buss and Hasinoff, 1995; Buss and Hasinoff, 1997) and enzymatic catalysis (Hasinoff et al., 1991; Hasinoff, 1993) have been examined; however very little is known about the enzymatic contribution to the hydrolysis of **B** and **C** to ADR-925. DHPase has been identified as an enzyme that would likely hydrolyze the ring opening of dexrazoxane to **B** and **C**, given the structural similarity of dexrazoxane to dihydrouracil and dihydrothymine. Likewise, given the structural similarity of **B** and **C** to dihydroorotate, the endogenous substrate of DHOase, it was decided to test the hypothesis that **B** and **C** could be enzymatically hydrolyzed to ADR-925 by DHOase. In Chapter 4, DHOase-mediated hydrolysis activation of **B** and **C** to ADR-925 was examined and Michaelis-Menton enzyme kinetics were derived.

Further in regards to the work done in Chapter 4, Chapter 5 investigates the *in vivo* inhibition of the hydrolysis activation of dexrazoxane to **B**, **C**, and ADR-925 was examined in an effort to determine the contribution of DHPase and DHOase in the hydrolysis activation of dexrazoxane and **B** and **C**, respectively. An enzymatically mediated mechanism of cardioprotection from anthracycline-induced cardiotoxicity was hypothesized for dexrazoxane that included DHPase-mediated hydrolysis of dexrazoxane

to **B** and **C**, and DHOase mediated hydrolysis of **B** and **C** to ADR-925. A rat model was used to determine the contribution of DHPase and DHOase in the hydrolysis of dexrazoxane to ADR-925 *in vivo*. The DHPase and DHOase inhibitor furosemide (Schroeder et al., 2002) and the DHOase inhibitor 5-aminoorotic acid (Christopherson and Jones, 1980; Krungkrai et al., 1992) were administered to the rat prior to dexrazoxane where the effect of DHPase and DHOase inhibition on ADR-925 plasma and tissue levels were determined.

In Chapter 6 primary cells from both neonatal rat myocyte and adult rat hepatocyte isolations were used to further investigate the role of DHOase-mediated metabolism of **C**. In addition, the DHOase inhibitors 5-aminoorotic acid and furosemide and the DHPase inhibitor 4-chlorobenzenesulfonamide were chosen to further define the contribution of DHPase and DHOase in the metabolism of dexrazoxane and **C** in primary cell suspensions. The hydrolysis of **C** in blood was also examined where the metal ion chelator diethylenetriaminepentaacetic acid was used to investigate the role of metal ions in the hydrolysis of **C** in an *in vitro* blood model.

1.6 References

Agen C, Bernardini N, Danesi R, Della Torre P, Costa M and Del Tacca M (1992) Reducing doxorubicin cardiotoxicity in the rat using deferred treatment with ADR-529. *Cancer Chemother Pharmacol* **30**:95-99.

Alderton P, Gross J and Green MD (1990) Role of (+-)-1,2-bis(3,5-dioxopiperazinyl-1-yl)propane (ICRF-187) in modulating free radical scavenging enzymes in doxorubicin-induced cardiomyopathy. *Cancer Res* **50**:5136-5142.

Alegria AE, Samuni A, Mitchell JB, Riesz P and Russo A (1989) Free radicals induced by adriamycin-sensitive and adriamycin-resistant cells: a spin-trapping study. *Biochemistry* **28**:8653-8658.

Arola OJ, Saraste A, Pulkki K, Kallajoki M, Parvinen M and Voipio-Pulkki LM (2000) Acute doxorubicin cardiotoxicity involves cardiomyocyte apoptosis. *Cancer Res* **60**:1789-1792.

Bakowski MT (1976) ICRF 159, (+/-) 1,2-di(3,5-dioxopiperazin-1-yl) propane NSC-129,943; razoxane. *Cancer Treat Rev* **3**:95-107.

Berrak SG, Ewer MS, Jaffe N, Pearson P, Ried H, Zietz HA and Benjamin RS (2001) Doxorubicin cardiotoxicity in children: reduced incidence of cardiac dysfunction associated with continuous-infusion schedules. *Oncol Rep* **8**:611-614.

Bonadonna G, Monfardini S, De Lena M and Fossati-Bellani F (1969) Clinical evaluation of adriamycin, a new antitumour antibiotic. *Br Med J* **3**:503-506.

Burden DA and Osheroff N (1998) Mechanism of action of eukaryotic topoisomerase II and drugs targeted to the enzyme. *Biochim Biophys Acta* **1400**:139-154.

Buss JL and Hasinoff BB (1993) The one-ring open hydrolysis product intermediates of the cardioprotective agent ICRF-187 (dexrazoxane) displace iron from iron-anthracycline complexes. *Agents Actions* **40**:86-95.

Buss JL and Hasinoff BB (1995) Ferrous ion strongly promotes the ring opening of the hydrolysis intermediates of the antioxidant cardioprotective agent dexrazoxane (ICRF-187). *Arch Biochem Biophys* **317**:121-127.

Buss JL and Hasinoff BB (1997) Metal ion-promoted hydrolysis of the antioxidant cardioprotective agent dexrazoxane (ICRF-187) and its one-ring open hydrolysis products to its metal-chelating active form. *J Inorg Biochem* **68**:101-108.

Cervantes A, Pinedo HM, Lankelma J and Schuurhuis GJ (1988) The role of oxygen-derived free radicals in the cytotoxicity of doxorubicin in multidrug resistant and sensitive human ovarian cancer cells. *Cancer Lett* **41**:169-177.

Christopherson RI and Jones ME (1980) The effects of pH and inhibitors upon the catalytic activity of the dihydroorotase of multienzymatic protein pyr1-3 from mouse Ehrlich ascites carcinoma. *J Biol Chem* **255**:3358-3370.

Comstock J (1995) *Anthracycline antibiotics: new analogues, methods of delivery, and mechanisms of action.* American Chemical Society, Salem, MA.

Corbett AH and Osheroff N (1993) When good enzymes go bad: conversion of topoisomerase II to a cellular toxin by antineoplastic drugs. *Chem Res Toxicol* **6**:585-597.

Costa L, Malatesta V, Morazzoni F, Scotti R, Monti E and Paracchini L (1988) Direct detection of paramagnetic species in adriamycin perfused rat hearts. *Biochem Biophys Res Commun* **153**:275-280.

Creighton AM, Hellmann K and Whitecross S (1969) Antitumour activity in a series of bisdiketopiperazines. *Nature* **222**:384-385.

Curran CF, Narang PK and Reynolds RD (1991) Toxicity profile of dexrazoxane (Zinecard, ICRF-187, ADR-529, NSC-169780), a modulator of doxorubicin cardiotoxicity. *Cancer Treat Rev* **18**:241-252.

Dawson KM (1975) Studies on the stability and cellular distribution of dioxopiperazines in cultured BHK-21S cells. *Biochem Pharmacol* **24**:2249-2253.

Della Torre P, Podesta A, Pinciroli G, Iatropoulos MJ and Mazue G (1996) Long-lasting effect of dexrazoxane against anthracycline cardiotoxicity in rats. *Toxicol Pathol* **24**:398-402.

Donelli MG, Zucchetti M and D'Incalci M (1992) Do anticancer agents reach the tumor target in the human brain? *Cancer Chemother Pharmacol* **30**:251-260.

Doroshow J (1995) *Role of reactive-oxygen metabolism in the cardiac toxicity of the anthracycline antibiotics.* American Chemical Society, Washington, DC.

Doroshow J, Burke, TG, VanBalgooy J, Akman S, and Verhoef V (1991) Cellular pharmacology of ICRF-187 in adult rat heart myocytes (M). *Proc Am Assoc Cancer Res* **32**:332.

Doroshow JH, Van Balgooy C, and Akman S (1990) Cellular pharmacology of ICRF-187 (187) in beating doxorubicin (D)-treated adult rat heart myocytes (M). *Proc Am Assoc Cancer Res* **31**:442.

27

Doroshow JH, Locker GY and Myers CE (1980) Enzymatic defenses of the mouse heart against reactive oxygen metabolites: alterations produced by doxorubicin. *J Clin Invest* **65:**128-135.

Dorr RT (1996) Cytoprotective agents for anthracyclines. *Semin Oncol* **23:**23-34.

El-Demerdash E, Ali AA, Sayed-Ahmed MM and Osman AM (2003) New aspects in probucol cardioprotection against doxorubicin-induced cardiotoxicity. *Cancer Chemother Pharmacol* **52:**411-416.

Gewirtz DA (1999) A critical evaluation of the mechanisms of action proposed for the antitumor effects of the anthracycline antibiotics adriamycin and daunorubicin. *Biochem Pharmacol* **57:**727-741.

Green MD, Alderton P, Gross J, Muggia FM and Speyer JL (1990) Evidence of the selective alteration of anthracycline activity due to modulation by ICRF-187 (ADR-529). *Pharmacol Ther* **48:**61-69.

Hande KR (1998) Clinical applications of anticancer drugs targeted to topoisomerase II. *Biochim Biophys Acta* **1400:**173-184.

Hasinoff BB (1990) The hydrolysis activation of the doxorubicin cardioprotective agent ICRF-187 [+)-1,2-bis(3,5-dioxopiperazinyl-1-yl)propane). *Drug Metab Dispos* **18:**344-349.

Hasinoff BB (1993) Enzymatic ring-opening reactions of the chiral cardioprotective agent (+) (S)-ICRF-187 and its (-) (R)-enantiomer ICRF-186 by dihydropyrimidine amidohydrolase. *Drug Metab Dispos* **21:**883-888.

Hasinoff BB (1994a) An HPLC and spectrophotometric study of the hydrolysis of ICRF-187 (dexrazoxane, (+)-1,2-bis(3,5-dioxopiperazinyl-1yl)propane and its one-ring opened intermediates. *Int. J. Pharm.* **107:**67-76.

Hasinoff BB (1994b) Pharmacodynamics of the hydrolysis-activation of the cardioprotective agent (+)-1,2-bis(3,5-dioxopiperazinyl-1-yl)propane. *J Pharm Sci* **83:**64-67.

Hasinoff BB, Reinders FX and Clark V (1991) The enzymatic hydrolysis-activation of the adriamycin cardioprotective agent (+)-1,2-bis(3,5-dioxopiperazinyl-1-yl)propane. *Drug Metab Dispos* **19:**74-80.

Hasinoff BB, Schnabl KL, Marusak RA, Patel D and Huebner E (2003a) Dexrazoxane (ICRF-187) protects cardiac myocytes against doxorubicin by preventing damage to mitochondria. *Cardiovasc Toxicol* **3:**89-99.

Hasinoff BB, Schroeder PE and Patel D (2003b) The metabolites of the cardioprotective drug dexrazoxane do not protect myocytes from doxorubicin-induced cytotoxicity. *Mol Pharmacol* **64:**670-678.

Hasinoff BB, Venkataram S, Singh M and Kuschak TI (1994) Metabolism of the cardioprotective agents dexrazoxane (ICRF-187) and levrazoxane (ICRF-186) by the isolated hepatocyte. *Xenobiotica* **24:**977-987.

Hellmann K (1999) Preventing the cardiotoxicity of anthracyclines by dexrazoxane. *BMJ* **319:**1085-1086.

Herman E, Ardalan B, Bier C, Waravdekar V and Krop S (1979) Reduction of daunorubicin lethality and myocardial cellular alterations by pretreatment with ICRF-187 in Syrian golden hamsters. *Cancer Treat Rep* **63:**89-92.

Herman EH, el-Hage A and Ferrans VJ (1988) Protective effect of ICRF-187 on doxorubicin-induced cardiac and renal toxicity in spontaneously hypertensive (SHR) and normotensive (WKY) rats. *Toxicol Appl Pharmacol* **92:**42-53.

Herman EH, el-Hage AN, Ferrans VJ and Ardalan B (1985a) Comparison of the severity of the chronic cardiotoxicity produced by doxorubicin in normotensive and hypertensive rats. *Toxicol Appl Pharmacol* **78:**202-214.

Herman EH and Ferrans VJ (1983) Influence of vitamin E and ICRF-187 on chronic doxorubicin cardiotoxicity in miniature swine. *Lab Invest* **49:**69-77.

Herman EH and Ferrans VJ (1986) Pretreatment with ICRF-187 provides long-lasting protection against chronic daunorubicin cardiotoxicity in rabbits. *Cancer Chemother Pharmacol* **16:**102-106.

Herman EH and Ferrans VJ (1993) Timing of treatment with ICRF-187 and its effect on chronic doxorubicin cardiotoxicity. *Cancer Chemother Pharmacol* **32:**445-449.

Herman EH, Ferrans VJ, Myers CE and Van Vleet JF (1985b) Comparison of the effectiveness of (+/-)-1,2-bis(3,5-dioxopiperazinyl-1-yl)propane (ICRF-187) and N-acetylcysteine in preventing chronic doxorubicin cardiotoxicity in beagles. *Cancer Res* **45:**276-281.

Herman EH, Mhatre RM and Chadwick DP (1974) Modification of some of the toxic effects of daunomycin (NSC-82,151) by pretreatment with the antineoplastic agent ICRF 159 (NSC-129,943). *Toxicol Appl Pharmacol* **27:**517-526.

Herman EH, Zhang J, Chadwick DP and Ferrans VJ (2000) Comparison of the protective effects of amifostine and dexrazoxane against the toxicity of doxorubicin in spontaneously hypertensive rats. *Cancer Chemother Pharmacol* **45:**329-334.

Herman EH, Zhang J and Ferrans VJ (1994) Comparison of the protective effects of desferrioxamine and ICRF-187 against doxorubicin-induced toxicity in spontaneously hypertensive rats. *Cancer Chemother Pharmacol* **35**:93-100.

Hochster H, Liebes L, Wadler S, Oratz R, Wernz JC, Meyers M, Green M, Blum RH and Speyer JL (1992) Pharmacokinetics of the cardioprotector ADR-529 (ICRF-187) in escalating doses combined with fixed-dose doxorubicin. *J Natl Cancer Inst* **84**:1725-1730.

Holm B, Jensen PB and Sehested M (1996) ICRF-187 rescue in etoposide treatment in vivo. A model targeting high-dose topoisomerase II poisons to CNS tumors. *Cancer Chemother Pharmacol* **38**:203-209.

Holm B, Sehested M and Jensen PB (1998) Improved targeting of brain tumors using dexrazoxane rescue of topoisomerase II combined with supralethal doses of etoposide and teniposide. *Clin Cancer Res* **4**:1367-1373.

Huang ZX, May PM, Quinlan KM, Williams DR and Creighton AM (1982) Metal binding by pharmaceuticals. Part 2. Interactions of Ca(II), Cu(II), Fe(II), Mg(II), Mn(II) and Zn(II) with the intracellular hydrolysis products of the antitumour agent ICRF 159 and its inactive homologue ICRF 192. *Agents Actions* **12**:536-542.

Imondi AR (1998) Preclinical models of cardiac protection and testing for effects of dexrazoxane on doxorubicin antitumor effects. *Semin Oncol* **25**:22-30.

Imondi AR, Della Torre P, Mazue G, Sullivan TM, Robbins TL, Hagerman LM, Podesta A and Pinciroli G (1996) Dose-response relationship of dexrazoxane for prevention of doxorubicin-induced cardiotoxicity in mice, rats, and dogs. *Cancer Res* **56**:4200-4204.

Ishida R, Hamatake M, Wasserman RA, Nitiss JL, Wang JC and Andoh T (1995) DNA topoisomerase II is the molecular target of bisdioxopiperazine derivatives ICRF-159 and ICRF-193 in Saccharomyces cerevisiae. *Cancer Res* **55**:2299-2303.

Ishida R, Miki T, Narita T, Yui R, Sato M, Utsumi KR, Tanabe K and Andoh T (1991) Inhibition of intracellular topoisomerase II by antitumor bis(2,6-dioxopiperazine) derivatives: mode of cell growth inhibition distinct from that of cleavable complex-forming type inhibitors. *Cancer Res* **51**:4909-4916.

Keizer HG, Pinedo HM, Schuurhuis GJ and Joenje H (1990) Doxorubicin (adriamycin): a critical review of free radical-dependent mechanisms of cytotoxicity. *Pharmacol Ther* **47**:219-231.

Koeller JM, Earhart RH and Davis HL (1981) Phase I trial of ICRF-187 by 48-hour continuous infusion. *Cancer Treat Rep* **65**:459-463.

Krungkrai J, Krungkrai SR and Phakanont K (1992) Antimalarial activity of orotate analogs that inhibit dihydroorotase and dihydroorotate dehydrogenase. *Biochem Pharmacol* **43**:1295-1301.

Lefrak EA, Pitha J, Rosenheim S and Gottlieb JA (1973) A clinicopathologic analysis of adriamycin cardiotoxicity. *Cancer* **32**:302-314.

Legha SS, Wang YM, Mackay B, Ewer M, Hortobagyi GN, Benjamin RS and Ali MK (1982) Clinical and pharmacologic investigation of the effects of alpha-tocopherol on adriamycin cardiotoxicity. *Ann N Y Acad Sci* **393**:411-418.

Li T and Singal PK (2000) Adriamycin-induced early changes in myocardial antioxidant enzymes and their modulation by probucol. *Circulation* **102**:2105-2110.

Liesmann J, Belt R, Haas C and Hoogstraten B (1981) Phase I evaluation of ICRF-187 (NSC-169780) in patients with advanced malignancy. *Cancer* **47**:1959-1962.

Lopez M, Vici P, Di Lauro K, Conti F, Paoletti G, Ferraironi A, Sciuto R, Giannarelli D and Maini CL (1998) Randomized prospective clinical trial of high-dose epirubicin and dexrazoxane in patients with advanced breast cancer and soft tissue sarcomas. *J Clin Oncol* **16**:86-92.

Malisza KL and Hasinoff BB (1995) Doxorubicin reduces the iron(III) complexes of the hydrolysis products of the antioxidant cardioprotective agent dexrazoxane (ICRF-187) and produces hydroxyl radicals. *Arch Biochem Biophys* **316**:680-688.

Mao SJ, Yates MT, Rechtin AE, Jackson RL and Van Sickle WA (1991) Antioxidant activity of probucol and its analogues in hypercholesterolemic Watanabe rabbits. *J Med Chem* **34**:298-302.

Myers C (1998) The role of iron in doxorubicin-induced cardiomyopathy. *Semin Oncol* **25**:10-14.

Myers C, Bonow R, Palmeri S, Jenkins J, Corden B, Locker G, Doroshow J and Epstein S (1983) A randomized controlled trial assessing the prevention of doxorubicin cardiomyopathy by N-acetylcysteine. *Semin Oncol* **10**:53-55.

Page E and McCallister LP (1973) Quantitative electron microscopic description of heart muscle cells. Application to normal, hypertrophied and thyroxin-stimulated hearts. *Am J Cardiol* **31**:172-181.

Postmus PE, Holthuis JJ, Haaxma-Reiche H, Mulder NH, Vencken LM, van Oort WJ, Sleijfer DT and Sluiter HJ (1984) Penetration of VP 16-213 into cerebrospinal fluid after high-dose intravenous administration. *J Clin Oncol* **2**:215-220.

Rajagopalan S, Politi PM, Sinha BK and Myers CE (1988) Adriamycin-induced free radical formation in the perfused rat heart: implications for cardiotoxicity. *Cancer Res* **48**:4766-4769.

Repta AJ, Baltezor MJ and Bansal PC (1976) Utilization of an enantiomer as a solution to a pharmaceutical problem: application to solubilization of 1,2-di(4-piperazine-2,6-dione)propane. *J Pharm Sci* **65**:238-242.

Roca J, Ishida R, Berger JM, Andoh T and Wang JC (1994) Antitumor bisdioxopiperazines inhibit yeast DNA topoisomerase II by trapping the enzyme in the form of a closed protein clamp. *Proc Natl Acad Sci U S A* **91**:1781-1785.

Sawyer DB, Fukazawa R, Arstall MA and Kelly RA (1999) Daunorubicin-induced apoptosis in rat cardiac myocytes is inhibited by dexrazoxane. *Circ Res* **84**:257-265.

Schimmel KJ, Richel DJ, van den Brink RB and Guchelaar HJ (2004) Cardiotoxicity of cytotoxic drugs. *Cancer Treat Rev* **30**:181-191.

Schroeder PE, Davidson JN and Hasinoff BB (2002) Dihydroorotase catalyzes the ring opening of the hydrolysis intermediates of the cardioprotective drug dexrazoxane (ICRF-187). *Drug Metab Dispos* **30**:1431-1435.

Schuchter LM, Hensley ML, Meropol NJ and Winer EP (2002) 2002 update of recommendations for the use of chemotherapy and radiotherapy protectants: clinical practice guidelines of the American Society of Clinical Oncology. *J Clin Oncol* **20**:2895-2903.

Schwartz RG, McKenzie WB, Alexander J, Sager P, D'Souza A, Manatunga A, Schwartz PE, Berger HJ, Setaro J, Surkin L and et al. (1987) Congestive heart failure and left ventricular dysfunction complicating doxorubicin therapy. Seven-year experience using serial radionuclide angiocardiography. *Am J Med* **82**:1109-1118.

Sehested M and Jensen PB (1996) Mapping of DNA topoisomerase II poisons (etoposide, clerocidin) and catalytic inhibitors (aclarubicin, ICRF-187) to four distinct steps in the topoisomerase II catalytic cycle. *Biochem Pharmacol* **51**:879-886.

Sehested M, Jensen PB, Sorensen BS, Holm B, Friche E and Demant EJ (1993) Antagonistic effect of the cardioprotector (+)-1,2-bis(3,5- dioxopiperazinyl-1-yl)propane (ICRF-187) on DNA breaks and cytotoxicity induced by the topoisomerase II directed drugs daunorubicin and etoposide (VP-16). *Biochem Pharmacol* **46**:389-393.

Seymour L, Bramwell V and Moran LA (1999) Use of dexrazoxane as a cardioprotectant in patients receiving doxorubicin or epirubicin chemotherapy for the treatment of cancer. The Provincial Systemic Treatment Disease Site Group. *Cancer Prev Control* **3**:145-159.

Shipp NG, Dorr RT, Alberts DS, Dawson BV and Hendrix M (1993) Characterization of experimental mitoxantrone cardiotoxicity and its partial inhibition by ICRF-187 in cultured neonatal rat heart cells. *Cancer Res* **53**:550-556.

Singal PK and Iliskovic N (1998) Doxorubicin-induced cardiomyopathy. *N Engl J Med* **339**:900-905.

Singal PK, Iliskovic N, Li T and Kumar D (1997) Adriamycin cardiomyopathy: pathophysiology and prevention. *Faseb J* **11**:931-936.

Siveski-Iliskovic N, Hill M, Chow DA and Singal PK (1995) Probucol protects against adriamycin cardiomyopathy without interfering with its antitumor effect. *Circulation* **91**:10-15.

Siveski-Iliskovic N, Kaul N and Singal PK (1994) Probucol promotes endogenous antioxidants and provides protection against adriamycin-induced cardiomyopathy in rats. *Circulation* **89**:2829-2835.

Sparano JA, Speyer J, Gradishar WJ, Liebes L, Sridhara R, Mendoza S, Fry D and Egorin MJ (1999) Phase I trial of escalating doses of paclitaxel plus doxorubicin and dexrazoxane in patients with advanced breast cancer. *J Clin Oncol* **17**:880-886.

Speyer JL, Green MD, Kramer E, Rey M, Sanger J, Ward C, Dubin N, Ferrans V, Stecy P and Zeleniuch-Jacquotte A (1988) Protective effect of the bispiperazinedione ICRF-187 against doxorubicin-induced cardiac toxicity in women with advanced breast cancer. *N Engl J Med* **319**:745-752.

Speyer JL, Green MD, Zeleniuch-Jacquotte A, Wernz JC, Rey M, Sanger J, Kramer E, Ferrans V, Hochster H and Meyers M (1992) ICRF-187 permits longer treatment with doxorubicin in women with breast cancer. *J Clin Oncol* **10**:117-127.

Steinherz LJ, Steinherz PG, Tan CT, Heller G and Murphy ML (1991) Cardiac toxicity 4 to 20 years after completing anthracycline therapy. *Jama* **266**:1672-1677.

Swain SM (1998) Adult multicenter trials using dexrazoxane to protect against cardiac toxicity. *Semin Oncol* **25**:43-47.

Swain SM and Vici P (2004) The current and future role of dexrazoxane as a cardioprotectant in anthracycline treatment: expert panel review. *J Cancer Res Clin Oncol* **130**:1-7.

Swain SM, Whaley FS, Gerber MC, Ewer MS, Bianchine JR and Gams RA (1997a) Delayed administration of dexrazoxane provides cardioprotection for patients with advanced breast cancer treated with doxorubicin-containing therapy. *J Clin Oncol* **15:**1333-1340.

Swain SM, Whaley FS, Gerber MC, Weisberg S, York M, Spicer D, Jones SE, Wadler S, Desai A, Vogel C, Speyer J, Mittelman A, Reddy S, Pendergrass K, Velez-Garcia E, Ewer MS, Bianchine JR and Gams RA (1997b) Cardioprotection with dexrazoxane for doxorubicin-containing therapy in advanced breast cancer. *J Clin Oncol* **15:**1318-1332.

Terasaki T, Iga T, Sugiyama Y and Hanano M (1984) Pharmacokinetic study on the mechanism of tissue distribution of doxorubicin: interorgan and interspecies variation of tissue-to-plasma partition coefficients in rats, rabbits, and guinea pigs. *J Pharm Sci* **73:**1359-1363.

Thomas C, Vile GF and Winterbourn CC (1993) The hydrolysis product of ICRF-187 promotes iron-catalysed hydroxyl radical production via the Fenton reaction. *Biochem Pharmacol* **45:**1967-1972.

Thornalley PJ and Dodd NJ (1985) Free radical production from normal and adriamycin-treated rat cardiac sarcosomes. *Biochem Pharmacol* **34:**669-674.

Van Vleet JF, Ferrans VJ and Weirich WE (1980) Cardiac disease induced by chronic adriamycin administration in dogs and an evaluation of vitamin E and selenium as cardioprotectants. *Am J Pathol* **99:**13-42.

Venturini M, Michelotti A, Del Mastro L, Gallo L, Carnino F, Garrone O, Tibaldi C, Molea N, Bellina RC, Pronzato P, Cyrus P, Vinke J, Testore F, Guelfi M, Lionetto R, Bruzzi P, Conte PF and Rosso R (1996) Multicenter randomized controlled clinical trial to evaluate cardioprotection of dexrazoxane versus no cardioprotection in women receiving epirubicin chemotherapy for advanced breast cancer. *J Clin Oncol* **14:**3112-3120.

Vile GF and Winterbourn CC (1990) dl-N,N'-dicarboxamidomethyl-N,N'-dicarboxymethyl-1,2-diaminopropane (ICRF-198) and d-1,2-bis(3,5-dioxopiperazine-1-yl)propane (ICRF-187) inhibition of Fe3+ reduction, lipid peroxidation, and CaATPase inactivation in heart microsomes exposed to adriamycin. *Cancer Res* **50:**2307-2310.

Vogel CL, Gorowski E, Davila E, Eisenberger M, Kosinski J, Agarwal RP and Savaraj N (1987) Phase I clinical trial and pharmacokinetics of weekly ICRF-187 (NSC 169780) infusion in patients with solid tumors. *Invest New Drugs* **5:**187-198.

Von Hoff DD, Layard MW, Basa P, Davis HL, Jr., Von Hoff AL, Rozencweig M and Muggia FM (1979) Risk factors for doxorubicin-induced congestive heart failure. *Ann Intern Med* **91**:710-717.

Von Hoff DD, Rozencweig M, Layard M, Slavik M and Muggia FM (1977) Daunomycin-induced cardiotoxicity in children and adults. A review of 110 cases. *Am J Med* **62**:200-208.

Von Hoff DD, Soares N, Gormley P and Poplack DG (1980) Pharmacokinetics of ICRF-187 in the cerebrospinal fluid of subhuman primates. *Cancer Treat Rep* **64**:734-736.

Yoda Y, Nakazawa M, Abe T and Kawakami Z (1986) Prevention of doxorubicin myocardial toxicity in mice by reduced glutathione. *Cancer Res* **46**:2551-2556.

Zhang J, Clark JR, Jr., Herman EH and Ferrans VJ (1996) Doxorubicin-induced apoptosis in spontaneously hypertensive rats: differential effects in heart, kidney and intestine, and inhibition by ICRF-187. *J Mol Cell Cardiol* **28**:1931-1943.

Zweier JL, Gianni L, Muindi J and Myers CE (1986) Differences in O_2 reduction by the iron complexes of adriamycin and daunomycin: the importance of the sidechain hydroxyl group. *Biochim Biophys Acta* **884**:326-336.

Chapter 2   The doxorubicin-cardioprotective drug dexrazoxane and its one-ring open intermediates undergo metabolism in the rat to its metal ion-chelating form ADR-925

2.1   Introduction

Dexrazoxane (ICRF-187, Figure 2.1) is clinically used to reduce doxorubicin-induced cardiotoxicity (Swain et al., 1997a; Swain et al., 1997b; Hasinoff, 1998; Hasinoff et al., 1998). The clinical use of dexrazoxane arose as a result of a series of careful preclinical animal studies that have been described in recent reviews (Hasinoff et al., 1998; Herman and Ferrans, 1998). Dexrazoxane likely acts as a cardioprotective agent by diffusing into the cell and hydrolyzing to its one-ring open intermediates **B** and **C**, and then to it fully rings-opened metal ion-chelating form ADR-925 (Figure 2.1), which has a structure similar to EDTA. ADR-925 may act by chelating free iron or displacing iron bound to the iron-doxorubicin complex (Hasinoff, 1989b; Buss and Hasinoff, 1993; Hasinoff, 1998; Hasinoff et al., 1998), thereby reducing iron-based oxygen radical formation.

Considerable evidence has accumulated that the cardiotoxicity of doxorubicin is due to iron-based oxygen radical-induced oxidative stress on the heart muscle which is relatively low in antioxidant enzymes (Gianni et al., 1985; Malisza and Hasinoff, 1995; Myers, 1998). The Fe^{3+}–doxorubicin complex is able to be reductively activated and redox cycle to produce the extremely damaging hydroxyl radical in a Fenton-type reaction (Zweier et al., 1986; Hasinoff, 1989b; Hasinoff, 1990b; Malisza and Hasinoff, 1995; Myers, 1998). Previous spectrophotometric and HPLC studies (Hasinoff, 1994b; Hasinoff, 1994a) showed that under physiological conditions dexrazoxane is only slowly

hydrolyzed to **B** and **C** ($t_{1/2}$ of 9.3 hr at 37°C and pH 7.4), and the final hydrolysis product

ADR-925 ($t_{1/2}$ of 23 h) according to the kinetic scheme shown in Figure 2. 1. Given the

slow rate at which hydrolysis-activation occurs *in vitro* it was, thus, unclear how

sufficient amounts of ADR-925 could be present in heart tissue to chelate iron and

prevent oxygen radical damage before dexrazoxane was eliminated ($t_{1/2\beta}$ of 4.2 ± 2.9 h in

humans) (Hochster et al., 1992). Considering ADR-925 is likely the pharmacologically

active metabolite of dexrazoxane, and because ADR-925 has not previously been

determined in an *in vivo* model, it was decided to develop a sensitive fluorescence assay

to measure its levels in plasma and tissues of rats dosed with dexrazoxane, a **B/C**

mixture, and ADR-925, such that a greater understanding of the metabolism and

cardioprotective effect of dexrazoxane could be obtained. Part of the work detailed in

this chapter has been accepted for publication (Schroeder and Hasinoff, 2002).
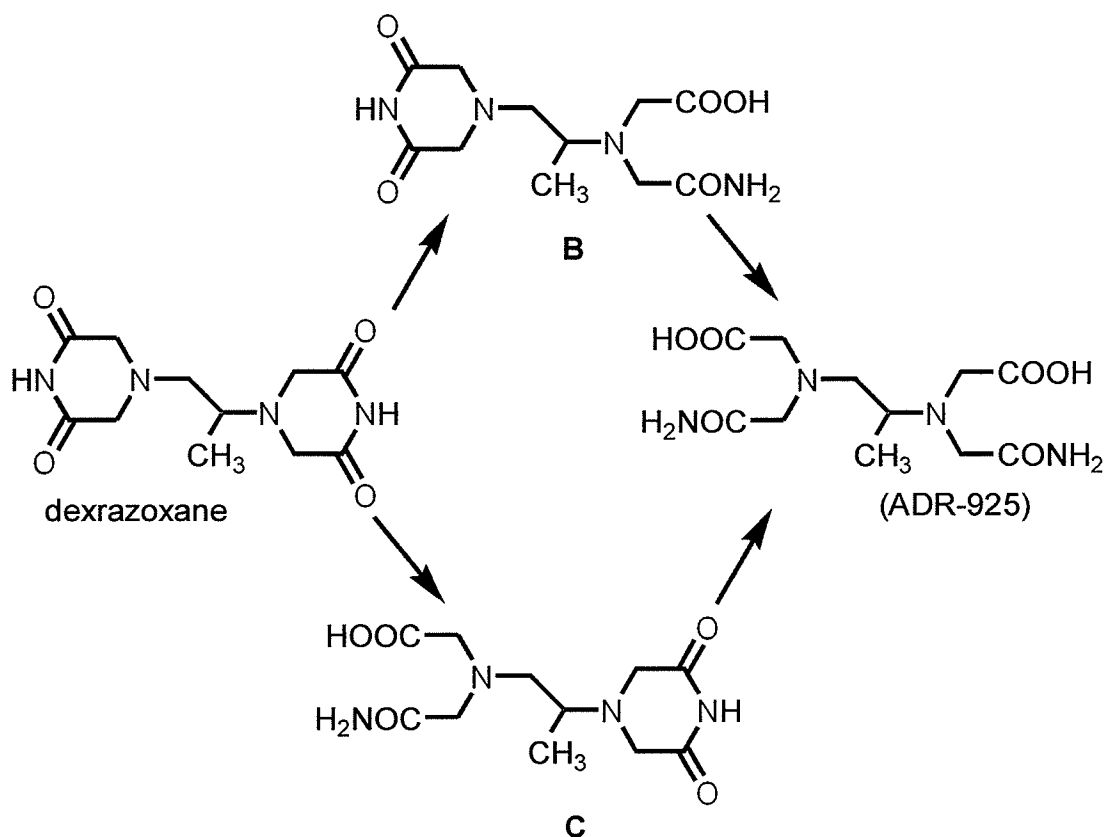
*Figure 2.1. Reaction scheme for the hydrolysis of dexrazoxane to intermediates **B** and **C**, and its strongly metal ion-chelating form ADR-925.*

2.2 Materials and Methods

2.2.1 Materials

Dexrazoxane hydrochloride and ADR-925 were gifts from Adria Laboratories (Columbus, OH). Calcein ("high purity") was from Molecular Probes (Eugene, OR). HPLC-grade methanol, phosphoric acid and cobalt chloride hexahydrate were from Fisher (Nepean, Canada) and heparin, reagent grade catalase, and 1-heptanesulfonic acid sodium salt were from Sigma (St. Louis, MO).

2.2.2 Animal handling and surgery

The male Sprague-Dawley (300-350 g) rats used for these experiments were held at the University of Manitoba Animal Holding Facility (UMAHF) in the department of Zoology where the animals were allowed food and water *ad libitum* prior to the study. The rats were transported to the Faculty of Pharmacy immediately prior to the commencement of the study and, thus, were not acclimatized prior to surgery. A combination of ketamine (90 mg/kg) and xylazine (10 mg/kg), administered as an intraperintoneal (i.p.) injection, was used to anaesthetize the rats. The surgical plane of anaesthesia was established and monitored through the pedal reflex of each foot where surgery was only performed after both pedal reflex responses were negative. The degree of anaesthesia was monitored every 5 min until the experiment was finished and the rat was euthanized. If the pedal reflex response was positive during surgery, a top up dose of anaesthetic (20 % of original dose) was administered i.p. Throughout the duration of the study, the rat was kept warm through an insulated electric heading pad. The rat was euthanized with Euthanol if at any point during the surgery or blood collection the animal appeared to be in pain, distress, or displayed an apparent resistance to the anaesthetic.

Once the surgical plane of anaesthesia was reached, a 2 cm incision was made through the skin above the left jugular vein. Once at least 1 cm of the jugular vein was completely separated from surrounding connective tissue, two 10 cm pieces of surgical silk were loosely tied 1 cm apart around the vein. Throughout the surgery, sterile saline (0.9 % wt/v NaCl) was liberally added to gauze and applied to the open wound to prevent dehydration. A 0.5 cm x 5 cm piece of flat stainless steel was inserted underneath the isolated jugular vein. The surgical silk furthest from the heart was tied tightly and double

knotted. The vein was cut such that the incision was diagonal and approximately half the width of the vein. One end of the cannula (Intramedic™ non-radiopaque polyethylene tubing, I.D. 0.58 mm O.D. 0.965 mm, obtained from Fisher, Canada) was inserted into a 23 G needle (Becton Dickinson, Fisher, Canada) and then attached to a 3-way valve (Becton Dickinson, Fisher, Canada) attached to a 10 ml Luer-Lok™ syringe (Becton Dickinson, Fisher, Canada) containing 10 ml of sterile saline containing heparin (10 units/ml). The other end of the cannula was cut at a slight angle with a dulled edge to prevent ripping the vein and inserted in the direction of the heart where light pressure was applied until resistance was felt (typically 2 – 3 cm). Blood was drawn into a 1 ml Luer-Lok™ syringe connected to the 3-way valve to determine if the appropriate flow rate was achieved or if the vein had collapsed on the cannula when adjustments could be easily made. Once the blood flow rate was satisfactory, the second piece of surgical silk was tied around the cannulated vein to secure the cannula. After the surgery was complete, a generously moistened piece of gauze was placed on the open wound for the duration of the experiment to prevent excessive dehydration. For every 1 ml of blood removed from the animal, 2 ml of sterile saline was infused. Typically surgery related blood loss did not exceed 100 µl. In an instance where surgery alone resulted in an estimated blood loss which exceeded 1 ml, the animal was not used for an *in vivo* metabolism study and the blood and tissue samples were collected for control studies. This protocol was approved by the University of Manitoba Animal Care Committee.

2.2.3   Dosing and sample collection

Dexrazoxane hydrochloride (freshly prepared, 10 mg/ml in sterile saline) was filtered using a sterile Fisherbrand™ 0.22 µm syringe filter (Fisher, Canada) and

administered at a dose of 40 mg/kg as an i.v. bolus infusion (2 ml/min) through the tail vein. Blood samples (500 μl) were removed from the left jugular vein from a group of 6 rats at times 5, 30, 60, 120, and 180 min post-dexrazoxane infusion, and at 60, 80, 100, 120, and 140 min post-dexrazoxane infusion from a second group of 6 rats. **B/C** (prepared as described in Section 2.2.4) and ADR-925 (prepared as described in Section 2.2.5) were administered at a dose of 20 mg/kg (as a 5 mg/ml solution in saline solution) as an i.v. bolus infusion (2 ml/min) through the tail vein. Blood samples (300 μl) were removed from the left jugular vein from a group of 3 rats at times 2, 15, 30, 45, 60, and 90 min. One 300 μl blood sample was drawn from each rat prior to the administration of **B/C** or ADR-925 as a control. The blood samples were added to heparin (10 μl of 1000 units/ml) and centrifuged for 5 min at 500 g. The plasma was removed and 20 μl of 5 M HCl per ml of plasma was added. The samples were stored at -80 °C to prevent further hydrolysis (Hasinoff, 1994b).

2.2.4 DHPase-mediated biosynthesis of the B/C mixture

Milligram quantities of **B/C** were biosynthetically prepared using the enzyme dihydropyrimidinase (DHPase, EC 3.5.2.2), for the animal studies where a bolus of a **B/C** mixture was used. It has been previously determined that DHPase can rapidly hydrolyze dexrazoxane to **B** and **C** but not to ADR-925 (Hasinoff et al., 1991; Hasinoff, 1993). DHPase-mediated biosynthesis of **B** and **C** from dexrazoxane resulted in relatively large quantities of a **B/C** mixture (20 mg per preparation as described in this Section). DHPase is present as a contaminant of catalase (obtained from Sigma, C-30). The catalase was dialyzed for 24 h at 4 °C using a Cellu Sep ™ regenerated cellulose tubular membrane (Fisher, Canada) with a molecular weight cut off of 12,000 - 14,000. The dialysis

41

membrane was filled with approximately 4 - 5 ml of crystaline catalase suspension and sealed by tying both ends with surgical silk. The catalase was dialyzed for 24 h in 4 l of distilled water.

Dexrazoxane hydrochloride was dissolved in water (30 mg/ml), titrated with 5 M NaOH to pH 7, and added to the dialyzed catalase/DHPase such that the final dexrazoxane solution concentration was 10 mg/ml. The reaction, carried out at room temperature, was monitored by HPLC (as described in Section 2.2.9) and typically reached completion in 45 to 60 min. The reaction was deemed complete when the dexrazoxane levels were less then 10 μM (or less then 0.03 mol % of initial dexrazoxane concentration). Acetonitrile (2:1, v/v) was used to precipitate proteins from the catalase and **B/C** mixture (as described in Section 2.2.6). Under these reaction conditions, dexrazoxane was hydrolyzed to **B** and **C** with a **B/C** ratio of 4.14:1, which is consistent with previous published enzyme kinetic reports of DHPase-mediated hydrolysis of dexrazoxane (Hasinoff, 1993). Once the **B/C** mixture was obtained, it was also analyzed for ADR-925 content via the calcein assay (as described in Section 2.2.11) and was found to contain less then 0.1 mol % ADR-925.

2.2.5 Preparation of ADR-925 from dexrazoxane for ADR-925 infusion studies

ADR-925 used for the animal experiments was prepared by adding 50 μl of 5 M NaOH per ml of 10 mg/ml dexrazoxane hydrochloride solution for 48 h. At 48 h, the reaction was quenched with 45 μl of 5 M HCl. The ADR-925 solution was titrated to pH 7 using 5 M NaOH. A sample was analyzed by HPLC (as described in Section 2.2.9) to ensure that the hydrolysis of dexrazoxane to ADR-925 was complete. ADR-925 prepared in this fashion contained less then 0.003, 0.006, and 0.006 mol % of

dexrazoxane, **B**, and **C**, respectively. The ADR-925 was filter sterilized using a Fisherbrand™ 0.22 μm syringe filter prior to animal use.

2.2.6 Precipitation of plasma proteins

Plasma samples to be analyzed for dexrazoxane and dexrazoxane metabolites were rapidly thawed in a 37 °C water bath, vortexed for 30 s, and titrated to a pH range of 5-6 with 5 M NaOH. To precipitate plasma proteins, a 300 μl aliquot of acetonitrile was added to 150 μl of plasma (2:1 acetonitrile/plasma, v/v) which was followed by 30 s of rapid vortex. The sample was then centrifuged at 10,000 *g* for 5 min upon which the supernatant was removed from the plasma protein pellet and placed in a 1.5 ml microcentrifuge tube and acidified with 5 μl of 5 M HCl. The acidified acetonitrile supernatant was evaporated to dryness by a stream of nitrogen gas at room temperature. Samples to be analyzed for dexrazoxane, **B**, and **C** analysis were dissolved in 10 mM HCl/500 μM Na$_2$EDTA reconstituted to their original volume just prior to analysis. Samples to be analyzed for ADR-925 by the calcein assay were dissolved in 10 mM HCl prior to analysis. Absolute recoveries from spiked plasma ranged from 90% to 100% over a 10 to 200 μM dexrazoxane range. Similarly, the recovery of **B** and **C** ranged from 77-98%, and 81-100%, respectively, over the range of 5-50 μM. Absolute recoveries from spiked plasma ranged from 90% to 98% over a 5 to 50 μM ADR-925 range.

2.2.7 Preparation of liver, heart, and brain homogenates

After the last blood collection time point (2 to 3 h post dexrazoxane or 90 min post **B/C** infusion), the heart, brain, and section of liver, were removed and weighed. Using surgical scissors, the organs were cut into small pieces (< 5 mm^3) and washed three

43

times in a 50 ml centrifuge tube by adding 30 ml of 10 mM HCl (pH 3) and swirling rapidly for about 1 min upon which the wash solution was drained. By the third wash the majority of organ blood was removed and the wash solution appeared clear. The washed minced organs were homogenized using a Polytron homogenizer (Kinematica GmbH, Switzerland) for 5 min. The homogenate was centrifuged at 0 °C for 2 h at ~18,000 g. The supernatant was removed and placed in 1.5 ml microcentrifuge tube and stored at -80°C until analysis. Homogenate supernatant proteins were precipitated as described in Section 2.2.6 and ADR-925 levels were subsequently measured via the calcein assay (as described in Section 2.2.11).

2.2.8 Treatment of liver, heart, and brain homogenates to determine total dexrazoxane, B, C, and ADR-925 tissue levels

In the case where rats were dosed with 40 mg/kg dexrazoxane hydrochloride, an experiment was done to determine the total concentration of dexrazoxane, **B**, **C**, and ADR-925. A 950 µl sample of tissue homogenate supernatants was treated with 50 µl of 5 M NaOH (such that the final NaOH concentration was 250 mM) for 15 hours to hydrolyze dexrazoxane, **B**, and **C** to ADR-925. Homogenate supernatant proteins were precipitated as described in Section 2.2.6 and ADR-925 levels were subsequently measured via the calcein assay (as described in Section 2.2.11).

2.2.9 HPLC separation of dexrazoxane, its one-ring open intermediates B and C, and ADR-925

2.2.9.1 Instrumentation

The HPLC apparatus consisted of a programmable Varian (Walnut Creek, CA) 9010 pump, Varian 9050 variable wavelength absorbance detector (detection wavelength

44

205 nm), Varian Star integrator software (Version 4.0), and a Gilson 234 autoinjector (Paris, France) with a 20 μl stainless steel sample loop. Prior to each injection, the sample loop was rinsed with 500 μl of 500 μM EDTA (pH 4.5). The column was a 10 μm μBondapak 3.9 X 300 mm reverse phase C_{18}-column (Waters, Mississauga, Canada). All HPLC solutions, with the exception of HPLC grade methanol, were filtered using a Millipore 0.4 μm cellulose filter (Fisher, Canada).

2.2.9.2 HPLC separation of dexrazoxane and C from peaks present in the acetonitrile-treated plasma sample

Ion-pair reverse phase HPLC was used to separate dexrazoxane and **C** from plasma peaks on the same run. The elution profile began with 500 μM Na_2EDTA/2 mM heptanesulfonic acid (pH 3.5) isocratically pumped through the column at a rate of 1 ml/min for 5 min. From 5 to 7 min, the methanol concentration was linearly increased to 20 % upon which a 500 μM Na_2EDTA in 2 mM heptanesulfonic acid/methanol (80:20 v/v) solution was isocratically pumped for 5 min. After the dexrazoxane peak eluted, at about 13 min, the methanol concentration was linearly increased from 20 to 80 % over 1 min and maintained for 20 min to remove any late eluting peaks present in the acetonitrile-treated plasma sample. The initial mobile phase of 500 μM Na_2EDTA/2 mM heptanesulfonic acid was isocratically pumped through the column for 30 min prior to the next injection to equilibrate the column.

2.2.9.3 HPLC separation of B from protein plasma peaks

Under the conditions described in Section 2.2.9.2, **B** co-eluted with a peak present in the acetonitrile-treated plasma sample and was thus determined separately under isocratic conditions. 500 μM Na_2EDTA (pH 3.5) was isocratically pumped through the

45

column at a rate of 1 ml/min for 6 min. From 6 to 8 min, the methanol concentration was linearly increased to 80 % and maintained for 20 min to remove any late eluting peaks. The initial mobile phase was isocratically pumped through the column for 20 min prior to the next injection.

2.2.9.4 Separation of ADR-925 from co-eluting plasma peaks

In order to compare the amount of ADR-925 obtained by HPLC and by the flow injection method (as described in section 2.2.11), ADR-925 was determined ($n = 4$) in the plasma of one rat by HPLC under isocratic conditions (500 µM Na_2EDTA/2 mM heptanesulfonic acid, pH 3.5, 1 ml/min). After ADR-925 eluted, the column was washed with 500 µM Na_2EDTA/methanol (20:80 v/v) for 20 min followed by re-equilibration with the initial mobile phase for 25 min.

2.2.9.5 HPLC separation of B and C from rats dosed with a B/C mixture

In the instance where rats were dosed with a **B/C** mixture, **B** and **C** were separated using a new 10 µm µBondapak 3.9 X 300 mm reverse phase C_{18}-column (Waters, Mississauga, Canada) with the same elution profile as outlined in Section 2.2.9.3 with the exception that the mobile phase of 500 µM Na_2EDTA was titrated to a pH of 4.5.

2.2.10 HPLC calibration plots: quantitation of dexrazoxane, B, C, and ADR-925 in rat plasma

The HPLC calibration (10 to 500 µM dexrazoxane, 2 to 50 µM **B** and **C**, and 20 to 100 µM ADR-925) were prepared by adding standards containing known amounts of dexrazoxane, **B**, **C** and ADR-925 (prepared as previously described (Hasinoff, 1994b)) to

blank rat plasma. The calibration plots for dexrazoxane, **B**, **C**, and ADR-925 were constructed by plotting arbitrary unit integration peak areas (as shown in Tables 2.2-2.7) as a function of drug or drug metabolite concentration as shown in Figures 2.7 through 2.12. Each concentration point of the calibration curves, prepared prior to sample analysis, was an average of two injections.

2.2.11 Analysis of ADR-925 using the fluorescent dye calcein

The low molar absorptivity of ADR-925 (Hasinoff, 1990a) lead to the necessity to develop a highly sensitive flow injection method of analysis for ADR-925. An assay was developed using the fluorescent metal ion-chelating indicator calcein (which does not bind calcium or magnesium at neutral pH). Calcein fluorescence is strongly quenched by Co^{2+} with which it forms a strong 1:1 ($K_f = 10^{6.8}$ M^{-1}) complex (Kendall and MacDonald, 1983). In this assay the free Co^{2+} not bound to ADR-925 in plasma was reacted with calcein. The free calcein remaining was then determined fluorometrically by either flow injection or fluorescence plate reader analysis or fluorescence analysis. As shown in equation 2.1 and 2.2, the free calcein is representative of ADR-925.

$$1\ Co^{2+} + x\ ADR\text{-}925\ \longrightarrow\ x\ Co^{2+}\text{-}ADR\text{-}925 + (1\text{-}x)\ Co^{2+} \qquad (2.1)$$

$$1\ calcein + (1\text{-}x)\ Co^{2+}\ \longrightarrow\ (1\text{-}x)\ Co^{2+}\text{-}calcein + x\ calcein \qquad (2.2)$$
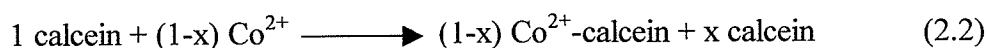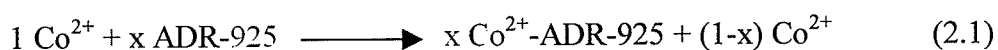
2.2.11.1 Experimental conditions for the calcein assay

Calibration plots of integrated fluorescence peak areas ($n = 6$) in the range 0 to 1.0 µM ADR-925 (as described in Table 2.1) were prepared as follows. A stock solution of 100 µM ADR-925 was prepared in blank plasma. To prepare blank plasma, blood samples were removed from a rat prior to dosing with any drug and plasma proteins were

precipitated with acetonitrile as described in Section 2.2.6. A stock solution of 50 µl of Co^{2+} (20 µM in 50 mM Tris buffer, pH 5.5) was added to 0 – 10 µl of 100 µM ADR-925 (prepared in blank plasma) in a Fisherbrand™ 3 ml glass test tube (Fisher). As noted in Table 2.1, the amount of plasma added to the reaction was kept constant at 10 µl. Thus for ADR-925 standards 0 to 0.8 µM, 10 to 2 µl of blank plasma was added to each standard. Samples were rapidly vortexed for 5 min to allow the reaction of ADR-925 with Co^{2+} to proceed to completion. Calcein (10 µl of 100 µM in distilled water) was then added and mixed for 30 s to allow for the reaction of the free Co^{2+} and calcein. Tris buffer (940 µl, 50 mM, pH 7.5) was added such that the final Co^{2+} concentration was 1.0 µM and the ADR-925 concentration ranged from 0 to 1.0 µM (as shown in Table 2.1).

Samples to be analyzed for ADR-925 in rats dosed with dexrazoxane, the **B/C** mixture, or ADR-925 were treated as described above and assessed for ADR-925 content relative to the standard curve. If the ADR-925 concentration exceeded 0.9 µM, as determined from the fluorescence signal, the plasma sample was diluted to bring it into the working range (0.2 – 0.9 µM). In order to reduce interfering heavy metal contaminants, the Tris buffer and calcein stock solutions were stirred with the chelating resin Chelex (Sigma, 1 g/100 ml) for 24 h prior to use. Calcein was also stored over Chelex (1 g/5 ml) at 4 °C. Care was also taken to ensure that the plasma samples only came in contact with plastic to prevent heavy metal contamination.

Table 2.1 Calcein assay standard ADR-925 curve to determine ADR-925 plasma levels.

Std #	Volume of 20 μM Co^{2+} in 50 mM Tris (pH 5.5) (μl)	Volume of 100 μM ADR-925 (μl)	Volume of blank plasma (μl)	Volume 100 μM calcein (μl)	Volume 50 mM Tris (pH 7.5) (μl)	Final ADR-925 concentration (μM)
1	50	0	10	10	930	0
2	50	2	8	10	930	0.2
3	50	4	6	10	930	0.4
4	50	6	4	10	930	0.6
5	50	8	2	10	930	0.8
6	50	10	0	10	930	1.0

2.2.11.2 Instrumental

2.2.11.2.1 Flow injection analysis of ADR-925

Once the plasma samples were prepared for ADR-925 analysis (as described in Section 2.2.11.1) 50 μl was injected into a Rheodyne (Cotati, CA) injector with a 20 μl Upchurch (Oak Harbor, WA) PEEK sample loop using a Teflon needle (Rheodyne). PEEK tubing (Upchurch) was used between the injector, a programmable Varian (Walnut Creek, CA) 9010 pump, and the Shimadzu (Columbia, MD) RF-551 fluorescence detector (λ_{ex} 496 nm, λ_{em} 517 nm). Aqueous Na$_2$EDTA (20 μM, 1 ml/min) was used as the mobile phase to complex metal ions present in the flow system. This concentration of EDTA was shown not to affect the assay because the brief time that the injected sample was in contact with EDTA was too short to allow any significant reaction to occur with the Co^{2+}–calcein complex. Samples were analyzed in triplicate.

2.2.11.2.2 Fluorescence plate reader analysis of ADR-925

The fluorescence measurements were also conducted on a BMG Lab Technologies Inc. (Durham, NC) Fluostar Galaxy fluorescence plate reader (λ_{ex} 485 nm, λ_{em} 520 nm) with excitation and emission probes directed to the bottom (bottom/bottom read) of a black plastic 96-well plate (obtained from Corning, NY). A gain was set such that 100 μl of 1 μM calcein would be 90 % of the maximum fluorescence value (which typically resulted in a gain range of 20 − 22). Preparation of the calibration curve and samples to be analyzed for ADR-925 were done exactly as described in Section 2.2.11.1 and 100 μl of prepared sample was added to each well. Samples were analyzed in duplicate.

2.2.12 ADR-925 calibration plots using the fluorescent dye calcein

Calibration plots of integrated peak areas ($n = 6$) in the range 0 to 1.0 μM ADR-925 (as shown in Tables 2.8 - 2.9) were repeated every 3 h during ADR-925 analysis for the calcein assay using the flow injection method (Section 2.2.11.2.1). In the instance where the fluorescence plate reader was used (Section 2.2.11.2.2), a standard curve was prepared for each individual plate containing samples to be analyzed for ADR-925 content. The limit of quantitation of ADR-925 in plasma was estimated to be 1 μM. This was determined by adding known amounts of ADR-925 to blank plasma samples (prepared as described in Section 2.2.11.1) and comparing the resulting fluorescence signal to the predicted signal based on the standard curve.

2.2.13 Data Analysis

Pharmacokinetic data were analyzed using the pharmacokinetic/pharmacodynamic modeling program WinNonlin (Pharsight, Mountain View, CA) for an *i.v.* bolus.

2.3 Results

2.3.1 HPLC separation of dexrazoxane, its one-ring open intermediates B and C, and ADR-925

Under the column conditions described in Section 2.2.9, dexrazoxane, **B**, **C**, and ADR-925 were all well separated from peaks present in the acetonitrile-treated plasma sample with retention times of 13.5, 4.9, 5.7, and 3.6 min, respectively. Representative chromatograms of the separation of dexrazoxane and its hydrolysis products are shown in Figures 2.2 to 2.5. In the instance where rats were dosed with a **B/C** mixture, **B** and **C** were well resolved on the same run with retention times of 4.8 min and 5.9 min, respectively, as shown in Figure 2.6.
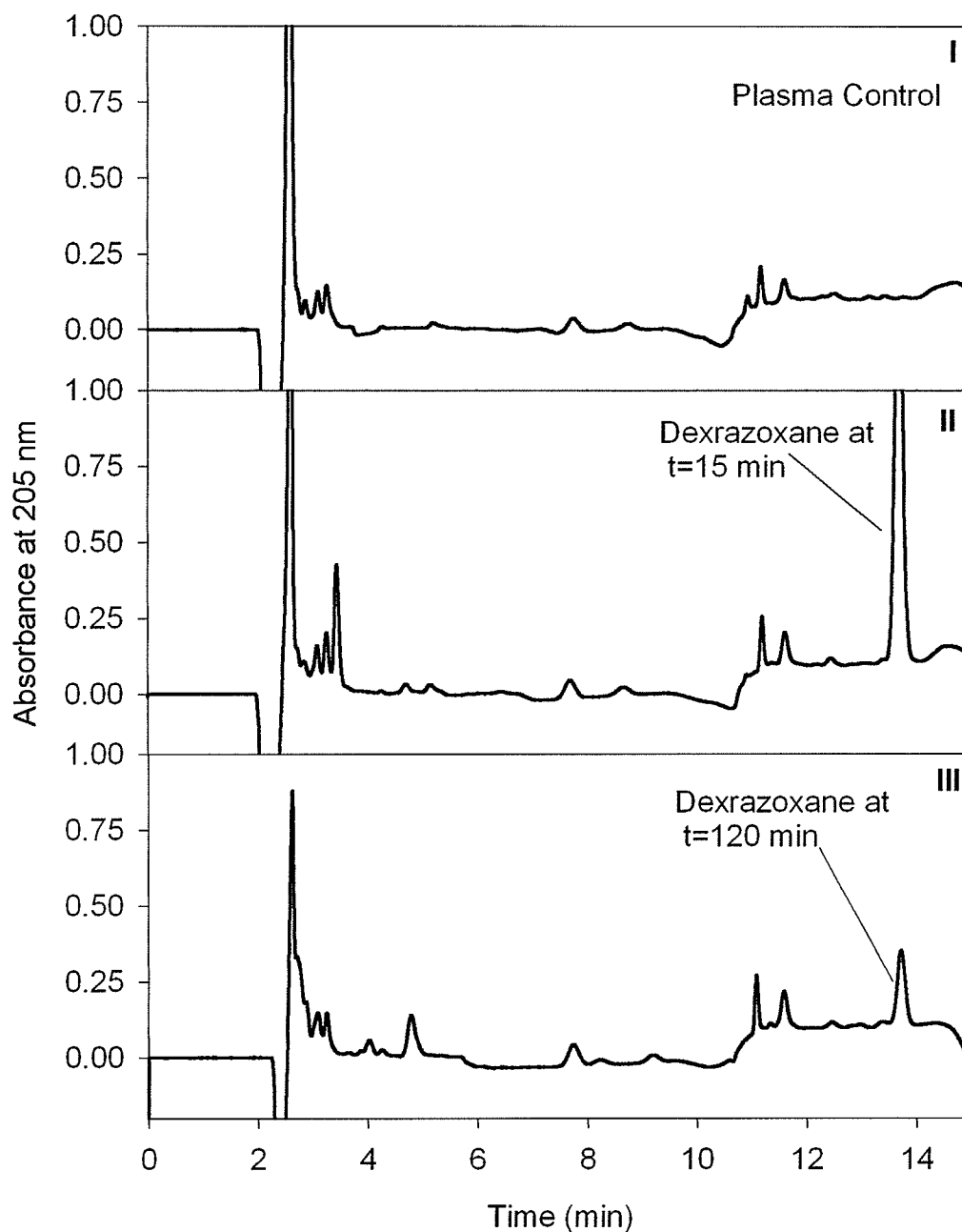
Figure 2.2   HPLC chromatograms of the separation of dexrazoxane in plasma from a rat dosed with an i.v. bolus of 40 mg/kg dexrazoxane hydrochloride.

Dexrazoxane was separated on a C_{18} reverse-phase column. A blank plasma sample is shown in chromatogram I.   HPLC chromatograms II and III were obtained after 15 and 120 min post dexrazoxane bolus (40 mg/kg), respectively.
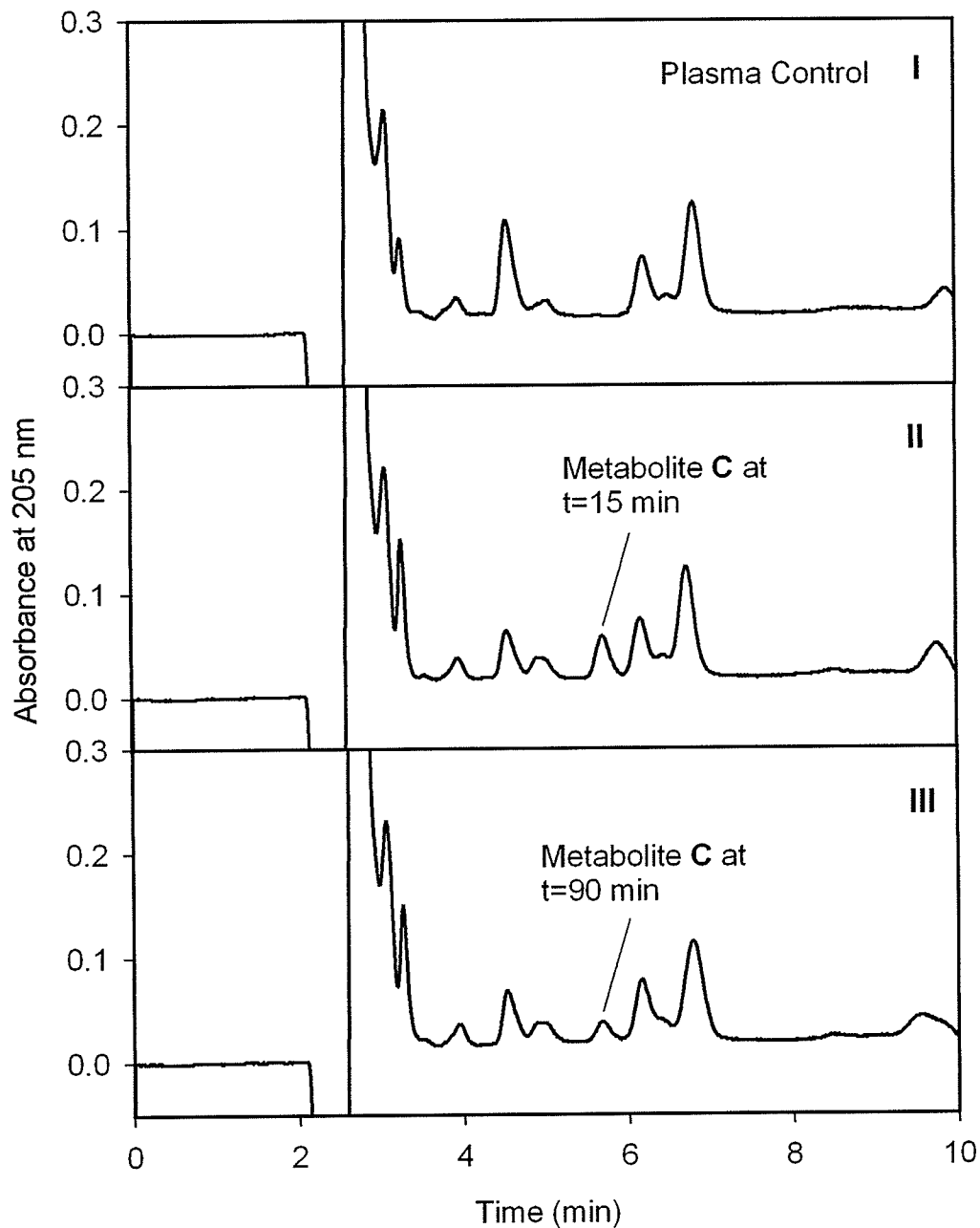
Figure 2.3   HPLC chromatograms of the separation of Metabolite C in plasma from a rat dosed with an i.v. bolus of 40 mg/kg dexrazoxane hydrochloride.

Metabolite **C** was separated on a C_{18} reverse-phase column. A blank plasma sample is shown in chromatogram I.   HPLC chromatograms II and III were obtained after 15 and 90 min post dexrazoxane bolus (40 mg/kg), respectively.
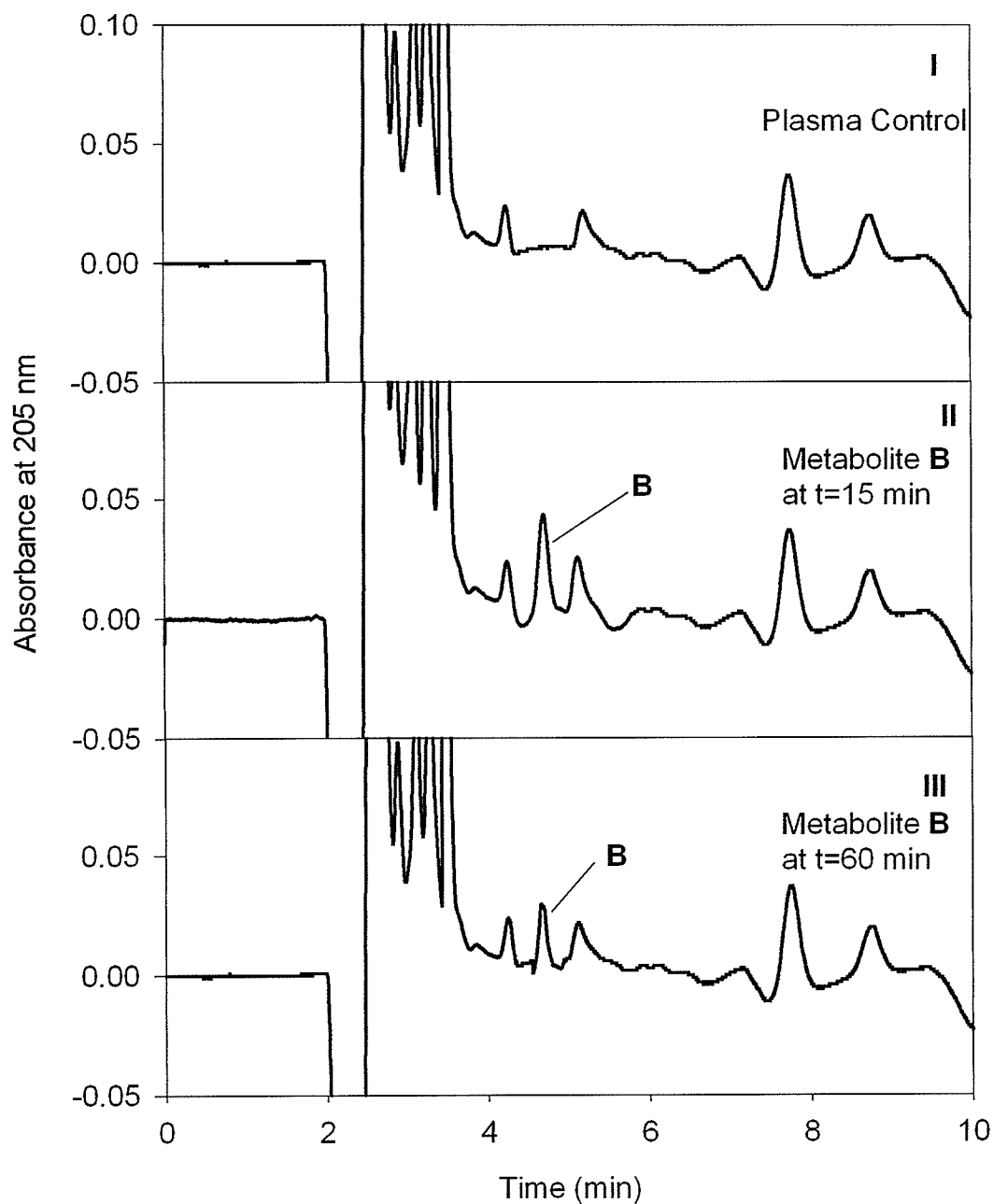
*Figure 2.4   HPLC chromatograms of the separation of Metabolite **B** in plasma from a
rat dosed with an i.v. bolus of 40 mg/kg dexrazoxane hydrochloride.*

Metabolite **B** was separated on a C_{18} reverse-phase column. A blank plasma sample is
shown in chromatogram I.   HPLC chromatograms II and III were obtained after 15 and
60 min post dexrazoxane bolus (40 mg/kg), respectively.
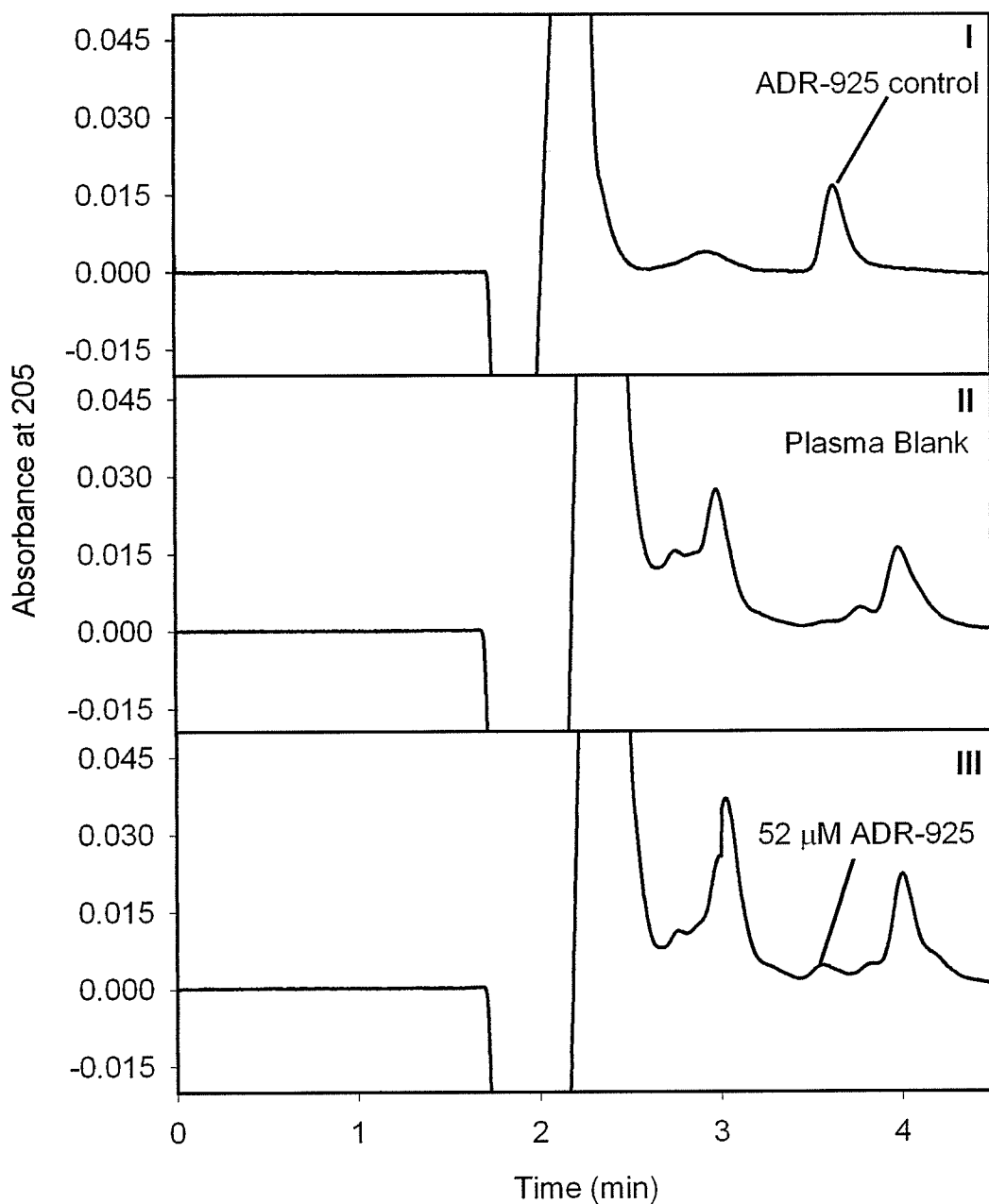
Figure 2.5   HPLC chromatograms of the separation of ADR-925in plasma from a dosed with an i.v. bolus of 40 mg/kg dexrazoxane hydrochloride.

ADR-925 was separated on a C_{18} reverse-phase column. A control sample of 500 μM ADR-925 is shown in HPLC chromatogram I. A blank plasma sample is shown in chromatogram II. HPLC chromatograms III was obtained after 120 min post dexrazoxane bolus (40 mg/kg), where the integrated ADR-925 peak area corresponds to 52 μM ADR-925.
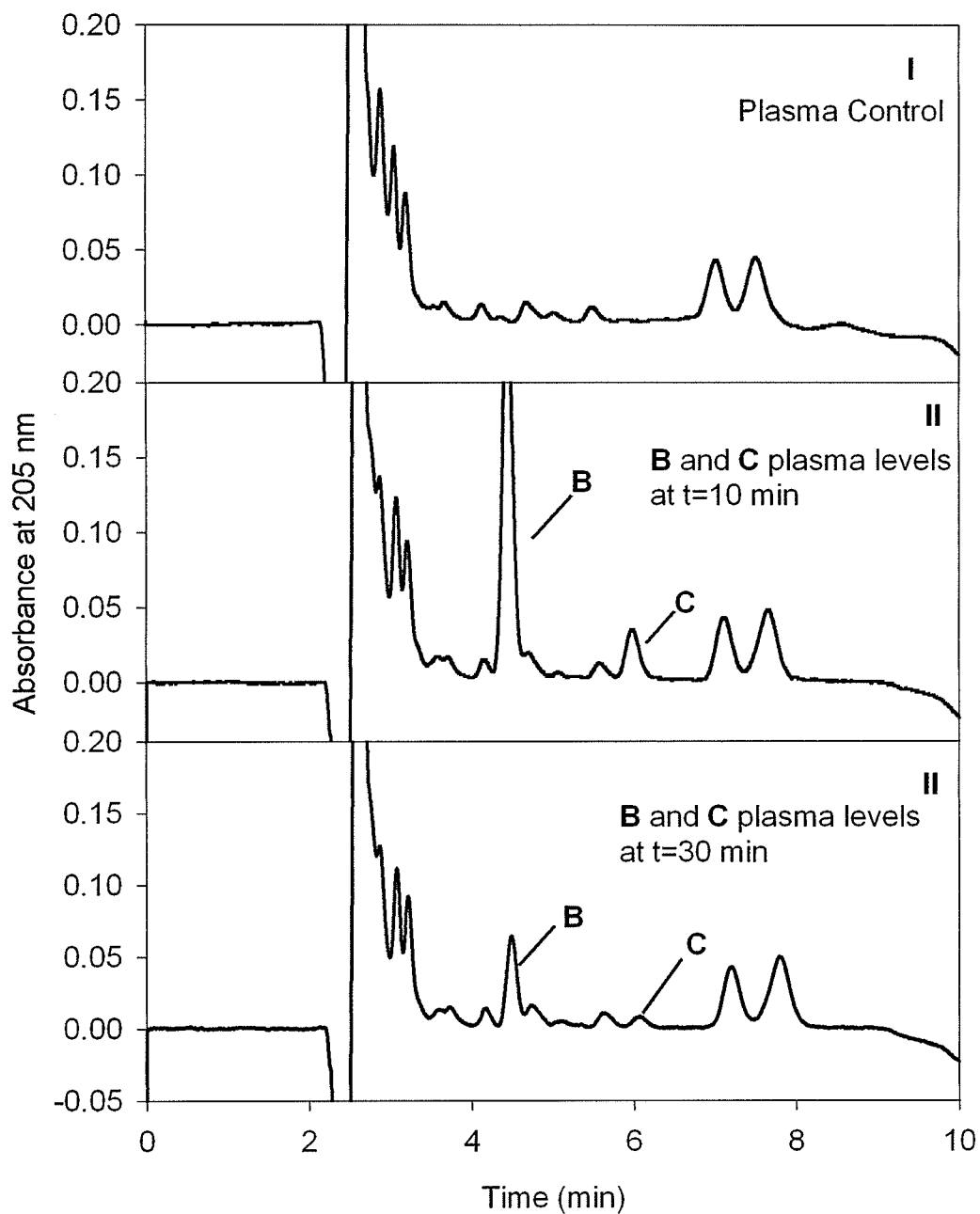
*Figure 2.6   HPLC chromatograms of the separation of Metabolite **B** and **C** in plasma from a rat dosed with an i.v. bolus of 20 mg/kg B/C mixture.*

Metabolite **B** and **C** were separated on a new C_{18} reverse-phase column. A blank plasma sample is shown in chromatogram I. HPLC chromatograms II and III were obtained after 10 and 30 min post **B/C** mixture bolus (20 mg/kg), respectively.

2.3.2 HPLC calibration plots: quantitation of dexrazoxane, B, C, and ADR-925 in rat plasma

The calibration plots for dexrazoxane, **B**, **C**, and ADR-925 were constructed by plotting arbitrary integration peak areas (as shown in Tables 2.2-2.7) as a function of drug or drug metabolite concentration as shown in Figures 2.7 through 2.12. Each concentration point of the calibration curves, prepared prior to sample analysis, was an average of two injections. The day-to-day variation of the slopes was found to be small and is expressed as a percent difference at the end of Tables 2.2-2.9. The limit of quantitation, estimated from three times the limit of detection, of dexrazoxane, **B**, **C**, and ADR-925 in plasma was 0.5, 1.0, 1.0, and 10 μM, respectively. The limit of detection was made through an estimate of drug/metabolite peak heights that exceeded the background noise three-fold.

Table 2.2 HPLC calibration curve of dexrazoxane (UV absorbance at 205 nm) in precipitated rat plasma for rats dosed with 40 mg/kg dexrazoxane hydrochloride.

Concentration (μM)	Average Peak Area (Arbitrary Units)
400	1324489
300	953100
200	667646
100	324312
50	152916
25	91418
10	45671
Slope[a]	3261
Y-intercept	3115
r^2	0.998

[a] Between-day variation in the slopes of the calibration plots was 11%.

Table 2.3   HPLC calibration curve of metabolite **C** (UV absorbance at 205 nm) in precipitated rat plasma for rats dosed with 40 mg/kg dexrazoxane hydrochloride.

Concentration (μM)	Average Peak Area (Arbitrary Units)
50	76388
30	42579
20	27292
10	16102
5	8272
2	3104
Slope [a]	1495
Y-intercept	-199
r^2	0.996

[a] Between-day variation in the slopes of the calibration plots was 2%.

Table 2.4   HPLC calibration curve of metabolite **B** (UV absorbance at 205 nm) in precipitated rat plasma for rats dosed with 40 mg/kg dexrazoxane hydrochloride.

Concentration (μM)	Average Peak Area (Arbitrary Units)
50	80543
30	49987
20	27041
10	14246
5	7978
2	3039
Slope [a]	1633
Y-intercept	-1375
r^2	0.994

[a] Between-day variation in the slopes of the calibration plots was 2%.

Table 2.5   HPLC calibration curve of ADR-925 (UV absorbance at 205 nm) in precipitated rat plasma for rats dosed with 40 mg/kg dexrazoxane hydrochloride.

Concentration (μM)	Average Peak Area (Arbitrary Units)
100	30241
70	19546
50	13954
35	11024
20	6124
10	3024
Slope	293
Y-intercept	20.6
r^2	0.994

Table 2.6   HPLC calibration curve of metabolite **B** (UV absorbance at 205 nm) in precipitated rat plasma for rats dosed with 20 mg/kg **B/C** mixture.

Concentration (μM)	Average Peak Area (Arbitrary Units)
500	773812
200	330132
100	159981
50	84046
25	40672
10	14294
5	6688
2	3028
Slope	1555
Y-intercept	3244
r^2	0.999

Table 2.7   HPLC calibration curve of metabolite **C** (UV absorbance at 205 nm) in precipitated rat plasma for rats dosed with 20 mg/kg **B/C** mixture.

Concentration (μM)	Average Peak Area (Arbitrary Units)
200	337383
100	158267
75	115942
50	75824
25	37877
10	16564
5	7338
2	3127
Slope[a]	1677
Y-intercept	-3866
r^2	0.998
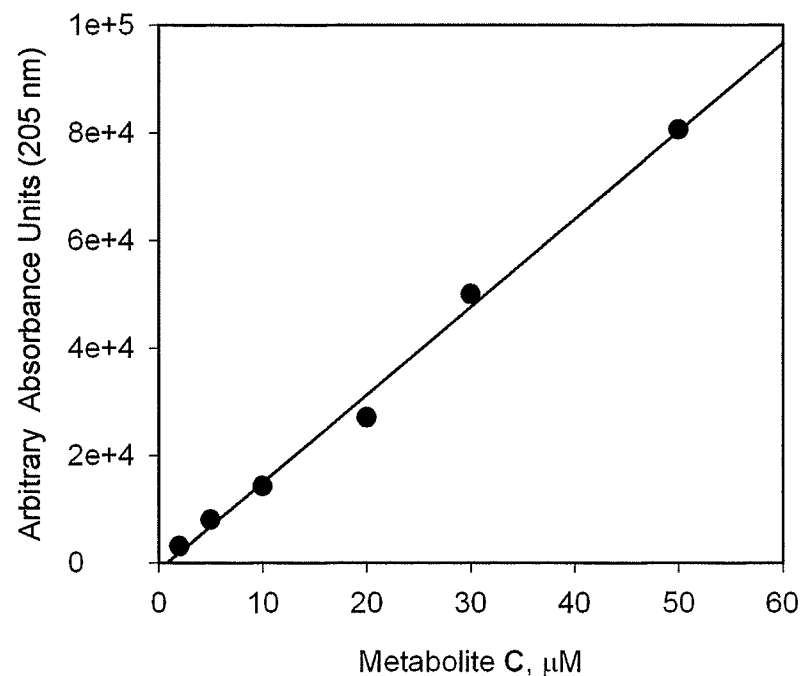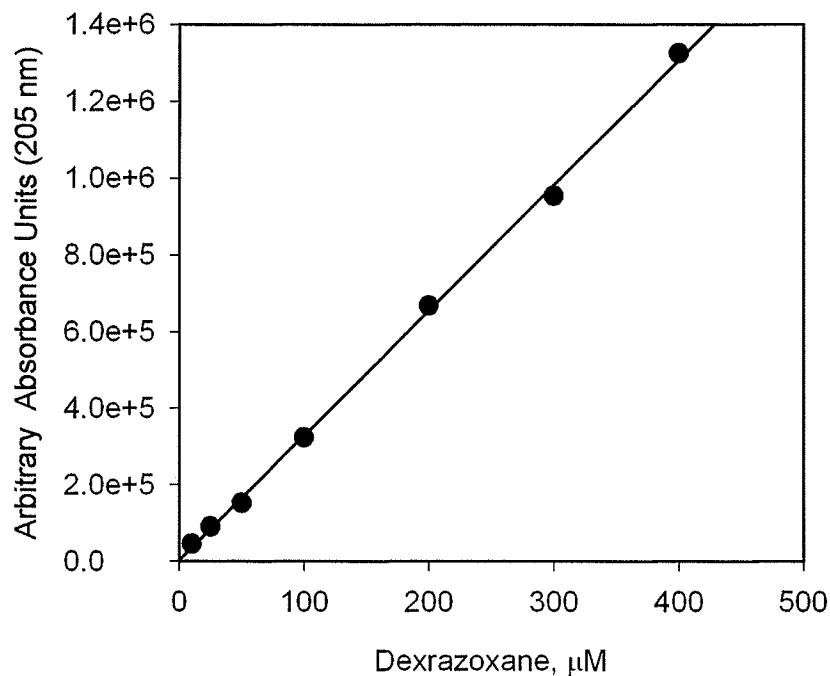
Figure 2.7 HPLC calibration curve of dexrazoxane in rat plasma *Figure 2.8 HPLC calibration curve of C in rat plasma*

HPLC calibration plots using integrated peak areas were prepared by adding standards containing known amounts of dexrazoxane and C to blank rat plasma. A mobile phase of 500 μM Na$_2$EDTA/2 mM heptanesulfonic acid (pH 3.5) (as described in Section 2.2.9.2) separated dexrazoxane (t_r 13.8 min) and C (t_r 5.8 min) from peaks present in the acetonitrile-treated plasma sample.
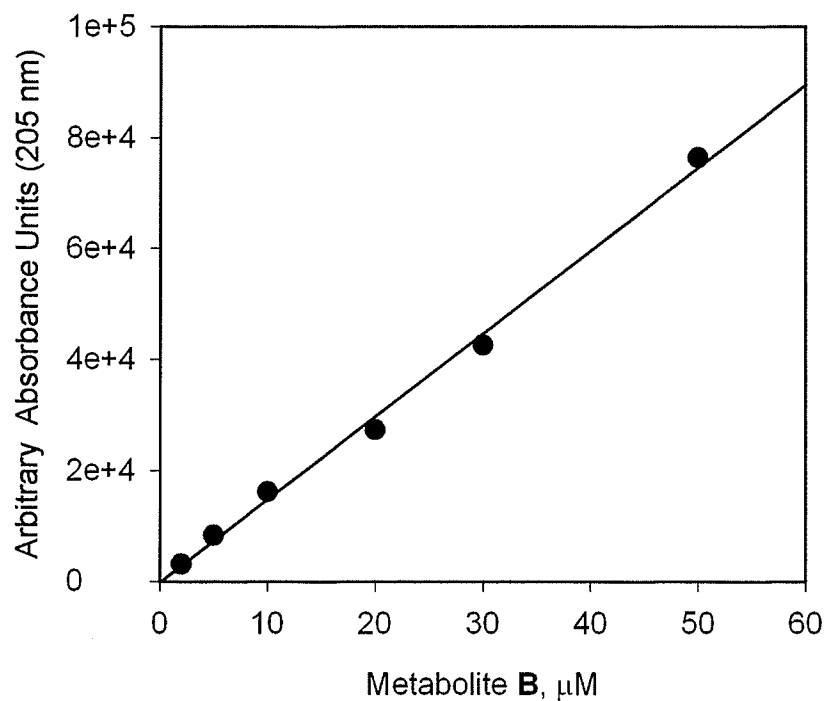
*Figure 2.9 HPLC calibration curve of **B** in rat plasma*
HPLC calibration plot using integrated peak areas was prepared by adding standards containing known amounts of **B** to blank rat plasma. A mobile phase of 500 µM Na$_2$EDTA (pH 3.5) (as described in Section 2.2.9.2) separated **B** (t_r 4.9 min) from peaks present in the acetonitrile-treated plasma sample.
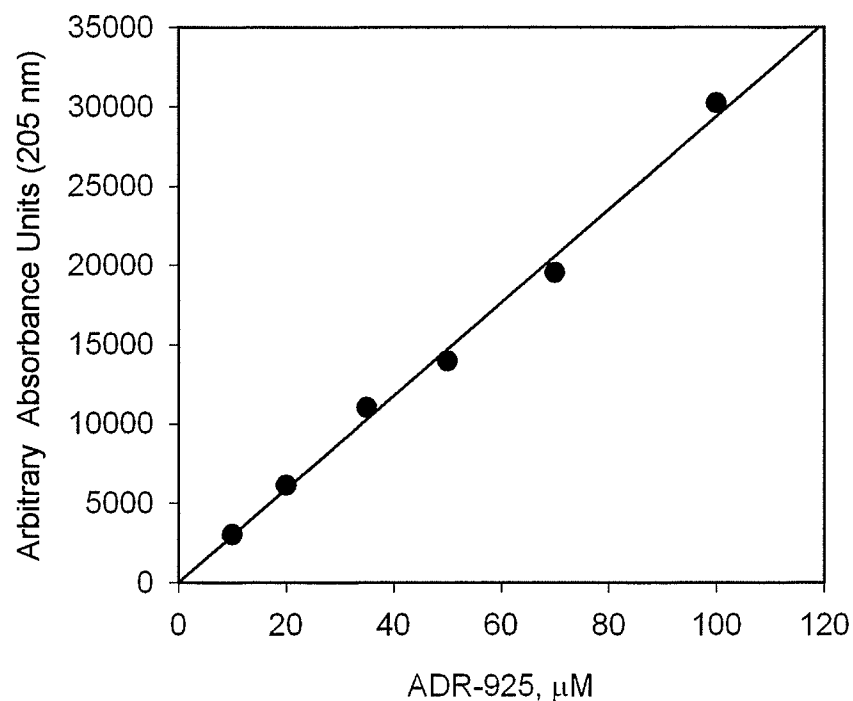
Figure 2.10 HPLC calibration curve of ADR-925 in rat plasma
HPLC calibration plot using integrated peak areas was prepared by adding standards containing known amounts of ADR-925 to blank rat plasma. A mobile phase of 500 µM Na$_2$EDTA/2 mM heptanesulfonic acid (pH 3.5) (as described in Section 2.2.9.4) separated ADR-925 (t_r 3.8 min) from protein peaks.
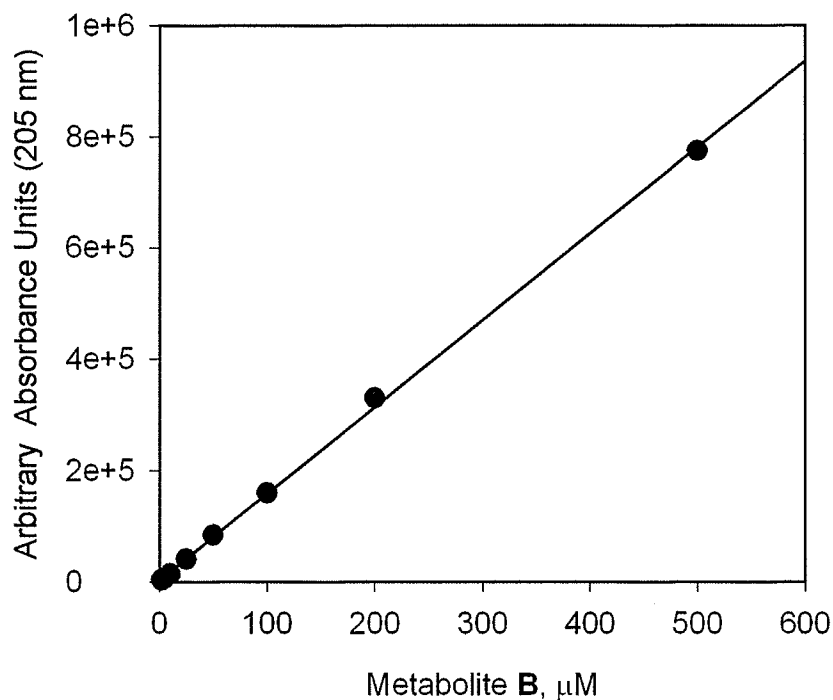
*Figure 2.11 HPLC calibration curve of **B** in rat plasma for rats   Figure 2.12 HPLC calibration curve of **C** in rat plasma for rats*
  *dosed with 20 mg/kg of a **B/C** mixture*   *dosed with 20 mg/kg of a **B/C** mixture*
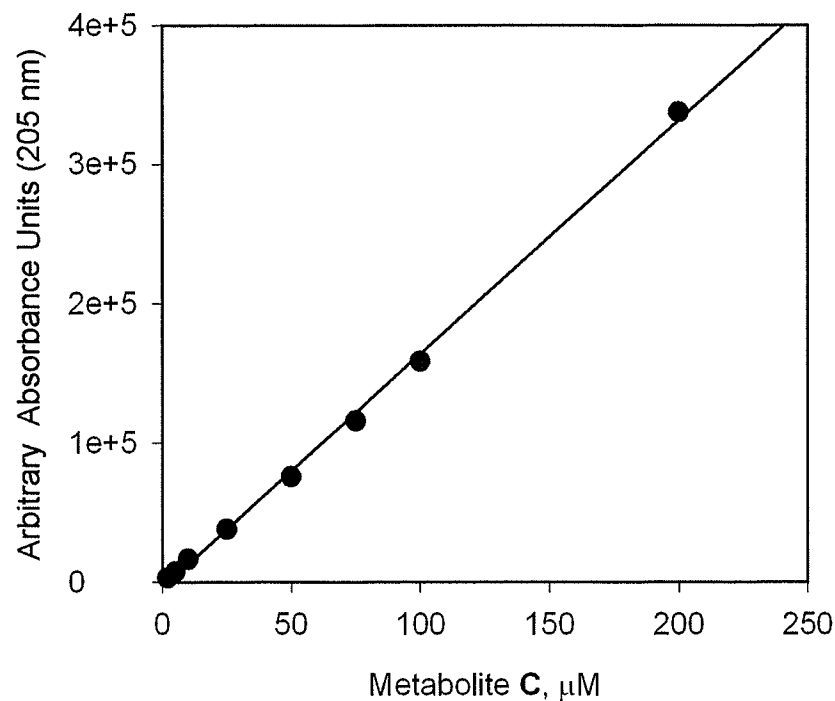
HPLC calibration plots using integrated peak areas were prepared by adding standards containing known amounts of **B** and **C** to blank rat plasma. A mobile phase of 500 μM Na_2EDTA (pH 4.5) (as described in Section 2.2.9.5) separated **B** (t_r 4.8 min) and **C** (t_r 5.9 min) from peaks present in the acetonitrile-treated plasma sample.

2.3.3 Selectivity of Co^{2+} for ADR-925

The calcein assay was shown to selectively detect only ADR-925 in the presence of a mixture of dexrazoxane, **B**, **C** and ADR-925 as shown in Figure 2.13. The added Co^{2+} was shown not to detectably promote the ring opening of **B** and **C** (Buss and Hasinoff, 1997) over 20 min, under the experimental conditions outlined in Section 2.2.11.1. All ADR-925 calibration curves were done in precipitated plasma (detailed in Section 2.2.6) and precipitated plasma components were shown not to interfere with the assay as the slopes of the calibration plots in water and reconstituted plasma were unchanged. Over the time the assay was conducted both the Co^{2+}–ADR-925 and Co^{2+}–calcein complexes were stable. The ADR-925 in plasma is likely complexed with Ca^{2+} and Mg^{2+} (K_f of $10^{6.9}$ and $10^{5.1}$ M^{-1}, respectively (Huang et al., 1982)). It was shown in control experiments containing typical plasma concentrations of Ca^{2+} and Mg^{2+}, that the added Co^{2+} was able to displace the Ca^{2+} and Mg^{2+} from their complexes with ADR-925 within 3 min, as seen in Figure 2.14. Figure 2.14 also shows that free calcein was not to be able to displace ADR-925 from Co^{2+}–ADR-925 over the time the assay was conducted.

While the calcein assay was not sensitive to either dexrazoxane, **B**, or **C**, the possibility existed that other dexrazoxane-derived chelating metabolites that the calcein assay might detect were formed. In order to test this possibility an experiment was carried out on a single rat in which a single large blood sample, sufficient to measure the ADR-925 level both by HPLC (as described in Section 2.2.9.4 and shown in Figure 2.5) and by the calcein assay (as described in Section 2.2.11), was taken at 120 min post-

dexrazoxane infusion. The plasma concentration of ADR-925 was measured to be 52 and 49 μM using the HPLC and calcein assays, respectively. The close agreement of these two values indicates that there were no other detectable dexrazoxane-derived Co^{2+} chelating metabolites formed *in vivo*.
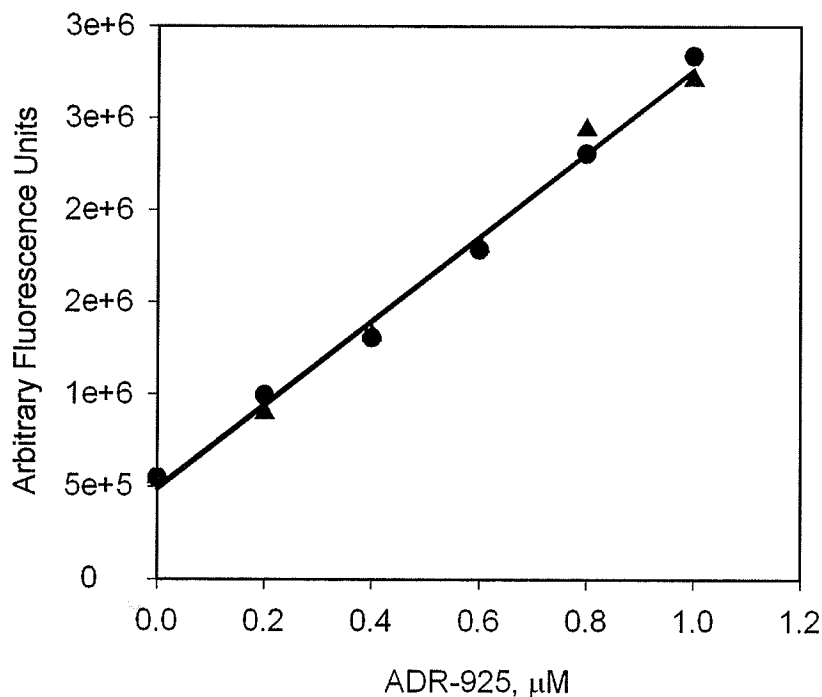
*Figure 2.13 Dexrazoxane, **B**, and **C** do not interfere with ADR-925 quantitation using the fluorescent dye calcein.*

The calcein fluorescence of a mixture of dexrazoxane, **B**, **C**, and ADR-925 (8:3:3:1, mol ratio) was compared to that of ADR-925 to determine whether dexrazoxane, **B**, or **C** interfered with the calcein assay. The standard curve from standards containing dexrazoxane, **B**, **C**, and ADR-925 mixture (●) and ADR-925 alone (▲) were shown not to be statistically different ($p > 0.5$) indicating that **B**, **C**, and dexrazoxane did not interfere with the calcein assay.
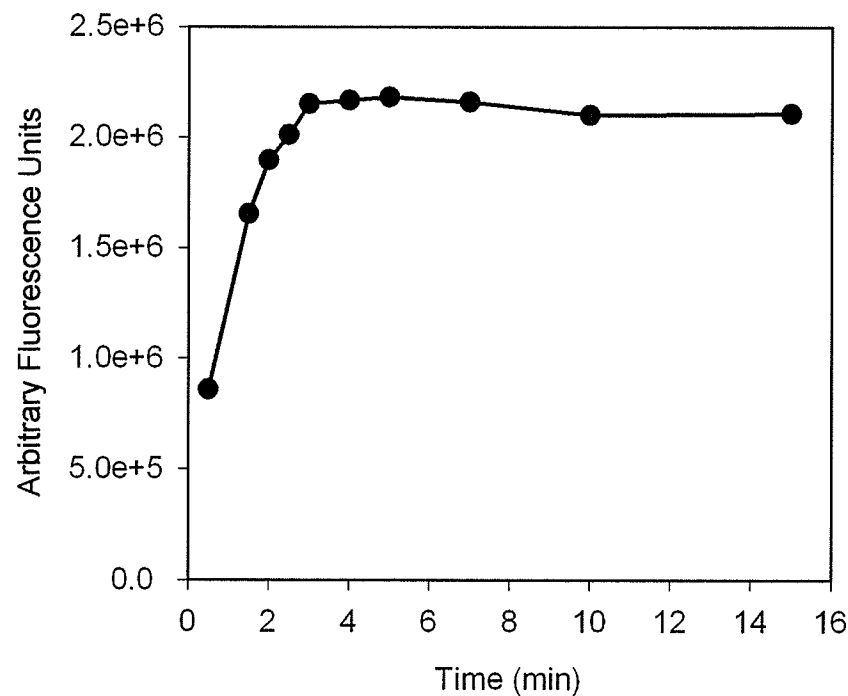
Figure 2.14 Displacement of Mg^{2+} and/or Ca^{2+} from the Mg^{2+}-ADR-925 or Ca^{2+}-ADR-925 complex by Co^{2+}.

The time measurement is the duration that 1 μM Co^{2+} was incubated with 1 μM ADR-925 (pre-incubated with rat plasma for 5 min) prior to calcein addition. ADR-925 content was determined through the calcein assay as described in Section 2.2.11.

66

2.3.4 ADR-925 calibration plots using the fluorescent dye calcein

Calibration plots of integrated peak areas ($n = 6$) in the range 0 to 1.0 µM ADR-925 (as shown in Tables 2.9 - 2.10) were repeated every 3 h during ADR-925 analysis for the calcein assay using the flow injection method (Section 2.2.11.2.1). In the instance where the fluorescence plate reader was used (Section 2.2.11.2.2), a standard curve was prepared for each individual plate containing samples to be analyzed for ADR-925 content. The limit of quantitation of ADR-925 in plasma was estimated to be 1 µM. At ADR-925 concentrations of 1 µM or larger, the observed and predicted fluorescence signal were in strong agreement (95 % or more). However, once ADR-925 concentration decreased to 0.5 µM or less, the agreement between the observed and predicted fluorescence values decreased dramatically. ADR-925 plasma concentrations were all above 5 µM and, thus, all above the limit of quantitation for this assay.

Table 2.8   Flow injection calibration curve of ADR-925 (using the fluorescent dye calcein, λ_{ex} 496 nm and λ_{em} 518 nm) in precipitated rat plasma

Concentration (µM)	Average Peak Area (Arbitrary Units)
0	548036
0.2	899273
0.4	1321833
0.6	1808228
0.8	2339384
1.0	2711249
Slope[a]	2 231 827
Y-intercept	488753
r^2	0.996

[a] Between-day variation in the slopes of the calibration plots was 3 %.

Table 2.9   Fluorescence plate reader calibration curve of ADR-925 (using the fluorescent dye calcein, λ_{ex} 485 nm and λ_{em} 520 nm) in precipitated rat plasma

Concentration (μM)	Average Peak Area (Arbitrary Units)
0	15640
0.2	22953
0.4	30591
0.6	40553
0.8	52070
1.0	57727
Slope[a]	43 964
Y-intercept	14 607
r^2	0.993

[a] Between-day variation in the slopes of the calibration plots was 2 %.
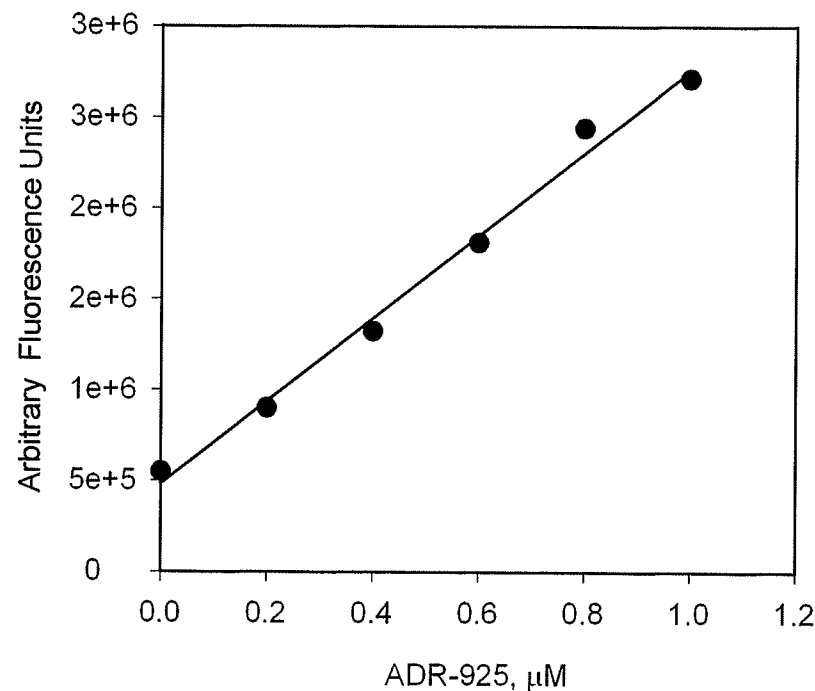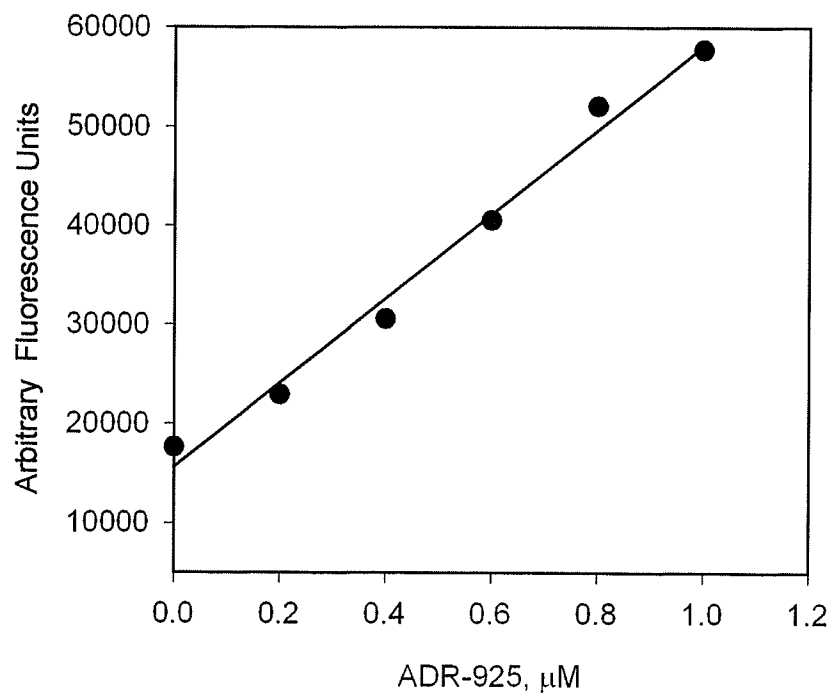
Figure 2.15   Fluorescence plate reader (λ_{ex} 485 nm, λ_{em} 520 nm) ADR-925 calibration curve in rat plasma

Figure 2.16   Fluorescence flow injection (λ_{ex} 496 nm, λ_{em} 518 nm) ADR-925 calibration curve in rat plasma

Calibration plots using the calcein assay on either a Flowstar Galaxy fluorescence plate reader (Figure 2.15) or flow injection (Figure 2.16). Calibration curves were prepared by adding standards containing known amounts of ADR-925 to blank rat plasma as described in section 2.2.11. A mobile phase of 20 μM Na$_2$EDTA (pH 4.5) was used for the flow injection method to chelate potential metal ions.

2.3.5 Metabolism of dexrazoxane to B and C after an i.v. bolus of dexrazoxane

The results shown in Figures 2.17 – 2.28 represent the dexrazoxane and dexrazoxane metabolite concentration-time profile for all 12 rats. The results shown in Figure 2.29 represent the average concentration-time data (shown in Tables 2.10-2.13) for all 12 rats. The results shown in Figure 2.29 for dexrazoxane, B, and C are very close to those previously obtained for rats likewise dosed at 40 mg/kg of dexrazoxane hydrochloride (Hasinoff and Aoyama, 1999a). The intermediates B and C appeared in the plasma very quickly after dexrazoxane administration and then remained almost constant after a rapid decrease over 30 min. It can also be seen from the data in Figure 2.30 that the concentration of B was always larger than that of C (by a nearly constant 4 fold) as previously observed (Hasinoff and Aoyama, 1999a). The peak plasma concentration of dexrazoxane of 529 ± 41 μM shown in Table 2.10 can be compared to that seen in humans of 340 ± 80 μM at a dose of 600 mg/m^2 (Hochster et al., 1992). ADR-925 also appeared in the plasma very quickly, increased with time, and its concentration exceeded B and C at 30 min. ADR-925 plasma levels peaked at about 80 min, and exceeded the concentration of dexrazoxane at that time, and then slowly decreased with time to 180 min. The sum of the plasma concentrations of dexrazoxane and its three metabolites is also plotted in Figure 2.29. The sum decreases rapidly over the first 60 min and then slowly decreases with time.

Table 2.10   Plasma concentrations (µM) of dexrazoxane after male Sprague-Dawley rats were dosed (i.v. bolus) with 40 mg/kg dexrazoxane hydrochloride.

Time (min)	Rat number												Average (µM)	SE (± µM)
	1	2	3	4	5	6	7	8	9	10	11	12		
5	489	646	451	589	391	609							529	41
30	297	96	120	80	178	205							163	33
60	70.0	63.1	50.5	50.3	76.7	80.1	69.4	64.1	49.5	51.3	75.7	81.5	65.2	5.0
80							60.5	55.5	45.5	47.9	62.9	74.6	57.8	4.4
100														
120	52.1	52.4	40.2	43.6	50.2	70.5							51.5	4.3
140							55.3	50.3	41.3				48.9	2.9
165							50.1	49.5	37.5	39.5	50.5	60.5	47.9	3.4
180	56.4	46.1	37.5	40.8	46.5	65.7							48.8	4.3

Table 2.11   Plasma concentrations (µM) of ADR-925 after male Sprague-Dawley rats were dosed (i.v. bolus) with 40 mg/kg dexrazoxane hydrochloride.

Time (min)	Rat number												Average (µM)	SE (± µM)
	1	2	3	4	5	6	7	8	9	10	11	12		
5	5.0	5.0	5.0	5.0	9.0	10.8							6.6	1.1
30	26.9	25.3	19.4	19.6	9.6	18.2							19.8	2.5
60	88.0	47.7	50.6	69.9	22.9	47.3	40.7	38.8	60.4	69.3	30.5	65.3	52.6	7.6
80							100.5	84.5	75.5	60.5	60.5	88.2	78.3	6.5
100							64.9	60.5	90.9	50.5	45.5	75.9	64.7	6.8
120	60.5	80.5	65.5	50.9	57.5	59.7	60.5	45.5	75.5	30.5	15.5	60.5	55.2	7.3
140							50.5		69.5	24.9		50.1	48.8	7.5
165							39.8	33.5	45.5			40.5	39.8	2.0
180	30.3	40.5	36.2		27.9	33.5							29.7	4.3

71

Table 2.12   Plasma concentrations (µM) of **B** after male Sprague-Dawley rats were dosed (i.v. bolus) with 40 mg/kg dexrazoxane hydrochloride.

Time (min)	\- Rat number \-												Average (µM)	SE (± µM)
	1	2	3	4	5	6	7	8	9	10	11	12		
5	31.4	42.3	48.3	37.6	81.9	48.4							48.3	7.2
30	15.9	18.2	13.3	8.6	10.4	13.4							13.3	1.4
60	15.0	16.5	13.5	10.5	12.0	13.9	17.0	15.5	14.5	9.5	13.0	12.9	13.7	0.9
80							14.1	14.8	13.8	8.6	13.6	15.5	13.4	1.0
100														
120	14.6	14.5	14.4	12.0	15.5	13.9							14.2	0.5
140							16.4	14.1	13.1				14.5	0.7
165							14.1	13.9	14.2	14.5	13.0	12.9	13.8	0.3
180	16.3	15.0	16.1	8.3	12.2	10.4							13.0	1.3

Table 2.13   Plasma concentrations (µM) of **C** after male Sprague-Dawley rats were dosed (i.v. bolus) with 40 mg/kg dexrazoxane hydrochloride.

Time (min)	\- Rat number \-												Average (µM)	SE (± µM)
	1	2	3	4	5	6	7	8	9	10	11	12		
5	13.5	20.5	12.5	15.7	12.5	18.9							15.6	1.4
30	3.3	7.5	4.6	3.5	2.5	3.5							4.2	0.7
60	3.0	4.5	3.5	4.0	2.8	3.1	2.0	5.5	2.5	5.0	1.8	4.5	3.5	0.5
80							2.5	3.0	3.0	2.6	2.2	3.0	2.7	0.1
100														
120	2.0	5.0	3.8	3.0	3.7	4.7				3.0	4.0	3.8	3.7	0.4
140							5.0	1.5	1.5				2.7	0.8
165							3.0	2.5	2.0	3.0	2.0	3.9	2.7	0.3
180	2.0	4.0	2.4	5.4	2.1	3.2							3.2	0.5
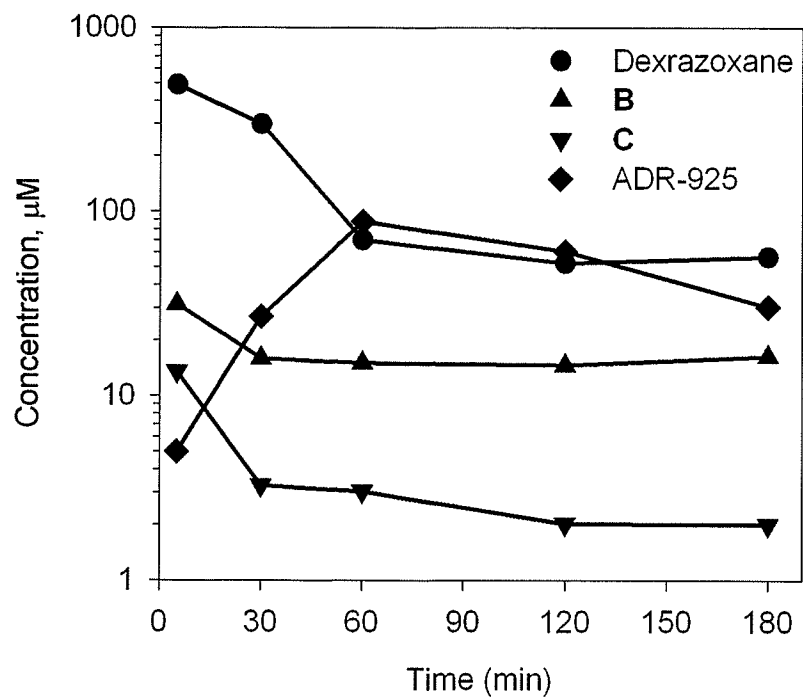
Figure 2.17 Plasma concentrations of dexrazoxane, **B**, **C**, and ADR-925 for rat 1 after an i.v. dose of 40 mg/kg of dexrazoxane hydrochloride.
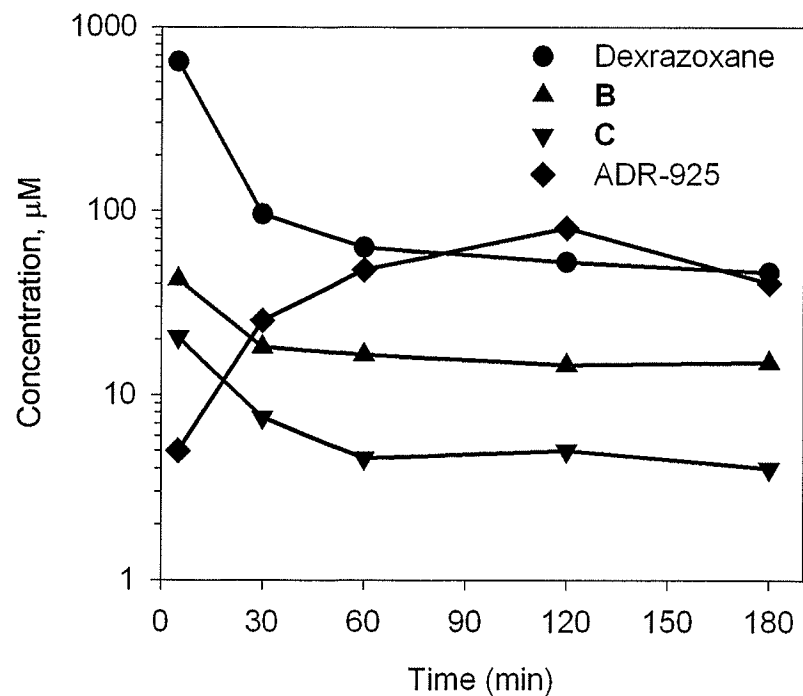
Figure 2.18 Plasma concentrations of dexrazoxane, **B**, **C**, and ADR-925 for rat 2 after an i.v. dose of 40 mg/kg of dexrazoxane hydrochloride.

73
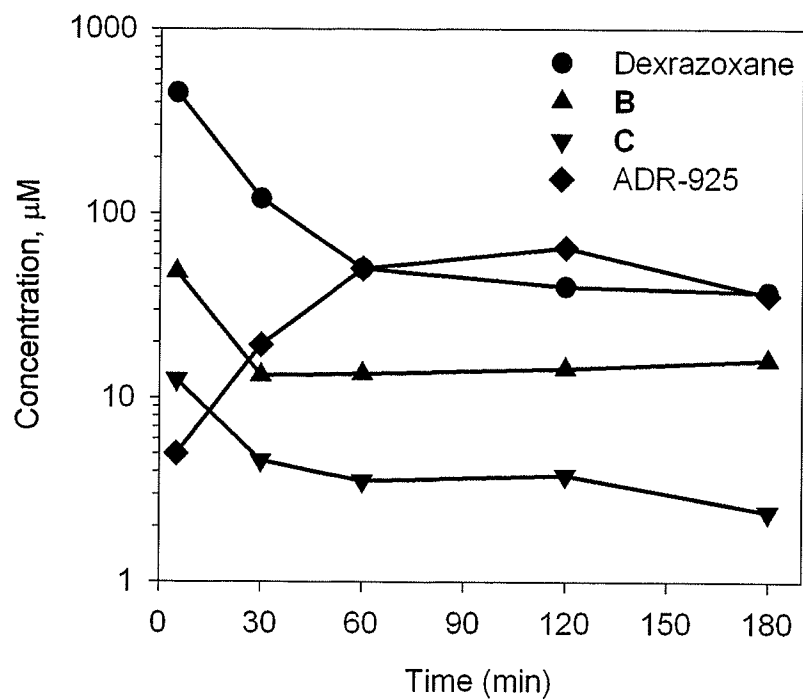
*Figure 2.19 Plasma concentrations of dexrazoxane, **B**, **C**, and ADR-925 for rat 3 after an i.v. dose of 40 mg/kg of dexrazoxane hydrochloride.*
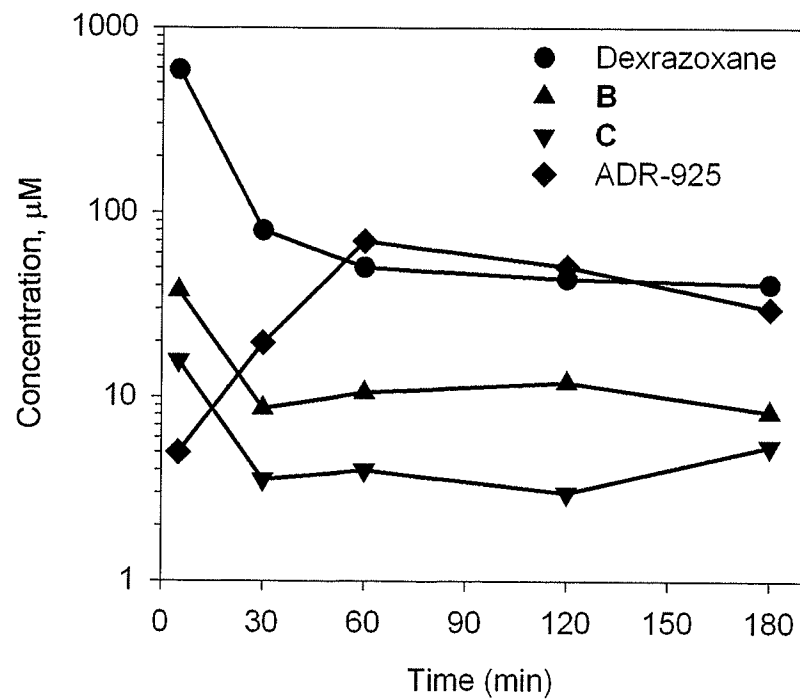
*Figure 2.20 Plasma concentrations of dexrazoxane, **B**, **C**, and ADR-925 for rat 4 after an i.v. dose of 40 mg/kg of dexrazoxane hydrochloride.*
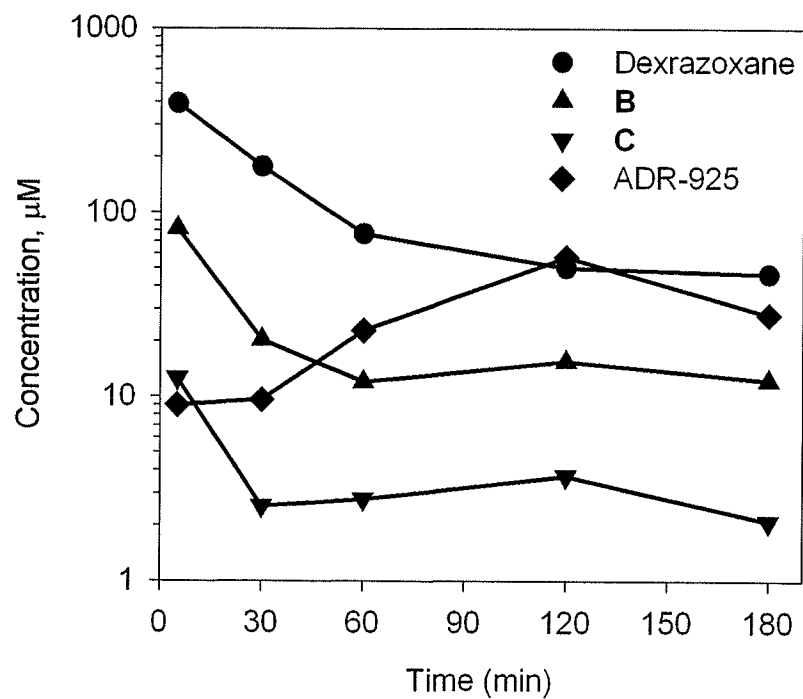
*Figure 2.21 Plasma concentrations of dexrazoxane, **B**, **C**, and ADR-925 for rat 5 after an i.v. dose of 40 mg/kg of dexrazoxane hydrochloride.*
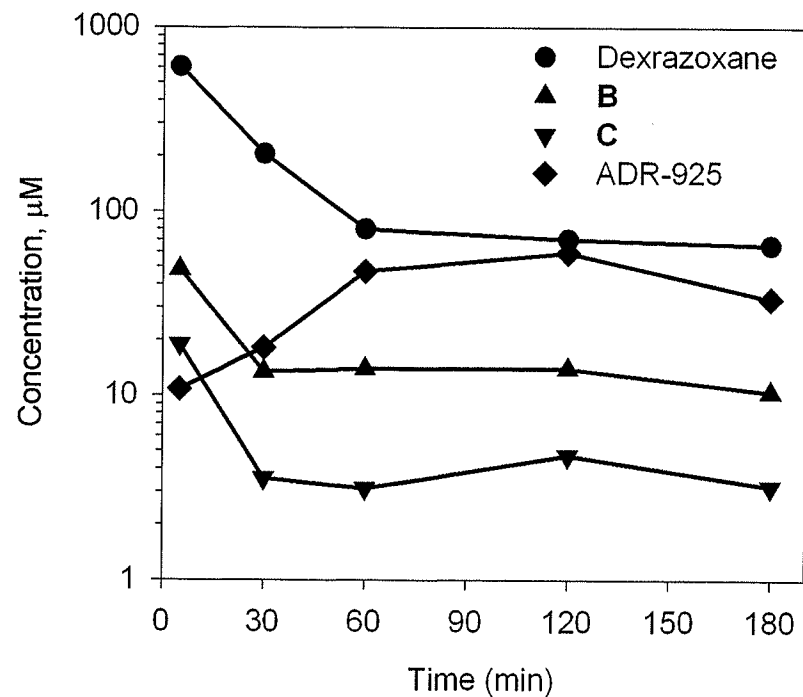
*Figure 2.22 Plasma concentrations of dexrazoxane, **B**, **C**, and ADR-925 for rat 6 after an i.v. dose of 40 mg/kg of dexrazoxane hydrochloride.*
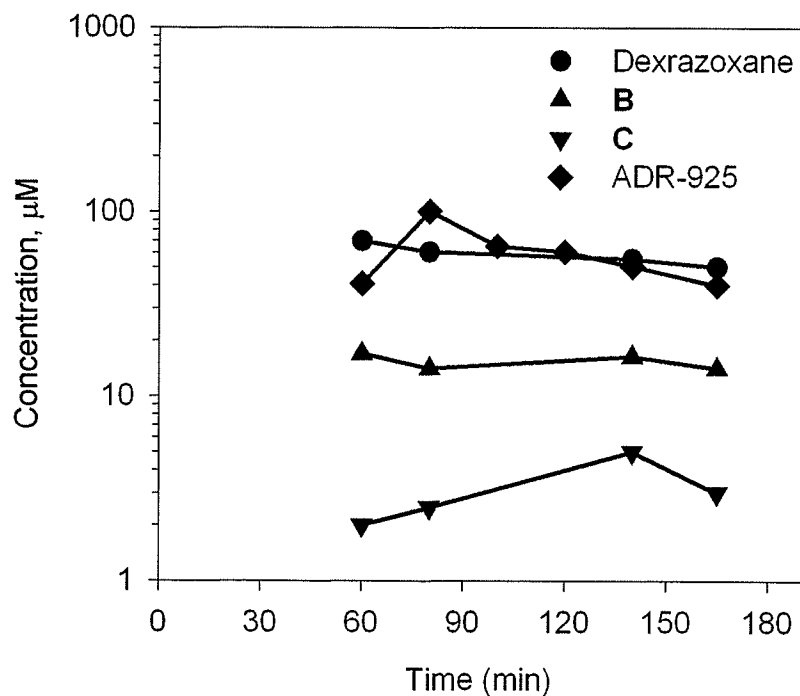
Figure 2.23 Plasma concentrations of dexrazoxane, **B**, **C**, and ADR-925 for rat 7 after an i.v. dose of 40 mg/kg of dexrazoxane hydrochloride.
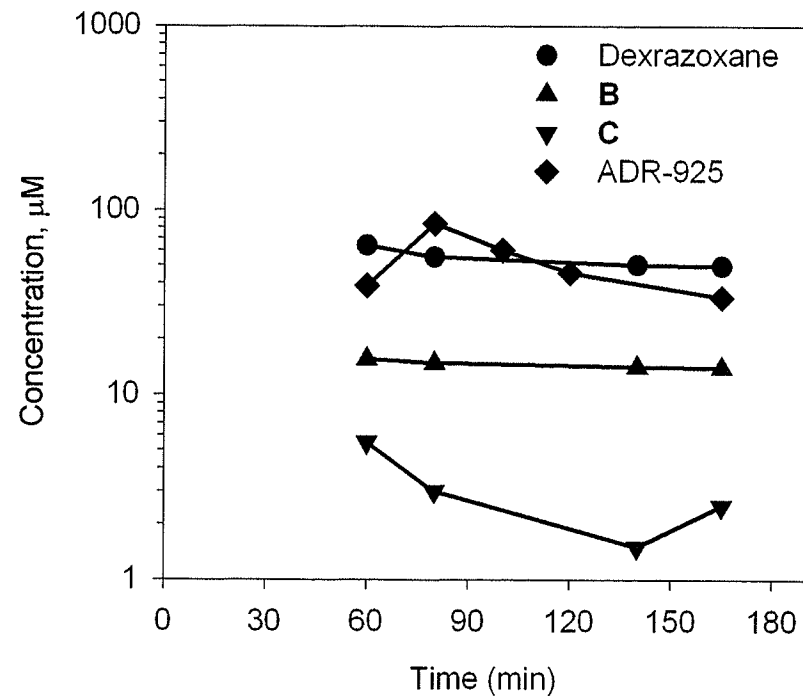
Figure 2.24 Plasma concentrations of dexrazoxane, **B**, **C**, and ADR-925 for rat 8 after an i.v. dose of 40 mg/kg of dexrazoxane hydrochloride.

76
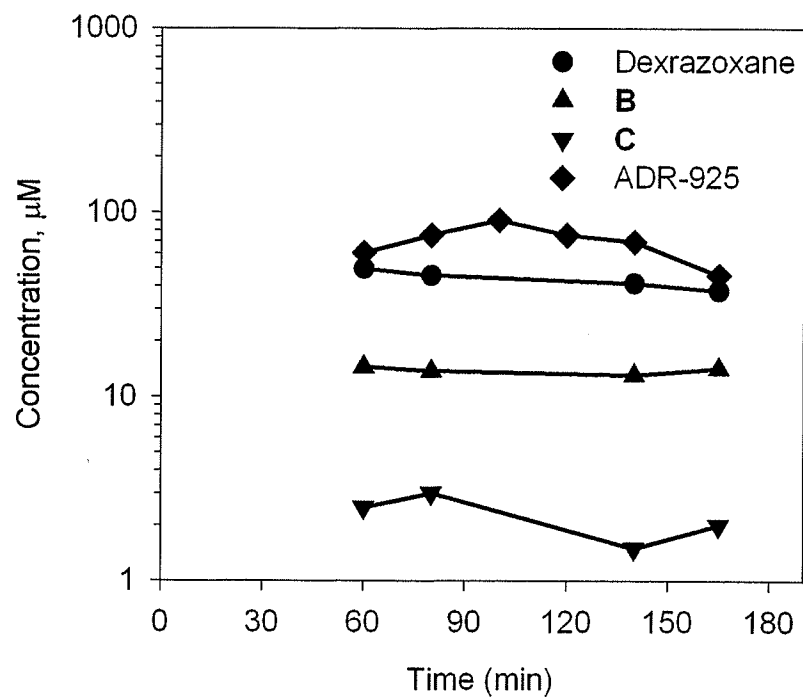
*Figure 2.25 Plasma concentrations of dexrazoxane, **B**, **C**, and ADR-925 for rat 9 after an i.v. dose of 40 mg/kg of dexrazoxane hydrochloride.*
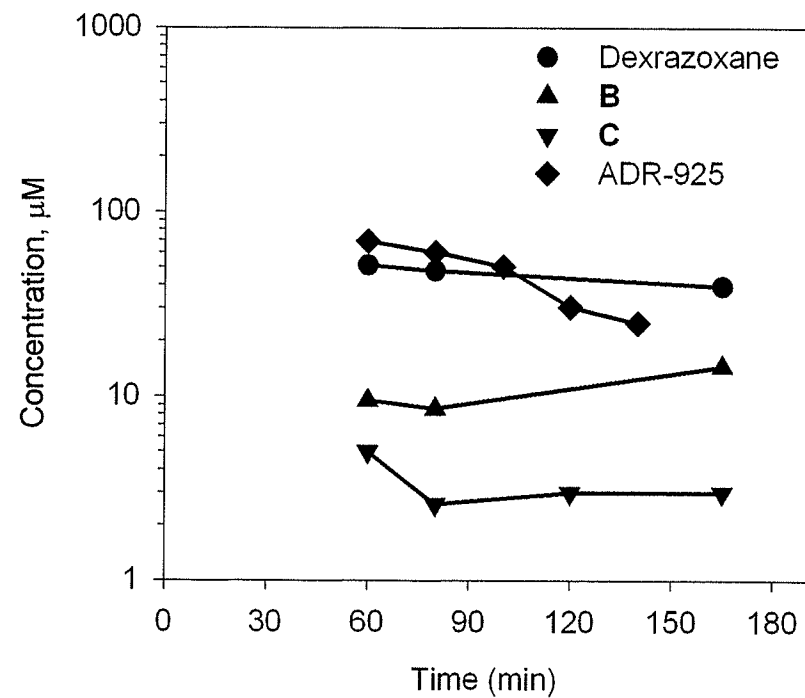
*Figure 2.26 Plasma concentrations of dexrazoxane, **B**, **C**, and ADR-925 for rat 10 after an i.v. dose of 40 mg/kg of dexrazoxane hydrochloride.*
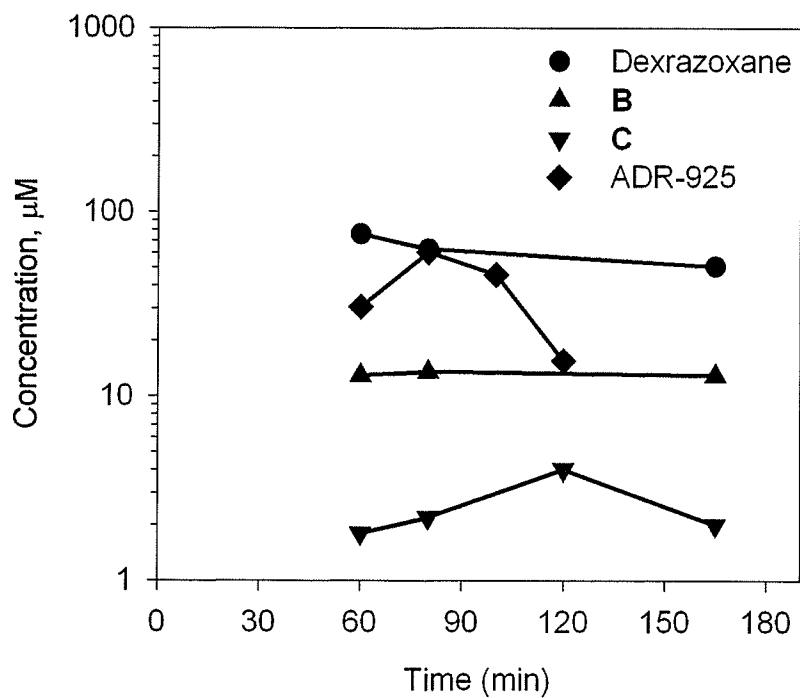
*Figure 2.27 Plasma concentrations of dexrazoxane, **B**, **C**, and ADR-925 for rat 11 after an i.v. dose of 40 mg/kg of dexrazoxane hydrochloride.*
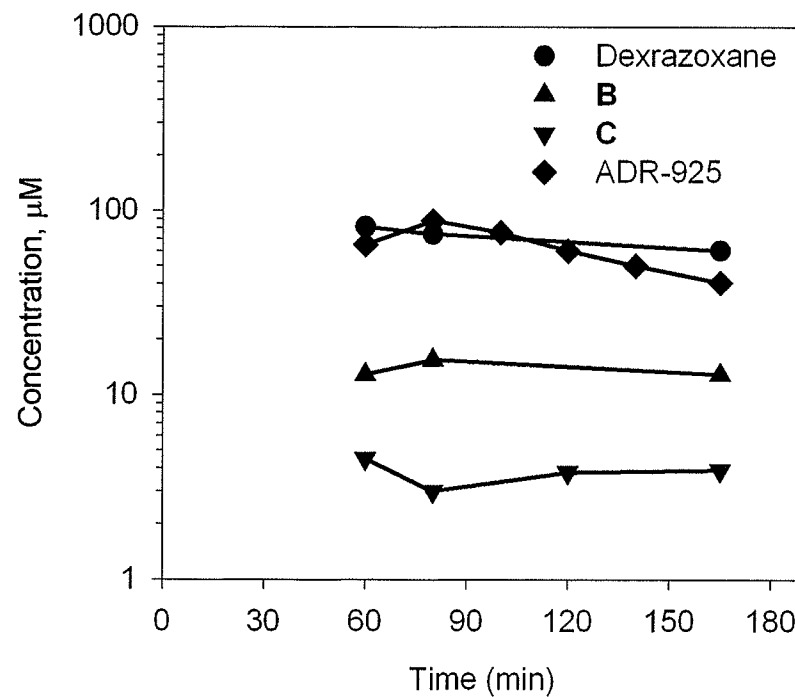
*Figure 2.28 Plasma concentrations of dexrazoxane, **B**, **C**, and ADR-925 for rat 12 after an i.v. dose of 40 mg/kg of dexrazoxane hydrochloride.*
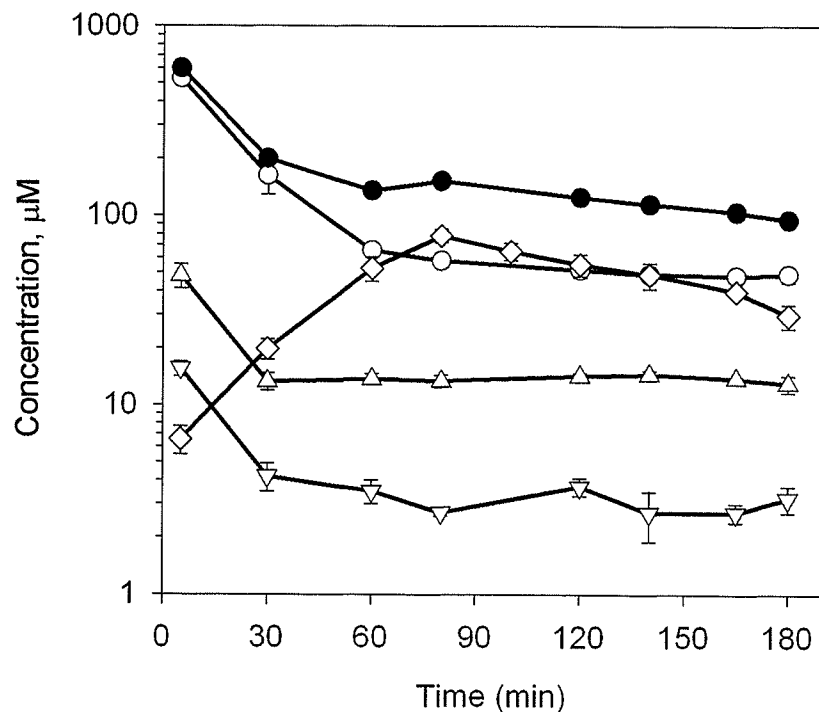
*Figure 2.29   Average rat plasma concentrations of dexrazoxane (○), **B** (△), **C** (▽), ADR-925 (◇), and sum of the concentrations of dexrazoxane, **B**, **C**, and ADR-925 (●) after an i.v. dose of 40 mg/kg of dexrazoxane hydrochloride.*

Error bars represent the SEMs from 6-12 rats per concentration-time point, except for 140 min data which are averaged from 3 rats.
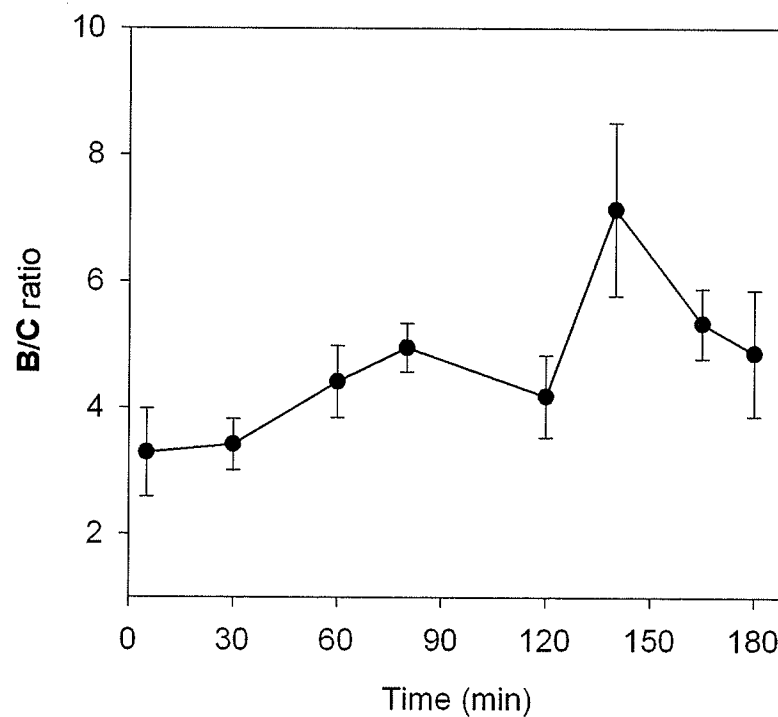
*Figure 2.30 Ratio of the averaged **B**:**C** plasma concentrations as a function of time.*

Error bars represent the SEMs of the ratios from 6-12 rats per concentration time point.

2.3.5.1 ADR-925 levels in tissue homogenate supernatants from rats dosed with 40 mg/kg dexrazoxane hydrochloride

ADR-925 levels in the heart, liver, and brain tissue homogenate supernatants of rats dosed with 40 mg/kg dexrazoxane hydrochloride are shown in Table 2.14. ADR-925 concentrations were approximately two-fold higher in liver homogenates relative to that of the heart, with average ADR-925 tissue concentrations of 0.0971 and 0.0515 μmol/g wet tissue, respectively. Interestingly, no detectable amounts of ADR-925 were found in brain homogenate (< 0.002 μmol/g wet tissue) suggesting that dexrazoxane does not cross the blood brain barrier of the rat in detectable levels. A significant 2-fold increase in the ADR-925 tissue levels was found in the heart ($p < 0.0001$) and liver ($p < 0.002$) after NaOH treatment (as shown in Table 2.14, described in Section 2.2.8), which strongly indicates that ADR-925 comprises approximately half of the total amount of dexrazoxane, **B**, **C**, and ADR-925 found in tissues. Also, no detectable amount of ADR-925 was found in the brain homogenates of rats likewise treated with NaOH, indicating that detectable amounts (< 0.002 μmol/g wet tissue) of dexrazoxane, **B**, or **C**, are not present in the brain after a dexrazoxane hydrochloride bolus.

Table 2.14 Brain, liver, and heart tissue homogenate supernatant concentrations of ADR-925 as determined by the calcein assay. Rat tissues were removed and treated as described in Section 2.2.7 and 2.2.8 at 2 – 3 h post-dexrazoxane infusion.

Rat Number	ADR-925 (μmol/g wet tissue)			Total ADR-925 (NaOH treated) (μmol/g wet tissue)		
	Heart	Liver	Brain	Heart	Liver	Brain
1	0.0281	0.0812	<LOD	0.118	0.344	<LOD
2	0.0405	0.0660	<LOD	0.090	0.186	<LOD
3	0.0384	0.0665	<LOD	0.070	0.167	<LOD
4	0.0650	0.1674	<LOD	0.107	0.215	<LOD
5	0.0728	0.1215	<LOD	0.168	0.251	<LOD
6	0.0507	0.0842	<LOD	0.116	0.246	<LOD
7	0.0651	0.0926	<LOD	0.101	0.232	<LOD
Ave	0.0515	0.0971	--	0.100	0.232	--
SE	0.0063	0.0137	--	0.0074	0.0255	--

2.3.6 Metabolism of B and C to ADR-925 after an i.v. bolus of B/C

2.3.6.1 Pharmacokinetic analysis of B, C, and ADR-925 from rats dosed with an *i.v.* bolus of B/C mixture (20 mg/kg)

The plasma pharmacokinetics for the *i.v.* bolus of a **B/C** mixture was fitted to an *i.v.* bolus one-compartment model (equation 2.1 and 2.2, WinNonlin Model 1) (WinNonlin 4.0, Pharsight, Mountain View, CA). The one-compartment model was used to describe the entire plasma concentration (C) versus time (t) curve fitted by a single exponential term where C_B and C_C refer to the zero-time intercepts and k_b and k_c refer to the elimination rate constants of the concentration-time curve of **B** (equation 2.1) and **C**, (equation 2.2.) respectively.

$$C_t = C_B \cdot e^{-k_b \cdot t}$$ 2.1

$$C_t = C_C \cdot e^{-k_c \cdot t}$$ 2.2

The elimination half life $(t_{\frac{1}{2}k})$ for **B** and **C** is defined by equations 2.3 and 2.4, respectively.

$$t_{\frac{1}{2}kb} = \frac{\ln 2}{k_b} \qquad\qquad 2.3$$

$$t_{\frac{1}{2}kc} = \frac{\ln 2}{k_c} \qquad\qquad 2.4$$

The apparent elimination rate of ADR-925 (k_{ADR}) was also determined by fitting the data

to a two-parameter single-exponential decay function (equation 2.5) where the apparent

elimination half life is estimated by equation 2.6.

$$C_t = C_{ADR} \cdot e^{-k_{ADR} \cdot t} \qquad\qquad 2.5$$

$$t_{\frac{1}{2}kADR} = \frac{\ln 2}{k_{ADR}} \qquad\qquad 2.6$$

The pharmacokinetic parameters for **B** and the apparent pharmacokinetic

parameters for ADR-925 were determined from the concentration-time data for the first

30 min after the **B/C** bolus where the concentration-time profile of **B** and ADR-925 was

linear. The pharmacokinetic parameters for **C** were determined from the concentration-

time data for the first 20 min after the **B/C** bolus as plasma concentrations for **C** were

lower then the limit of quantitation after 20 min.

The results in Tables 2.15 - 17 and in Figures 2.31-2.33 show that when a **B/C**

mixture is given as an i.v. bolus both metabolites are rapidly eliminated with half-lives of

4.9 ± 0.84 and 3.2 ± 0.96 min, respectively, as shown in Table 2.18. The C_0 for **B** and **C**

was determined to be 417 ± 39 and 73.7 ± 12.7, respectively, as shown in Table 2.18.

The peak plasma concentration of ADR-925 of 134 ± 10.3 μM is shown in Figure 2.34.

ADR-925 appeared in the plasma very rapidly and was found to be at a maximum value

at 2 min post **B/C** bolus, the first data collection time point. Unlike the ADR-925

concentration-time profile after a dexrazoxane infusion, when **B/C** was infused the ADR-925 levels rapidly decrease with an apparent half life of elimination of 8.5 ± 1.2 min (shown in Table 2.18). The sum of the plasma concentrations of **B**, **C**, and ADR-925 metabolites is also plotted in Figure 2.34. The sum decreases rapidly over the first 30 min and then slowly decreases with time.

Table 2.15 Plasma concentrations of **B** after dosing (i.v. bolus) male Sprague-Dawley rats with 20 mg/kg of a **B/C** mixture.

Time	Rat number			Average	SE
(min)	1	2	3	(μM)	($\pm \mu$M)
2	249.5	306.3	390.0	315.3	41.6
10	55.2	120.6	108.3	94.7	20.4
20	13.6	38.3	56.8	36.2	12.7
30	4.0	1.4	19.8	8.4	5.9
45	1.2	<LOD	7.0	4.1	--
60	<LOD	<LOD	6.6	6.6	--
90	<LOD	<LOD	2.3	2.3	--

Table 2.16   Plasma concentrations of **C** after dosing (i.v. bolus) male Sprague-Dawley rats with 20 mg/kg of a **B/C** mixture.

Time	Rat number			Average	SE
(min)	1	2	3	(μM)	($\pm \mu$M)
2	35.6	62.8	45.5	48.0	8.1
10	5.6	6.1	11.9	7.9	2.1
20	3.6	1.4	4.3	2.1	1.1
30	2.3	<LOD	2.3	--	--
45	2.6	<LOD	2.0	--	--
60	<LOD	<LOD	<LOD	--	--
90	<LOD	<LOD	<LOD	--	--

Table 2.17   Plasma concentrations of ADR-925, as determined by the calcein fluorescence assay, after dosing (i.v. bolus) male Sprague-Dawley rats with 20 mg/kg of a **B/C** mixture.

Time (min)	Rat number			Average (μM)	SE (± μM)
	1	2	3		
2	140	89.2	114.0	114	14.8
10	54.4	62.3	59.1	58.6	2.3
20	17.6	36.6	25.4	26.5	5.6
30	1.8	21.3	12.9	12.0	5.8
45	7.1	10.0	4.0	7.0	1.8
60	4.3	3.8	3.4	3.8	0.2
90	4.3	5.6	6.8	5.6	0.7

Table 2.18   Pharmacokinetic parameters for the elimination of **B** and **C** and apparent elimination of ADR-925 in the rat following a **B/C** bolus (20 mg/kg)

Rat number	**B**			**C**			ADR-925		
	n	k_b (min^{-1})	C_B (μM)	n	k_c (min^{-1})	C_C (μM)	n	k_{ADR} (min^{-1})	C_{ADR} (μM)
1	4	0.18	360	3	0.22	54.3	4	0.12	177
2	4	0.12	389	3	0.29	111	4	0.050	99.5
3	4	0.14	512	3	0.16	62.4	4	0.082	134
Mean[a]	--	0.15	420	--	0.22	75.9	--	0.084	137
SE	--	0.019	47	--	0.038	18	--	0.020	22.8
Ave[b]	4	0.14	417	3	0.22	73.7	4	0.082	134
SE	--	0.024	39	--	0.065	12.7	--	0.011	10.3

n, is the number of plasma concentration-time points for each rat used to obtain the pharmacokinetic parameters.

[a] Average pharmacokinetic parameters for the individual concentration-time data of **B**, **C**, and ADR-925 for the first 30 min from rats 1-3 where errors are expressed as standard errors.

[b] Pharmacokinetic parameters for the individual concentration-time data of rats 1-3 over the first 30 min where standard errors were obtained from modeling data to equation 2.1, 2.2, and 2.5.
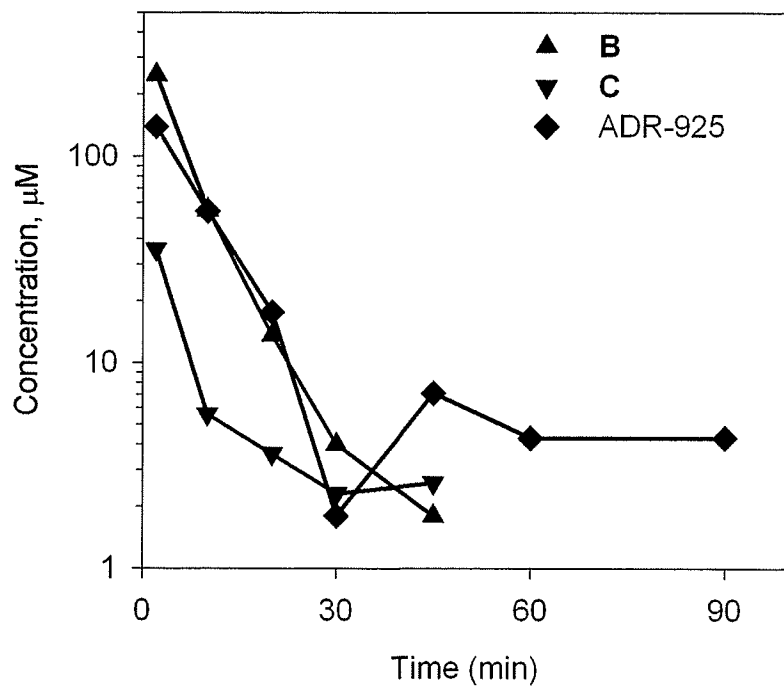
Figure 2.31 Plasma concentrations of B, C, and ADR-925 for rat 1 after a 20 mg/kg dose (i.v. bolus) of a B/C mixture.
After 45 min, **B** and **C** concentration-time data were below the limit of quantitation (LOQ).
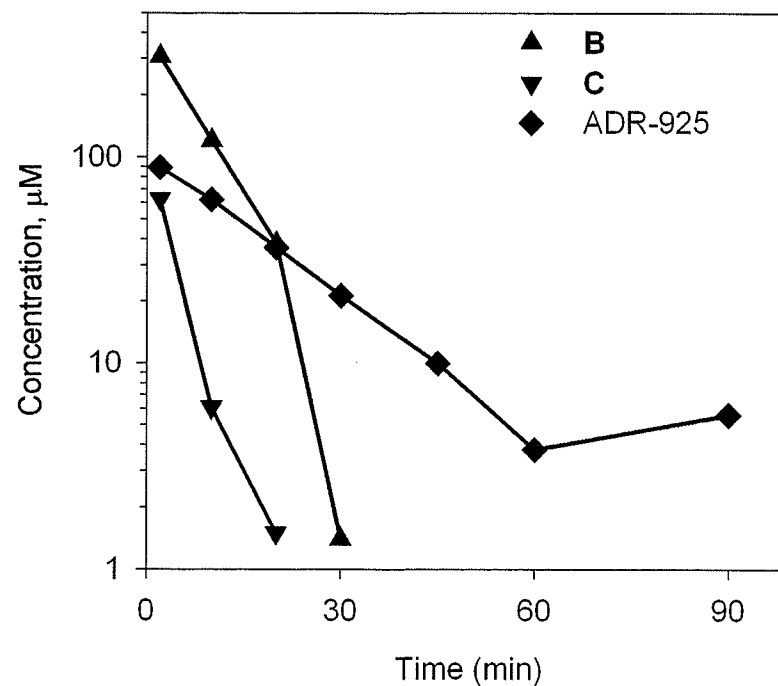
Figure 2.32 Plasma concentrations of B, C, and ADR-925 for rat 2 after a 20 mg/kg dose (i.v .bolus) of a B/C mixture.
After 30 min for **B** and 20 min for **C** concentration-time data were below the limit of quantitation (LOQ).
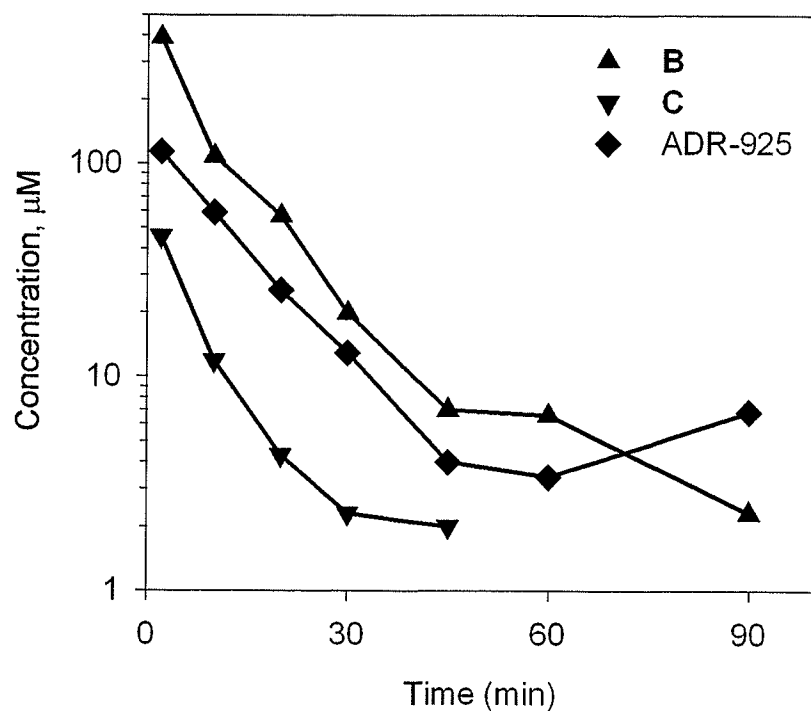
Figure 2.33 Plasma concentrations of B, C, and ADR-925 for rat 3 after a 20 mg/kg dose (i.v. bolus) of a B/C mixture.
After 45 min **C** concentration-time data was below the limit of quantitation (LOQ).
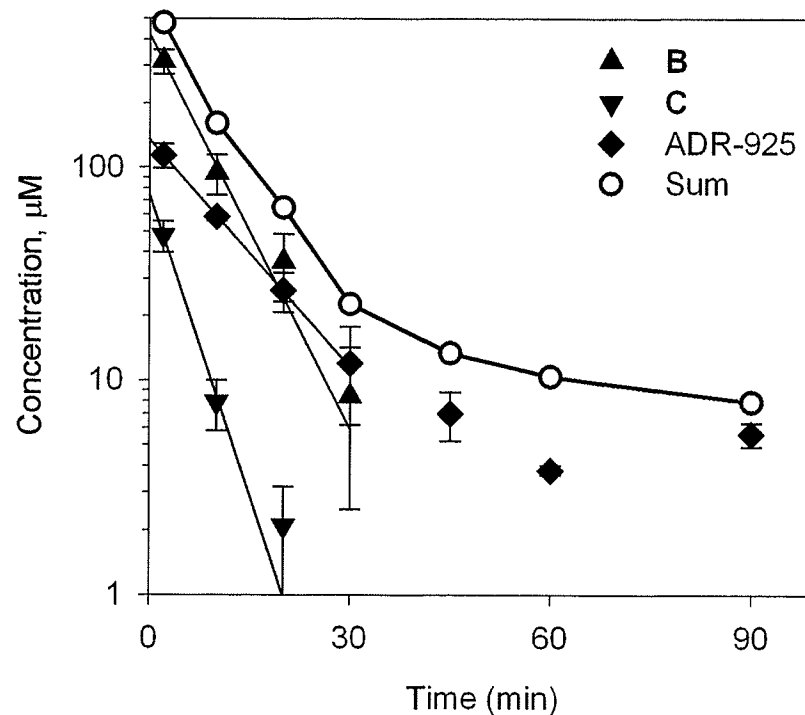
Figure 2.34 Average plasma concentrations of B, C, and ADR-925 and the sum of the concentrations of dexrazoxane, B, C, and ADR-925 after a 20 mg/kg dose (i.v .bolus) of a B/C mixture.
Error bars represent the relative S.E. from **B**, **C**, and ADR-925 concentration-time determinations of 3 rats. The smooth line through **B**, **C**, and ADR-925 concentration-time data was calculated from eqn. 2.1.

86

2.3.6.2 Description of the ADR-925 concentration-time curve following a 20 mg/kg B/C bolus.

A linear two-compartment model, where the parent compounds (**B** and **C**) are eliminated solely by metabolism to ADR-925 through a first-order process, was used to describe ADR-925 plasma levels following a 20 mg/kg bolus of the **B/C** mixture. Because of the rapid appearance of ADR-925, this model assumes **B** and **C** are eliminated exclusively through metabolism, where the formation of ADR-925 is dependent on both **B** and **C** and where C_t is the concentration of ADR-925 as a function of time. Thus, k_{fb} is defined as the formation rate constant of **B** to ADR-925 and k_{fc} is defined as the formation rate constant of **C** to ADR-925. It is assumed that because the ADR-925 formed is highly polar it is, subsequently, completely eliminated via a first-order process with a rate constant k_{mu} (Jackson et al., 2004). These assumptions for the initial first order formation of ADR-925 can be described for the first 30 min by equation 2.7 (Jackson et al., 2004). Where C_B is the zero time intercept of **B** (defined from

$$C_t = \frac{k_{fb} \cdot C_B \, (e^{-k_{mu}t} - e^{-k_{fb}t})}{(k_{fb}-k_{mu})} + \frac{k_{fc} \cdot C_C \, (e^{-k_{mu}t} - e^{-k_{fc}t})}{(k_{fc}-k_{mu})} \qquad 2.7$$

equation 2.8, data from the first 30 min) and C_C is the zero time intercept of **C** (defined from equation 2.9, data from the first 20 min).

$$C_t = C_B \cdot e^{-k_{fb} \cdot t} \qquad 2.8$$

$$C_t = C_C \cdot e^{-k_{fc} \cdot t} \qquad 2.9$$

The primary parameters; k_{fb}, k_{fc}, k_{mu}, C_B, and C_C, were derived through modeling the whole concentration data set (as shown in Tables 2.15-2.17) to all three functions

87

simultaneously (equations 2.7, 2.8, and 2.9 with a 1/yhat weighting, where 1/yhat is the reciprocal of the predicted or fitted value) in WinNonlin using the model described in Table 2.19.

Table 2.19   WinNonlin model for describing the concentration-time curve of ADR-925 after a 20 mg/kg B/C mixture bolus in the rat.

```
MODEL
remark    ******************************************************
remark    Developer:
remark    Model Date:       11-18-2004
remark    Model Version:    1.0
remark    ******************************************************
remark
remark - define model-specific commands
COMMANDS
NFUNCTIONS 3
NPARAMETERS 5
PNAMES   'Cb', 'Cc', 'kfb', 'kfc', 'kmu'
END
remark - define temporary variables
TEMPORARY
t=x
END
remark - define algebraic functions
FUNCTION 1
t=x
F=Cb*exp(-kfb*t)
END
FUNCTION 2
t=x
F=Cc*exp(-kfc*t)
END
FUNCTION 3
t=x
F=((kfb*Cb)/((kfb-kmu)))*(((exp(-kmu*t))-(exp(-kfb*t))))+((kfc*Cc/((kfc-
kmu)))*(((exp(-kmu*t))-(exp(-kfc*t)))))
END
remark - define any secondary parameters
remark - end of model
EOM
```

Equation 2.7 describes the formation of ADR-925 as being dependent on both **B** (with formation rate constants k_{fb} and zero-point intercept C_B) and **C** (with formation rate constants k_{fc} and zero-point intercept C_C). Therefore the elimination rate constants, k_b and k_c from equations 2.1 and 2.2, respectively, are assumed to be equal to the formation rate constants (k_{fb} and k_{fc}) for **B** and **C**, respectively. From Table 2.18, the elimination

half life of **B** and **C** determined (using equation 2.1 and 2.2) to be 4.9 ± 0.84 and 3.2 ±

0.96 min, respectively, is in good agreement with the formation rate constants of **B** and **C**

(as defined by equation 2.7) of 5.2 ± 0.42 and 3.4 ± 0.88 min, respectively as shown in

Table 2.20. Due to the polar nature of ADR-925, the model also assumes complete

elimination via a first-order process with a rate half life k_{mu} (determined to be 2.2 ± 0.3

min, as shown in Table 2.20) which is an estimate of the rate of total elimination and is

not equivalent to the apparent elimination of ADR-925, k_{ADR}, as described by equation

2.5. The elimination of ADR-925 over the first 30 min is essentially parallel to that of

the **B** and **C**, indicating that the appearance of ADR-925 is formation rate limited. The

smooth lines in Figure 2.35 show the predicted values of the concentration-time curve of

B, **C**, ADR-925 following a **B/C** mixture bolus when data are modeled to equations 2.7,

2.8, and 2.9 using the model shown in Table 2.19.

Table 2.20   Pharmacokinetic parameters for the formation of ADR-925 following a **B/C**
bolus (20 mg/kg)

	B			**C**			ADR-925	
	n	k_{fb} (min^{-1})	C_B (μM)	n	k_{fc} (min^{-1})	C_C (μM)	n	k_{mu} (min^{-1})
Ave[a]	3	0.13	442	2	0.20	75.7	3	0.32
SE	--	0.012	40.1	--	0.051	21.7	--	0.044

n, is the number of plasma concentration-time points for each rat used to obtain the
pharmacokinetic parameters.
[a] Pharmacokinetic parameters for the individual concentration-time data of 3 rats where
standard errors were obtained from modeling data to equation 2.7, 2.8, and 2.9 over the
first 30 min.
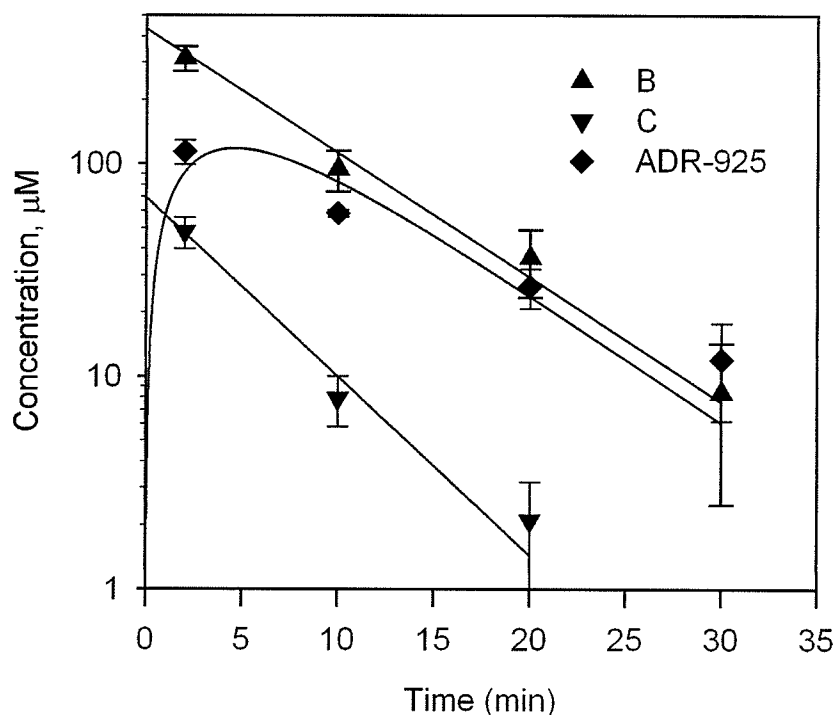
Figure 2.35   Metabolite pharmacokinetic modeling of ADR-925 to equation 2.7 in rats dosed with 20 mg/kg of a B/C mixture for the first 30 min.

The smooth lines were calculated from eqn. 2.7, 2.8, and 2.9. The best fit to this data yielded C_B 442 µM, k_{fb} 0.132 min⁻¹, C_C 75.7 µM, k_{fc} 0.206 min⁻¹, and k_{mu} 0.312 min⁻¹.

2.3.6.3 Determination of ADR-925 levels in tissues from rats dosed with 20 mg/kg B/C mixture

ADR-925 levels in the heart, liver, and brain tissue homogenates of rats dosed with 20 mg/kg B/C are shown in Table 2.21. As in the case when rats were dosed with dexrazoxane, ADR-925 concentrations found in the liver were greater then those found in the heart for rats dosed with B/C. ADR-925 was not detected in brain homogenate (< 0.002 µmol/g wet tissue, where the LOD is 0.002 µmol/g wet tissue) suggesting that neither B nor C crosses the blood brain barrier of the rat at detectable levels.

90

Table 2.21   Brain, liver, and heart tissue homogenate supernatant concentrations of ADR-925 as determined by the calcein assay. Rat tissues were removed and treated as described in Section 2.2.7 at 90 min post-**B/C** infusion.

Rat Number	ADR-925 (μmol/g wet tissue)		
	Heart	Liver	Brain
1	0.03459	0.05533	<LOD
2	0.02411	0.03929	<LOD
3	0.02365	0.02396	<LOD
Average	0.02745	0.03953	--
SE	0.00618	0.01569	--

2.3.7 Distribution of ADR-925 after a 20 mg/kg ADR-925 bolus

2.3.7.1 Pharmacokinetic analysis ADR-925 from rats dosed with an i.v. bolus of ADR-925 (20 mg/kg)

The plasma distribution and elimination curve for ADR-925 plasma levels after a 20 mg/kg ADR-925 i.v. bolus was fitted to an i.v. bolus two-compartment model (equation 2.10) (WinNonlin 4.0, Model 7). The two-compartment model was used to describe the entire plasma ADR-925 concentration (C) versus time (t) curve fitted by the sum of two exponential terms where A and B refer to the corresponding zero-time intercepts (equation 2.10). The first term describes the disposition of ADR-925 (where α is the disposition rate constant) while the second term describes dexrazoxane

$$C_t = A \cdot e^{-\alpha t} + B \cdot e^{-\beta t} \qquad\qquad 2.10$$

elimination (where β describes the terminal phase rate constant). Once the alpha and beta rate constants are determined, the secondary pharmacokinetic parameters; alpha half life ($t_{\frac{1}{2}\alpha}$, equation 2.11), beta half life ($t_{\frac{1}{2}\beta}$, equation 2.12), maximum concentration (C_0, equation 2.13), elimination rate constant (k_{10}, equation 2.14), and elimination half life ($t_{1/2k10}$, equation 2.15) can be determined.

$$t_{\frac{1}{2}\alpha} = \frac{\ln 2}{\alpha} \qquad\qquad 2.11$$

$$t_{\frac{1}{2}\beta} = \frac{\ln 2}{\beta} \qquad\qquad 2.12$$

$$C_0 = A + B \qquad\qquad 2.13$$

$$k_{10} = \frac{\alpha \cdot \beta (A+B)}{A \cdot \beta + B \cdot \alpha} \qquad\qquad 2.14$$

$$t_{\frac{1}{2}k10} = \frac{\ln 2}{k_{10}} \qquad\qquad 2.15$$

The results shown in Figure 2.38 and Table 2.23 show that ADR-925 is rapidly distributed with a alpha half life of 3.3 ± 0.1 min with a relatively slow terminal phase with a beta half life of 26.2 ± 1.5 min. The elimination half-life of ADR-925 was determined to be 7.2 ± 1.4 min (as described by equation 2.15).

Table 2.22   Plasma concentrations of ADR-925, as determined by the calcein fluorescence assay, after dosing (i.v. bolus) male Sprague-Dawley rats with 20 mg/kg of ADR-925.

Time (min)	Rat number			Average (µM)	SE (± µM)
	1	2	3		
2	357	361	467	395	62.4
10	92.2	184	114	130	47.9
20	62.3	61.2	68.0	63.8	3.6
30	34.9	38.7	55.9	43.2	11.2
45	24.5	27.5	29.9	27.3	2.7
60	11.6	22.9	24.0	19.5	6.9
90	<LOD	11.0	9.3	10.1	1.2 [a]

[a] error calculated as average deviation

Table 2.23 Two-compartment pharmacokinetic parameters for the distribution and elimination of ADR-925 in the rat following an ADR-925 bolus (20 mg/kg)

Rat number	ADR-925				
	n	k_{10} (min^{-1})	C_0 (μM)	α (min^{-1})	β (min^{-1})
1	6	0.26	1210	0.77	0.041
2	7	0.042	440	0.10	0.0032
3	7	0.13	820	0.34	0.028
Mean[a]	--	0.14	820	0.40	0.024
SE	--	0.064	226	0.20	0.011
Ave[b]	--	0.096	557	0.21	0.026
SE	--	0.0019	4.8	0.0064	0.0015

n, is the number of plasma concentration-time points for each rat used to obtain the pharmacokinetic parameters.

[a] Average pharmacokinetic parameters for the individual concentration-time data of ADR-925 from rats 1-3 where errors are expressed as standard errors.

[b] Pharmacokinetic parameters for the individual concentration-time data of 3 rats where standard errors were obtained from modeling data to equation 2.15.
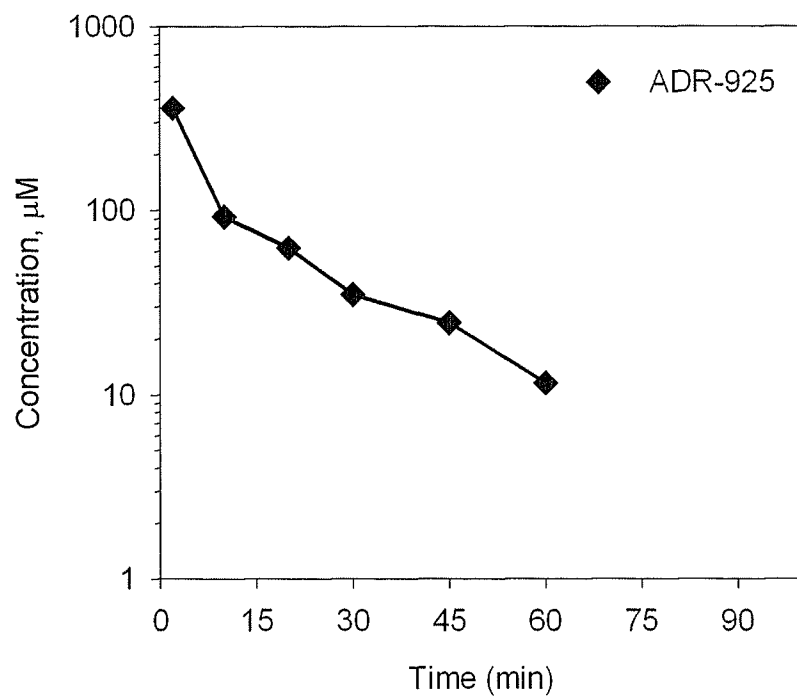
Figure 2.36 Plasma concentrations of the distribution of ADR-925 for rat 1 after an ADR-925 i.v. dose of 20 mg/kg.
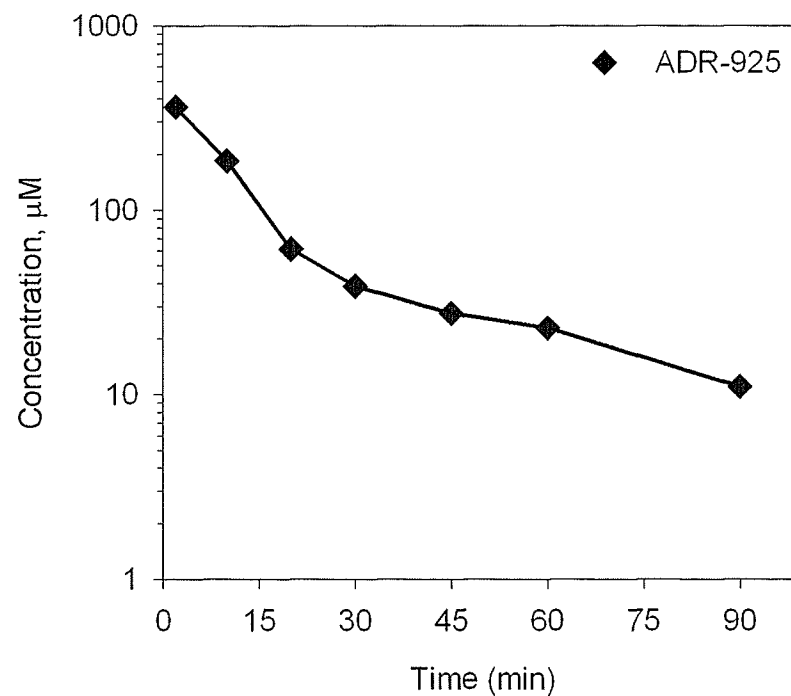
Figure 2.37 Plasma concentrations of the distribution of ADR-925 for rat 2 after an ADR-925 i.v. dose of 20 mg/kg.
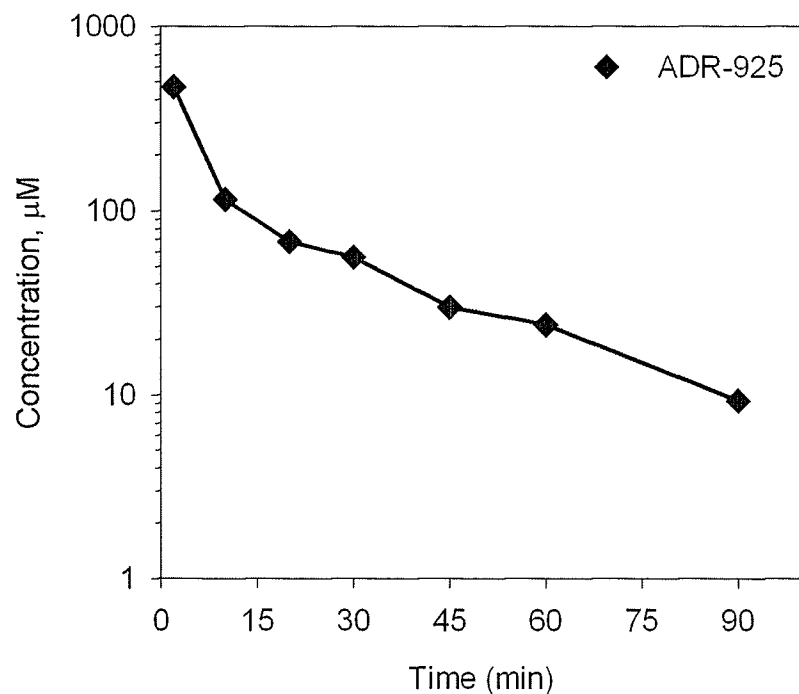
Figure 2.38 Plasma concentrations of the distribution of ADR-925 for rat 3 after an ADR-925 i.v. dose of 20 mg/kg.
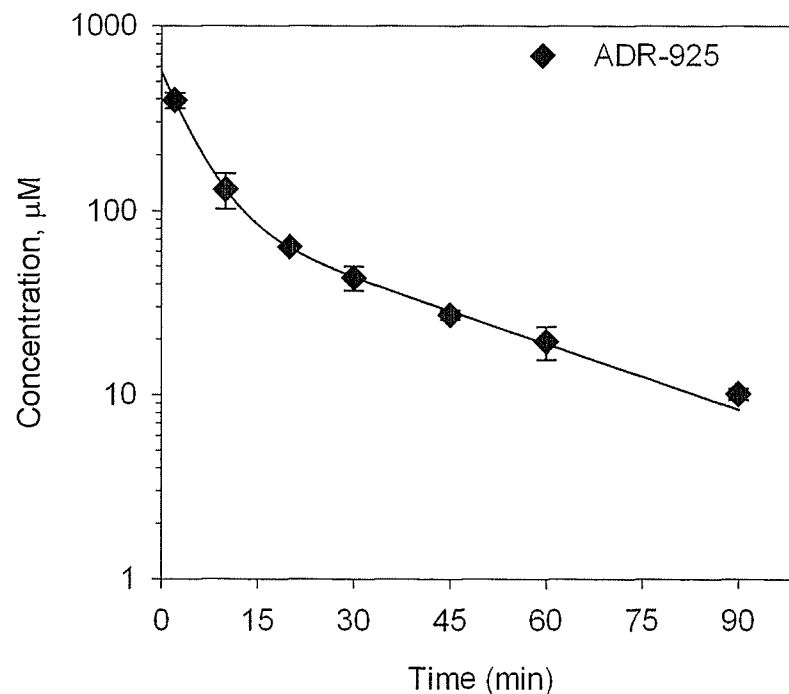
Figure 2.39 Average plasma concentrations of ADR-925 after dosing the rats with 20 mg/kg ADR-925.

Error bars represent the relative S.E. from ADR-925 concentration-time determinations of 3 rats (with the exception of the 90 min time point which is an average of 2 rats). The smooth line was calculated from eqn. 2.10. The best fit to this data yielded $t_{1/2\alpha}$ 3.3 min, $t_{1/2\beta}$ 25.4 min, and C_0 559 µM. Error bars on data points present the SEs.

95

2.3.7.2 ADR-925 accumulation in tissues from rats dosed with 20 mg/kg ADR-925

ADR-925 levels in the heart, liver, and brain tissue homogenates of rats dosed with 20 mg/kg ADR-925 are shown in Table 2.24. As when the rat was given dexrazoxane and **B/C** infusions, ADR-925 levels were highest in liver tissue (0.011 ± 0.0007 μmol/g wet tissue) and greater than that of the heart (0.0074 ± 0.0016 μmol/g wet tissue). ADR-925 was not detected in brain homogenate (< 0.002 μmol/g wet tissue, where the LOD is 0.002 μmol/g wet tissue) suggesting that ADR-925 does not cross blood brain barrier of the rat at detectable levels.

Table 2.24   Brain, liver, and heart tissue homogenate supernatant concentrations of ADR-925 as determined by the calcein assay. Rat tissues were removed and treated as described in Section 2.2.7 at 90 min post-ADR-925 infusion.

Rat Number	ADR-925 (μmol/g wet tissue)		
	Heart	Liver	Brain
1	0.00891	0.00985	<LOD
2	0.00852	0.01118	<LOD
3	0.00630	0.01078	<LOD
Average	0.00741	0.01061	--
SE	0.00157	0.00068	--

2.3.8 Determination of ADR-925 bound to transition metals in rat plasma

Experiments were done to determine the relative amount of free ADR-925 in plasma as the calcein assay measures only free ADR-925. In preliminary experiments it was shown that stirring Chelex with preformed Fe^{3+}–ADR-925 at pH 5.5 resulted in complete displacement of Fe^{3+} from its complex with ADR-925 within 20 min. The amount of free ADR-925 in plasma samples collected from a rat at 5, 60, and 180 min where found to be 5.0, 88, and 30 μM, respectively. After a 20 min Chelex treatment,

ADR-925 levels were found to be 6.1, 84, and 32 µM, for the 5, 60, and 180 min sample time points, respectively. This indicates that there is not a measurable increase in ADR-925 levels after Chelex treatment which further suggests that the relative amount of transition metal ion-complexed ADR-925 in plasma was very small.

2.4 Discussion

2.4.1 Metabolism of dexrazoxane, B, C, and the distribution of ADR-925

The presence of ADR-925 *in vivo*, the presumably active metabolite of dexrazoxane, has not been measured before. The rapid appearance of ADR-925 in plasma suggests that either **B** or **C**, or both, were rapidly metabolized to ADR-925. The relative slow elimination in plasma levels of ADR-925 after 80 min suggests that this metabolite was in a steady state. ADR-925, when given as an i.v. bolus as shown in Figure 2.38, has a rapid disposition and elimination (alpha and beta half lives of 3.3 and 26.2 min, respectively, as shown in Table 2.23). Also, when metabolites **B/C** are given as a mixture, as shown in Figure 2.34, their disposition is also very rapid with apparent elimination half lives of 4.9 ± 0.31 and 3.1 ± 0.26 min, respectively (as shown in Table 2.18). Thus, the slow elimination of ADR-925 after a dexrazoxane bolus (Figure 2.29) is a good indication that, throughout the 3 h duration of this study, both metabolites **B** and **C** as well as ADR-925 are being continually produced, eliminated, and in the case of dexrazoxane, **B**, and **C**, metabolized. This could occur through distribution and excretion and possibly even further metabolism of ADR-925. The relatively small changes in either **B** or **C** after 30 min indicate that the one-ring open intermediates were also produced in a

manner close to that expected for a dynamic steady-state due to their rapid metabolism and excretion.

A study (Sadee et al., 1975) utilizing ^{14}C-razoxane at 120 mg/kg i.v. in the rat found that intact razoxane (Figure 1.3) accounted for 46% of the total radioactivity at 2 h in the plasma which suggested that a rapid metabolism of razoxane had occurred. For comparison the results of Figure 2.29 show that dexrazoxane accounted for 41% of the total of the concentrations of dexrazoxane and its three metabolites. The good agreement between these two values strongly suggests that all of the major circulating metabolites of dexrazoxane have been accounted for. The elimination of **B/C** (as described by equation 2.1 and 2.2) is very rapid with elimination half lives of 4.9 ± 0.84 and 3.2 ± 0.96 min (Table 2.18), for **B** and **C** respectively. The rapid appearance of ADR-925 in plasma suggests that **B**, **C**, or both, were rapidly metabolized to ADR-925. The **B/C** mixture (prepared as described in Section 2.2.4) was synthesized at a 4:1 ratio for **B** and **C**, respectively. The initial plasma concentrations, estimated by equations 2.1 and 2.2, were determined to be a 5.5:1 ratio (417 ± 39 and 73.7 ± 12.7, respectively, as shown in Table 2.18). Considering the rapid elimination half life of **B** and **C**, this initial plasma concentration estimate is in fair agreement with the starting dose ratio.

Unlike the ADR-925 plasma levels of the dexrazoxane study (Figure 2.29) the **B/C** study has maximum ADR-925 levels occurring immediately following the **B/C** bolus. Interestingly, ADR-925 is also very rapidly eliminated with an apparent elimination half life of 8.5 ± 1.2 min (Table 2.18) differing from the slow apparent elimination of ADR-925 after a dexrazoxane bolus (Figure 2.29). The relatively rapid elimination in plasma levels of ADR-925 suggests that **B** and **C** are being rapidly

metabolized, either in the blood or in tissue, and releasing ADR-925 which, in turn, is rapidly eliminated. The ADR-925 found in plasma is probably a combination of tissue enzyme and blood mediated hydrolysis of **B** and **C**. The rate of ADR-925 formation was determined by assuming that **B** and **C** were eliminated exclusively through metabolism, and is mathematically described using equation 2.7. Using this model, it was also determined that the appearance of ADR-925 in plasma was formation dependant where all ADR-925 is eliminated through the kidneys.

The concentration-time profile of ADR-925 following a **B/C** mixture bolus is formation dependent, thus the apparent elimination of ADR-925 (as determined by equation 2.5) is not a good estimate of the elimination of ADR-925 by the kidney. As seen when rats are given a bolus of ADR-925 (Figure 2.38), the alpha phase is very rapid with a $t_{1/2}$ of 3.3 ± 0.1 min (as shown in Table 2.23). After a **B/C** mixture bolus, modeling the ADR-925 concentration-time data of the first 30 min to equation 2.7 yields an elimination (defined as k_{mu}) half life of 2.2 ± 0.3 min. The agreement between these two values indicates that equation 2.7 is a reasonable model to estimate the elimination of ADR-925 following a **B/C** mixture bolus. Thus, the relatively slow decrease in ADR-925 plasma levels in rats dosed with dexrazoxane alone strongly suggests that the ADR-925 plasma levels in rats dosed with dexrazoxane is the result of the continuous and rapid metabolism of dexrazoxane to **B** and **C** which are further metabolized to ADR-925.

2.4.2 Detection of ADR-925 in tissue homogenate supernatants of rats dosed with dexrazoxane, B/C mixture, or ADR-925

ADR-925 levels in the heart, liver, and brain tissue homogenates of rats dosed with dexrazoxane, a **B/C** mixture, and ADR-925 are shown in Tables 2.14, 2.21, and

2.24. In all dosing cases, ADR-925 was not found in rat brain homogenate at detectable levels (< 0.002 μmol/g wet tissue). Although this is an interesting result, it is consistent with the hydrophilic nature of dexrazoxane that has been previously thought not to cross the blood brain barrier, an assumption that has been paramount to a variety of preclinical and clinical work (and also a key hypothesis for work described in Chapter 4). Thus, considering the hydrophilic (log P_{oct} −1.8 (Hasinoff et al., 1995)) nature of dexrazoxane and the very preliminary observation that ADR-925 does not collect in brain tissue, an argument can be made that dexrazoxane does not (in detectable quantities) cross the blood brain barrier.

The dexrazoxane, **B/C** mixture, and ADR-925 bolus infusions resulted in ADR-925 levels being highest in the liver homogenate supernatant. It has been previously determined that dexrazoxane underwent an enzymatic ring-opening hydrolysis by the 105,000 g soluble supernatant fraction of porcine liver homogenates (Hasinoff et al., 1991) and in adult rat primary hepatocytes (Hasinoff et al., 1994). However, the same study found that there was no significant hydrolysis of dexrazoxane in the supernatant fraction of the heart. In animals dosed with dexrazoxane and the **B/C** mixture, there are detectable levels of ADR-925 in the heart homogenate supernatant leading to the conclusion that **B** and **C** are very likely permeable to heart tissue. Also, there is likely an enzyme present in the heart which hydrolyses **B** and/or **C** to ADR-925 considering the relatively substantial levels of ADR-925 in the heart. ADR-925 heart tissue levels obtained with the **B/C** mixture infusion are approximately half of those obtained after an i.v. bolus of dexrazoxane which is consistent with the rapid elimination of **B** and **C** (4.9

and 3.1 min, respectively) and rapid apparent elimination of ADR-925 (8.5 min), following the **B/C** mixture bolus.

2.4.3 Iron chelation by ADR-925, the active form of dexrazoxane

ADR-925, the rings-opened hydrolysis product of dexrazoxane and analog of EDTA, is a strong chelator of Fe^{2+} (K_f $10^{10.0}$ M^{-1}) (Huang et al., 1982) and of Fe^{3+} (K_f $10^{18.2}$ M^{-1}) (Diop et al., 2000). It has been previously shown that ADR-925 is able to quickly ($t_{1/2}$ 1.7 min) and efficiently remove Fe^{3+} from its complex with doxorubicin (Hasinoff, 1989a; Buss and Hasinoff, 1993; Hasinoff, 1998; Hasinoff et al., 1998) and, thus, prevent iron-based doxorubicin mediated free radical oxidative stress on the heart muscle (Gianni et al., 1985; Malisza and Hasinoff, 1995; Myers, 1998). The free iron or non-transferrin-bound iron concentration is very low (< 0.4 μM) in human plasma (Durken et al., 2000). The ADR-925 plasma levels measured, even 5 min post-dexrazoxane infusion, greatly exceeded this value and thus, these results which showed that no detectable fraction of ADR-925 was complexed to iron is consistent with this result. This result also indicates that if ADR-925 complexes iron in tissues it is not being measurably transported to the plasma.

2.4.4 Enzymatic contribution of dexrazoxane and B/C hydrolysis to ADR-925

DHPase, which is present in the liver and the kidney, has been shown to efficiently hydrolyze dexrazoxane (Hasinoff et al., 1991; Hasinoff, 1993; Hasinoff, 1994c; Hasinoff et al., 1994; Hasinoff and Aoyama, 1999b) and is likely the enzyme that is primarily responsible for the metabolism of dexrazoxane to **B** and **C**. DHPase is unable to convert the one-ring open intermediates **B** and **C** into ADR-925 (Hasinoff et al.,

1991). Thus, the rapid appearance of ADR-925 in the plasma (Figure 2.29) suggests that there is another unknown enzyme that metabolically converts **B** and **C** into ADR-925.

Dexrazoxane undergoes a slow base-catalyzed hydrolysis (Figure 2.1) to **B** and **C** ($t_{1/2}$ of 9.3 h) and then to ADR-925 ($t_{1/2}$ of 23 h) under physiological conditions (37 °C and pH 7.4) (Hasinoff, 1994b; Hasinoff, 1994a). Given the slow rate of the *in vitro* hydrolysis of dexrazoxane under physiological conditions, little of the **B**, **C**, or ADR-925 seen *in vivo* could have been formed from base-catalyzed hydrolysis (Hasinoff, 1994b; Hasinoff, 1994a), and therefore must have resulted from rapid metabolism. Previous animal studies have shown that the timing of dexrazoxane dosing is critical for it to exert it protective effects (Herman et al., 1983; Herman and Ferrans, 1993). Maximal protective effects were seen when dexrazoxane was given between 3 h before and 3 h after daunorubicin treatment of Syrian golden hamsters (Herman et al., 1983). Likewise, doxorubicin-induced cardiomyopathy was greater in beagle dogs receiving dexrazoxane simultaneously than those that received dexrazoxane 2 h after doxorubicin (Herman and Ferrans, 1993). These results were the basis for the recommendation that in a clinical setting after completing the infusion of dexrazoxane and prior to a total elapsed time of 30 min (from the beginning of the dexrazoxane infusion), the intravenous injection of doxorubicin should be given. The results of this study that shows that ADR-925 rapidly appeared in the plasma after dexrazoxane administration now provides a pharmacodynamic basis for this dosing schedule.

This study does not directly address how dexrazoxane exerts its cardioprotective effects in the heart. While rat primary hepatocytes (Hasinoff, 1994c) and supernatants of liver and kidney homogenates did hydrolyze dexrazoxane, that of heart did not (Hasinoff

et al., 1991). Dexrazoxane is, however, permeable to cells (Dawson, 1975). Thus, it follows that even if dexrazoxane is not metabolized in the heart, the metabolites are probably cell permeable enough and present at high enough concentrations to chelate free iron in the heart and prevent the formation of the Fe^{3+}–doxorubicin complex. One enzyme that may be responsible for the conversion of **B** and **C** into ADR-925 in the heart is dihydroorotase (DHOase, EC 3.5.2.3). The continuation of this study, to identify the Michaelis-Menten enzyme kinetics of DHOase-mediated hydrolysis of **B** and **C**, is fully described in Chapter 4.

2.5 References

Buss JL and Hasinoff BB (1993) The one-ring open hydrolysis product intermediates of the cardioprotective agent ICRF-187 (dexrazoxane) displace iron from iron-anthracycline complexes. *Agents Actions* **40**:86-95.

Buss JL and Hasinoff BB (1997) Metal ion-promoted hydrolysis of the antioxidant cardioprotective agent dexrazoxane (ICRF-187) and its one-ring open hydrolysis products to its metal-chelating active form. *J Inorg Biochem* **68**:101-108.

Dawson KM (1975) Studies on the stability and cellular distribution of dioxopiperazines in cultured BHK-21S cells. *Biochem Pharmacol* **24**:2249-2253.

Diop NK, Vitellaro LK, Arnold P, Shang M and Marusak RA (2000) Iron complexes of the cardioprotective agent dexrazoxane (ICRF-187) and its desmethyl derivative, ICRF-154: solid state structure, solution thermodynamics, and DNA cleavage activity. *J Inorg Biochem* **78**:209-216.

Durken M, Herrnring C, Finckh B, Nagel S, Nielsen P, Fischer R, Berger HM, Moison RM, Pichlmeier U, Kohlschutter B, Zander AR and Kohlschutter A (2000) Impaired plasma antioxidative defense and increased nontransferrin-bound iron during high-dose chemotherapy and radiochemotherapy preceding bone marrow transplantation. *Free Radic Biol Med* **28**:887-894.

Gianni L, Zweier JL, Levy A and Myers CE (1985) Characterization of the cycle of iron-mediated electron transfer from Adriamycin to molecular oxygen. *J Biol Chem* **260**:6820-6826.

Hasinoff BB (1989a) The interaction of the cardioprotective agent ICRF-187 (+)-1,2-bis(3,5-dioxopiperazinyl-1-yL)propane); its hydrolysis product (ICRF-198); and other chelating agents with the Fe(III) and Cu(II) complexes of adriamycin. *Agents Actions* **26**:378-385.

Hasinoff BB (1989b) Self-reduction of the iron(III)-doxorubicin complex. *Free Radic Biol Med* **7**:583-593.

Hasinoff BB (1990a) The hydrolysis activation of the doxorubicin cardioprotective agent ICRF-187 (+)-1,2-bis(3,5-dioxopiperazinyl-1-yl)propane). *Drug Metab Dispos* **18**:344-349.

Hasinoff BB (1990b) Oxyradical production results from the Fe3(+)-doxorubicin complex undergoing self-reduction by its alpha-ketol group. *Biochem Cell Biol* **68**:1331-1336.

Hasinoff BB (1993) Enzymatic ring-opening reactions of the chiral cardioprotective agent (+) (S)-ICRF-187 and its (-) (R)-enantiomer ICRF-186 by dihydropyrimidine amidohydrolase. *Drug Metab Dispos* **21**:883-888.

Hasinoff BB (1994a) An HPLC and spectrophotometric study of the hydrolysis of ICRF-187 (dexrazoxane, (+)-1,2-bis(3,5-dioxopiperazinyl-1yl)propane and its one-ring opened intermediates. *Int. J. Pharm.* **107**:67-76.

Hasinoff BB (1994b) Pharmacodynamics of the hydrolysis-activation of the cardioprotective agent (+)-1,2-bis(3,5-dioxopiperazinyl-1-yl)propane. *J Pharm Sci* **83**:64-67.

Hasinoff BB (1994c) Stereoselective hydrolysis of ICRF-187 (dexrazoxane) and ICRF-186 by dihydropyrimidine amidohydrolase. *Chirality* **6**:213-215.

Hasinoff BB (1998) Chemistry of dexrazoxane and analogues. *Semin Oncol* **25**:3-9.

Hasinoff BB and Aoyama RG (1999a) Relative plasma levels of the cardioprotective drug dexrazoxane and its two active ring-opened metabolites in the rat. *Drug Metab Dispos* **27**:265-268.

Hasinoff BB and Aoyama RG (1999b) Stereoselective metabolism of dexrazoxane (ICRF-187) and levrazoxane (ICRF-186). *Chirality* **11**:286-290.

Hasinoff BB, Hellmann K, Herman EH and Ferrans VJ (1998) Chemical, biological and clinical aspects of dexrazoxane and other bisdioxopiperazines. *Curr Med Chem* **5**:1-28.

Hasinoff BB, Kuschak TI, Yalowich JC and Creighton AM (1995) A QSAR study comparing the cytotoxicity and DNA topoisomerase II inhibitory effects of bisdioxopiperazine analogs of ICRF-187 (dexrazoxane). *Biochem Pharmacol* **50**:953-958.

Hasinoff BB, Reinders FX and Clark V (1991) The enzymatic hydrolysis-activation of the adriamycin cardioprotective agent (+)-1,2-bis(3,5-dioxopiperazinyl-1-yl)propane. *Drug Metab Dispos* **19**:74-80.

Hasinoff BB, Venkataram S, Singh M and Kuschak TI (1994) Metabolism of the cardioprotective agents dexrazoxane (ICRF-187) and levrazoxane (ICRF-186) by the isolated hepatocyte. *Xenobiotica* **24**:977-987.

Herman EH, El-Hage AN, Ferrans VJ and Witiak DT (1983) Reduction by ICRF-187 of acute daunorubicin toxicity in Syrian golden hamsters. *Res Commun Chem Pathol Pharmacol* **40**:217-231.

Herman EH and Ferrans VJ (1993) Timing of treatment with ICRF-187 and its effect on chronic doxorubicin cardiotoxicity. *Cancer Chemother Pharmacol* **32**:445-449.

Herman EH and Ferrans VJ (1998) Preclinical animal models of cardiac protection from anthracycline-induced cardiotoxicity. *Semin Oncol* **25**:15-21.

Hochster H, Liebes L, Wadler S, Oratz R, Wernz JC, Meyers M, Green M, Blum RH and Speyer JL (1992) Pharmacokinetics of the cardioprotector ADR-529 (ICRF-187) in escalating doses combined with fixed-dose doxorubicin. *J Natl Cancer Inst* **84**:1725-1730.

Huang ZX, May PM, Quinlan KM, Williams DR and Creighton AM (1982) Metal binding by pharmaceuticals. Part 2. Interactions of Ca(II), Cu(II), Fe(II), Mg(II), Mn(II) and Zn(II) with the intracellular hydrolysis products of the antitumour agent ICRF 159 and its inactive homologue ICRF 192. *Agents Actions* **12**:536-542.

Jackson AJ, Robbie G and Marroum P (2004) Metabolites and bioequivalence: past and present. *Clin Pharmacokinet* **43**:655-672.

Kendall DA and MacDonald RC (1983) Characterization of a fluorescence assay to monitor changes in the aqueous volume of lipid vesicles. *Anal Biochem* **134**:26-33.

Malisza KL and Hasinoff BB (1995) Production of hydroxyl radical by iron(III)-anthraquinone complexes through self-reduction and through reductive activation by the xanthine oxidase/hypoxanthine system. *Arch Biochem Biophys* **321**:51-60.

Myers C (1998) The role of iron in doxorubicin-induced cardiomyopathy. *Semin Oncol* **25**:10-14.

Sadee W, Staroscik J, Finn C and Cohen J (1975) Determination of (plus or minus)-1, 2-bis(3, 5-dioxopiperazinyl) propane plasma levels in rats, rabbits, and humans by GLC and mass fragmentography. *J Pharm Sci* **64**:998-1001.

Schroeder PE and Hasinoff BB (2002) The doxorubicin-cardioprotective drug dexrazoxane undergoes metabolism in the rat to its metal ion-chelating form ADR-925. *Cancer Chemother Pharmacol* **50**:509-513.

Swain SM, Whaley FS, Gerber MC, Ewer MS, Bianchine JR and Gams RA (1997a) Delayed administration of dexrazoxane provides cardioprotection for patients with advanced breast cancer treated with doxorubicin-containing therapy. *J Clin Oncol* **15**:1333-1340.

Swain SM, Whaley FS, Gerber MC, Weisberg S, York M, Spicer D, Jones SE, Wadler S, Desai A, Vogel C, Speyer J, Mittelman A, Reddy S, Pendergrass K, Velez-Garcia

E, Ewer MS, Bianchine JR and Gams RA (1997b) Cardioprotection with dexrazoxane for doxorubicin-containing therapy in advanced breast cancer. *J Clin Oncol* **15**:1318-1332.

Zweier JL, Gianni L, Muindi J and Myers CE (1986) Differences in O2 reduction by the iron complexes of adriamycin and daunomycin: the importance of the sidechain hydroxyl group. *Biochim Biophys Acta* **884**:326-336.

Chapter 3: The metabolism of dexrazoxane used as a rescue agent in cancer patients treated with high-dose etoposide

3.1 Introduction

The *Laboratory of Experimental Medical Oncology*, in Copenhagen, Denmark, initiated a phase I/II clinical trial in order establish whether dexrazoxane can increase the maximum tolerable dose of etoposide in patients with brain metastases from primary small cell lung cancer. Preclinical studies have shown that dexrazoxane can antagonize etoposide and daunorubicin DNA strand breaks and cytotoxicity (Sehested et al., 1993; Jensen and Sehested, 1997) and doxorubicin cytotoxicity (Hasinoff et al., 1996). Dexrazoxane-mediated antagonism of etoposide has been found to extend to an *in vivo* mouse model where dexrazoxane in combination with etoposide allowed for a 3.6-fold dose escalation (Holm et al., 1996). Furthermore, mice inoculated with L1210 or EHR2 cells into the central nervous system (CNS) and treated with dexrazoxane and etoposide had a significant increase in life span relative to mice treated with an equitoxic dose of etoposide alone (Holm et al., 1998).

These preclinical findings led to the hypothesis that dexrazoxane can be used in combination with etoposide in a clinical setting to protect against etoposide-mediated systemic toxicity and ultimately allow for significant escalations of etoposide dose. It is proposed that the hydrophilic dexrazoxane (*log P_{oct}* of −1.8, (Hasinoff et al., 1995)) does not cross the blood-brain barrier, in contrast to the lipophilic etoposide. Thus, dexrazoxane-mediated antagonism of etoposide would be systemic and not extend to the CNS, which could possibly allow for significant escalations in etoposide dose. The

Laboratory of Experimental Medical Oncology evaluated this concept in an early phase I/II study where patients with brain metastases from primary small cell lung cancer provided the patient population for the study. The objectives of this study were; to establish the maximum tolerable dose of etoposide in combination with dexrazoxane, to evaluate the toxicity and tolerability of the drug combination, and to determine the response rate of the patient population.

There has been no published report concerning the pharmacokinetics of dexrazoxane metabolites other than the report on the metabolism of the conversion of dexrazoxane to **B** and **C** (Hasinoff and Aoyama, 1999) and the conversion of **B** and **C** to ADR-925 (Figure 1.4) (Schroeder and Hasinoff, 2002) in the rat. Thus, it was decided to measure the blood plasma levels of dexrazoxane, and dexrazoxane metabolites in this patient population in order to obtain a greater understanding of the metabolism and the mechanism of the protective effects of dexrazoxane. Plasma samples have also been analyzed for etoposide. The pharmacokinetics of etoposide and dexrazoxane (parent drug only) have been studied in detail; however, this study also examined whether the pharmacokinetics of etoposide and dexrazoxane differed significantly when the two drugs were co-administered. This work has been accepted for publication (Schroeder et al., 2003a; Schroeder et al., 2003b).

3.2 Materials and Methods

3.2.1 Materials

Dexrazoxane hydrochloride (Cardioxane®) for the clinical studies was obtained from Chiron (Amsterdam, The Netherlands) as a lyophilized powder in 500 mg vials. It

was reconstituted in 25 ml sterile water, and then mixed with isotonic glucose to a total volume of 250 ml. Etoposide was obtained from Bristol-Myers Squibb (Vepesid®, New York, NY) as a ready-to-administer liquid solution (100 mg etoposide in 5 ml). Dexrazoxane hydrochloride and ADR-925 used in the HPLC assays were gifts from Adria Laboratories (Columbus, OH). Calcein ("high purity") was from Molecular Probes (Eugene, OR). Cobalt chloride hexahydrate and HPLC-grade methanol were from Fisher (Nepean, Canada), and the 1-heptanesulfonic acid and 1-octanesulfonic acid sodium salts were from Sigma (St. Louis, MO).

3.2.2 Patient eligibility and characteristics

The trial inclusion criteria that the *Laboratory of Experimental Medical Oncology* (Copenhagen, Denmark) stipulated were: histologically verified small-cell lung cancer together with CT- or MR-evaluable brain-metastasis and age > 18 y. In addition, only one prior chemotherapy regimen which included etoposide was allowed, and which was terminated no later than 3 weeks prior to inclusion, was permitted. The ECOG performance score had to be $\leq$ 2, and life expectancy > 3 months. Adequate organ function to enter the trial was defined as: WBC > 3.0 x 10^9/l, platelets > 100 x 10^9/l, total bilirubin < 1.25 X upper normal limit, aspartate aminotransferase < 2 X upper normal limit, or < 5 X upper normal limit in the presence of verified liver-metastases and serum creatinine < 1.5 X upper normal limit. The patient had to understand the objective of the study, and must have signed an informed consent. The study was approved by the Danish Medical Authorities and by the local ethics committee. Three males and two females were included in this pharmacokinetic study. They had a median age of 67 y (range 58-74 y). They had a median weight of 68 kg (range 53-80 kg). Four patients had received one

110

prior chemotherapy regimen consisting of etoposide, carboplatin and vincristine, while the fifth patient had been treated with one series of topotecan, carboplatin, cisplatin, etoposide and vincristine.

3.2.3 Therapy

Patients in the study group were treated every 3 weeks. The pharmacokinetic studies were done only on the first day of treatment, except for one patient dosed with 500 mg/m^2 etoposide and 1500 mg/m^2 dexrazoxane who was studied for 5 consecutive treatments at 3-week intervals. Three patients were dosed with 500 mg/m^2 etoposide and 1500 mg/m^2 dexrazoxane. One patient was dosed with 1000 mg/m^2 etoposide and 1000 mg/m^2 dexrazoxane, and one patient was dosed with 650 mg/m^2 etoposide and 1500 mg/m^2 dexrazoxane.

Both etoposide and dexrazoxane were administered through a vascular port catheter. Dexrazoxane was administered over 15 min, followed by the infusion of etoposide over 90 min. The etoposide was infused undiluted within 15 min of the completion of the infusion of dexrazoxane. All patients were treated intravenously 30 min prior to the infusion of dexrazoxane and etoposide with 80 mg Solu-Medrol® (methylprednisolone sodium succinate, Pharmacia & Upjohn, Kalamazoo, MI) and 2 mg Tavegyl® (clemastine, Novartis, Basel, Switzerland) for prevention of anaphylactic reactions to the infusion of etoposide and 100 mg Nizax® (nizatidine, Eli Lilly, Indianapolis, IN) for protection of the gastric mucosa.

3.2.4 Sample collection and treatment

Blood samples were withdrawn at predetermined times (0, 0.25, 0.50, 1.0, 2, 3, 4, 8, 12, 16 and 24 h) starting directly after the completion of the infusion of dexrazoxane (defined as time zero). A blood sample was also taken as an HPLC control before the infusion of any drugs. Blood (5 ml) was collected in BD (Franklin Lakes, NJ) Vacutainers® containing lithium heparin (143 I. U.). Blood sampling was from a peripheral vein during infusion of drugs and after completion of treatment the blood was withdrawn from a vascular port catheter (Port-á-Cath, PAC®). The plasma was separated by centrifugation at 650 g for 5 min and then split in two. The portion for analysis of dexrazoxane and its metabolites were generally treated with 10 µl of 5 M HCl/ml of plasma in order to bring the pH to 3 to reduce hydrolysis of dexrazoxane and its metabolites (Hasinoff, 1994a). The portion to be analyzed for etoposide was not treated with HCl. Both portions were stored at −80 °C.

3.2.5   Precipitation of plasma proteins

Plasma samples to be analyzed for dexrazoxane and dexrazoxane metabolites were thawed for 2 min in a 37 °C water bath and rapidly vortexed for 30 s. 200 µl aliquots of plasma were removed and placed in a 1.5 ml microcentrifuge tube. The pH of the sample (typically pH ~ 3) was titrated to a pH range of 5-6 with 5M NaOH. A 400 µl aliquot of acetonitrile (2:1 acetonitrile/plasma, v/v) was added to precipitate plasma proteins. The samples were vortexed at rapid speed for 30 s and allowed to settle for 5 min prior to centrifugation at 10,000 g for 5 min. The supernatant was removed from the plasma protein pellet and placed in a 1.5 ml microcentrifuge tube with 5 µl of 5 M HCl/per 475 µl supernatant. The acidified acetonitrile supernatant was evaporated to dryness by a stream of nitrogen gas at room temperature. Samples to be analyzed for

dexrazoxane, **B**, and **C** analysis were reconstituted in 10 mM HCl/500 µM Na$_2$EDTA to their original volume just prior to analysis. Samples to be analyzed for ADR-925 were reconstituted in 10 mM HCl prior to analysis. Absolute recoveries from spiked plasma ranged from 90% to 100% over a 10 to 200 µM dexrazoxane range. Similarly, the recovery of **B** and **C** ranged from 77-98%, and 81-100%, respectively, over the range of 5-50 µM. Absolute recoveries from spiked plasma ranged from 90% to 98% over a 5 to 50 µM ADR-925 range.

3.2.6 HPLC separation of dexrazoxane, its one-ring open intermediates B and C, and ADR-925

The HPLC apparatus and software set up for the analysis of dexrazoxane and its metabolites using a reversed phase C$_{18}$-column has been previously described in Section 2.2.9. The separation of **B**, **C**, and dexrazoxane from plasma peaks involved two separate HPLC column conditions, one to separate dexrazoxane and **B** from plasma peaks and one to separate **C** from co-eluting plasma peaks. To separate **B** and dexrazoxane from the plasma peaks 2 mM heptanesulfonic acid in 500 µM EDTA (pH 3.5) was isocratically pumped through a 10-µm µBondapak 3.9 × 300 mm reversed-phase C$_{18}$ column connected to an absorbance detector (205 nm) at a rate of 1 ml/min for 5 min to elute **B** with a retention time, t_r, of 5.4 min (as shown in Figure 3.1). The HPLC grade methanol concentration was linearly increased over 1 min from 0 to 20% (v/v) to elute the dexrazoxane peak, t_r of 12.1 min (as shown in Figure 3.2). After the dexrazoxane peak eluted, the methanol was linearly increased from 20 to 80% (v/v) over 2 min and maintained for 20 min to remove any late eluting plasma protein peaks. 2 mM heptanesulfonic acid in 500 µM EDTA (pH 3.5) was isocratically pumped through the

113

column for 30 min prior to the next sample to equilibrate the column. To separate **C** from plasma peaks, 500 μM of EDTA (pH 3.5) was isocratically pumped through a 10-μm μBondapak 3.9 × 300 mm reversed-phase C_{18} column connected to an absorbance detector (205 nm) at a rate of 1 ml/min. As shown in the HPLC chromatogram (Figure 3.3), **C** was separated from early eluting plasma protein peaks with a t_r 6.2 min. After the elution of **C**, the column was washed with methanol/500 μM EDTA (80:20, v/v) for 10 min to remove remaining plasma proteins from the column. The column was then re-equilibrated in 500 μM EDTA (pH 3.5) for 15 min prior to the next sample injection. Samples were run in duplicate. In order to compare the amount of ADR-925 obtained by HPLC and by the flow injection method (as described in section 3.2.9), ADR-925 was determined ($n = 4$) in the plasma of one patient by HPLC (t_r 3.6 min) under isocratic conditions (500 μM Na_2EDTA/10 mM octanesulfonic acid, pH 2.8, 1 ml/min). As shown in Figure 3.4, the ADR-925 peak is relatively well separated from the solvent front plasma peaks. The limit of quantitation, estimated from three times the limit of detection, of dexrazoxane, **B**, **C**, and ADR-925 in plasma was 1, 1.5, 1.5, and 10 μM, respectively. The limit of detection was made through a conservative estimate of drug/metabolite peak heights that exceeded the background noise five fold. A 5 mM stock solution of Cardioxane® (dexrazoxane hydrochloride, obtained from Chiron) was prepared to determine the mol% of **B**, **C**, and ADR-925. Dexrazoxane, **B**, and **C** concentrations were determined by the HPLC assay mentioned above. The ADR-925 concentration was determined using the calcein fluorescence flow injection assay described in Section 3.2.8. The dexrazoxane hydrochloride that was infused into the patients was found to contain less than 0.49% **B**, 0.20% **C**, and 0.29% ADR-925 (mol%).

3.2.7   HPLC calibration plots: quantitation of dexrazoxane, B, C, and ADR-925 in human plasma

The HPLC calibration plots using integrated peak areas (10 to 400 µM dexrazoxane, 2 to 70 µM **B**, 2 to 30 µM **C**, and 10 to 70 µM ADR-925) were prepared by adding standards containing known amounts of dexrazoxane, **B**, **C** and ADR-925 (prepared as previously described (Hasinoff, 1994a)) to blank plasma.   The calibration plots were constructed by plotting arbitrary integration peak areas (as shown in Tables 3.1-3.4) as a function of drug or drug metabolite concentration as shown in Figures 3.6 through 3.9.   Calibration curves were prepared prior to each series of sample analysis and each concentration point is an average of two injections.   A total of three calibration curves for dexrazoxane, two calibration curves for **B** and **C**, and one calibration curve for ADR-925 were performed.   The day to day variation of the slopes was found to be small and is expressed as a percent difference at the end of each table.

3.2.8   Fluorescence flow injection analysis of ADR-925

The flow injection apparatus, experimental protocol and software set up has been previously described in Section 2.2.9.   The samples treated for analysis were injected (n=3) into a Rheodyne (Cotati, CA) injector with a 20 µl PEEK sample loop (Upchurch, Oak Harbor, WA) using a Teflon needle (Rheodyne). PEEK tubing (Upchurch) was used between the injector and the Shimadzu (Columbia, MD) RF-551 fluorescence detector (λ_{ex} 496 nm, λ_{em} 517 nm). Aqueous Na$_2$EDTA (20 µM, 1 ml/min) was used as the mobile phase to complex metal ions present in the flow system.   Human plasma components were shown not to interfere with the assay as the slopes of the calibration plots in water and reconstituted plasma were not significantly different.   Because the calcein assay

measures only free ADR-925, experiments were also done to determine the relative amount of free ADR-925 in plasma. In preliminary experiments it was shown that stirring the chelating resin Chelex (Sigma), with preformed Fe^{3+}–ADR-925 at pH 5.5 resulted in complete displacement of Fe^{3+} from its complex with ADR-925 within 20 min. Thus, the ADR-925 levels reported here are representative of Chelex treated plasma samples and are thus representative of the total plasma ADR-925 levels. The limit of detection in plasma was estimated to be 1 μM (concentration of ADR-925 in plasma) and was estimated from the loss of linearity in the concentration-fluorescence relationship.

3.2.9   Precipitation of plasma proteins

Plasma samples were treated as previously described in Section 3.2.5. Etoposide is stable in plasma (over 99 % protein bound) (Robieux et al., 1996). However, once acetonitrile is added to precipitate plasma proteins, etoposide is no longer stable and undergoes isomerisation of *trans*-etoposide to the inactive compound *cis*-etoposide (Mader et al., 1991; Cai et al., 1999). Therefore, to ensure the stability of etoposide after the acetonitrile protein precipitation, samples were reconstituted in methanol/ddH$_2$O/glacial acetic acid (49/50/1 (v/v/v), pH 3.5) after they were dried under nitrogen to ensure etoposide stability.

3.2.10 Detection of etoposide in human plasma

The HPLC apparatus and software set up has been previous described in Section 2.2.9. To separate etoposide from plasma peaks, methanol/ddH$_2$O/glacial acetic acid (49/50/1, v/v/v) titrated with 5M NaOH to pH 3.5, was isocratically pumped through a 120 Å10-μm μBondapak 3.9 × 300 mm reversed-phase phenyl column connected to an

absorbance detector (235 nm) at a rate of 1 ml/min. The chromatogram in Figure 3.5 shows that under these conditions, etoposide is well separated from early eluting plasma peaks with a t_r of 16.3 min. The column was washed with 100% methanol every 25 runs to remove the late eluting plasma proteins and ensure reproducibility.

3.2.11 HPLC quantitation of etoposide in human plasma

The HPLC calibration plot using integrated peak areas (2 to 300 μM etoposide, Table 3.5) is shown in Figure 3.11. Standards for the calibration curve were prepared by adding known amounts of etoposide to blank plasma. Absolute recoveries from spiked plasma ranged from 80 to 97% over a 10 to 300 μM etoposide concentration range. The limit of detection was determined by an estimate of etoposide peak heights that exceeded the background noise three fold. The limit of quantitation was determined to be three times the limit of detection and found to be 2 μM.

3.2.12 Data analysis

The plasma distribution and elimination curve for dexrazoxane was fit to an *i.v.* bolus two-compartment model (Model 7 WinNonlin 4.0, Pharsight, Mountain View, CA) as previously described for dexrazoxane (Earhart et al., 1982; Jakobsen et al., 1994). The etoposide concentration-time curves were fitted to an *i.v.* infusion one-compartment model (Model 201 WinNonlin 4.0, Pharsight, Mountain View, CA) where the elimination kinetic parameters were derived.

3.3 Results

3.3.1 HPLC separation of etoposide, dexrazoxane, B, C, and ADR-925

The separation of dexrazoxane, **B**, **C**, and ADR-925 from plasma peaks involved three separate HPLC column conditions, all on a 10-μm μBondapak 3.9 × 300 mm reversed-phase C_{18} column as described in Section 3.2.6. Under the previously described conditions, dexrazoxane, **B**, **C**, and ADR-925 were separated with retention times of 12.1, 5.4, 6.2, and 3.6 min, respectively as shown in Figures 3.1 to 3.4. Etoposide was separated on a 120 Å10-μm μBondapak 3.9 × 300 mm reversed-phase phenyl column (as described in Section 3.2.10) and was well separated from early eluting plasma peaks, t_r of 16.3 min as shown in Figure 3.5.
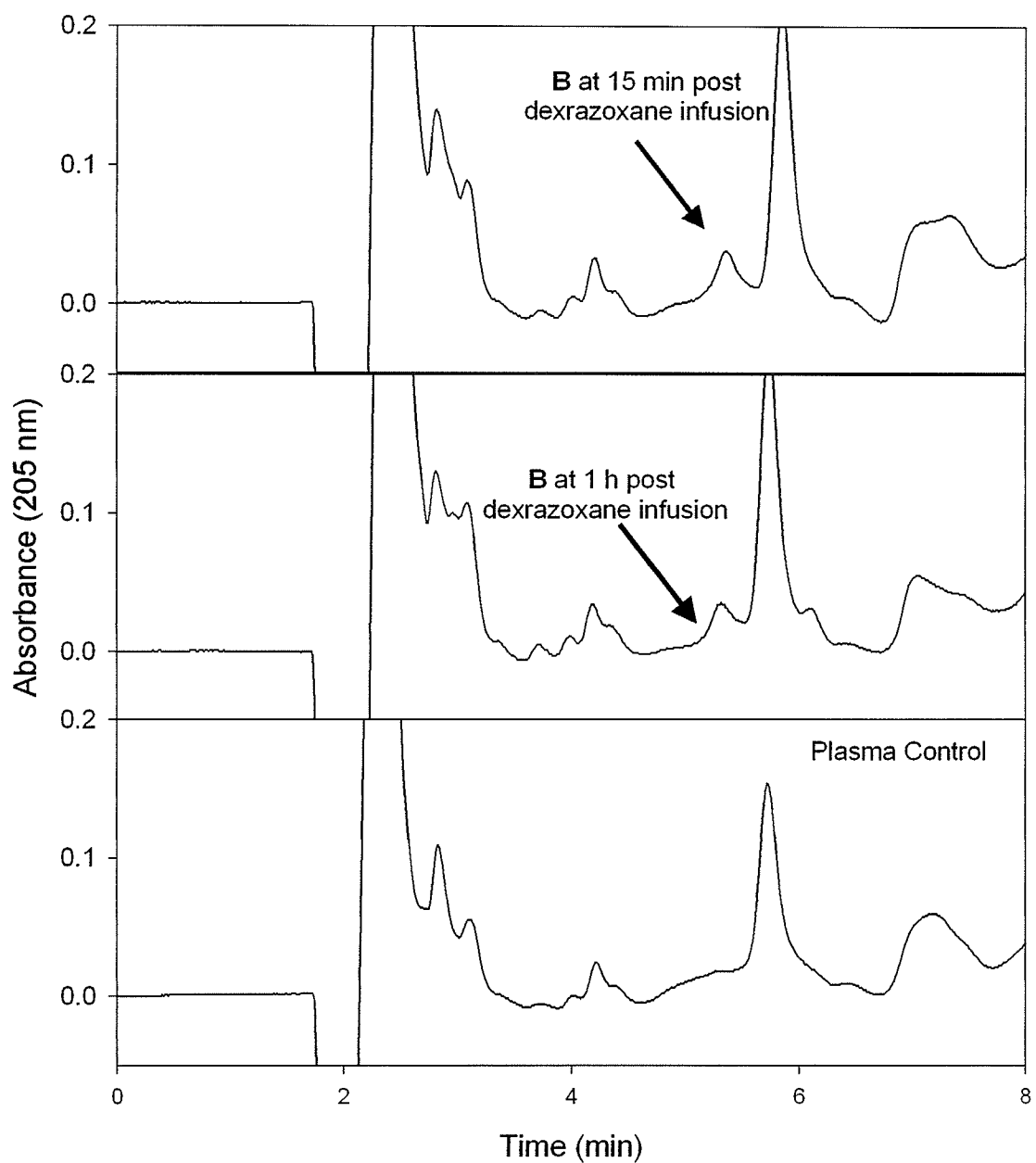
Figure 3.1. *HPLC chromatogram of the separation of B in the plasma of patient 5 who received an i.v. bolus of 1000 mg/m^2 dexrazoxane.*

Integrated **B** peak areas at 15 min and 1 h corresponds to 12.9 μM and 9.4 μM **B**, respectively.
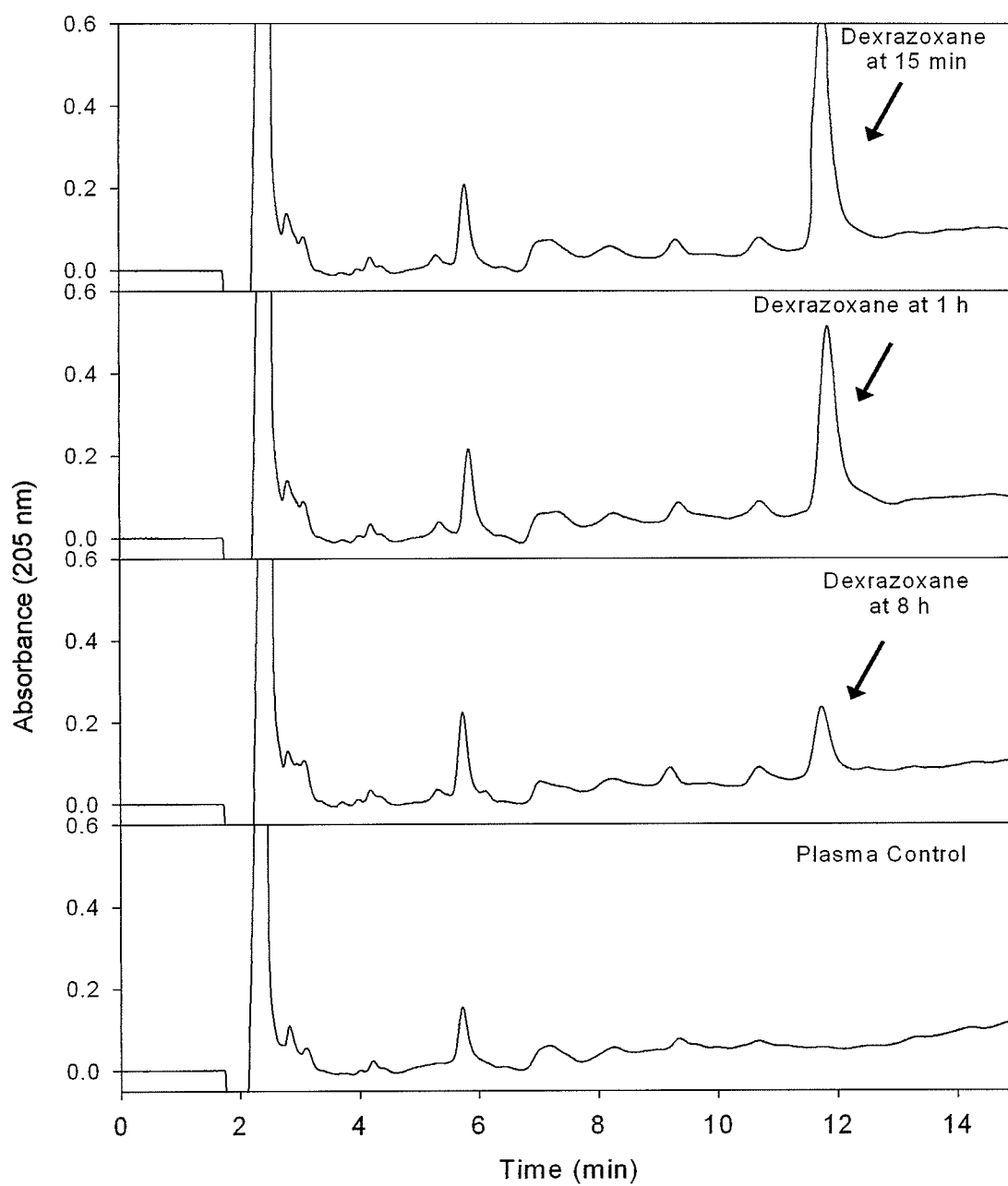
Figure 3.2. HPLC chromatogram of the separation of dexrazoxane in the plasma of patient 5.

Integrated dexrazoxane peak areas at 15 min, 1 h, and 8 h corresponds to 130 μM, 90 μM, and 12.5 μM dexrazoxane, respectively.

120
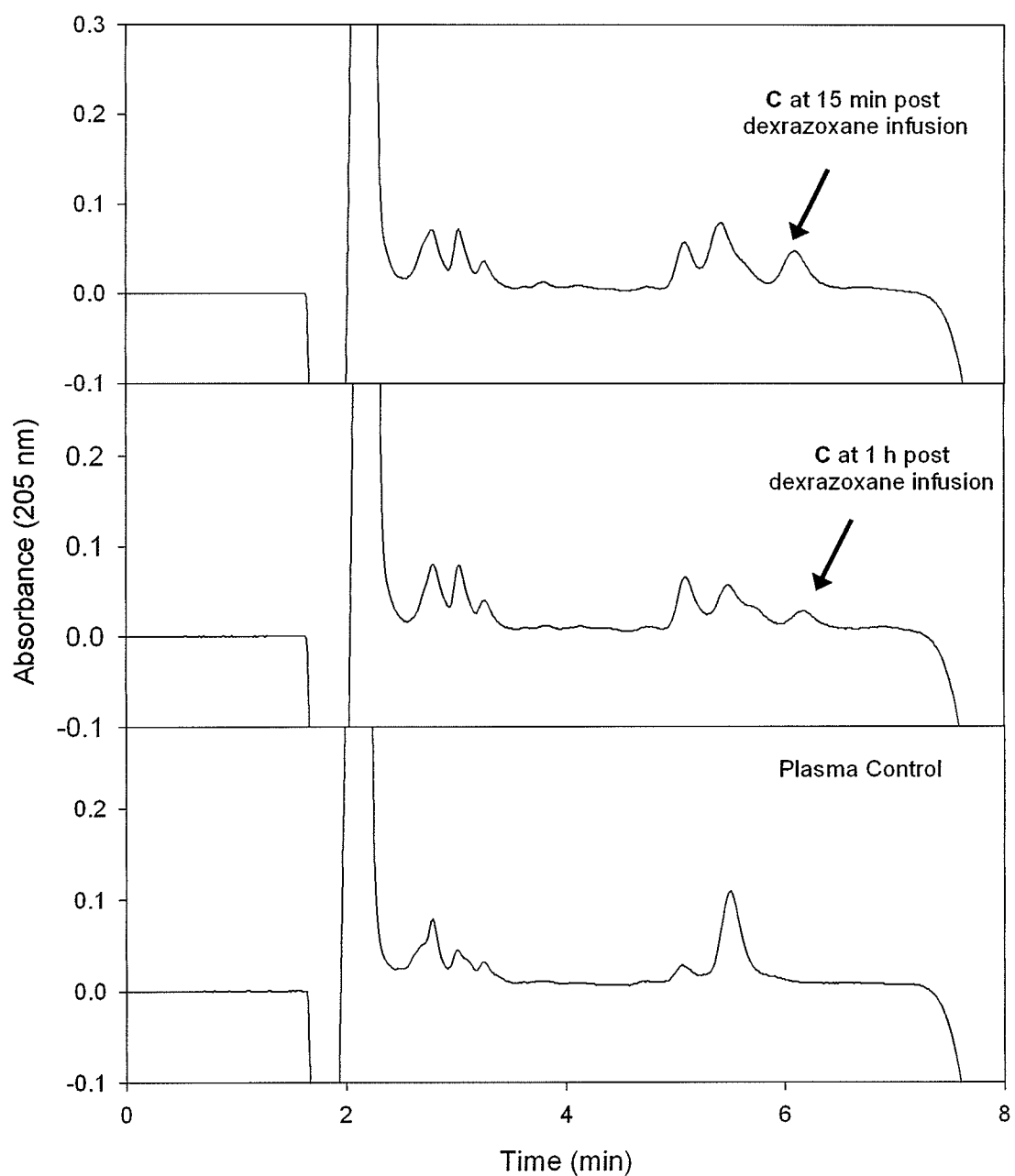
Figure 3.3. HPLC chromatogram of the separation of **C** *in the plasma of patient 5.*

Integrated **C** peak areas at 15 min and 1 h corresponds to 8.6 μM and 4.1 μM **C**, respectively.

121
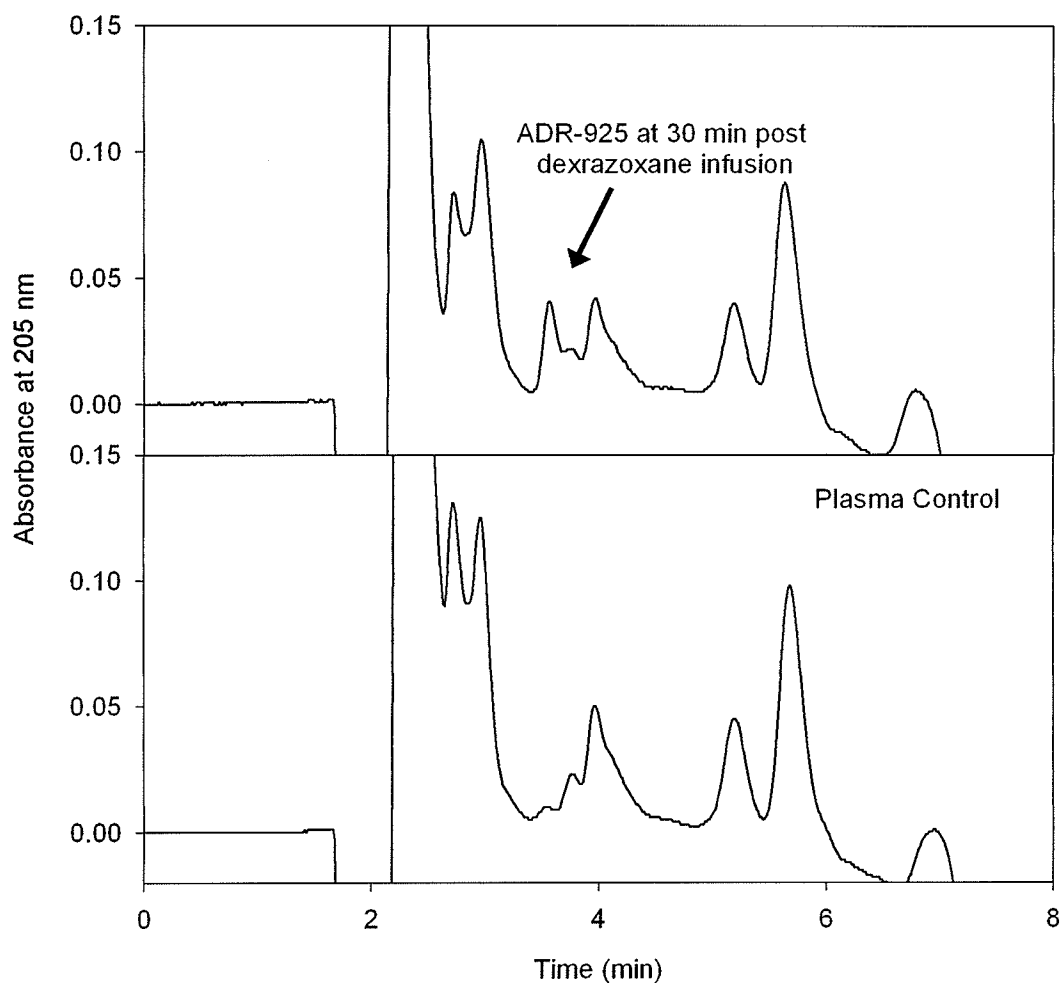
Figure 3.4. HPLC chromatogram of ADR-925 separation in human plasma.

The plasma ADR-925 concentration obtained by HPLC was compared to the ADR-925 concentration found by the fluorescence assay (see Section 3.2.8) to determine whether any other Co^{2+} chelating dexrazoxane metabolites were formed that would lead to an overestimation of ADR-925 plasma levels determined through the calcein assay. Integrated ADR-925 peak areas at 30 min corresponds to an ADR-925 concentration of 34 μM.
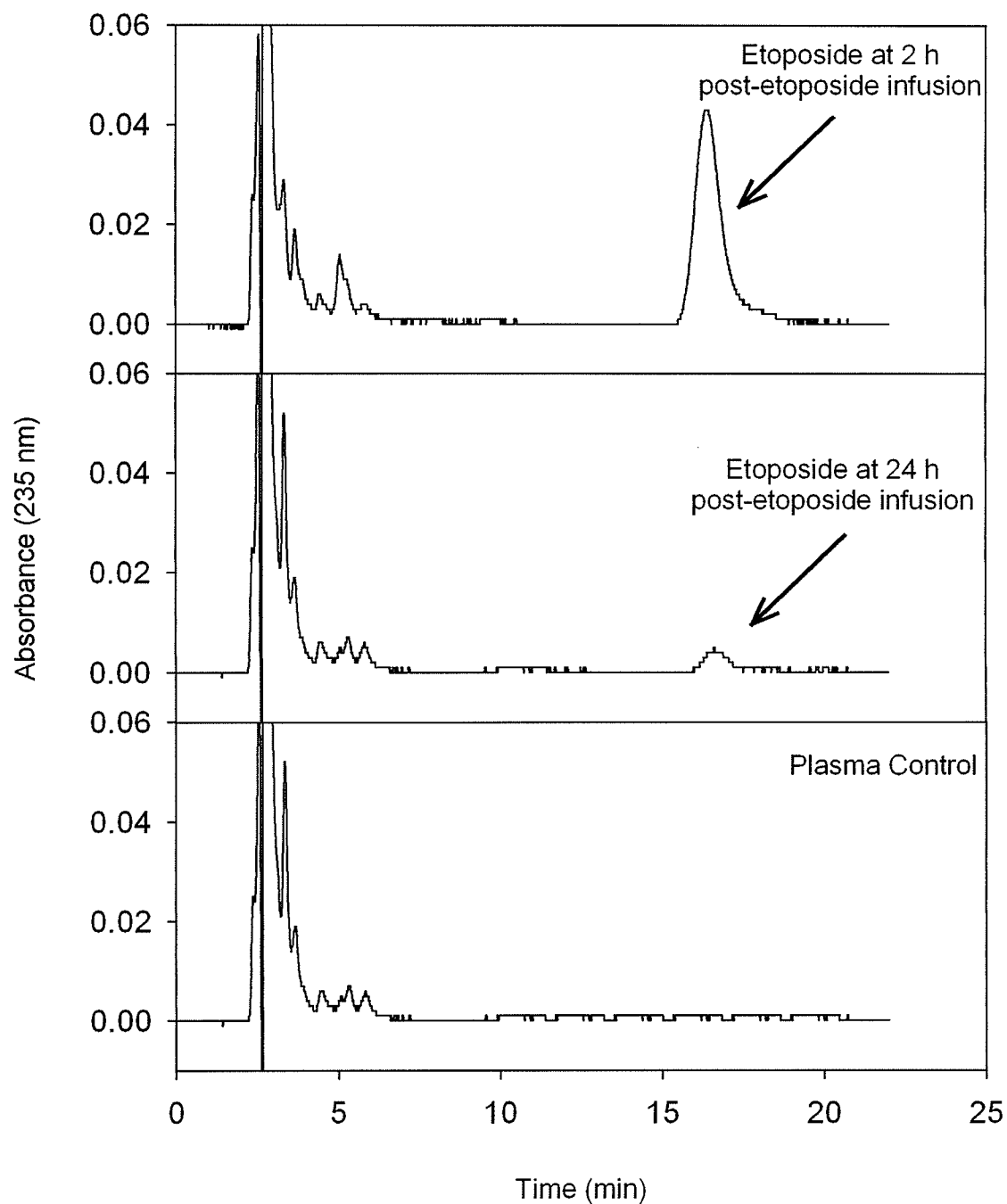
Figure 3.5. HPLC chromatogram of the separation of etoposide in the plasma of patient 4 who received an etoposide dose of 500 mg/.m².

Integrated etoposide peak areas at 2 h, and 24 h corresponds to 173 μM and 15 μM etoposide plasma concentrations, respectively.

3.3.2 Calibration plots: quantitation of etoposide, dexrazoxane, B, C, and ADR-925

The calibration plots were constructed by plotting arbitrary integration peak areas (as shown in Tables 3.1-3.6) as a function of drug or drug metabolite concentration as shown in Figures 3.6 through 3.11. Calibration curves were prepared prior to each series of sample analysis and each concentration point is an average of two injections. A total of three calibration curves for dexrazoxane, two calibration curves for **B** and **C**, and one calibration curve for ADR-925 were performed. The day-to-day variation of the slopes was found to be small and is expressed as a percent difference at the end of each table. The HPLC calibration plot using integrated peak areas (2 to 300 μM etoposide, Table 3.5) is shown in Figure 3.11. Standards for the calibration curve were prepared by adding known amounts of etoposide to blank plasma. Absolute recoveries from spiked plasma ranged from 80 to 97% over a 10 to 300 μM etoposide concentration range. The limit of detection was determined by an estimate of etoposide peak heights that exceeded the background noise three fold. The limit of quantitation was determined to be three times the limit of detection and found to be 2 μM.

The fluorescence calibration plot using integrated peak areas (0 to 1 μM ADR-925, Table 3.6) is shown in Figure 3.10. Calibration plots of integrated peak areas ($n = 6$) in the range 0 to 1.0 μM ADR-925 were repeated every 3 h during analysis and were found to be linear ($r^2 > 0.997$).

Table 3.1. HPLC calibration curve of dexrazoxane (UV absorbance at 205 nm) in precipitated human plasma for patients dosed with 1500 mg/m^2 dexrazoxane.

Concentration (μM)	Average Peak Area (Arbitrary Units)
400	1324489
300	953100
200	667646
100	324312
50	152916
25	91418
10	45671
Slope [a]	3261
Y-intercept	3115
r^2	0.9982

[a] Between-day variation in the slopes of the calibration plots was 7 %.

Table 3.2. HPLC calibration curve of **B** (UV absorbance at 205 nm) in precipitated human plasma for patients dosed with 1500 mg/m^2 dexrazoxane.

Concentration (μM)	Average Peak Area (Arbitrary Units)
70	109350
50	82538
30	48390
20	37461
10	21206
5	13026
2	9150
Slope [a]	1487
Y-intercept	6149
r^2	0.998

[a] Between-day variation in the slopes of the calibration plots was 2%.

Table 3.3. HPLC calibration curve of **C** (UV absorbance at 205 nm) in precipitated human plasma for patients dosed with 1500 mg/m^2 dexrazoxane.

Concentration (µM)	Average Peak Area (Arbitrary Units)
30	48457
20	36760
15	26349
10	18856
5	11545
2	7254
Slope [a]	1511
Y-intercept	4222
r^2	0.991

[a] Between-day variation in the slopes of the calibration plots was 0.3%.

Table 3.4. HPLC calibration curve of ADR-925 (UV absorbance at 205 nm) in precipitated human plasma for patients dosed with 1500 mg/m^2 dexrazoxane.

Concentration (µM)	Average Peak Area (Arbitrary Units)
70	21546
50	14232
35	10542
20	6256
10	3365
Slope	297
Y-intercept	190
r^2	0.995

Table 3.5. HPLC calibration curve of etoposide (UV absorbance at 230 nm) in precipitated human plasma for patients dosed with 500 mg/m² etoposide.

Concentration (µM)	Average Peak Area (Arbitrary Units)
500	795770
200	316867
100	174659
50	82855
25	41605
10	21491
5	12940
2	6375
Slope	1583
Y-intercept	5021
r^2	0.995

Table 3.6. Flow injection calibration curve of ADR-925 (using the fluorescent dye calcein, λ_{ex} 496 nm and λ_{em} 518 nm) in precipitated human plasma for patients dosed with 1500 mg/m² dexrazoxane.

Concentration (µM)	Average Peak Area (Arbitrary Units)
0	539,159
0.2	912,234
0.4	1,231,389
0.6	1,573,033
0.8	2,015,882
1.0	2,298,371
Slope [a]	1,792,205
Y-intercept	496,747
r^2	0.997

[a] Between-day variation in the slopes of the calibration plots was 2%.
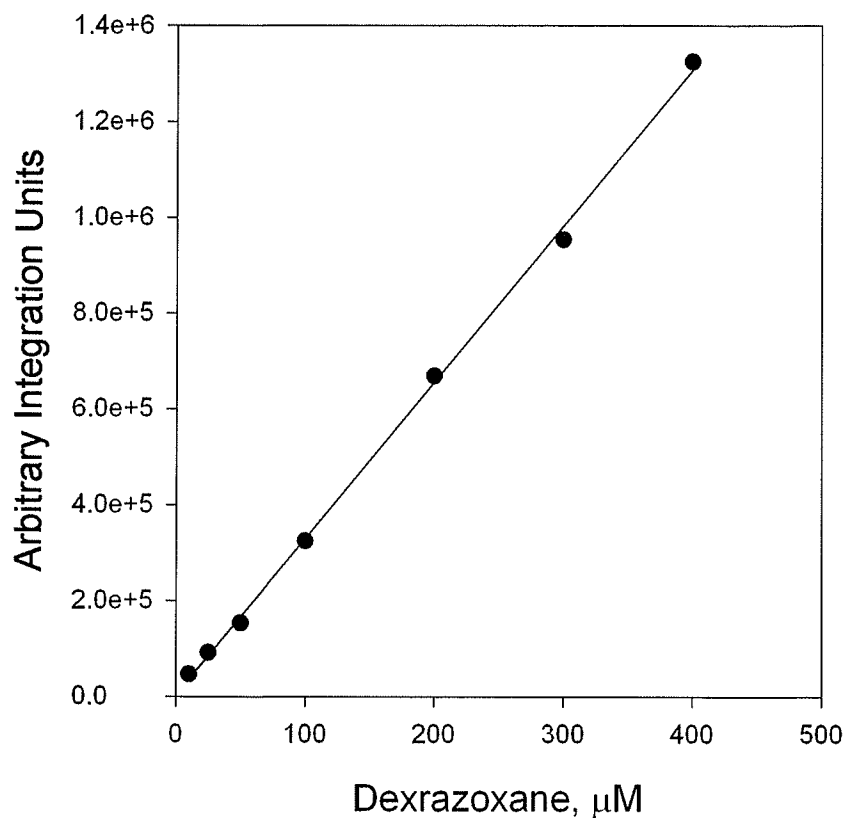
Figure 3.6. Dexrazoxane calibration curve
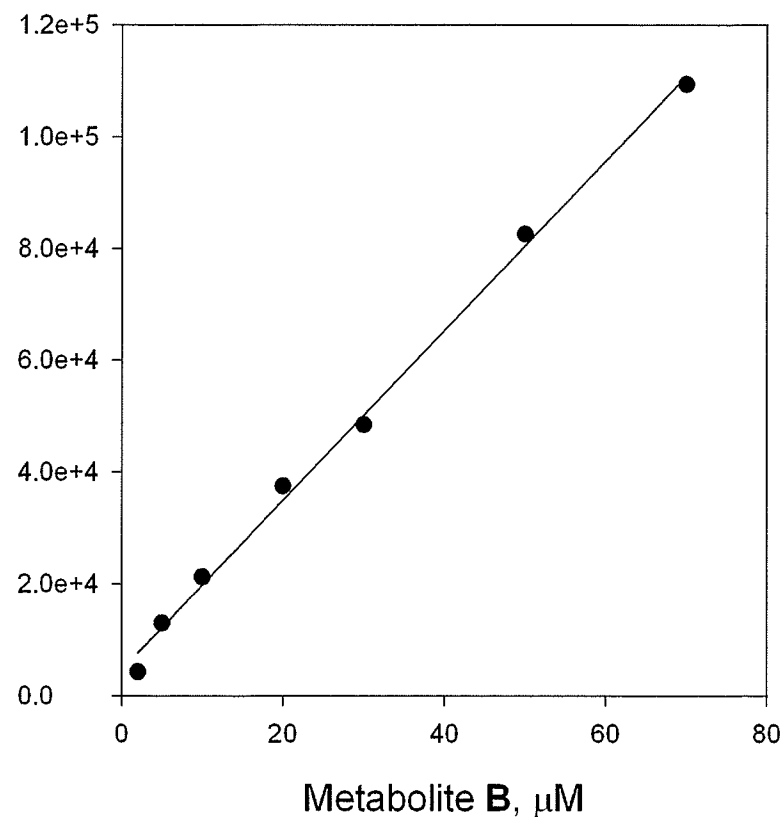
*Figure 3.7. **B** calibration curve*

HPLC calibration plots using integrated peak areas were prepared by adding standards containing known amounts of dexrazoxane and **B** to blank human plasma. A mobile phase of 2 mM heptanesulfonic acid/500 μM EDTA (as described in Section 3.2.6) separated dexrazoxane (t_r 12.1 min) and **B** (t_r 5.4 min) from co-eluting plasma protein peaks.
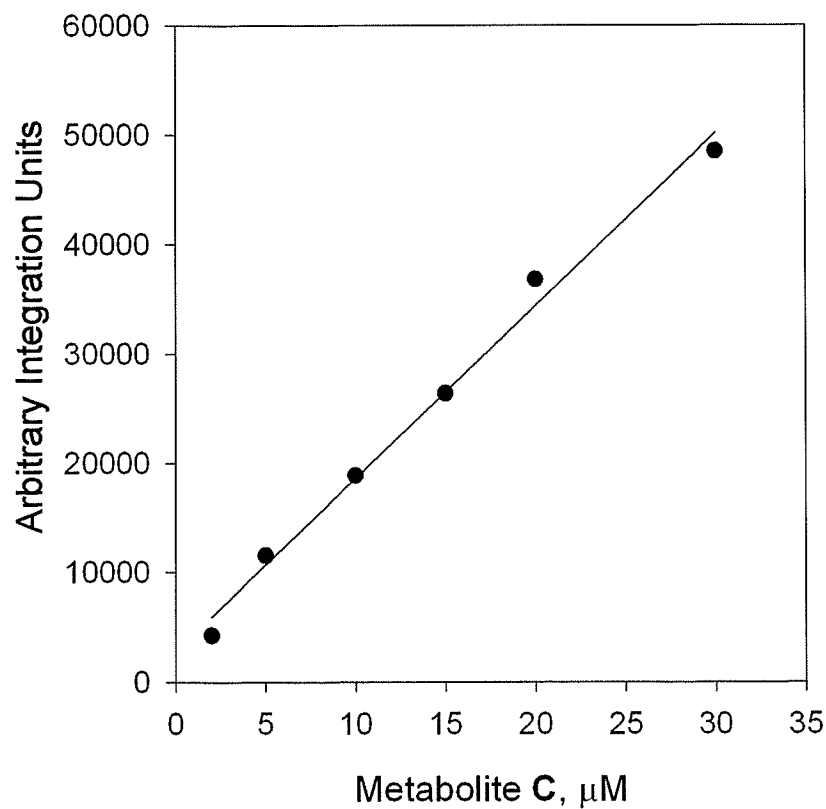
Figure 3.8 *C calibration curve*

HPLC calibration plot was prepared by adding standards containing known amounts of C to blank human plasma. A mobile phase of 500 μM EDTA (as described in Section 3.2.6) separated C (t_r 6.4 min) from co-eluting plasma peaks.
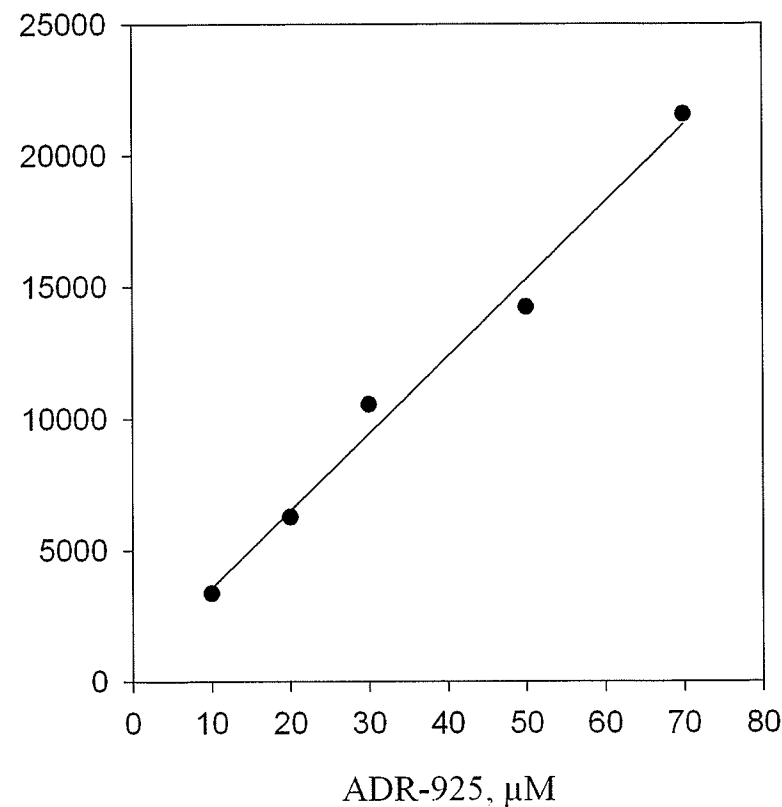
Figure 3.9 *ADR-925 calibration curve*

HPLC calibration plot was prepared by adding standards containing known amounts of ADR-925 to blank human plasma. 500 μM EDTA/10 mM octanesulfonic acid was used to separate ADR-925 (t_r 2.8 min) from co-eluting plasma protein peaks (as described in Section 3.2.6).
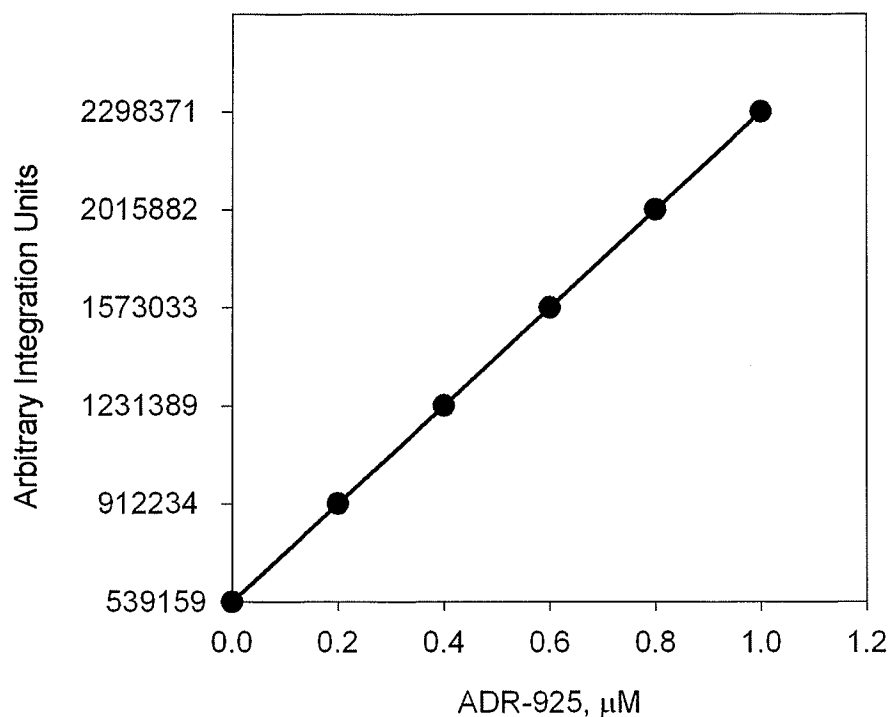
Figure 3.10. ADR-925 calibration curve using the fluorescent dye calcein

Flow injection calibration plot of ADR-925 using calcein fluorescence integrated peak areas were prepared by adding standards containing known amounts of ADR-925 to blank human plasma (as described in Section 3.2.8).
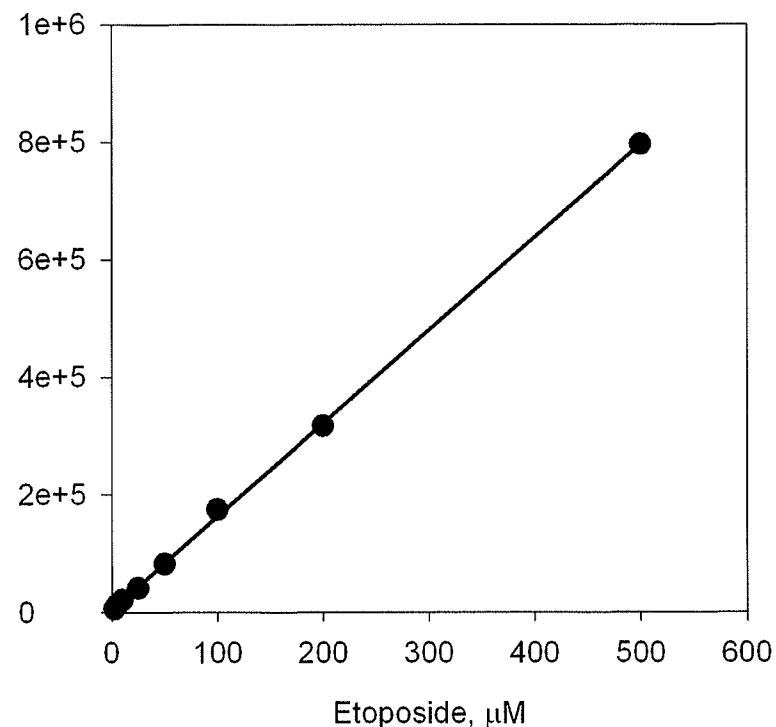
Figure 3.11. Etoposide calibration curve

HPLC etoposide calibration plot using integrated peak areas was prepared by adding standards containing known amounts of etoposide to blank human plasma. A mobile phase of methanol/ddH$_2$O/glacial acetic acid (49/50/1, v/v/v) (as described in Section 3.2.10) separated etoposide (t_r 16.3) from co-eluting plasma protein peaks.

130

3.3.3 Data analysis

The plasma distribution and elimination curve for dexrazoxane was fitted to an *i.v.* infusion two-compartment model (equation 3.1) (WinNonlin 4.0, Pharsight, Mountain View, CA) as previously described for dexrazoxane (Earhart et al., 1982; Jakobsen et al., 1994). A two-compartment model was used to describe the entire plasma dexrazoxane concentration (C) versus time (t) curve that was fitted by the sum of two exponential terms where A and B refer to the corresponding zero-time intercepts (equation 3.1). The

$$C_t = A \cdot e^{-\alpha t} + B \cdot e^{-\beta t} \qquad\qquad 3.1$$

first term describes the disposition of dexrazoxane (where α is the disposition rate constant) while the second term describes dexrazoxane elimination (where β partially describes the elimination). Once the alpha and beta rate constants are determined, the secondary pharmacokinetic parameters; total area under the concentration-time curve ($AUC_{0-\infty}$, equation 3.2), alpha half life ($t_{\frac{1}{2}\alpha}$, equation 3.3), beta half life ($t_{\frac{1}{2}\beta}$, equation 3.4), maximum concentration (C_0, equation 3.5), and total clearance (Cl_{tot}, equation 3.6) can be determined from:

$$AUC_{0-\infty} = \frac{A}{\alpha} + \frac{B}{\beta} \qquad\qquad 3.2$$

$$t_{\frac{1}{2}\alpha} = \frac{\ln 2}{\alpha} \qquad\qquad 3.3$$

$$t_{\frac{1}{2}\beta} = \frac{\ln 2}{\beta} \qquad\qquad 3.4$$

$$C_0 = A + B \qquad\qquad 3.5$$

$$Cl_{tot} = \frac{Dose}{AUC_{0-\infty}} \qquad\qquad 3.6$$

The apparent elimination half-lives for intermediates **B** and **C** were determined by fitting

the combined data from all patients to a two-parameter single-exponential decay function

(equation 3.7) where the beta half life is estimated by equation 3.4.

$$C_t = C_0 \cdot e^{-\beta t} \qquad\qquad 3.7$$

The etoposide concentration-time curves were fitted to an *i.v.* infusion one-

compartment model (Model 201 WinNonlin 4.0, Pharsight, Mountain View, CA) where

the elimination kinetic parameters were derived from equation 3.8.   Where t_i is the

infusion time and $t_* = t{-}t_i$, at all times less then the infusion time ($t \leq t{-}t_i$). At times

greater then the infusion time ($t > t{-}t_i$), $t^*{=}0$ and the concentration-time curve is estimated

as a monoexponential equation (equation 3.7).

$$C_t = \frac{C_0 \cdot (e^{-k\beta\,t}{}_* - e^{-k\beta t})}{t_i \cdot k_\beta} \qquad\qquad 3.8$$

3.3.4   Dexrazoxane pharmacokinetics

The plasma levels of dexrazoxane for the 5 patients obtained after dexrazoxane

infusion are tabulated in Table 3.7. Dexrazoxane displayed first order elimination kinetics

as has been well described before (Earhart et al., 1982; Hochster et al., 1992; Jakobsen et

al., 1994; Tetef et al., 2001) and shown in Figures 3.13 to 3.18. Analysis of the data from

five individual patients for which there was sufficient data gave an average $t_{\frac{1}{2}\alpha}$ of 0.8 ±

0.3 h (range 0.51 − 1.3 h) and $t_{\frac{1}{2}\beta}$ of 9.1 ± 5.4 h (range 4.3 - 16.4 h). Analysis of the

averaged data from all 5 patients treated gave a $t_{\frac{1}{2}\alpha}$ of 0.4 ± 0.1 h and a $t_{\frac{1}{2}\beta}$ of 5.8 ± 1.0 h.

All patients but one were dosed at 1500 mg/m^2 of dexrazoxane. The data for the one

patient that was dosed at 1000 mg/m^2 of dexrazoxane were included in the data set by

multiplying the concentration of dexrazoxane and its metabolites by 1.5 as previous

132

studies have shown that dexrazoxane plasma concentration is dose-linear. (Hochster et al., 1992; Jakobsen et al., 1994; Tetef et al., 2001). The post-infusion C_0 for the averaged data was 226 μM (range 152-314 μM). The post-infusion concentration-time area-under-the-curve $AUC_{0-\infty}$, calculated as described (Earhart et al., 1982), had a value of 609 μM·h (range 350-1210).

Table 3.7. Plasma concentrations (μM) of dexrazoxane for patients treated with a 1500 mg/m[2b] bolus of dexrazoxane hydrochloride 15 min prior to a 90 min infusion of etoposide.

Time (hr)	Patient number									Average[c] μM	SE $\pm \mu$M
	1	2	3[a]	3[a]	3[a]	3	4	5	5[b]		
0	230		359	460	333	191		130	195	295	43.9
0.25	171	295				126	201			198	35.7
0.5	131	249				73.0	148	123	185	157	29.2
1	99.7	159				65.0	118	90.0	135	115	15.9
2	66.8	114				21.0	80.6	41.9	62.9	69.1	15.0
3	36.5						52.9			44.7	8.2
4		51.2				9.0		15.6	23.4	27.9	12.4
8								12.5	18.7	18.7	NA
12								7.9	11.9	11.9	NA
16								3.3	5.0	5.0	NA
24	1					2	15	1.0	1	4.8	3.4

[a] Initial dexrazoxane concentrations for patient 3 obtained from 3 separate treatments.
[b] The concentration-time data for patient 5 has been normalized to a dexrazoxane dose of 1500 mg/m^2.
[c] Average dexrazoxane plasma concentrations of all 5 patients where the normalized concentration-time points for patient 5 is included.

134

Table 3.8. Pharmacokinetic parameters for the distribution and elimination of dexrazoxane following a 1500 mg/m^{2a} dexrazoxane hydrochloride bolus.

Patient number	Dexrazoxane (mg/m^2)	Sex	$t_{1/2\alpha}$ (h)	$t_{1/2\beta}$ (h)	C_0 (µM)	$AUC_{0-\infty}$ (µM·h)	Cl_{tot} (ml·m^2·min^{-1})
1	1500	F	0.7	4.3	210	460	202
2	1500	M	1.3	ND^b	314	580	161
3	1500	F	0.5	9.8	165	270	345
4	1500	M	0.9	16.4	215	1210	77
5	1000	M	0.8	5.9	152	350	266
Mean			0.8	9.1	226^a	609^a	210
SD			0.3	5.4	54	355	101
Ave^c	1500		0.4	5.8	280	617	151
SE^d			0.1	1.0	16	48	12

^{a} Mean where the dose-linear parameters C_0 and $AUC_{0-\infty}$ were normalized to a dose of 1500 mg/m^2 of dexrazoxane for patient 5.

^{b} Not determined as plasma concentration-time points were only collected to 4 h.

^{c} Pharmacokinetic parameters obtained from the combined concentration-time points of all 5 patients (where patient 5 concentration-time points were normalized to a dexrazoxane dose of 1500 mg/m^2). Also includes patient 3 whose time-concentration data was obtained for t=0 from a total of four treatment schedules.

^{d} Standard errors obtained from modeling data to equation 3.1.

3.3.5 Pharmacokinetics of the dexrazoxane metabolites

The plasma levels of **B** and **C** are shown in Tables 3.9 and 3.10, respectively. The intermediates **B** and **C** appeared in the plasma very quickly after dexrazoxane administration and then continuously decreased to below detectable limits (1.5 µM) by 4 h and 16 h, respectively (Figures 3.13-3.18). The level of **C** was a nearly constant 3-5% of dexrazoxane plasma levels. The level of **B** increased from an initial 8% to maximally 29% of the dexrazoxane plasma levels at 3 h. As can be seen from Figure 3.18 the semi-log plots of the **B** and **C** data are approximately linear and thus, the data was empirically fit to a two-parameter exponential decay equation. The apparent half-lives for the disappearance of intermediates **B** and **C** had values of 2.5 ± 1.1 and 0.6 ± 0.2 h,

respectively. The apparent C_0 values for intermediates **B** and **C** were 19.3 ± 5.2 and 9.1 ± 3.0 μM, respectively. These are apparent values only because **B** and **C** are intermediates that are both being formed, distributed, metabolized and eliminated simultaneously. It can also be seen from the data in Figure 3.18 that the concentration of **B** was always larger than that of **C**. The ratio **B/C** (Figure 3.12) increased from an initial value of 2.4 to 6.4 at 3 h.

Table 3.9. Plasma concentrations (μM) of **B** for patients treated with a 1500 mg/m[2a] bolus of dexrazoxane hydrochloride.

Time (hr)	Patient number						Average[b]	SE
	1	2	3	4	5	5 [a]		
0	12.0		25.7		8.6	12.9	16.87	4.42
0.25	15.9	19.4	18.5	27.5			20.33	2.50
0.5	14.5	19.3	15.2	20.4	7.7	11.5	16.18	1.63
1	12.5	15.7	16.4	18.4	6.3	9.4	14.48	1.59
2	7.0	12.2	12.9	12.5	3.7	5.6	10.04	1.55
3	10.0			15.7	1.6	2.1	9.27	3.94
4		7.4	<LOD				7.40	
8					1.9	2.9	2.90	
12								
16					<LOD	<LOD		
24	<LOD		<LOD	2.8	<LOD	<LOD	2.80	

[a] The concentration-time data for patient 5 has been normalized to a dexrazoxane dose of 1500 mg/m^2.
[b] Average **B** plasma concentrations of all 5 patients where the normalized concentration-time points for patient 5 is included.
<LOD, below the limit of detection

136

Table 3.10. Plasma concentrations (μM) of **C** for patients treated with a 1500 mg/m^{2a} bolus of dexrazoxane hydrochloride.

Time (hr)	1	2	3	4	5	5 [a]	Average[b]	SE
0	7.6		5.0		5.7	8.6	7.07	1.07
0.25	4.8	<LOD	<LOD	10.0			7.40	
0.5	2.7	<LOD	<LOD	7.2	4.8	7.2	5.70	1.50
1	<LOD	<LOD	<LOD	5.0	2.7	4.1	4.55	0.64
2	<LOD	<LOD	<LOD	2.1	<LOD	<LOD	2.10	
3	2.0			<LOD	<LOD	<LOD	2.00	
4		<LOD	<LOD				<LOD	
8					<LOD	<LOD	<LOD	
12								
16					<LOD	<LOD	<LOD	
24	<LOD		<LOD	<LOD	<LOD	<LOD	<LOD	

[a] The concentration-time data for patient 5 has been normalized to a dexrazoxane dose of 1500 mg/m^2.
[b] Average **C** plasma concentrations of all 5 patients where the normalized concentration-time points for patient 5 is included.
<LOD, below the limit of detection

Table 3.11. Pharmacokinetic parameters for the apparent half lives of **B** and **C** of patients treated with a 1500 mg/m^{2a} dexrazoxane hydrochloride bolus.

Patient number	B			C		
	n	$t_{\frac{1}{2}\beta}$ (h)	C_0 (μM)	n	$t_{\frac{1}{2}\beta}$ (h)	C_0 (μM)
1	6	3.9	14.4	4	0.5	6.3
2	5	2.6	21.1	–	ND	ND
3	5	2.1	22.1	–	ND	ND
4	6	2.9	25.4	4	0.8	12.2
5	5	0.9	13.3	3	0.5	8.9
Mean		2.5	19.3		0.6	9.1
SD		1.1	5.2		0.2	3.0

n, is the number of plasma concentration-time points for each patient used to obtain the pharmacokinetic parameters.
[a] Mean where the dose-linear parameters C_0 and $t_{1/2}$ were normalized to a dose of 1500 mg/m^2 of dexrazoxane for patient 5.
ND, not determined
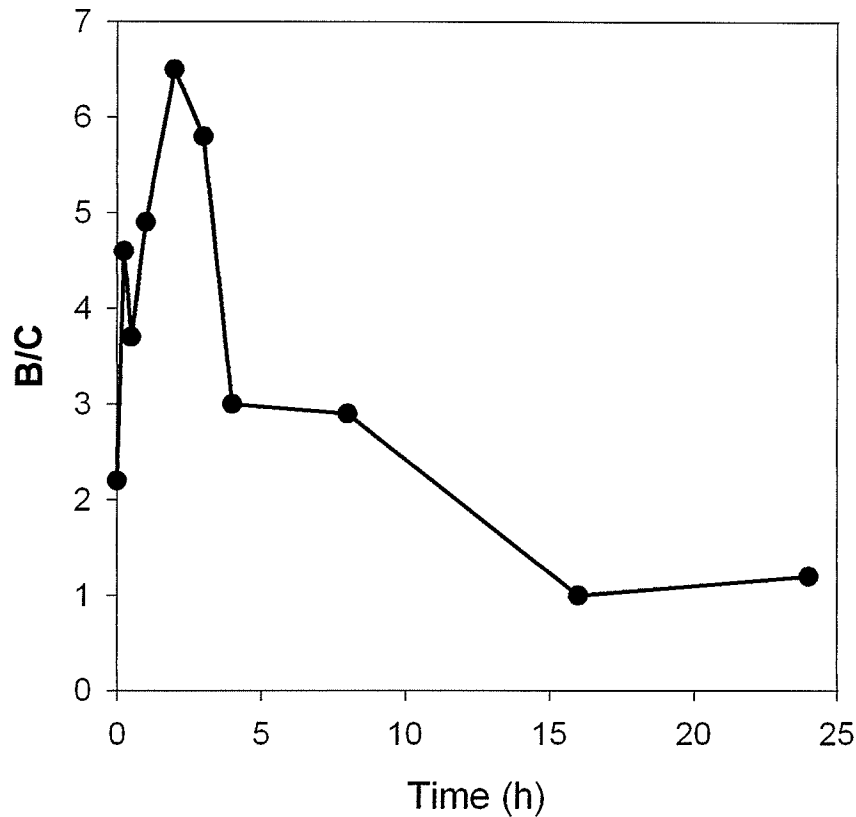
*Figure 3.12. The ratio of the averaged intermediate **B/C** plasma concentrations as a function of time.*

Metabolite concentrations for patient 5 was normalized to an initial infusion dose of 1500 mg/m^2 by multiply the metabolite concentrations by 1.5.

3.3.6 Pharmacokinetics of ADR-925

The ADR-925 plasma levels are tabulated in Table 3.12. The total ADR-925 levels are also plotted in Figure 3.13-3.18. ADR-925 was already detectable (9.5 ± 2.8 μM) in the plasma at the end of the dexrazoxane infusion period when the first sample was taken at $t = 0$ (Figure 3.18). ADR-925 then rapidly increased nearly three-fold to 29 ± 9 μM at 15 min post-infusion, remained relatively constant for the next 2-4 h and

then slowly deceased by about half at 24 h. By 16 h total ADR-925 levels exceeded that

of dexrazoxane, **B** or **C**.

Table 3.12. Plasma concentrations (μM) of ADR-925 for patients treated with a 1500 mg/m[2a] bolus of dexrazoxane hydrochloride.

Time (hr)	Patient number						Average[b]	SE
	1	2	3	4	5	5 [a]		
0	12.5		12.0		2.7	4.0	9.5	2.8
0.25	20.6	16.3	45.0	8.7			28.7	8.6
0.5	26.6	19.4	34.0	40.8	17.3	25.9	30.6	4.3
1	23.3	18.9	40.5	40.9	15.4	23.1	29.3	4.7
2	29.5	23.9	40.6	32.3	11.0	16.5	28.6	4.0
3	26.9			34.6	19.8	29.7	31.7	2.0
4		30.8	35.5		13.7	20.5	23.3	4.5
8					10.1	15.1	15.1	
12								
16					6.8	10.2	10.2	
24	7.6		10.0	35.6	5.5	8.3	17.2	8.0

[a] The concentration-time data for patient 5 has been normalized to a dexrazoxane dose of 1500 mg/m^2.

[b] Average ADR-925 plasma concentrations of all 5 patients where the normalized concentration-time points for patient 5 is included.

While the calcein assay was not sensitive to either dexrazoxane, **B**, or **C**, the possibility existed that other dexrazoxane-derived chelating metabolites that the calcein assay might detect were formed. In order to test this possibility an experiment was carried out on a single plasma sample obtained at 0.5 h post-dexrazoxane infusion, which when concentrated contained sufficient ADR-925 to measure both by HPLC and by the calcein assay. The plasma concentration of ADR-925 was measured to be 34 (as shown in Figure 3.4) and 40 μM using the HPLC and calcein assays, respectively. The agreement of these two values indicates that there were no other major detectable dexrazoxane-derived chelating metabolites formed *in vivo*.
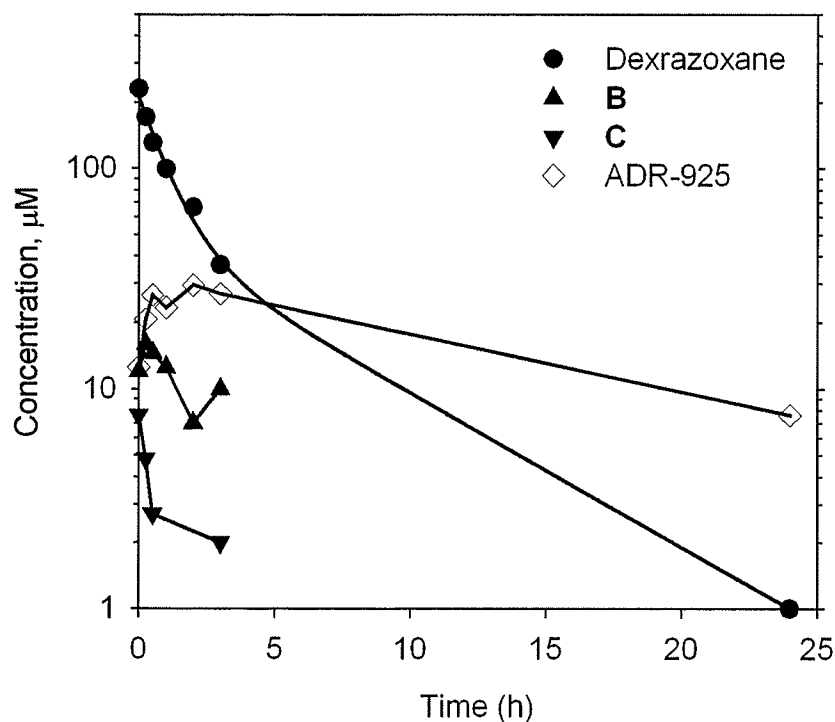
Figure 3.13. Plasma levels of dexrazoxane and dexrazoxane metabolites for patient 1 dosed with 1500 mg/m²dexrazoxane.

The smooth line was calculated from eqn. 3.1. The best fit to this data yielded $t_{1/2\alpha}$ 0.7 h, $t_{1/2\beta}$ 4.3 h, C_0 210 μM, $AUC_{0-\infty}$ 460 μM·h, and Cl_{tot} 202 ml·min⁻¹·m².
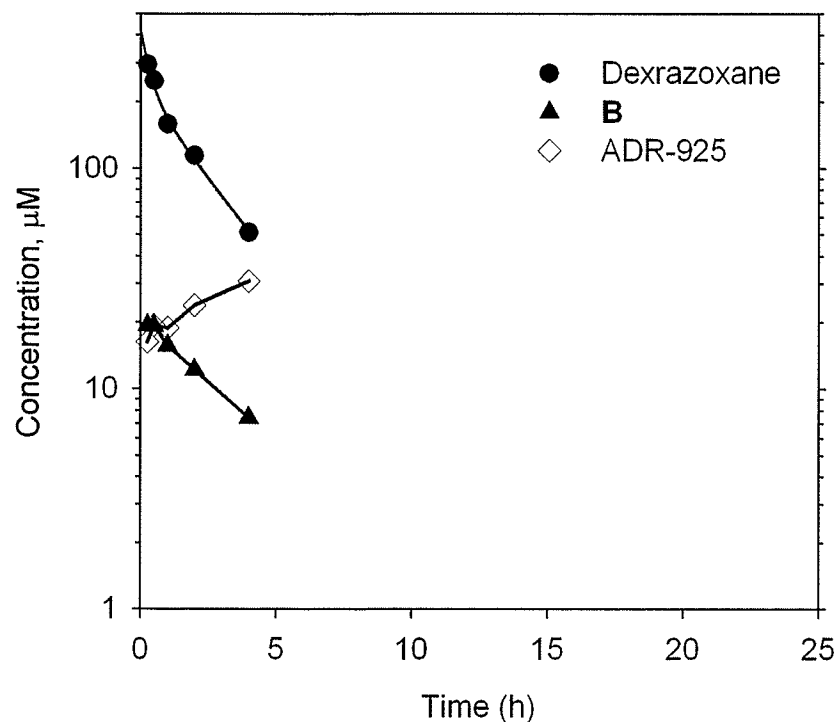
Figure 3.14. Plasma levels of dexrazoxane and dexrazoxane metabolites for patient 2 dosed with 1500 mg/m²dexrazoxane.

The smooth line was calculated from eqn. 3.1. The best fit to this data yielded $t_{1/2\alpha}$ 1.3 h, C_0 314 μM, $AUC_{0-\infty}$ 580 μM·h, and Cl_{tot} 161 ml·min⁻¹·m². The $t_{1/2\beta}$ for this patient was not calculated due to limited sampling (out to 4 h)

140
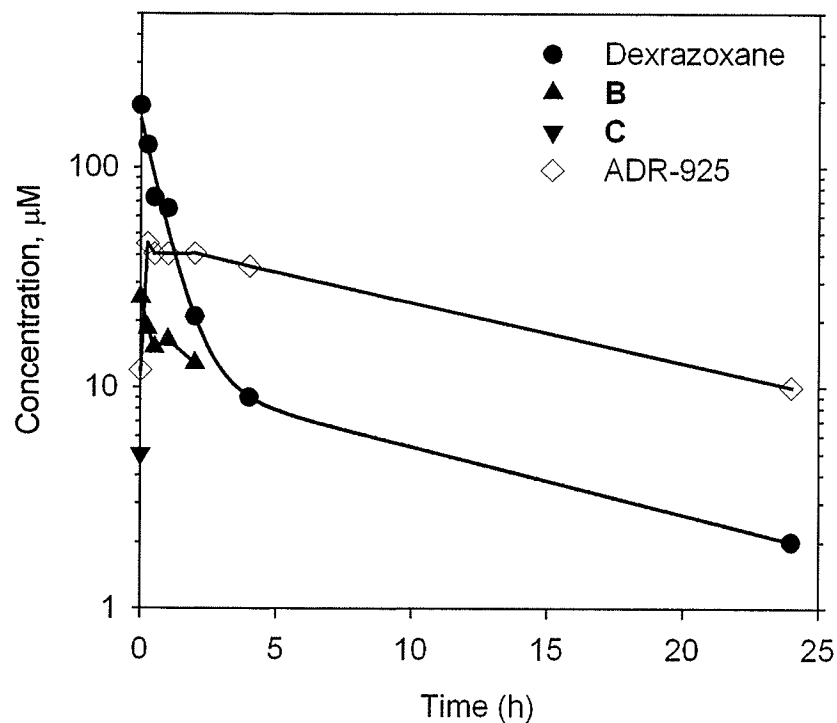
Figure 3.15. Plasma levels of dexrazoxane and dexrazoxane metabolites for patient 3 dosed with 1500 mg/m^2 dexrazoxane.

The smooth line was calculated from eqn. 3.1. The best fit to this data yielded $t_{1/2\alpha}$ 0.5 h, $t_{1/2\beta}$ 9.8 h, C_0 165 μM, $AUC_{0-\infty}$ 270 μM·h, and Cl_{tot} 345 ml·min^{-1}·m^2.
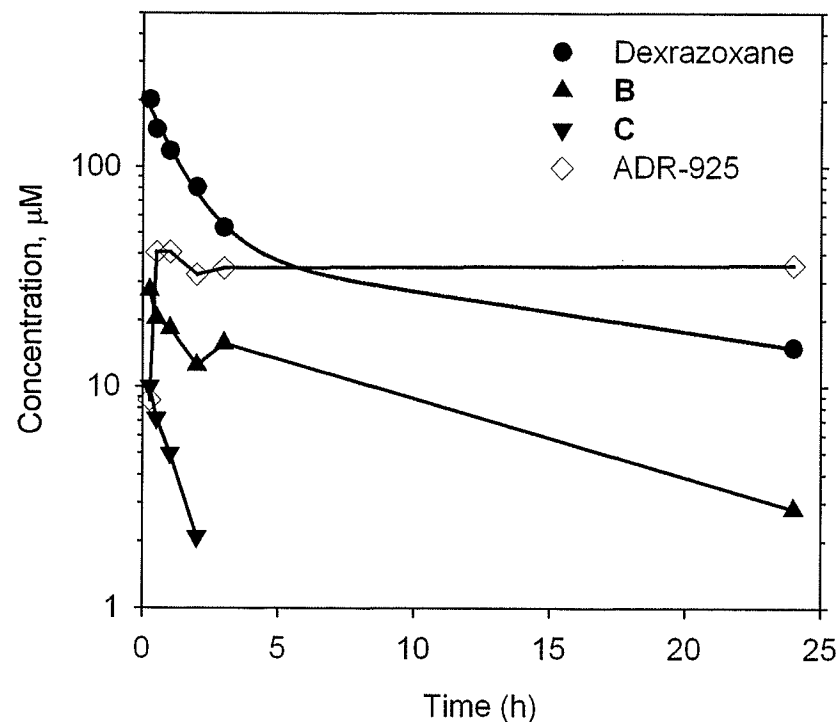
Figure 3.16. Plasma levels of dexrazoxane and dexrazoxane metabolites for patient 4 dosed with 1500 mg/m^2 dexrazoxane.

The smooth line was calculated from eqn. 3.1. The best fit to this data yielded $t_{1/2\alpha}$ 0.9 h, $t_{1/2\beta}$ 16.4 h, C_0 215 μM, $AUC_{0-\infty}$ 1210 μM·h, and Cl_{tot} 77 ml·min^{-1}·m^2.

141

Figure 3.17. Plasma levels of dexrazoxane and dexrazoxane metabolites for patient 5 dosed with 1000 mg/m² not dexrazoxane.

The smooth line was calculated from eqn. 3.1. The best fit to this data yielded $t_{1/2\alpha}$ 0.8 h, $t_{1/2\beta}$ 5.9 h, C_0 152 µM, $AUC_{0-\infty}$ 350 µM·h, and Cl_{tot} 266 ml·min⁻¹·m².

*Figure 3.18. Average plasma concentrations of dexrazoxane and dexrazoxane metabolites (both normalized to 1500 mg/m²) and the sum of the concentrations of dexrazoxane, **B**, **C**, and ADR-925 for all 5 patients after an i.v. dose of 1500 mg/m² dexrazoxane.*

The smooth line was calculated from eqn. 3.1. The best fit to this data yielded $t_{1/2\alpha}$ 0.4 h, $t_{1/2\beta}$ 5.8h, C_0 280 µM, $AUC_{0-\infty}$ 617 µM·h, and Cl_{tot} 151 ml·min⁻¹·m². Error bars on data points present the SEs. Least squares calculated straight lines are drawn through the averaged **B** and **C** data.

Figure 3.17. Plasma levels of dexrazoxane and dexrazoxane metabolites for patient 5 dosed with 1000 mg/m² dexrazoxane.

The smooth line was calculated from eqn. 3.1. The best fit to this data yielded $t_{1/2\alpha}$ 0.8 h, $t_{1/2\beta}$ 5.9 h, C_0 152 µM, $AUC_{0-\infty}$ 350 µM·h, and Cl_{tot} 266 ml·min⁻¹·m².

*Figure 3.18. Average plasma concentrations of dexrazoxane and dexrazoxane metabolites (both normalized to 1500 mg/m²) and the sum of the concentrations of dexrazoxane, **B**, **C**, and ADR-925 for all 5 patients after an i.v. dose of 1500 mg/m² dexrazoxane.*

The smooth line was calculated from eqn. 3.1. The best fit to this data yielded $t_{1/2\alpha}$ 0.4 h, $t_{1/2\beta}$ 5.8h, C_0 280 µM, $AUC_{0-\infty}$ 617 µM·h, and Cl_{tot} 151 ml·min⁻¹·m². Error bars on data points present the SEs. Least squares calculated straight lines are drawn through the averaged **B** and **C** data.

3.3.7 Etoposide pharmacokinetics

Plasma etoposide levels are shown in Table 3.13. The concentration-time curves of etoposide is shown in Figures 3.19 - 3.24 and is well described by a one-compartment model defined by a monoexponential decay. Describing the concentration-time data biexponentially, did not significantly improve the fit of the data for any patient.

Table 3.13. Plasma concentrations (μM) of etoposide for patients treated with a 500 mg/m^{2a,b} 90 min infusion of etoposide

Time (hr)	Patient number							Ave [c]	SE
	1	1 [a]	2	3	4	5	5 [b]		
0.25			33.6	44.7	11.7			30.0	9.7
0.5	4.8	3.7	72.8	98.6	40.6	19.2	9.6	45.1	18.2
1	65.8	50.6	121.3	145.0	79.7	62.0	31.0	85.5	21.3
2	148.8	114.4	77.3	89.7	173.2	190.6	95.3	110.0	16.9
3	65.4	50.3			166.9			108.6	82.4
4			62.7	66.6		155.7	77.8	69.0	4.5
8						115.2	57.6	57.6	
12						71.6	35.8	35.8	
16						46.2	23.1	23.1	
24	1.7	1.3		2.2	15.0	3.1	1.6	5.0	3.3

[a] The concentration-time data for patient 1 (650 mg/m^2) has been normalized to an etoposide dose of 500 mg/m^2 by multiplying the concentration by 0.77.

[b] The concentration-time data for patient 5 (1000 mg/m^2) has been normalized to an etoposide dose of 500 mg/m^2 by multiplying the concentration by 0.5.

[c] Average etoposide plasma concentrations of all 5 patients where the normalized concentration-time points for patient 1 and 5 is included.

Three patients were dosed at 500 mg/m^2, one was dosed at 650 mg/m^2 and one was dosed at 1000 mg/m^2 of etoposide. Etoposide plasma levels are dose-linear (Hande et al., 1984; Holthuis et al., 1986; Green et al., 1988; Newman et al., 1988; Schwinghammer, 1994; Wurthwein and Boos, 2002), thus pharmacokinetic analysis involving the average of all patients was accomplished by normalizing the etoposide dose to 500 mg/m^2. For the patients dosed with 1000 mg/m^2 and 650 mg/m^2 of etoposide the observed plasma

concentrations were multiplied by 0.5 and 0.77, respectively. Table 3.14 contains the pharmacokinetic parameters for the individual patients. The maximum plasma etoposide concentration ranged from 85 to 180 μM with a mean value of 133 ± 43 μM. The $t_{1/2\beta}$ ranged from 2.6 to 7.4 h with a mean value of 5.2 ± 2.4 h. The plasma etoposide clearance ranged from 8.0 to 25 ml·min^{-1}·m^2 with a mean value of 16.2 ± 7.0 ml·min^{-1}·m^2. Because blood sampling after completion of etoposide infusion from some patients was sparse, deriving the pharmacokinetic parameters from the combination of all the patients' concentration-time points was deemed appropriate. For this determination, patients dosed with 650 and 1000 mg/m^2 were normalized to 500 mg/m^2. The etoposide $t_{1/2\beta}$ and plasma clearance derived from the concentration-time curve of from all the patients concentration-time data was 5.9 h and 12 ml·min^{-1}·m^2, respectively.

Table 3.14. Pharmacokinetic parameters for the elimination of dexrazoxane following a 500 mg/m^{2a} etoposide infusion.

Patient number	Etoposide dose (mg/m^2)	Sex	$t_{1/2\beta}$ (h)	C_0 (μM)	AUC$_{0-\infty}$ (μM·h)	Cl$_{tot}$ ml·min^{-1}·m^2
1[a]	650	F	3.8	88	560	25
2	500	M	ND	150	ND	ND
3	500	F	2.6	180	820	17
4	500	M	7.2	160	1770	8.0
5[a]	1000	M	7.4	85	980	15
Mean[b]			5.2	133	1030	16.2
SE			2.4	43	520	7.0
Average[c]	500		5.9	125	1150	12.0
SE[d]			1.2	12.2	203	2.1

[a] Etoposide plasma concentration-time data for patients 1 and 5 were normalized to 500 mg/m^2.

[b] Mean Value of C_0 and AUC$_{0-inf}$ for patients 1 and 5 have been normalized to 500 mg/m^2 by multiplying parameters C_0 and AUC$_{0-\infty}$ by 0.77 and 0.5 respectively.

[c] Pharmacokinetic parameters obtained from the individual concentration-time points of all 5 patients (where patients 1 and 5 concentration-time points were normalized to an etoposide dose of 500 mg/m^2) modeled to equation 3.8.

[d] Standard errors obtained from modeling data to equation 3.8.

144
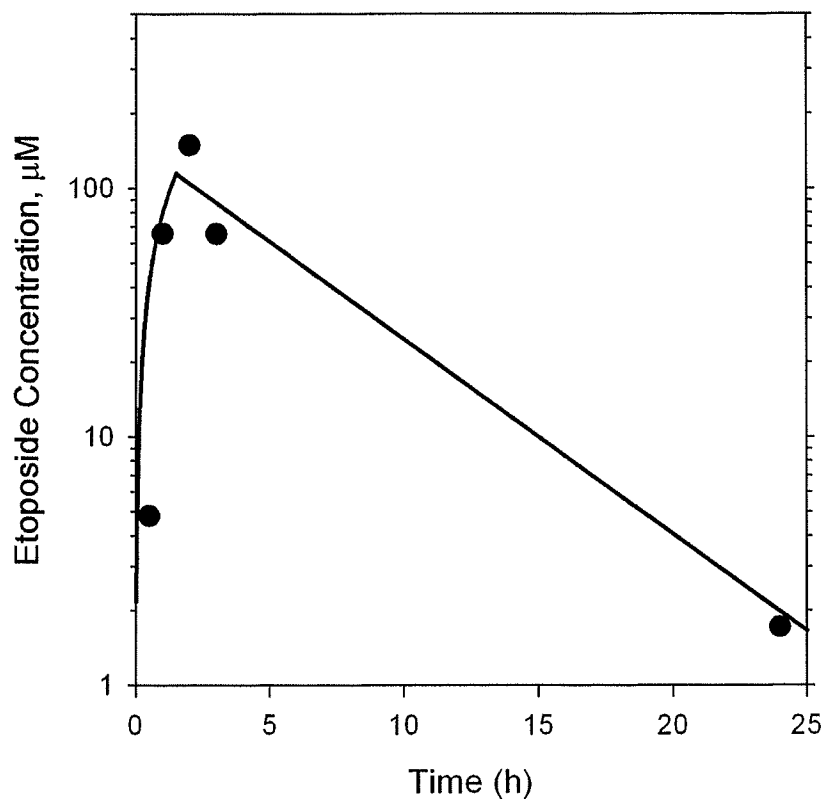
Figure 3.19 Plasma concentration of etoposide for patient 1 after an i.v. *dose of 650 mg/m² etoposide.*

The best fit to this data yielded $t_{\frac{1}{2}\beta}$ 3.8 h, C_0 88 μM, $AUC_{0-\infty}$ 560 μM·h, and Cl_{tot} 25 ml·min^{-1}·m².
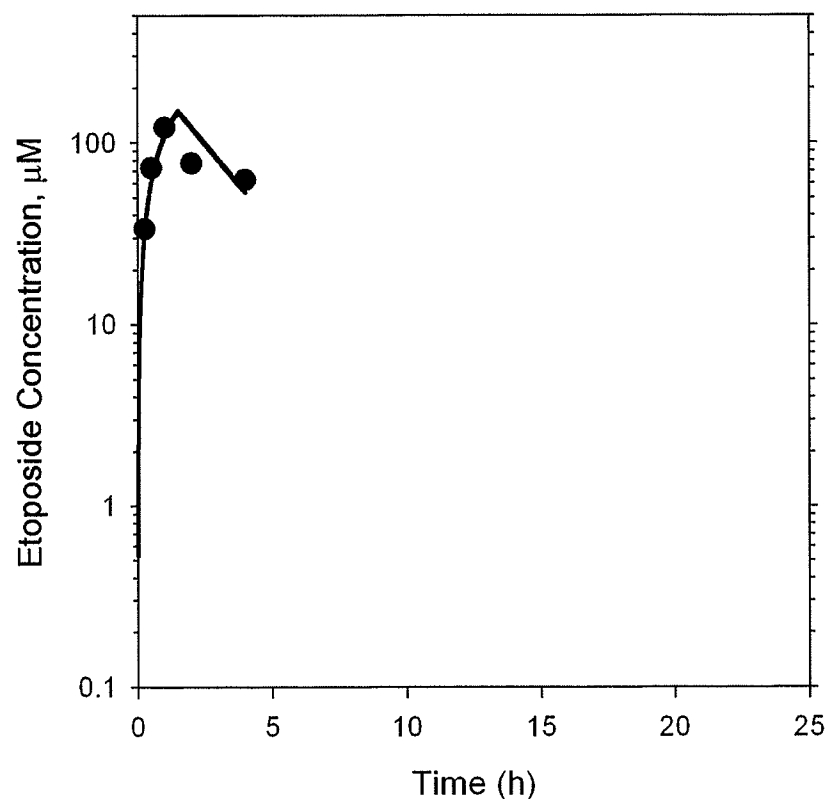
Figure 3.20 Plasma concentration of etoposide for patient 2 after an i.v. *dose of 500 mg/m² etoposide.*

The best fit to this data yielded C_0 150 μM. Other pharmacokinetic parameters where not determined due to limited sampling times (to 4 h).
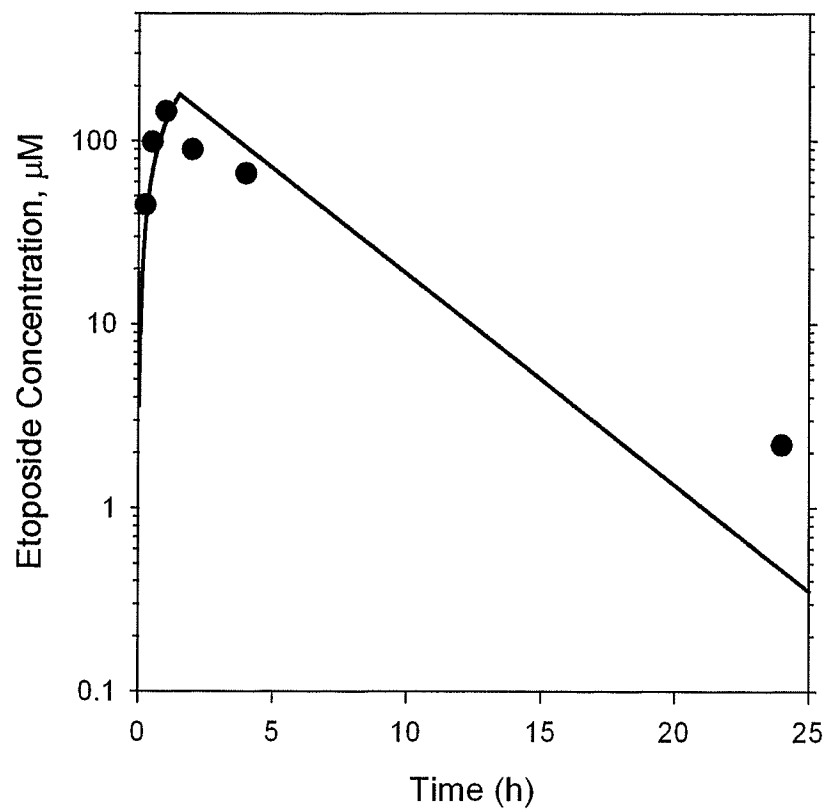
Figure 3.21 Plasma concentration of etoposide for patient 3 after an i.v. *dose of 500 mg/m² etoposide.*

The best fit to this data yielded $t_{1/2\beta}$ 2.6 h, C_0 180 μM, $AUC_{0-\infty}$ 820 μM·h, and Cl_{tot} 17 ml·min⁻¹·m².
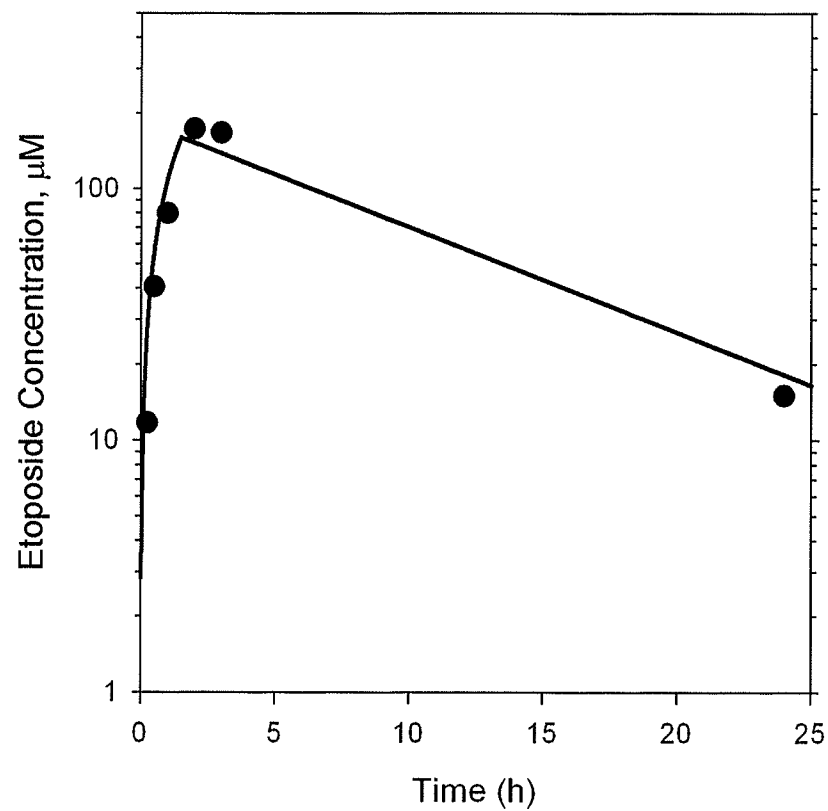
Figure 3.22 Plasma concentration of etoposide for patient 4 after an i.v. *dose of 500 mg/m² etoposide.*

The best fit to this data yielded $t_{1/2\beta}$ 7.2 h, C_0 160 μM, $AUC_{0-\infty}$ 1770 μM·h, and Cl_{tot} 8 ml·min⁻¹·m².

146
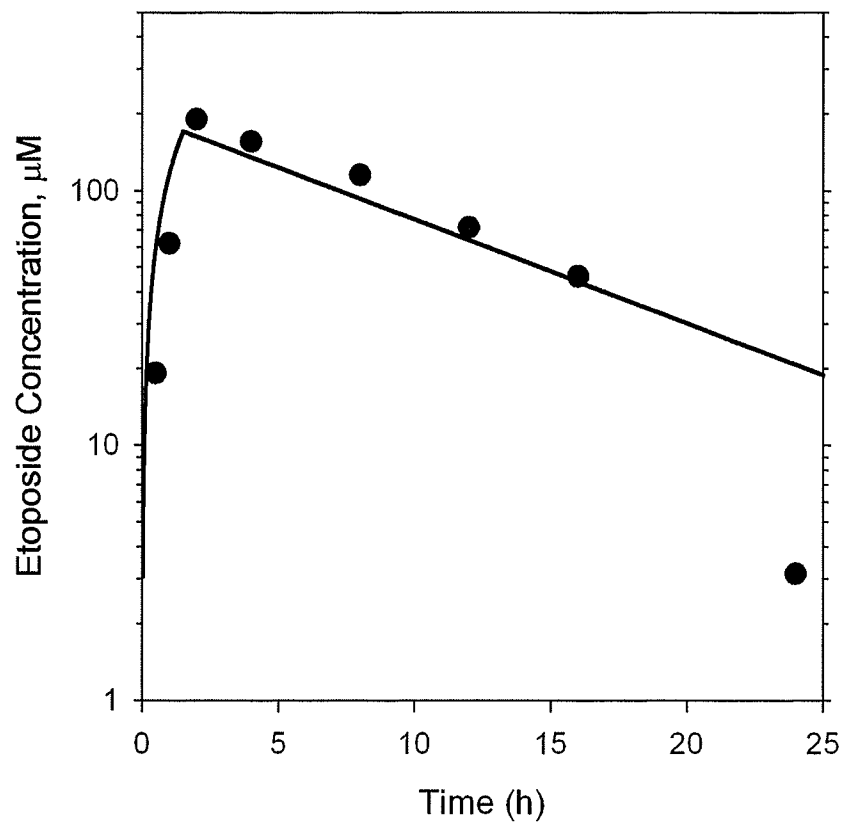
Figure 3.23 Plasma concentration of etoposide for patient 5 after an i.v. *dose of 1000 mg/m² etoposide.*

The best fit to this data yielded $t_{1/2\beta}$ 7.4 h, C_0 85 μM, $AUC_{0-\infty}$ 980 μM·h, and Cl_{tot} 15 ml·min^{-1}·m².
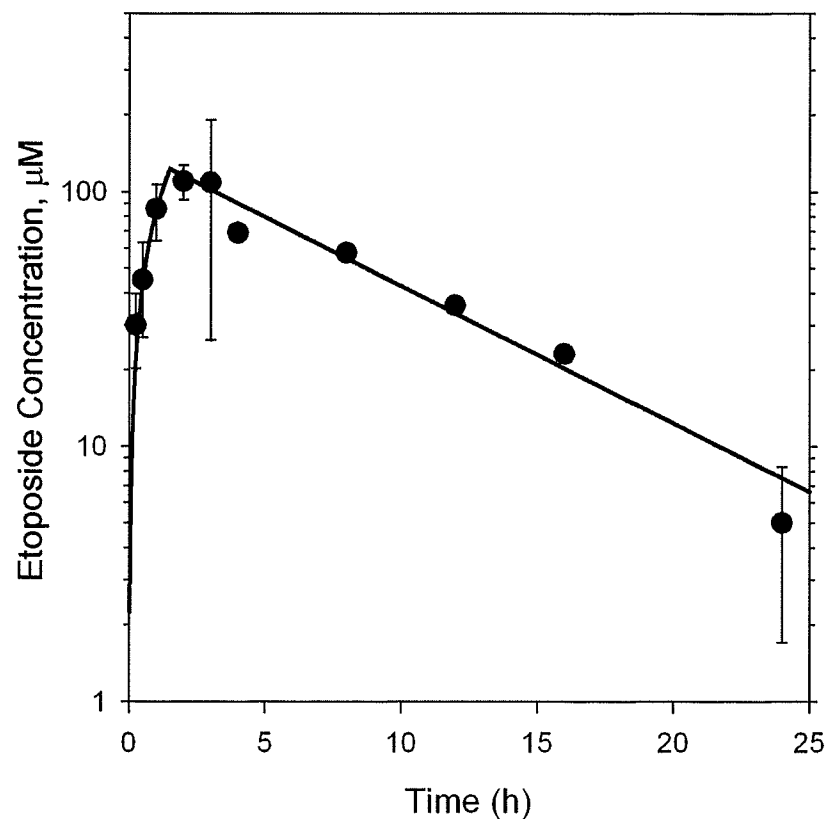
Figure 3.24 Average plasma concentration of etoposide (normalized to 500 mg/m²) for all 5 patients after an i.v. *dose of 500 mg/m² etoposide.*

The best fit to this data yielded $t_{1/2\beta}$ 5.9 h, C_0 125 μM, $AUC_{0-\infty}$ 1150 μM·h, and Cl_{tot} 12 ml·min^{-1}·m².

147

3.4 Discussion

3.4.1 Pharmacokinetics of dexrazoxane

The values of $t_{1/2\alpha}$ of 0.8 ± 0.3 h and a $t_{1/2\beta}$ of 9.1 ± 5.4 h determined in this study agreed well with those of Hochster (Hochster et al., 1992) in which a $t_{1/2\alpha}$ of 0.46 ± 0.30 h and a $t_{1/2\beta}$ of 4.2 ± 2.9 h was obtained. A variety of other studies found $t_{1/2\alpha}$ values ranging from 0.17 to 0.47 h and $t_{1/2\beta}$ values ranging from 1.1 to 13.9 h, determined with (Hochster et al., 1992; Jakobsen et al., 1994), and without (Earhart et al., 1982; Myers, 1998; Tetef et al., 2001) anthracycline treatment. While this study was not specifically designed to test whether high-dose etoposide treatment affected dexrazoxane pharmacokinetics, the agreement of our results with these other studies suggest that etoposide treatment did not affect dexrazoxane pharmacokinetics.

3.4.2 Dexrazoxane metabolism to intermediates B and C

No other study in humans has shown the presence of dexrazoxane intermediates **B** and **C** after dexrazoxane treatment, though it was previously demonstrated that **B** and **C** rapidly appeared in the plasma of the dexrazoxane-treated rat (maximally reaching 24 and 9%, respectively, of the dexrazoxane concentration at 2 h) (Hasinoff and Aoyama, 1999). The results of this study that showed that the percentage **B** ranged from an initial value of 8 to 29% of the dexrazoxane value at 4 h, and that the percentage **C** was a nearly constant 3 to 5% of dexrazoxane levels, are not greatly different from that found in the rat, suggesting that the two species have common dexrazoxane metabolic pathways. The **B/C** ratio (Figure 3.12) seen at time zero of 2.4 and its increase with time to 6.4 at 3 h is also similar to that seen previously in a rat model in which an initial value of 2.7 at 5 min and

6.5 at 3 h was seen (Hasinoff and Aoyama, 1999). While sampling was sparse for these time points, these results tentatively suggest that the metabolism in these two species was similar.

Dihydropyrimidinase (DHPase) is the second enzyme in the breakdown of the pyrimidine bases, catalyzing the degradation of dihydrouracil and dihydrothymine to β-ureidopropionic acid and β-ureidoisobutyric acid (Kikugawa et al., 1994), respectively, and has been shown to enzymatically hydrolyze dexrazoxane (Hasinoff et al., 1991; Hasinoff, 1993; Hasinoff, 1994c). Purified DHPase has been shown to catalyze the ring opening of dexrazoxane to give a **B/C** ratio of 2.9-6.1 depending upon the pH (Hasinoff, 1993). In primary rat hepatocytes treated with dexrazoxane, the initial **B/C** ratio was found to be 2.7 (Hasinoff et al., 1994). Thus the initial **B/C** ratio of 2.4 seen in this study is consistent with dexrazoxane being metabolized by DHPase as previously concluded in the *in vivo* rat model (Hasinoff and Aoyama, 1999) and rat hepatocyte model studies (Hasinoff et al., 1994). The increase in the **B/C** ratio with time seen here (Figure 3.12) and in the rat (Hasinoff and Aoyama, 1999) suggests that **C** was metabolized to ADR-925 at a faster rate than **B** by some unknown enzyme. This enzyme cannot be DHPase as DHPase is unable to convert the one-ring open intermediates **B** and **C** into ADR-925 (Hasinoff et al., 1991; Hasinoff, 1993). The increase in the **B/C** ratio with time is unlikely due to differences in distribution or elimination rates of **B** and **C** as their structures are so similar.

Dexrazoxane undergoes a slow base-catalyzed hydrolysis to **B** and **C** ($t_{\frac{1}{2}}$ of 9.3 h) and then to ADR-925 ($t_{\frac{1}{2}}$ of 23 h) under physiological conditions (37 °C and pH 7.4) (Hasinoff, 1990a; Hasinoff, 1994a). Given the slow rate of the *in vitro* hydrolysis of

dexrazoxane under physiological conditions little of the **B** and **C** seen *in vivo* could have been formed from base-catalyzed hydrolysis of dexrazoxane ((Hasinoff, 1990a), (Hasinoff, 1994a). Therefore, the appearance of metabolites **B** and **C** must have resulted from rapid metabolism of dexrazoxane.

3.4.3   B and C metabolism to ADR-925

The presence of ADR-925, the presumably active iron-chelating metabolite of dexrazoxane, in the plasma of patients administered dexrazoxane has not been previously determined. The data of Figure 3.18 show that ADR-925 was rapidly produced after dexrazoxane administration, which suggests that either **B** or **C**, or both, were rapidly metabolized to ADR-925. The relative lack of change in the level of ADR-925 after 10 h suggested that ADR-925 was in a dynamic steady state.

ADR-925, the rings-opened hydrolysis product of dexrazoxane and analog of EDTA, is a strong chelator of Fe^{2+} (K_f $10^{10.0}$ M^{-1}) (Huang et al., 1982) and of Fe^{3+} (K_f $10^{18.2}$ M^{-1}) (Diop et al., 2000). ADR-925 is able to quickly ($t_{1/2}$ 1.7 min) and efficiently remove Fe^{3+} from its complex with doxorubicin (Hasinoff, 1989a; Buss and Hasinoff, 1993; Hasinoff, 1998; Hasinoff et al., 1998), and thus prevent iron-based doxorubicin-mediated free radical oxidative stress on the heart muscle (Gianni et al., 1985; Malisza and Hasinoff, 1995; Myers, 1998).

Previous animal studies have shown that the timing of dexrazoxane dosing is critical for it to exert its protective effects (Herman et al., 1983; Herman and Ferrans, 1993). Maximal protective effects are seen when dexrazoxane is given between 3 h before and 3 h after daunorubicin treatment of Syrian golden hamsters (Herman et al., 1983). Likewise, doxorubicin-induced cardiomyopathy was reduced in beagle dogs

receiving dexrazoxane simultaneously compared to those that received dexrazoxane 2 h after doxorubicin treatment (Herman and Ferrans, 1993). These results were the basis for the recommendation that in a clinical setting after completing the infusion of dexrazoxane, and prior to a total elapsed time of 30 min (from the beginning of the dexrazoxane infusion), the intravenous injection of doxorubicin should be given. The results of this study show that ADR-925 rapidly appeared in the plasma after dexrazoxane administration and now provide a pharmacodynamic basis for this dosing schedule.

This study did not directly address how dexrazoxane exerts its doxorubicin cardioprotective effects in the heart. It has been previously shown that while a suspension of rat primary hepatocytes (Hasinoff et al., 1994) and supernatants of liver and kidney homogenates did enzymatically hydrolyze dexrazoxane, that of heart did not (Hasinoff et al., 1991). DHPase was shown to be responsible for this enzymatic hydrolysis (Hasinoff et al., 1991; Hasinoff, 1993; Hasinoff, 1994b; Hasinoff et al., 1994). Dexrazoxane is cellular permeable (Dawson, 1975) and should thus be readily taken up by tissues. The fact that dexrazoxane was not metabolized *in vitro* in plasma, and that **B**, **C**, and ADR-925 rapidly appeared in the plasma (Figure 3.18), indicated that dexrazoxane was rapidly metabolized in tissues and that **B** and **C** were cell permeable enough to be rapidly released into the blood. Thus, it follows that even if dexrazoxane is not metabolized in the heart, **B** and **C** are probably cell permeable enough to be taken up by heart tissue and to be present at high enough concentrations to chelate free iron in the heart and prevent the formation of the Fe^{3+}–doxorubicin complex or remove Fe^{3+} from the Fe^{3+}–doxorubicin complex.   Thus, it remains difficult to determine whether the ADR-925

blood plasma levels are representative of ADR-925 that was released from tissues or hydrolysis of C in the blood.

3.4.4 Pharmacokinetics of etoposide

The pharmacokinetic parameters of etoposide at the doses studied here did not differ significantly from those cited in the literature (Hande et al., 1984; Holthuis et al., 1986; Green et al., 1988; Newman et al., 1988; Kohl et al., 1992). However, the alpha phase in the concentration-time curve, which is generally reflective of etoposide distribution, was not significantly observed in any patient. This was probably due to a combination of a relatively long infusion time of 90 min and sparse blood sampling during the theoretical alpha phase of the etoposide distribution curve.

The average values of $t_{\frac{1}{2}\beta}$ determined in this study are comparable to $t_{\frac{1}{2}\beta}$ values cited in the literature ranging from 3 to 8 h (Hande et al., 1984; Holthuis et al., 1986; Green et al., 1988; Newman et al., 1988; Kohl et al., 1992). The mean plasma clearance of etoposide, found in this study to be 16.2 ml·min^{-1}·m^2, was also consistent with that found in the literature ranging from 17.7 to 28.0 ml·min^{-1}·m^2 (Hande et al., 1984; Sinkule et al., 1984; Holthuis et al., 1986; Newman et al., 1988). These results are also consistent with previously published data concluding that these parameters are independent of dose and are comparable between high and low etoposide dose regimens (Hande et al., 1984; Holthuis et al., 1986; Newman et al., 1988).

This study also does not directly address how dexrazoxane exerts its extracerebral etoposide rescue effects. There is considerable *in vivo* evidence that doxorubicin-induced cardiotoxicity is due to iron-based oxidative stress (Gianni et al., 1985; Hasinoff, 1989b; Hasinoff, 1990b; Malisza and Hasinoff, 1995; Myers, 1998). Likewise, there is also some

evidence that etoposide toxicity may also be due to oxidative stress as it has been shown that etoposide can be activated by peroxidase (Kagan et al., 1999; Kagan et al., 2001) and tyrosinase (Usui and Sinha, 1990; Tyurina et al., 1995) to form etoposide phenoxyl free radicals. These radicals have been shown to deplete antioxidant cellular sulfhydryl compounds, the oxidation of which can lead to superoxide and H_2O_2 formation, leading to iron-based oxygen radical damage. Alternatively, the etoposide rescue effect of dexrazoxane may be due to the fact that it is a strong catalytic inhibitor of topoisomerase II (Hasinoff et al., 1995) which is able to antagonize (Sehested et al., 1993; Hasinoff et al., 1996; Jensen and Sehested, 1997) etoposide-induced cytotoxicity and cellular damage.

The premise behind this treatment schedule is that etoposide, a relatively lipophilic drug, will cross the blood brain barrier, where the hydrophilic drug, dexrazoxane will not, lending the possibility of dexrazoxane-mediated protection against extracerebral etoposide toxicity. Although this Phase I/II study does not explain the mechanism of dexrazoxane rescue, it does indicate that etoposide pharmacokinetics are not affected by dexrazoxane co-administration. This, along with encouraging preclinical animal studies, lends a potential for the clinical use of dexrazoxane as a rescue agent in the future.

3.5 References

Buss JL and Hasinoff BB (1993) The one-ring open hydrolysis product intermediates of the cardioprotective agent ICRF-187 (dexrazoxane) displace iron from iron-anthracycline complexes. *Agents Actions* **40:**86-95.

Cai X, Woo MH, Edick MJ and Relling MV (1999) Simultaneous quantitation of etoposide and its catechol metabolite in human plasma using high-performance liquid chromatography with electrochemical detection. *J Chromatogr B Biomed Sci Appl* **728:**241-250.

Dawson KM (1975) Studies on the stability and cellular distribution of dioxopiperazines in cultured BHK-21S cells. *Biochem Pharmacol* **24:**2249-2253.

Diop NK, Vitellaro LK, Arnold P, Shang M and Marusak RA (2000) Iron complexes of the cardioprotective agent dexrazoxane (ICRF-187) and its desmethyl derivative, ICRF-154: solid state structure, solution thermodynamics, and DNA cleavage activity. *J Inorg Biochem* **78:**209-216.

Earhart RH, Tutsch KD, Koeller JM, Rodriguez R, Robins HI, Vogel CL, Davis HL and Tormey DC (1982) Pharmacokinetics of (+)-1,2-di(3,5-dioxopiperazin-1-yl)propane intravenous infusions in adult cancer patients. *Cancer Res* **42:**5255-5261.

Gianni L, Zweier JL, Levy A and Myers CE (1985) Characterization of the cycle of iron-mediated electron transfer from Adriamycin to molecular oxygen. *J Biol Chem* **260:**6820-6826.

Green JA, Tarpey AW and Warenius HM (1988) Pharmacokinetic study of high dose etoposide infusion in patients with small cell lung cancer. *Acta Oncol* **27:**819-822.

Hande KR, Wedlund PJ, Noone RM, Wilkinson GR, Greco FA and Wolff SN (1984) Pharmacokinetics of high-dose etoposide (VP-16-213) administered to cancer patients. *Cancer Res* **44:**379-382.

Hasinoff BB (1989a) The interaction of the cardioprotective agent ICRF-187 [+)-1,2-bis(3,5- dioxopiperazinyl-1-yL)propane); its hydrolysis product (ICRF-198); and other chelating agents with the Fe(III) and Cu(II) complexes of adriamycin. *Agents Actions* **26:**378-385.

Hasinoff BB (1989b) Self-reduction of the iron(III)-doxorubicin complex. *Free Radic Biol Med* **7:**583-593.

Hasinoff BB (1990a) The hydrolysis activation of the doxorubicin cardioprotective agent ICRF-187 (+)-1,2-bis(3,5-dioxopiperazinyl-1-yl)propane). *Drug Metab Dispos* **18:**344-349.

Hasinoff BB (1990b) Oxyradical production results from the Fe3(+)-doxorubicin complex undergoing self-reduction by its alpha-ketol group. *Biochem Cell Biol* **68:**1331-1336.

Hasinoff BB (1993) Enzymatic ring-opening reactions of the chiral cardioprotective agent (+) (S)-ICRF-187 and its (-) (R)-enantiomer ICRF-186 by dihydropyrimidine amidohydrolase. *Drug Metab Dispos* **21:**883-888.

Hasinoff BB (1994a) Pharmacodynamics of the hydrolysis-activation of the cardioprotective agent (+)-1,2-bis(3,5-dioxopiperazinyl-1-yl)propane. *J Pharm Sci* **83:**64-67.

Hasinoff BB (1994b) Stereoselective hydrolysis of ICRF-187 (dexrazoxane) and ICRF-186 by dihydropyrimidine amidohydrolase. *Chirality* **6:**213-215.

Hasinoff BB (1994c) Stereoselective hydrolysis of ICRF-187 (dexrazoxane) and ICRF-186 by dihydropyrimidine amidohydrolase. *Chirality* **6:**213-215.

Hasinoff BB (1998) Chemistry of dexrazoxane and analogues. *Semin Oncol* **25:**3-9.

Hasinoff BB and Aoyama RG (1999) Relative plasma levels of the cardioprotective drug dexrazoxane and its two active ring-opened metabolites in the rat. *Drug Metab Dispos* **27:**265-268.

Hasinoff BB, Hellmann K, Herman EH and Ferrans VJ (1998) Chemical, biological and clinical aspects of dexrazoxane and other bisdioxopiperazines. *Curr Med Chem* **5:**1-28.

Hasinoff BB, Kuschak TI, Yalowich JC and Creighton AM (1995) A QSAR study comparing the cytotoxicity and DNA topoisomerase II inhibitory effects of bisdioxopiperazine analogs of ICRF-187 (dexrazoxane). *Biochem Pharmacol* **50:**953-958.

Hasinoff BB, Reinders FX and Clark V (1991) The enzymatic hydrolysis-activation of the adriamycin cardioprotective agent (+)-1,2-bis(3,5-dioxopiperazinyl-1-yl)propane. *Drug Metab Dispos* **19:**74-80.

Hasinoff BB, Venkataram S, Singh M and Kuschak TI (1994) Metabolism of the cardioprotective agents dexrazoxane (ICRF-187) and levrazoxane (ICRF-186) by the isolated hepatocyte. *Xenobiotica* **24:**977-987.

Hasinoff BB, Yalowich JC, Ling Y and Buss JL (1996) The effect of dexrazoxane (ICRF-187) on doxorubicin- and daunorubicin- mediated growth inhibition of Chinese hamster ovary cells. *Anticancer Drugs* **7:**558-567.

Herman EH, El-Hage AN, Ferrans VJ and Witiak DT (1983) Reduction by ICRF-187 of acute daunorubicin toxicity in Syrian golden hamsters. *Res Commun Chem Pathol Pharmacol* **40:**217-231.

Herman EH and Ferrans VJ (1993) Timing of treatment with ICRF-187 and its effect on chronic doxorubicin cardiotoxicity. *Cancer Chemother Pharmacol* **32:**445-449.

Hochster H, Liebes L, Wadler S, Oratz R, Wernz JC, Meyers M, Green M, Blum RH and Speyer JL (1992) Pharmacokinetics of the cardioprotector ADR-529 (ICRF-187) in escalating doses combined with fixed-dose doxorubicin. *J Natl Cancer Inst* **84:**1725-1730.

Holm B, Jensen PB and Sehested M (1996) ICRF-187 rescue in etoposide treatment in vivo. A model targeting high- dose topoisomerase II poisons to CNS tumors. *Cancer Chemother Pharmacol* **38:**203-209.

Holm B, Sehested M and Jensen PB (1998) Improved targeting of brain tumors using dexrazoxane rescue of topoisomerase II combined with supralethal doses of etoposide and teniposide. *Clin Cancer Res* **4:**1367-1373.

Holthuis JJ, Postmus PE, Van Oort WJ, Hulshoff B, Verleun H, Sleijfer DT and Mulder NH (1986) Pharmacokinetics of high dose etoposide (VP 16-213). *Eur J Cancer Clin Oncol* **22:**1149-1155.

Huang ZX, May PM, Quinlan KM, Williams DR and Creighton AM (1982) Metal binding by pharmaceuticals. Part 2. Interactions of Ca(II), Cu(II), Fe(II), Mg(II), Mn(II) and Zn(II) with the intracellular hydrolysis products of the antitumour agent ICRF 159 and its inactive homologue ICRF 192. *Agents Actions* **12:**536-542.

Jakobsen P, Sorensen B, Bastholt L, Mirza MR, Gjedde SB, Mouridsen HT and Rose C (1994) The pharmacokinetics of high-dose epirubicin and of the cardioprotector ADR-529 given together with cyclophosphamide, 5-fluorouracil, and tamoxifen in metastatic breast-cancer patients. *Cancer Chemother Pharmacol* **35:**45-52.

Jensen PB and Sehested M (1997) DNA topoisomerase II rescue by catalytic inhibitors: a new strategy to improve the antitumor selectivity of etoposide. *Biochem Pharmacol* **54:**755-759.

Kagan VE, Kuzmenko AI, Tyurina YY, Shvedova AA, Matsura T and Yalowich JC (2001) Pro-oxidant and antioxidant mechanisms of etoposide in HL-60 cells: role of myeloperoxidase. *Cancer Res* **61:**7777-7784.

Kagan VE, Yalowich JC, Borisenko GG, Tyurina YY, Tyurin VA, Thampatty P and
    Fabisiak JP (1999) Mechanism-based chemopreventive strategies against
    etoposide-induced acute myeloid leukemia: free radical/antioxidant approach. *Mol
    Pharmacol* **56**:494-506.

Kikugawa M, Kaneko M, Fujimoto-Sakata S, Maeda M, Kawasaki K, Takagi T and
    Tamaki N (1994) Purification, characterization and inhibition of
    dihydropyrimidinase from rat liver. *Eur J Biochem* **219**:393-399.

Kohl P, Koppler H, Schmidt L, Fritsch HW, Holz J, Pfluger KH and Jungclas H (1992)
    Pharmacokinetics of high-dose etoposide after short-term infusion. *Cancer
    Chemother Pharmacol* **29**:316-320.

Mader RM, Steger GG, Moser K, Rainer H, Krenmayr P and Dittrich C (1991) Instability
    of the anticancer agent etoposide under in vitro culture conditions. *Cancer
    Chemother Pharmacol* **27**:354-360.

Malisza KL and Hasinoff BB (1995) Production of hydroxyl radical by iron(III)-
    anthraquinone complexes through self-reduction and through reductive activation
    by the xanthine oxidase/hypoxanthine system. *Arch Biochem Biophys* **321**:51-60.

Myers C (1998) The role of iron in doxorubicin-induced cardiomyopathy. *Semin Oncol*
    25:10-14.

Newman EM, Doroshow JH, Forman SJ and Blume KG (1988) Pharmacokinetics of
    high-dose etoposide. *Clin Pharmacol Ther* **43**:561-564.

Robieux I, Aita P, Sorio R, Toffoli G and Boiocchi M (1996) Determination of unbound
    etoposide concentration in ultrafiltered plasma by high-performance liquid
    chromatography with fluorimetric detection. *J Chromatogr B Biomed Appl*
    686:35-41.

Schroeder PE and Hasinoff BB (2002) The doxorubicin-cardioprotective drug
    dexrazoxane undergoes metabolism in the rat to its metal ion-chelating form
    ADR-925. *Cancer Chemother Pharmacol* **50**:509-513.

Schroeder PE, Hofland KF, Jensen PB, Sehested M, Langer SW and Hasinoff BB
    (2003a) Pharmacokinetics of etoposide in cancer patients treated with high-dose
    etoposide and with dexrazoxane (ICRF-187) as a rescue agent. *Cancer Chemother
    Pharmacol* **22**:22.

Schroeder PE, Jensen PB, Sehested M, Hofland KF, Langer SW and Hasinoff BB
    (2003b) Metabolism of dexrazoxane (ICRF-187) used as a rescue agent in cancer
    patients treated with high-dose etoposide. *Cancer Chemother Pharmacol* **52**:167-
    174.

Schwinghammer TL (1994) Safety, pharmacokinetics, and pharmacodynamics of high-dose etoposide. *J Clin Oncol* **12:**2768-2769.

Sehested M, Jensen PB, Sorensen BS, Holm B, Friche E and Demant EJ (1993) Antagonistic effect of the cardioprotector (+)-1,2-bis(3,5- dioxopiperazinyl-1-yl)propane (ICRF-187) on DNA breaks and cytotoxicity induced by the topoisomerase II directed drugs daunorubicin and etoposide (VP-16). *Biochem Pharmacol* **46:**389-393.

Sinkule JA, Hutson P, Hayes FA, Etcubanas E and Evans W (1984) Pharmacokinetics of etoposide (VP16) in children and adolescents with refractory solid tumors. *Cancer Res* **44:**3109-3113.

Tetef ML, Synold TW, Chow W, Leong L, Margolin K, Morgan R, Raschko J, Shibata S, Somlo G, Yen Y, Groshen S, Johnson K, Lenz HJ, Gandara D and Doroshow JH (2001) Phase I trial of 96-hour continuous infusion of dexrazoxane in patients with advanced malignancies. *Clin Cancer Res* **7:**1569-1576.

Tyurina YY, Tyurin VA, Yalowich JC, Quinn PJ, Claycamp HG, Schor NF, Pitt BR and Kagan VE (1995) Phenoxyl radicals of etoposide (VP-16) can directly oxidize intracellular thiols: protective versus damaging effects of phenolic antioxidants. *Toxicol Appl Pharmacol* **131:**277-288.

Usui N and Sinha BK (1990) Tyrosinase-induced free radical formation from VP-16,213: relationship to cytotoxicity. *Free Radic Res Commun* **10:**287-293.

Wurthwein G and Boos J (2002) Low dose--high dose: what is the right dose? Pharmacokinetic modeling of etoposide. *Cancer Chemother Pharmacol* **49:**303-308.

4.0 Chapter 4: Dihydroorotase catalyzes the ring opening of the hydrolysis intermediates of the cardioprotective drug dexrazoxane

4.1 Introduction

Spectrophotometric and HPLC studies (Hasinoff, 1994a; Hasinoff, 1994b) show that, under *in vitro* physiological conditions, dexrazoxane is slowly hydrolyzed to **B** and **C** ($t_{\frac{1}{2}}$ of 9.3 h at 37 °C and pH 7.4), and the final hydrolysis product ADR-925 ($t_{\frac{1}{2}}$ of 23 h) according to the kinetic scheme shown in Figure 4.1a Clinical pharmacokinetic trials, where dexrazoxane was administered with and without anthracycline, show that the beta phase half life of dexrazoxane elimination ($t_{\frac{1}{2}\beta}$) ranged from 2.6 to 4.2 h (Earhart et al., 1982; Hochster et al., 1992; Jakobsen et al., 1994; Vogel et al., 1987). Given the slow rate of *in vitro* hydrolysis-activation of dexrazoxane to ADR-925, it is unclear how sufficient amounts of ADR-925 could be present in heart tissue to chelate iron and prevent oxygen radical damage.

Cells are permeable to dexrazoxane (Dawson, 1975) and has been shown to rapidly hydrolyze to **B** and **C** in both an *in vitro* primary rat hepatocyte suspension (Hasinoff et al., 1994), and in an *in vivo* rat model (Hasinoff & Aoyama, 1999). In the hepatocyte model, it was determined that the conversion of dexrazoxane to **B** and **C** did not account for all the metabolites formed, strongly suggesting the presence of the third dexrazoxane metabolite, ADR-925 (Hasinoff et al., 1994), where **B** and **C** were hydrolyzed to ADR-925 by some unknown enzyme. These results were both consistent with dexrazoxane being metabolized by dihydropyrimidine amidohydrolase (DHPase, EC 3.5.2.2) which has been shown to hydrolyze dexrazoxane to **B** and **C**, but did not

159

enzymatically hydrolyze **B** and **C** to ADR-925 (Hasinoff, 1993; Hasinoff et al., 1991). A previous pharmacokinetic study in the rat showed that **B** and **C** reached relatively low steady state levels (Hasinoff & Aoyama, 1999). Preliminary pharmacokinetic studies in the rat (Chapter 2) and humans (Chapter 3) showed that dexrazoxane was rapidly hydrolyzed to ADR-925 *in vivo,* suggesting that the conversion of **B** and **C** to ADR-925 is enzymatically mediated.

The first three steps of *de novo* synthesis of the pyrimidines, uracil and thymine, are carried out by the multifunctional protein called CAD (Davidson et al., 1993; Simmer et al., 1990). In mammals CAD is a trifunctional protein which contains carbamyl phosphate synthetase, (CPSase, EC 6.3.5.5), aspartate transcarbamylase (ATCase, EC 2.1.3.2) and the zinc hydrolase dihydroorotase, (DHOase, EC 3.5.2.3) (Davidson et al., 1981; Kelly et al., 1986; Simmer et al., 1990). DHOase catalyzes the reversible cyclization of N-carbamyl-L-aspartate to form L-5,6-dihydroorotate (Figure 4.1b) which is the third reaction in the *de novo* pyrimidine biosynthetic pathway (Carrey, 1993; Evans et al., 1993).

DHPase has been identified as an enzyme that would likely hydrolyze the ring opening of dexrazoxane to **B** and **C**, given the structural similarity of dexrazoxane to dihydrouracil and dihydrothymine (Hasinoff et al., 1991). Likewise, given the structural similarity of **B** and **C** to dihydroorotate (Figure 4.1 b), the endogenous substrate of DHOase, it was decided to test the hypothesis that **B** and **C** could be enzymatically hydrolyzed to ADR-925 by DHOase, and thus, that DHOase might be ultimately responsible converting dexrazoxane metabolites **B** and **C** to ADR-925. In this chapter,

160

DHOase-catalyzed hydrolysis of **B** and **C** to ADR-925 was determined and Michealis Menten parameters were established. Results from this chapter have been accepted for publication (Schroeder et al., 2002).

a.

b.

c.
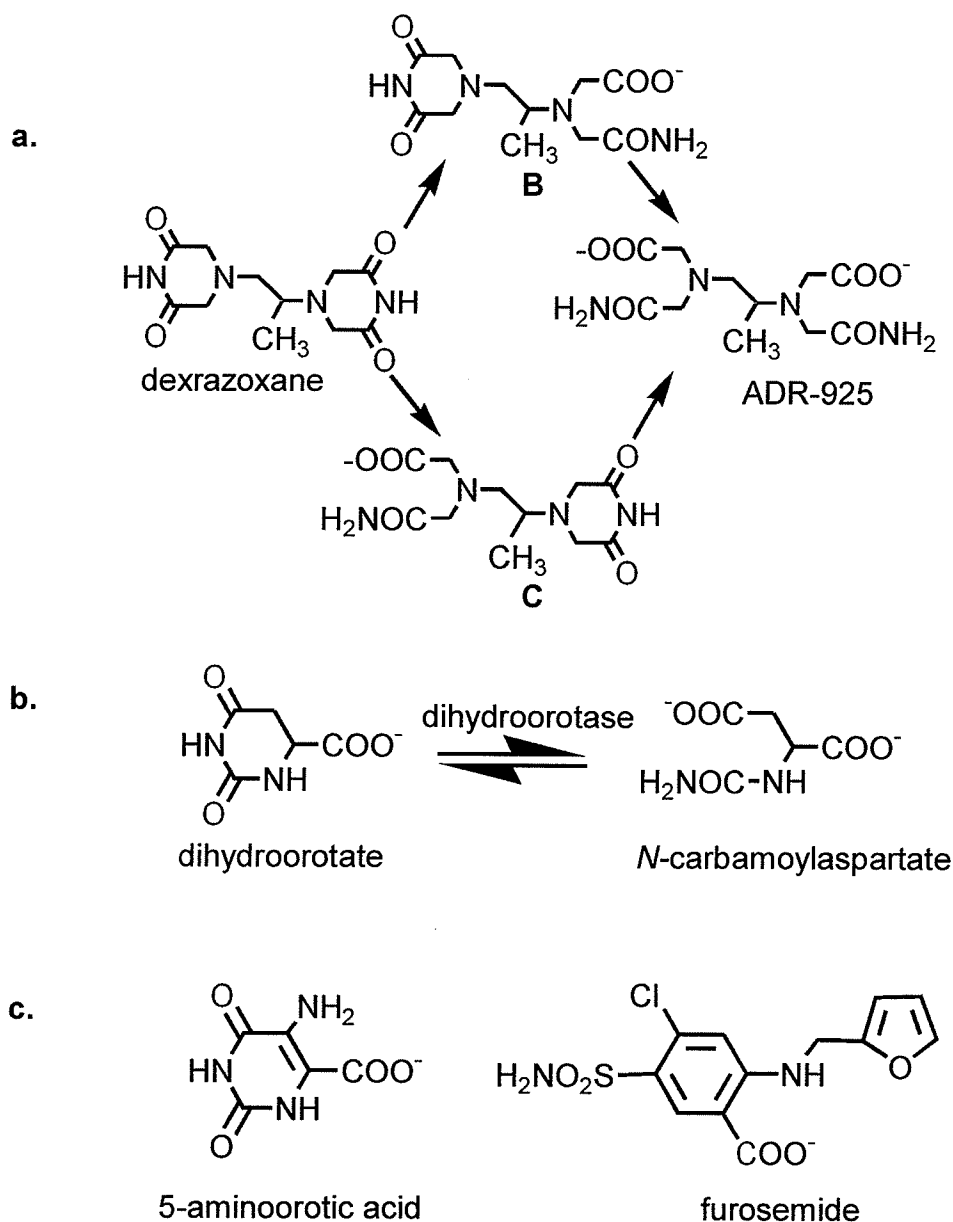
*Figure 4.1 a, reaction scheme for the hydrolysis of dexrazoxane to **B** and **C** and ADR-925; b, DHOase-catalyzed reversible reaction of L-dihydroorotate to N-carbamoyl-aspartate; c, structure of the DHOase inhibitors 5-aminoorotic acid and furosemide.*

4.2 Materials and Methods

4.2.1 Materials

Dexrazoxane hydrochloride and ADR-925 were gifts from Adria Laboratories (Columbus, OH). HPLC-grade methanol was from Fisher (Nepean, Canada). Tris, Chelex resin, 5-aminoorotic acid, furosemide, L-dihydroorotic acid and 1-octanesulfonic acid were from Sigma (St. Louis, MO). 4-Chlorobenzenesulfonamide was from Aldrich (Milwaukee, WI). Six-histidine-tagged CAD protein (198 μg/ml, stored in 30 % (v/v) DMSO, 5% (wt/v) glycerol, 12 mM Tris buffer, pH 7.9, 0.3 M NaCl, 0.6 M imidazole, and 1 mM 1,4-dithiothreitol.) purified from transfected hamster cells (Qiu & Davidson, 2000) was a gift from J. Davidson (University of Kentucky, Lexington, Kentucky).

4.2.2 Preparation and separation of B and C

Microgram quantities of **B** and **C** were prepared by hydrolyzing 5 mg/ml dexrazoxane with NaOH (8 μl/ml of 5 M NaOH) at 25 °C for 40 min and quenching the reaction with HCl (10 μl/ml of 5 M HCl) to pH 3 as described (Hasinoff, 1994a). Under these conditions a mixture of dexrazoxane, **B**, **C** and ADR-925 are produced with a typical mole ratio of 0.2, 0.3, 0.3, and 0.2, respectively. Dexrazoxane was efficiently removed from the mixture by loading 1 ml of the mixture on a Sep-Pak Plus C18 cartridge (Waters, Mississauga, Canada) with a plastic 1 ml syringe at a flow rat of 1 ml/min and eluting B, C, and ADR-925 with 2 % (v/v) methanol with a 5 ml plastic syringe at a flow rate of 5 ml/min. While dexrazoxane was highly retained on the cartridge, **B**, **C** and ADR-925 eluted together and were collected at elution volumes between 1.5 and 2.5 ml. This

fraction was then analyzed by HPLC to confirm that dexrazoxane was not present at detectable levels. This 1 ml fraction (pH 6) was loaded on three Sep-Pak Accell Plus QMA (Waters, Mississauga, Canada) ion exchange cartridges connected in series and eluted with 2 % (v/v) methanol at a flow rate of 5 ml/min. Fractions containing **B** were collected at elution volumes between 3 and 4.5 ml, and those containing **C** between 5 and 15 ml.

4.2.3 Determination of the purity of B and C by HPLC

After the synthesis and separation of **B** and **C** (as described in Section 4.2.2) the fractions were brought to pH 2 with 5 M HCl and evaporated to dryness under a stream of nitrogen. Fractions containing **B** and **C** were reconstituted in 10 mM HCl (pH ~ 3) and analyzed by HPLC (Section 4.2.9) to determine metabolite concentration and purity. **B** and **C** stock solutions were also analyzed for ADR-925 via the calcein assay (as described in Section 2.2.11). Under these conditions the **B** stock solution contained less than 0.1 mol % and 0.01 mol % of **C** and ADR-925, respectively. The **C** stock solution contained less than 0.1 mol % **B** and 0.05 mol % of ADR-925, respectively. Both fractions had undetectable amounts of dexrazoxane (less then 0.001 mol %). Typical yields of **B** and **C** were 50 μg and 20 μg, respectively.

4.2.4 Kinetics of DHOase-catalyzed hydrolysis of B, C and dihydroorotate

The DHOase-catalyzed hydrolysis of **B**, **C**, and dihydroorotate was determined by measuring the decrease of substrate concentration by HPLC as a function of time in order to obtain the initial velocities (v_o). The 60 μl reaction mixture contained Chelex-treated 10

mM Tris buffer (pH 7.4 at 15 °C), 2 µg/ml DHOase, and substrate (**B**, **C**, or dihydroorotate) at 15 °C. DHOase (198 µg/ml in 30 % (v/v) DMSO, 5% (wt/v) glycerol, 12 mM Tris buffer, pH 7.9, 0.3 M NaCl, 0.6 M imidazole, and 1 mM 1,4-dithiothreitol) was thawed for one min at 37 °C, vortexed briefly, and diluted with distilled H_2O to a stock solution concentration of 12 µg/ml. DHOase (10 µl of the 12 µg/ml stock) was added to 35 µl of Tris buffer (17.2 mM, pH 7.4 at 15 °C) such that the final DHOase concentration was 2 µg/ml. Lastly, 15 µl of substrate (**B**, **C**, or dihydroorotate in distilled H_2O) was added to the reaction mixture and then mixed two times with a 200 µl pipette upon which a sample was immediately taken (defined as t = 0). Tris buffer was incubated in a 15 °C water bath at least 15 min prior to the start of the experiment. A reaction temperature of 15 °C was found to greatly minimize the background hydrolysis of **B** and **C** while retaining good DHOase activity. Under these conditions, non-enzymatic hydrolysis of either **B** or **C** was not detectable at 45 min. After incubation periods of 0, 10, 20, 30, and 45 min post-DHOase addition, aliquots (10 µl) were removed and added to 25 µl of 3 mM HCl (pH 2) and stored at -80 °C to stop the reaction and prevent further hydrolysis of **B** or **C** (Hasinoff, 1994a). The initial velocities of the reaction for the decrease of **B** and **C** concentrations were calculated from a linear least squares fit of the above mentioned 5 substrate concentration-time data points as shown in Figures 4.10 – 4.11. The initial velocities of the reaction for the decrease in dihydroorotate concentration were calculated from 4 concentration-time data points as shown in Figure 4.12.

4.2.5   Inhibition of DHOase-mediated hydrolysis of C

When inhibitors were used 1 mM of either 5-aminoorotic acid, furosemide, or 4-

chlorobenzenesulfonamide were incubated with DHOase in the reaction buffer for 1 min

prior to addition of C, upon which samples were treated as described in Section 4.2.4.

4.2.6   Test to determine whether ADR-925 is a DHOase inhibitor

An experiment was done to determine if ADR-925, the rings fully open hydrolysis

product of **B** and **C**, inhibited DHOase. To test this 100 µM ADR-925 was added to the

DHOase reaction mixture (15 °C, pH 7.4, as described in Section 4.2.4) and incubated for

5 min prior to the addition of the 25 µM dihydroorotate. A control experiment where the

initial velocity of 25 µM dihydroorotate was monitored in the absence of ADR-925 was

run under the same experimental conditions.

4.2.7   Test to determine whether dexrazoxane is a substrate for DHOase

An experiment was also done to determine if dexrazoxane was a substrate for

DHOase (Figure 4.18). The hydrolysis of 500 µM dexrazoxane in the presence of 2 µg/ml

DHOase was followed for 2 h (15 °C, pH 7.4, as described in Section 4.3.4). A control

experiment followed the hydrolysis of dexrazoxane under the same reaction conditions and

during the same time in the absence of 2 µg/ml DHOase.

4.2.8   Quantitation of ADR-925, the product of DHOase-catalyzed hydrolysis of B and C

The initial velocities were derived by measuring the decrease in the amount of **B** or

C as a function of time. It was therefore necessary to determine whether the product of

DHOase-catalyzed hydrolysis of **B** and **C** was ADR-925. In order to test this **B** and **C** (1

mM) were separately incubated with 2 µg/ml DHOase for 120 min (10 mM Tris, pH 7.4 at

15 °C, as described in Section 4.2.4). The change in the amount of **B** and **C** (as determined by HPLC and described in Section 4.2.9) over two hours was compared to the amount of ADR-925 produced (as determined by HPLC and described in Section 4.2.9).

4.2.9 HPLC analysis of B, C, ADR-925

The HPLC analysis of **B** and **C** using an ion-pair reagent with the reversed phase C_{18}-column (detection wavelength 205 nm) has been described in Section 2.2.9. Briefly, 2 mM heptanesulfonic acid in 500 µM EDTA (pH 4.5) was isocratically pumped through a 10-µm µBondapak 3.9 × 300 mm reversed-phase C_{18} column (Waters) connected to an absorbance detector (205 nm) at a rate of 1 ml/min for 7 min to elute **B** or **C** with a retention time, t_r, of 6.5 and 9.5 min, respectively (as shown in Figures 4.2 and 4.3). At 7 min, HPLC grade methanol (Fisher) concentration was linearly increased over 2 min from 0 to 80% (v/v) 2 and maintained for 15 min. To equilibrate the column, 2 mM heptanesulfonic acid in 500 µM EDTA (pH 4.5) was isocratically pumped through the column for 30 min prior to the next sample injection. ADR-925 was determined separately under isocratic conditions (500 µM Na₂EDTA/2 mM octanesulfonic acid, pH 3.5, 1 ml/min). After ADR-925 eluted (t_r 3.5 min, as shown in Figure 4.4) the column was washed with 500 µM Na₂EDTA/methanol (20:80 v/v) for 20 min followed by re-equilibration with the initial mobile phase for 25 min. Duplicate determinations were carried out on each sample.

4.2.10 HPLC analysis of dihydroorotate

An ion-pair HPLC assay was developed to determine (wavelength of 205 nm)

dihydroorotate using a 10 mm µBondapak 3.9 x 300 mm reversed phase C_{18}-column (Waters). The elution profile was 10 mM 1-octanesulfonic acid (pH 2.5, 1 ml/min) for 5 min after which the methanol concentration was linearly increased over 1 min from 0 to 40% (v/v) and maintained for 20 min. The column was re-equilibrated with the initial mobile phase of 10 mM 1-octanesulfonic acid for 30 min prior to the next injection. Under these conditions dihydroorotate eluted at 2.5 min as seen in Figure 4.5. Duplicate determinations were carried out on each sample.

4.2.11 HPLC calibration plots: quantitation of B, C, ADR-925, and dihydroorotate

The HPLC calibration plots using integrated peak areas (100 µM to 10 mM **B** and **C**, 20 to 140 µM ADR-925, and 5-25 µM dihydroorotate) were prepared by adding standards containing known amounts of **B**, **C** and ADR-925 (prepared as previously described (Hasinoff, 1994a)) and dihydroorotate in 0.09 % DMSO (v/v). As shown in Figure 4.2 I, the major peak (t_r 4 min) was DMSO (0.09 % DMSO (v/v) as the concentration-time samples had been diluted 3.5 fold for HPLC analysis). Because of the possibility of integration interference from DMSO tailing (especially with metabolite **B**, t_r 6.5), standard curves were constructed with DMSO.

4.2.12 Data Analysis

The initial velocities for the reaction of **B** and **C** to ADR-925, and dihydroorotate to N-carbamoyl aspartate were determined from the linear least-squares fit of five and four substrate concentration-time data points, respectively.   Michaelis-Menten kinetic

parameters for the DHOase-catalyzed hydrolysis of **B**, **C**, and dihydroorotate were achieved through the dependence of the initial velocities on the concentration of the respective substrate and fit to equation 4.1 by nonlinear least-squares analysis (SigmaPlot; Jandel Scientific, San Rafael, CA).

$$v = \frac{V_{max}[S]}{(K_m + [S])} \qquad (4.1)$$

4.3 Results

4.3.1 HPLC quantitation of dihydroorotate, B, C, and ADR-925

The HPLC analysis of **B** and **C** using an ion-pair reagent as described in Section 4.2.9 eluted **B** and **C** with a retention time, t_r, of 6.5 and 9.5 min, respectively (as shown in Figures 4.2 and 4.3). ADR-925, determined separately under isocratic conditions (500 µM Na$_2$EDTA/2 mM octanesulfonic acid, pH 3.5, 1 ml/min).], eluted at t_r 3.5 min, as shown in Figure 4.4. Dihydroorotate was separated using the ion-pair agent 1-octanesulfonic acid and these conditions dihydroorotate eluted at 2.5 min as seen in Figure 4.5.
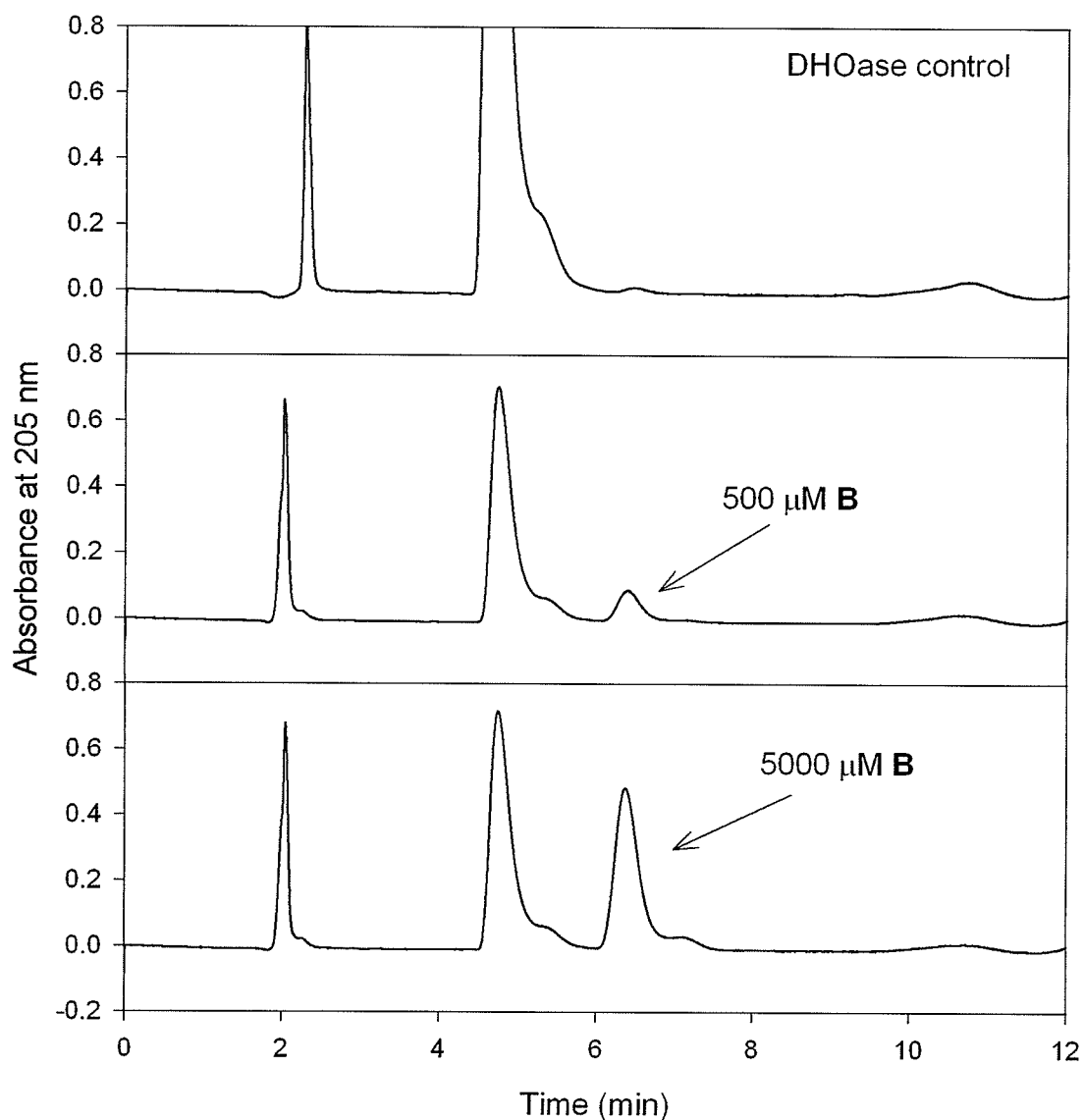
*Figure 4.2   HPLC chromatogram of the separation of metabolite **B** from CAD protein stabilizing components*

B was separated on a C_{18} reverse-phase column. A blank 2 μg/ml DHOase protein chromatogram is shown in chromatogram I.   HPLC chromatograms II and III were obtained at t = 0 for initial velocity studies of 500 and 5000 μM **B**, respectively, in the presence of 2 μg/ml DHOase.
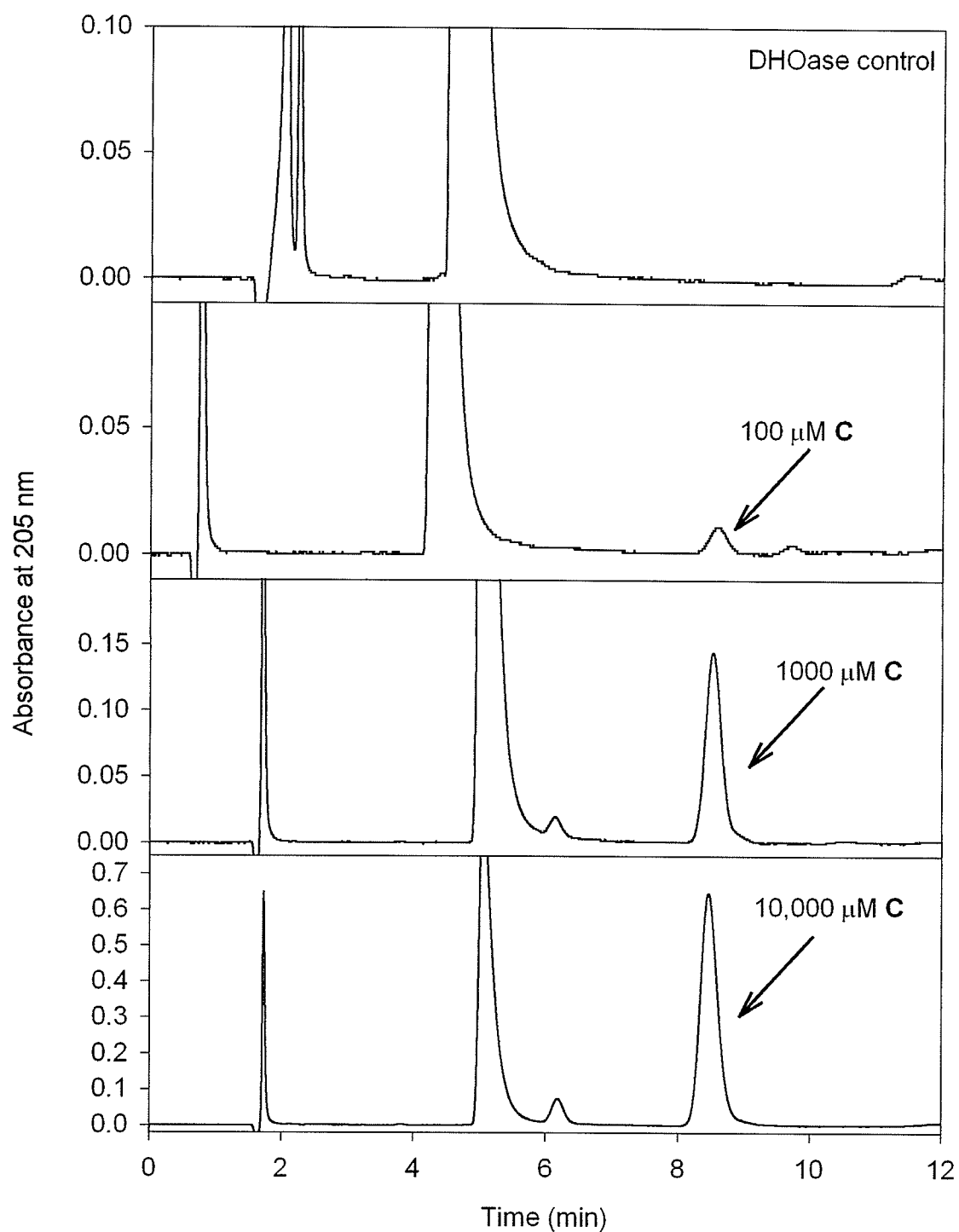
Figure 4.3 HPLC chromatogram of the separation of metabolite C from CAD protein stabilizing components

C was separated on a C_{18} reverse-phase column. A blank 2 μg/ml DHOase protein chromatogram is shown in chromatogram I. HPLC chromatograms II, III, and IV were obtained at t = 0 for initial velocity studies of 100, 1000, and 10,000 μM **B**, respectively, in the presence of 2 μg/ml DHOase.
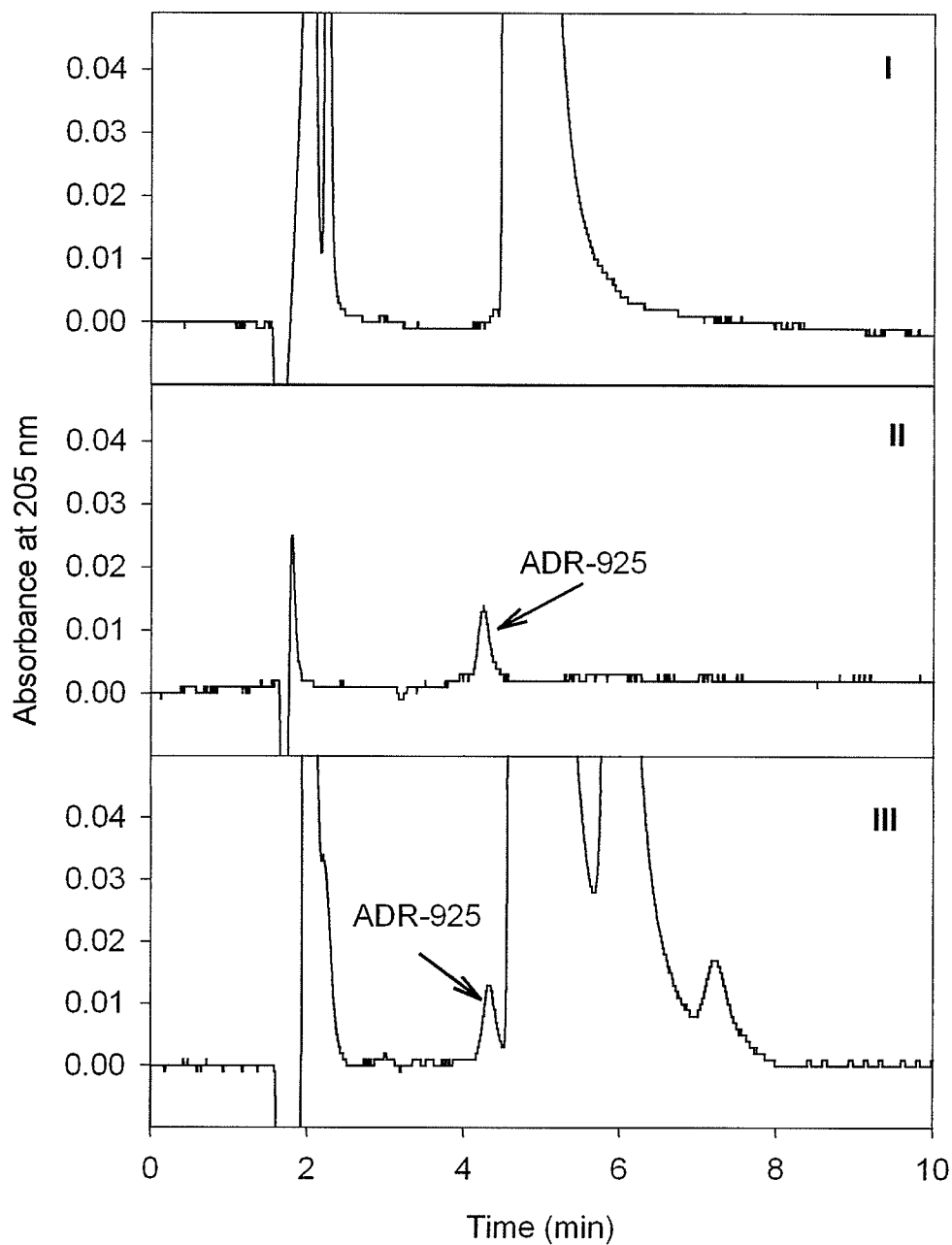
Figure 4.4   HPLC chromatogram of the separation of ADR-925 from CAD protein stabilizing components

ADR-925 was separated on a C_{18} reverse-phase column. A blank 2 µg/ml DHOase protein chromatogram is shown in chromatogram I.   ADR-925 (200 µM) in distilled water is shown in chromatogram II.   Chromatogram III was obtained at t = 120min after 1 mM C was added 2 µg/ml DHOase.
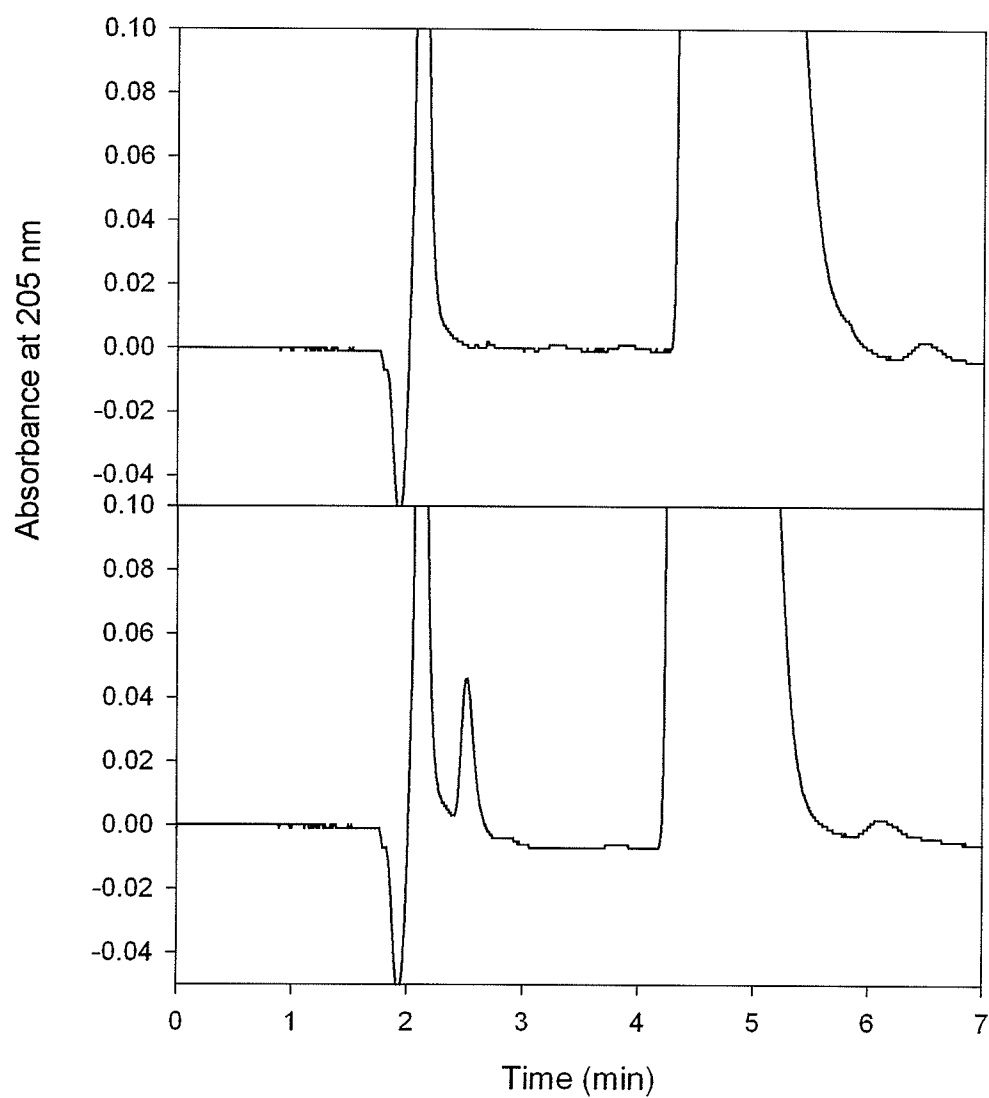
Figure 4.5   HPLC chromatogram of the separation of dihydroorotate from CAD protein stabilizing components

Dihydroorotate was separated on a C_{18} reverse-phase column. A blank 2 µg/ml DHOase protein chromatogram is shown in chromatogram I.   HPLC chromatogram II was obtained at t = 30 min after 20 µM dihydroorotate was incubated with 2 µg/ml DHOase.

4.3.2 HPLC calibration curves for dihydroorotate, B, C, and ADR-925

The calibration plots were constructed by plotting arbitrary integration peak areas (as shown in Tables 4.1-4.4) as a function of substrate or metabolite concentration as shown in Figures 4.6 through 4.9. Calibration curves for **B**, **C**, ADR-925, and dihydroorotate were performed once prior to the analysis of the **B**, **C**, and dihydroorotate concentration-time samples. All concentration points were run in duplicate. The limit of quantitation was estimated to be three times the limit of detection (that was determined through an estimate of drug/metabolite or substrate peak heights that exceeded the background noise 3-fold). The limit of quantitation for **B**, **C**, ADR-925, and dihydroorotate was estimated to be 1.5, 1.5, 10, and 0.5 µM respectively.

Table 4.1. HPLC Calibration curve of **B** in 0.09 % DMSO (v/v)

Concentration (µM)	Average Peak Area (Arbitrary Units)
10,000	15933414
7000	10221372
5000	7054806
3000	4044684
1000	1072368
700	680112
500	498584
100	130565
slope	1585
intercept	-42012
r^2	0.9982

Table 4.2. HPLC Calibration curve of **C** in 0.09 % DMSO (v/v)

Concentration (μM)	Average Peak Area (Arbitrary Units)
10,000	16033414
7000	11165206
5000	7013432
3000	4022444
1000	1158378
700	658082
500	485376
100	129224
slope	1627
intercept	-48315
r^2	0.997

Table 4.3. HPLC Calibration curve of dihydroorotate in 0.09 % DMSO (v/v)

Concentration (μM)	Average Peak Area (Arbitrary Units)
25	37827
20	31369
15	22507
10	17702
7	13961
5	10956
slope	1333
intercept	4064
r^2	0.994

Table 4.4. HPLC Calibration curve of ADR-925 in 0.09 % DMSO (v/v)

Concentration (μM)	Average Peak Area (Arbitrary Units)
200	56852
140	37655
110	26452
90	23123
70	17546
50	13232
20	6256
slope	294
intercept	-1246
r^2	0.991
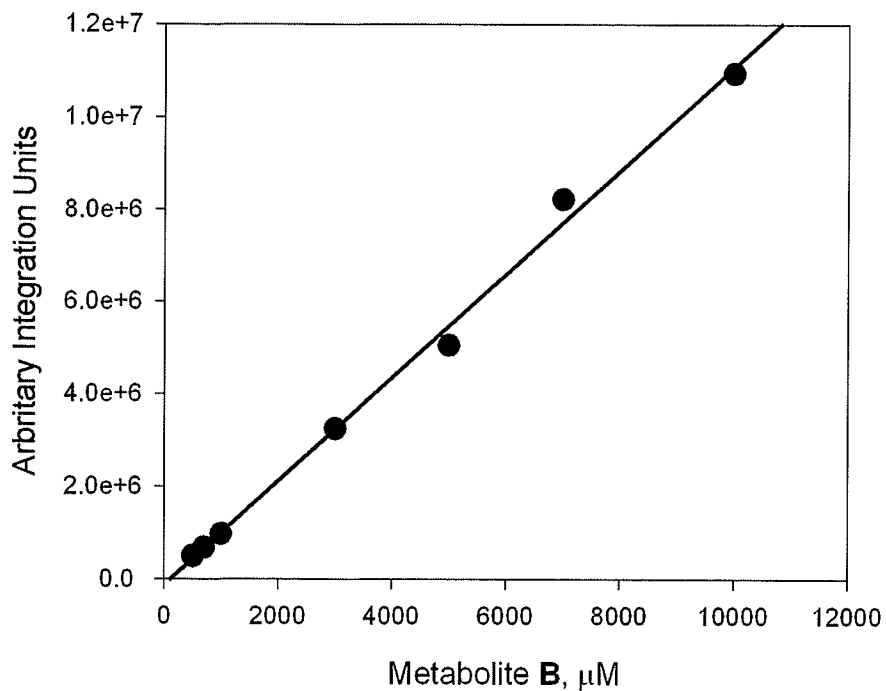
*Figure 4.6 HPLC calibration curve of **B** in 0.09 % DMSO (v/v)*
The HPLC calibration plot was prepared by adding standards containing known amounts of **B** to 0.09 % DMSO (v/v). A mobile phase of 2 mM heptanesulfonic 500 μM Na_2EDTA, pH 4.5 (as described in Section 4.2.9) was used to separate **B** (t_r 6.5 min).
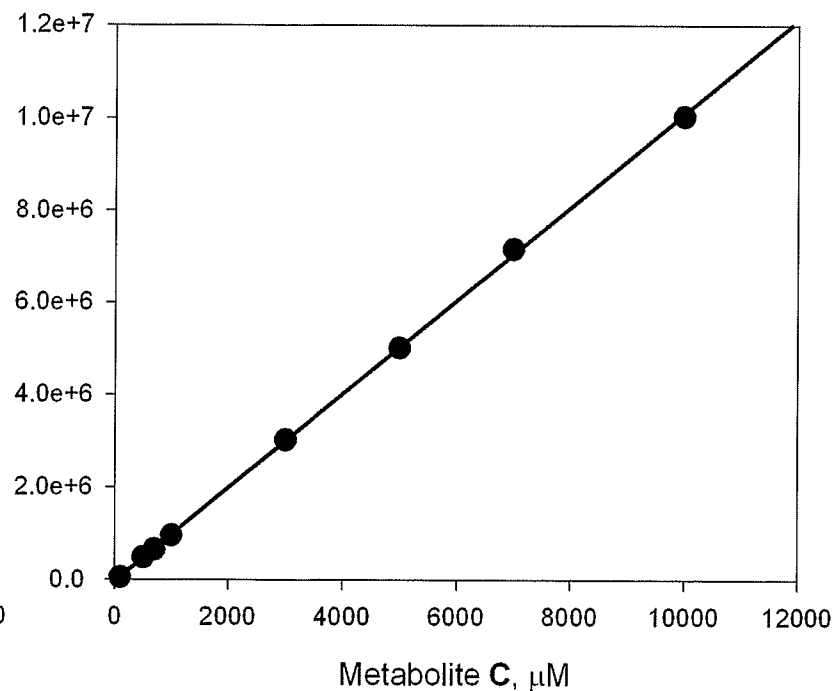
*Figure 4.7 HPLC calibration curve of **C** in 0.09 % DMSO (v/v)*
The HPLC calibration plot was prepared by adding standards containing known amounts of **C** to 0.09 % DMSO (v/v). A mobile phase of 2 mM heptanesulfonic 500 μM Na_2EDTA, pH 4.5 (as described in Section 4.2.9) was used to separate **C** (t_r 9.5 min).
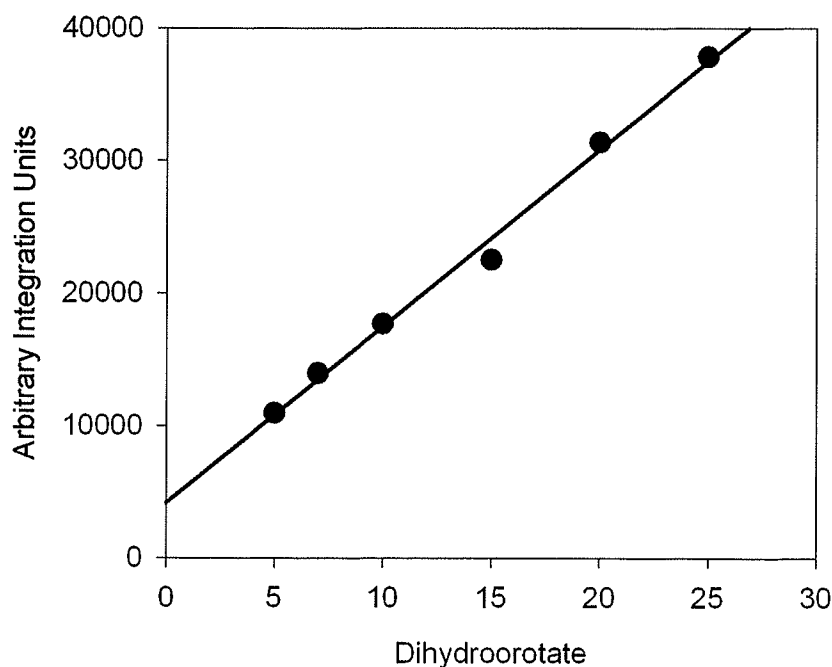
Figure 4.8 HPLC calibration curve of Dihydroorotate in 0.09 % DMSO (v/v)

The HPLC calibration plot was prepared by adding standards containing known amounts of dihydroorotate to 0.09 % DMSO (v/v). A mobile phase of 10 mM octanesulfonic acid, pH 4.5 (as described in Section 4.2.10) was used to separate dihydroorotate (t_r 3.5 min).
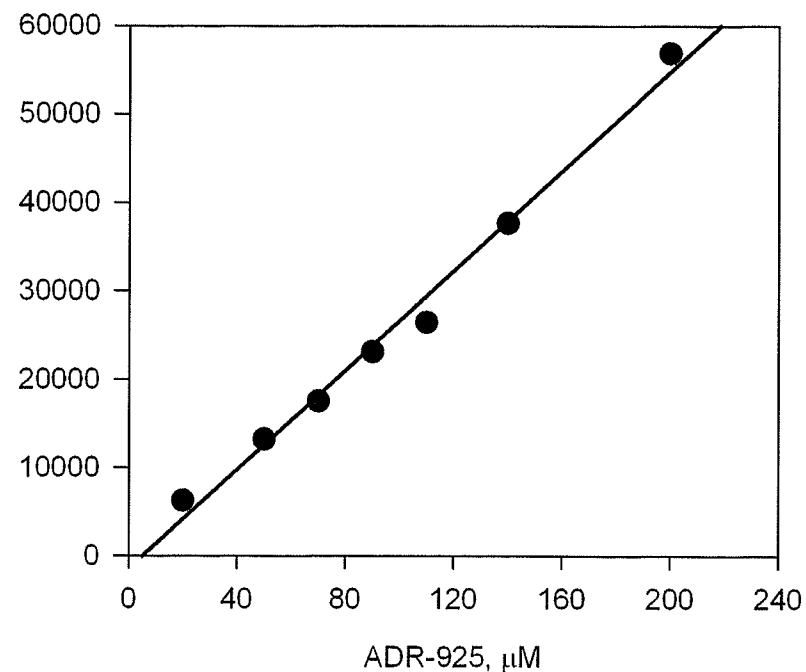
Figure 4.9 HPLC calibration curve of ADR-925 in 0.09 % DMSO (v/v)

The HPLC calibration plot was prepared by adding standards containing known amounts of ADR-925 to 0.09 % DMSO (v/v). A mobile phase of 2 mM heptanesulfonic/500 µM Na$_2$EDTA, pH 4.5 (as described in Section 4.2.9) was used to separate ADR-925 (t_r 3.5 min).

4.3.3 Initial velocities of DHOase-catalyzed hydrolysis of dihydroorotate, B and C

The DHOase-catalyzed hydrolysis of **B**, **C**, and dihydroorotate was determined by measuring the decrease of substrate concentration as a function of time to obtain the initial velocities (v_o) as shown in Tables 4.5-4.7 and in Figures 4.10-4.12.

Table 4.5 Initial velocities for the rate of loss of Metabolite **B** by the action of DHOase

Time (min)	Metabolite **B** Concentration (μM)						
	500	700	1000	3000	5000	7000	10,000
0	500	713	1134	3034	4992	7024	10,034
10	490	704	1110	3017	4928	6954	10,004
20	478	697	1092	2983	4888	6873	9915
30	453	684	1076	2938	4829	6841	9805
45	428	673	1053	2906	4805	6797	9775
v_o (μM·min^{-1})	1.66	0.91	1.77	3.04	4.23	5.06	6.43
r^2	0.981	0.994	0.991	0.981	0.954	0.944	0.940

Table 4.6 Initial velocities for the rate of loss of Metabolite **C** by the action of DHOase

Time (min)	Metabolite **C** Concentration (μM)							
	100	500	700	1000	3000	5000	7000	10,000
0	97	522	690	983	2994	4935	7032	10,032
10	94	517	679	951	2924	4859	6877	9933
20	90	513	660	941	2877	4842	6740	9858
30	86	507	642	915	2837	4768	6683	9696
45	77	492	626	887	2807	4646	6567	9619
v_o (μM·min^{-1})	0.40	0.64	1.47	2.05	4.09	6.15	10.1	9.57
r^2	0.985	0.963	0.990	0.983	0.921	0.969	0.960	0.974

Table 4.7 Initial velocities for the rate of loss of dihydroorotate by the action of DHOase

Time (min)	Dihydroorotate Concentration (μM)				
	7	10	15	20	25
0	7.0	10.0	15.0	20.9	24.9
10	4.6	7.46	11.4	16.6	19.2
20	3.1	4.09	8.08	12.1	15.6
30	1.2	1.60	3.59	8.63	11.3
v_0 (μM·min^{-1})	0.19	0.286	0.377	0.412	0.444
r^2	0.991	0.996	0.996	0.997	0.991
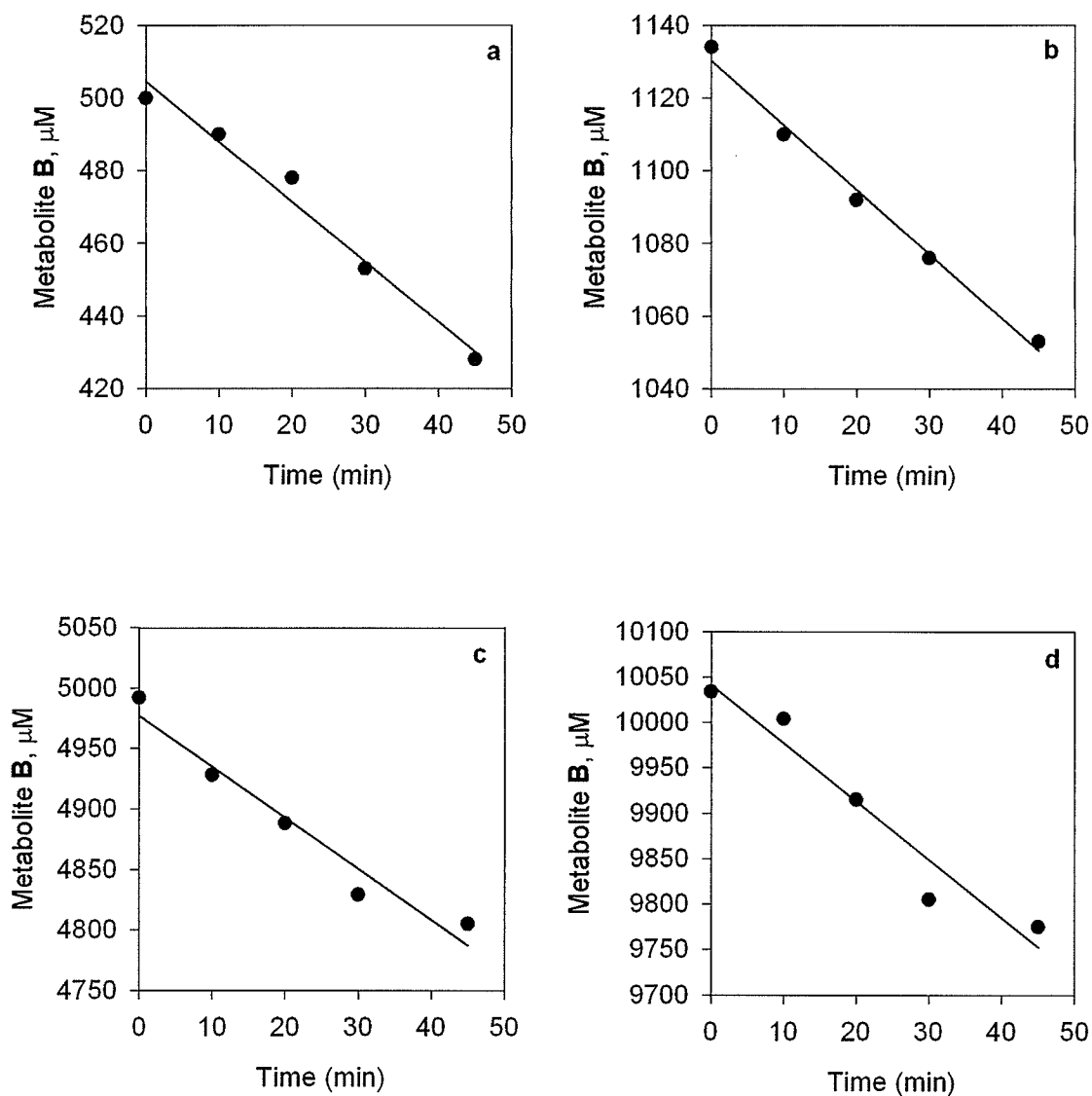
*Figure 4.10 Initial velocity plots for the DHOase-catalyzed hydrolysis of **B***

The initial velocities of the reaction for the DHOase mediated decrease of **B** were calculated from a linear least squares fit of 5 substrate concentration-time data points with initial **B** concentrations ranging from 500 to 10,000 μM. The reaction was carried out in Tris buffer (pH 7.4 at 15 °C) in the presence of 2 μg/ml DHOase with 500 (a), 1000 (b), 5000 (c), and 10,000 (d) μM **B**.
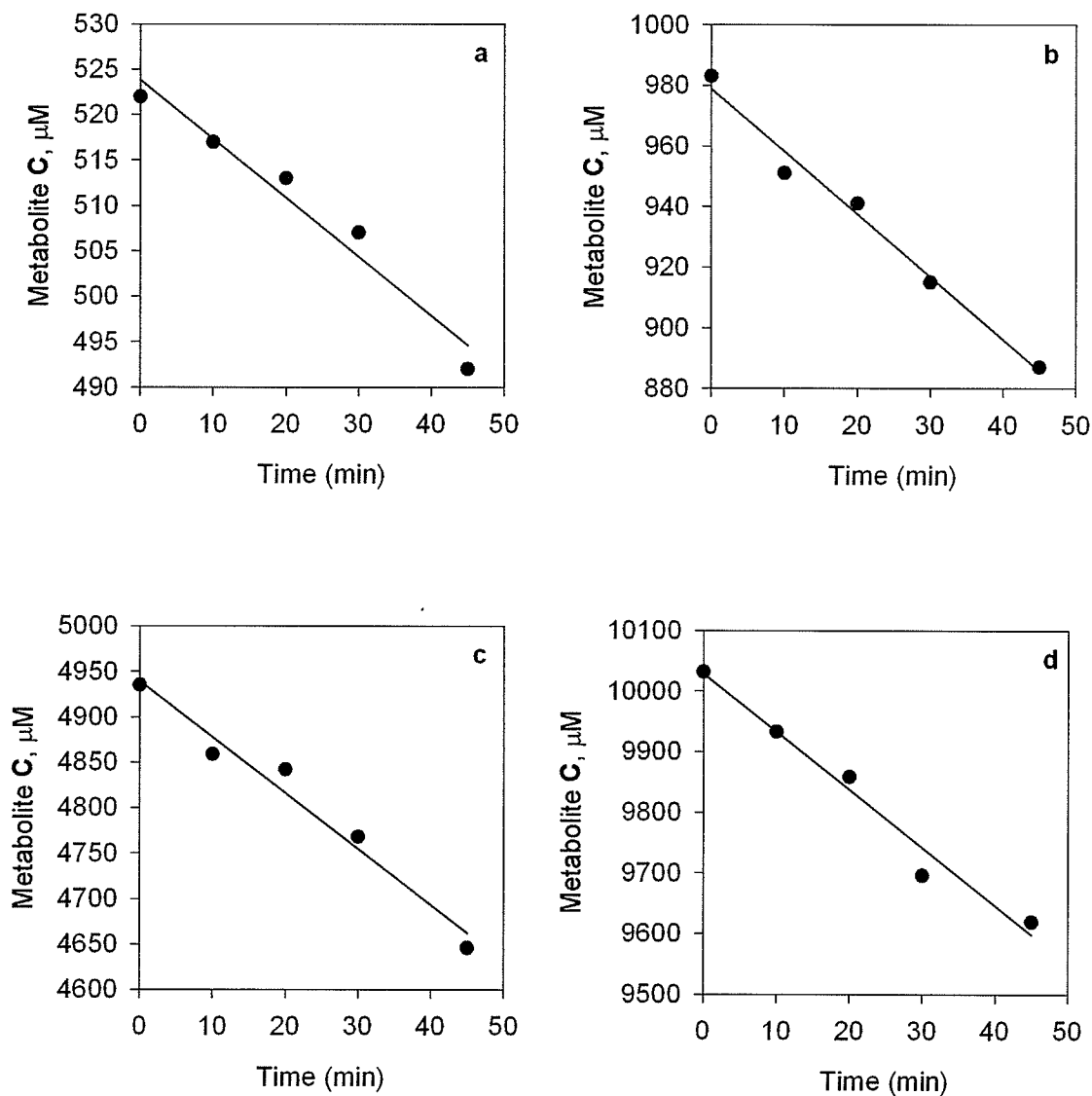
Figure 4.11 Initial velocity plots for the DHOase-catalyzed hydrolysis of C

The initial velocities of the reaction for the DHOase mediated decrease of **C** were calculated from a linear least squares fit of 5 substrate concentration-time data points with initial **C** concentrations ranging from 500 to 10,000 μM. The reaction was carried out in Tris buffer (pH 7.4 at 15 °C) in the presence of 2 μg/ml DHOase with 500 (a), 1000 (b), 5000 (c), and 10,000 (d) μM **C**.
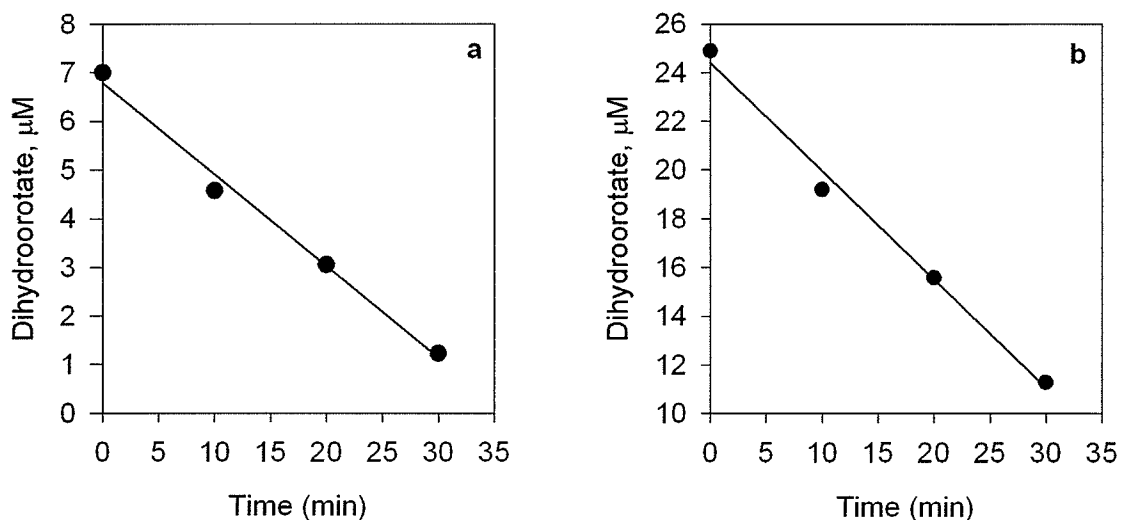
Figure 4.12   Initial velocity plots for the DHOase-catalyzed hydrolysis of dihydroorotate

The initial velocities of the reaction for the DHOase mediated decrease of dihydroorotate were calculated from a linear least squares fit of 4 substrate concentration-time data points with initial dihydroorotate concentrations ranging from 7 to 25 μM.   The reaction was carried out in Tris buffer (pH 7.4 at 15 °C) in the presence of 2 μg/ml DHOase with 7 (a) and 25 (b) μM dihydroorotate.

4.3.4   Kinetics of DHOase-catalyzed hydrolysis of dihydroorotate, B and C

The dependence of the initial velocity on the concentration of dihydroorotate, **B** and **C** are shown in Figure 4.13-4.15 and show that DHOase catalyzes the ring-opening reaction of **B** and **C**. The initial velocities were fit to Michaelis-Menten kinetics by nonlinear least squares analysis (SigmaPlot, Jandel Scientific, San Rafael, CA) of the data in the following equation:

$$v = V_{max}[S]/(K_m + [S]) \qquad (4.1)$$

The specific V_{max} and K_m values are given in Table 4.8.
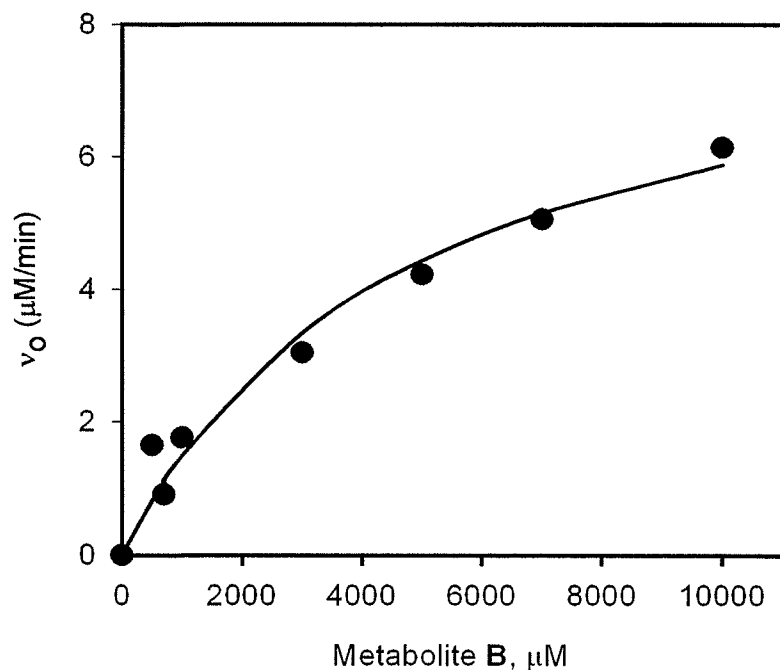
*Figure 4.13 Initial velocities (v_o) for the rate of loss of **B** by the action of DHOase.*

Solid line is obtained from the nonlinear least squares fit of the data to the Michaelis-Menten kinetics (eqn. 4.1). The best fit to this data yielded V_{max} 4.35 μmol•min^{-1}•mg^{-1}, K_m 4800 μM, and V_{max}/K_m 0.9 l•min^{-1}•g^{-1}. DHOase-catalyzed hydrolysis of **B** was measured in 10 mM Tris buffer (pH 7.4) at 15 °C with a DHOase concentration of 2.0 μg/ml.
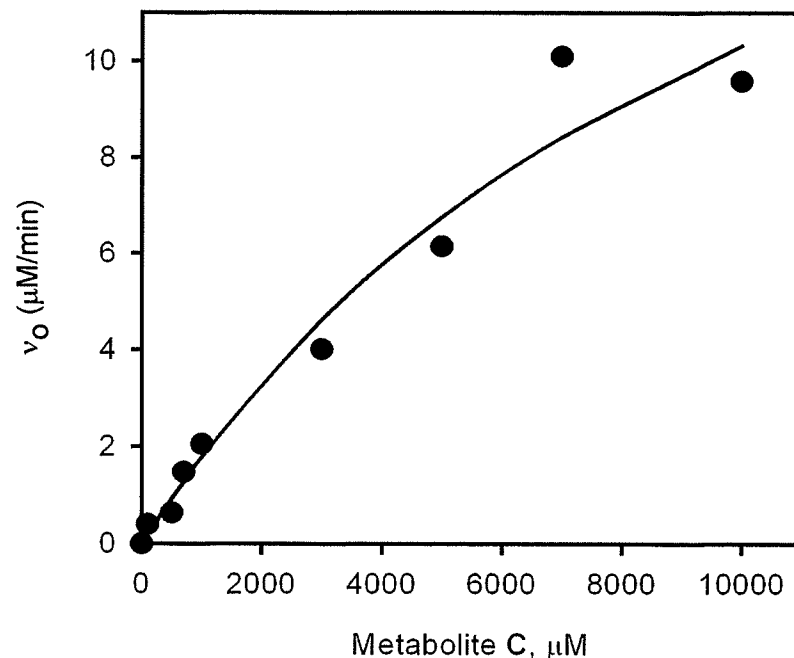
*Figure 4.14 Initial velocities (v_o) for the rate of loss of **C** by the action of DHOase.*

Solid line is obtained from the nonlinear least squares fit of the data to the Michaelis-Menten kinetics (eqn. 4.1). The best fit to this data yielded V_{max} 10.9 μmol•min^{-1}•mg^{-1}, K_m 11,000 μM, and V_{max}/K_m 0.98 l•min^{-1}•g^{-1}. DHOase-catalyzed hydrolysis of **C** was measured in 10 mM Tris buffer (pH 7.4) at 15 °C with a DHOase concentration of 2.0 μg/ml.

-183-
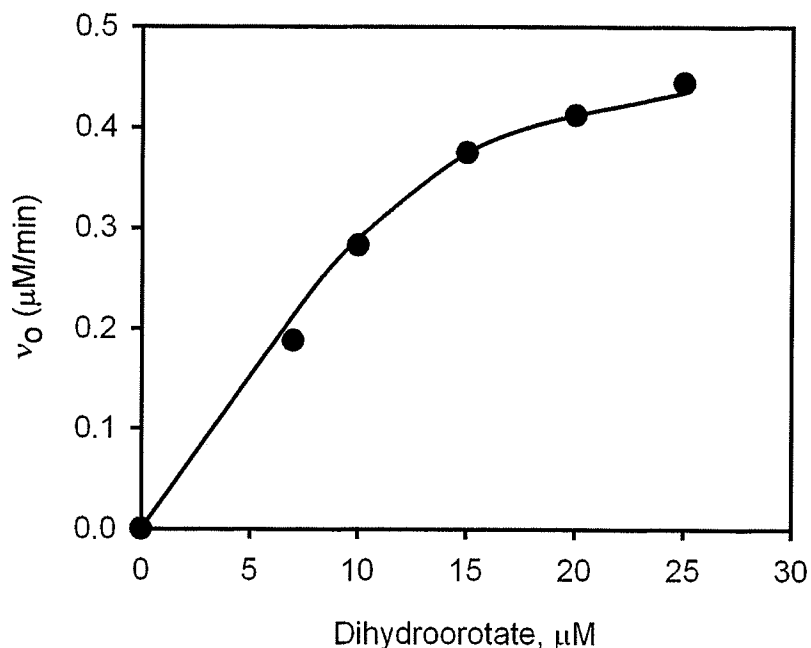
Figure 4.15 *Initial velocities (v_o) for the rate of loss of dihydroorotate by the action of DHOase.*

Solid line is obtained from the nonlinear least squares fit of the data to the Michaelis-Menten kinetics (eqn. 4.1). The best fit to this data yielded V_{max} 0.41 $\mu mol \cdot min^{-1} \cdot mg^{-1}$, K_m 20 μM, and V_{max}/K_m 20.6 $l \cdot min^{-1} \cdot g^{-1}$. DHOase-catalyzed hydrolysis of dihydroorotate was measured in 10 mM Tris buffer (pH 7.4) at 15 °C with a DHOase concentration of 2.0 $\mu g/ml$.
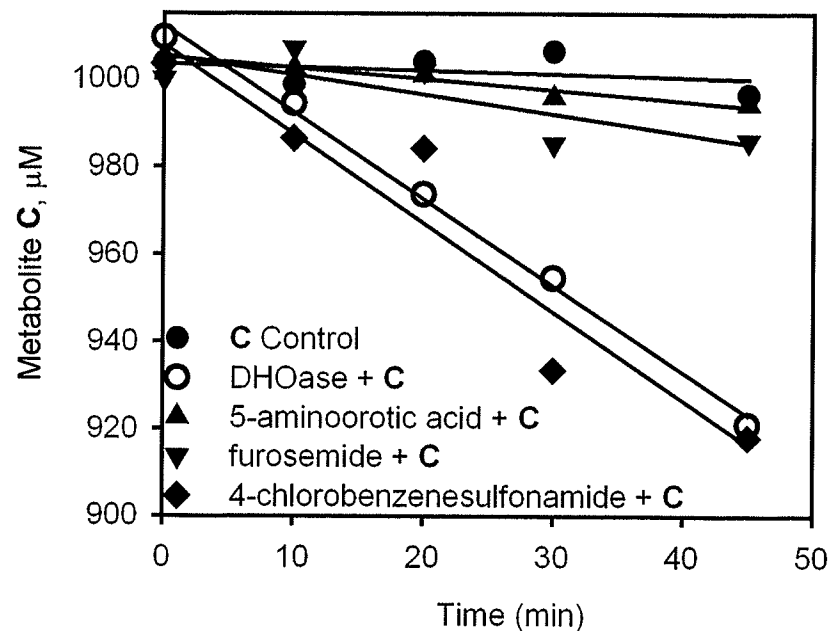
Figure 4.16 *Initial velocity plots for the DHOase-catalyzed hydrolysis of C without DHOase (●) and with DHOase(O) in the presence of 1 mM 5-aminoorotic acid (▲), furosemide (▼), and 4-chlorobenzenesulfonamide (♦) in Tris buffer (pH 7.4) at 15 °C in the presences of 2 mg/ml DHOase.*

5-aminoorotic acid and furosemide inhibited DHOase-catalyzed hydrolysis of C by 91 and 80 %, respectively. 4-chlorobenzenesulfonamide was not inhibitory.

Table 4.8 Michaelis-Menten kinetic parameters for the DHOase-catalyzed hydrolysis of dihydroorotate and **B** and **C**

| Substrate | V_{max} | K_m | V_{max}/K_m |
	($\mu mol \cdot min^{-1} \cdot mg^{-1}$)	(μM)	($l \cdot min^{-1} \cdot g^{-1}$)
dihydroorotate	0.41 ± 0.07	20 ± 6	20.6
B	4.35 ± 0.70	4800 ± 1700	0.9
C	10.9 ± 3.8	$11,000 \pm 6300$	0.98

The reaction was carried out in 10 mM Tris buffer (pH 7.4) at 15 °C and substrate concentrations were assayed by HPLC. The errors shown are standard errors obtained from the non-linear least squares analysis of the data in the Michaelis-Menten equation (equation 4.1).

4.3.5 ADR-925 does not cause product inhibition of DHOase

An experiment was done to determine if ADR-925 inhibited DHOase. To test this 100 μM ADR-925 was added to the DHOase reaction mixture prior to the addition of the 25 μM dihydroorotate. The initial velocity of the DHOase-catalyzed hydrolysis of dihydroorotate was measured in the presence and absence of 100 μM. The ADR-925 slopes were not significantly different (t-test $p > 0.5$, $n = 5$), which indicated that ADR-925 did not inhibit DHOase (as seen in Figure 4.17).

4.3.6 Dexrazoxane is not a substrate for DHOase

An experiment was also done to determine if dexrazoxane was a substrate for DHOase. The hydrolysis of 500 μM dexrazoxane in the presence and absence of 2 $\mu g/ml$ DHOase was followed for 2 h (15 °C, pH 7.4). No statistically significant (t-test $p > 0.1$, $n = 5$) enzymatic hydrolysis (as measured by their respective slopes) was detected above
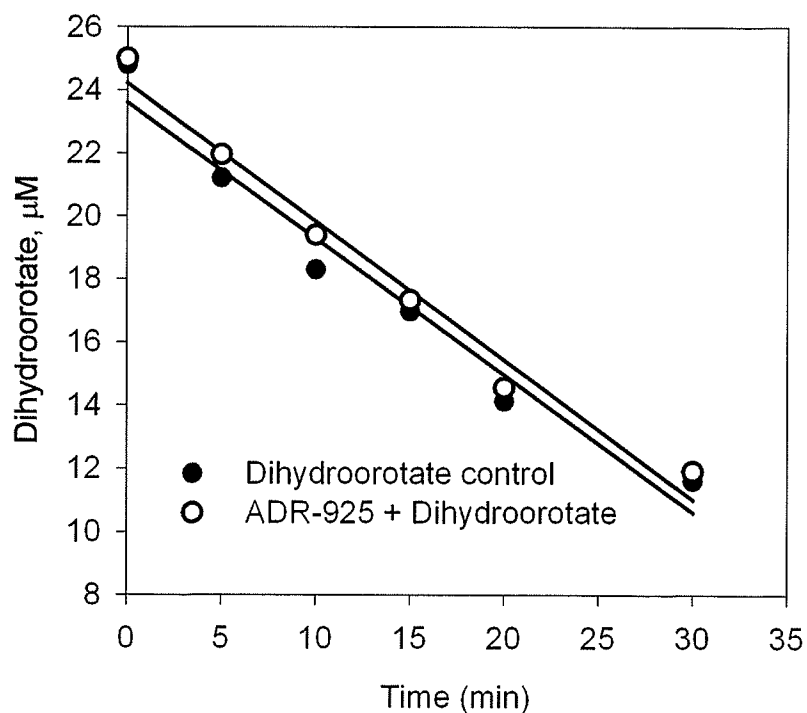
Figure 4.17 Initial velocity plots for the DHOase-catalyzed hydrolysis of dihydroorotate by the action of DHOase with (O) and without (●) ADR-925.

Hydrolysis of 25 μM dihydroorotate in the presence of 2 μg/ml DHOase buffered with 10 mM Tris (pH 7.4 at 15 °C). The hydrolysis rate of dihydroorotate with and without ADR-925, as measured by their respective slopes, was found not to be significant ($p > 0.5$).
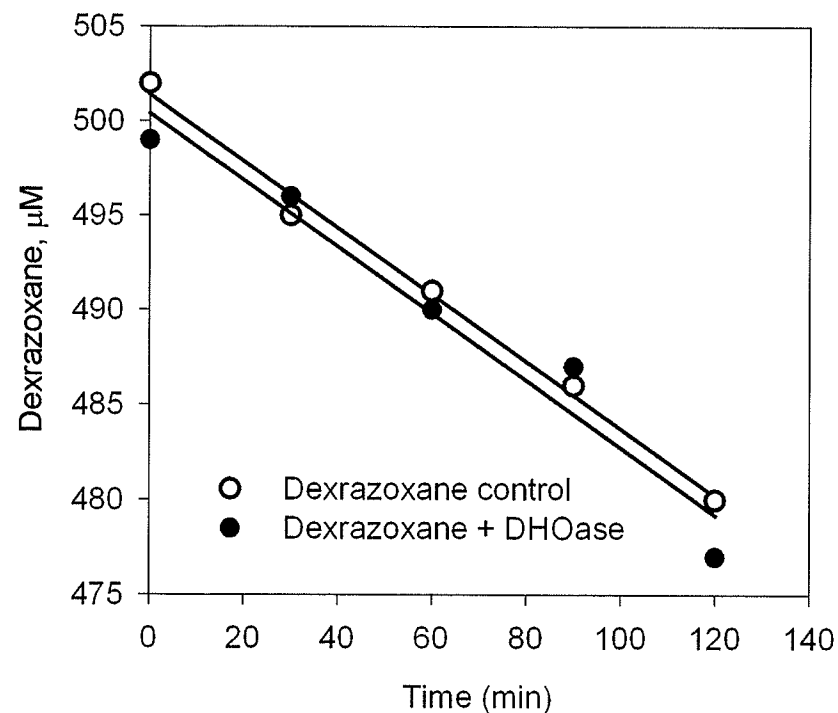
Figure 4.18 Hydrolysis of dexrazoxane with (●) and without (O) DHOase

Hydrolysis of 500 μM dexrazoxane in the presence of 2 μg/ml DHOase buffered with 10 mM Tris (pH 7.4 at 15 °C). The hydrolysis rate of dexrazoxane with and without ADR-925, as measured by their respective slopes, was found not to be significant ($p > 0.5$).

that observed for the dexrazoxane control (as seen in Figure 4.18) which indicated that neutral dexrazoxane was not a substrate for DHOase.

4.3.7 ADR-925 is the product of DHOase mediated hydrolysis of B and C

Experiments were also done to prove that the product of the DHOase-catalyzed hydrolysis of 1 mM **B** and **C** was ADR-925. The concentrations of ADR-925 were determined by HPLC at 2 h were found to be 137 μM and 184 μM for **B** and **C**, respectively. The amount of **B** and **C** in the DHOase reaction mixture at two hours was also assayed and found to be 870 and 774 μM, respectively. Thus, by subtraction, the amount of ADR-925 produced was 130 μM and 226 μM, respectively for **B** and **C**. The agreement with the ADR-925 concentration measured directly by HPLC and the ADR-925 concentration measured through subtraction indicated that DHOase catalyzed the hydrolysis of **B** and **C** to ADR-925.

4.3.8 The effect of DHOase inhibitors on DHOase-catalyzed hydrolysis of C

Given that DHOase is only one of the three activities of the multifunctional CAD enzyme, the kinetics of DHOase-catalyzed hydrolysis of **C** was determined in the presence of specific inhibitors of DHOase in order to determine if the hydrolysis of **B** and **C** was due to the DHOase domain. 5-Aminoorotic acid is an inhibitor (K_i of 6 μM) of mammalian DHOase-catalyzed hydrolysis of dihydroorotate, though 4-nitrobenzenesulfonamide did not (Christopherson & Jones, 1980). 4-Chlorobenzenesulfonamide and 4-nitrobenzenesulfonamide, are however, non-competitive inhibitors (K_i 200 and 1100 μM, respectively) of bacterial DHOase (Pradhan & Sander, 1973). Furosemide (Fig. 4.1) was

included because it is a sulfonamide with a carboxylate group. As shown in Fig. 4.16, 1 mM 4-chlorobenzenesulfonamide did not inhibit DHOase. However, 1 mM 5-aminoorotic acid and furosemide inhibited DHOase by 91 and 80 %, respectively.

4.4   Discussion

4.4.1   DHOase-mediated hydrolysis of Dihydroorotate

The specific V_{max} value of 0.41 $\mu mol \cdot min^{-1} \cdot mg^{-1}$ (10 mM Tris buffer, pH 7.4, 15 °C) for the hydrolysis of dihydroorotate by the recombinant 6-histidine tagged hamster DHOase (Qiu & Davidson, 2000) used in this study is smaller than the recombinant hamster DHOase specific V_{max} values of 1.2 - 2.1 $\mu mol \cdot min^{-1} \cdot mg^{-1}$ (50 mM HEPES buffer, pH 7.4, 37 °C, 100 μM ZnCl$_2$) (Huang et al., 1999; Williams et al., 1995) and 1.2 $\mu mol \cdot min^{-1} \cdot mg^{-1}$ (100 mM Tris buffer, pH 7.4, 37 °C, 25 mM MgCl$_2$, 0.1 M KCl, 3.3 mM glutamine, 15 mM L-aspartate, DTT, 7.5 % DMSO) (Kelly et al., 1986). However, given the different reaction conditions (buffer, presence of activating ZnCl$_2$, and temperature) and that a histidine-tagged DHOase was used in this study, the agreement is reasonable. The K_m of 20 μM determined in this study is in the range of previously observed K_m values of 4-20 μM (Christopherson et al., 1989; Huang et al., 1999; Kelly et al., 1986; Williams et al., 1995).

4.4.2   DHOase-mediated hydrolysis of B and C

The results of Table 4.8 show that both **B** and **C** are good substrates for DHOase. The specific V_{max} values for **B** and **C** are 11- and 27-fold higher than the endogenous substrate dihydroorotate. The reason for the high V_{max} for **B** and **C** probably lies with the

fact that the imide bond in **B** and **C** is much more easily hydrolyzed than is the imide bond in dihydroorotate. It has been previously shown that **B** and **C** underwent non-enzymatic hydrolysis (pH 7.4, 37 °C) with $t_{1/2}$ of 17 and 8.4 h, respectively (Hasinoff, 1994a), whereas dihydroorotate is very stable under these conditions. The K_m values for both **B** and **C** are, however, 240- and 550-fold larger than for dihydroorotate. This result suggests that neither **B** nor **C** is a good fit in the active site of DHOase. A comparison of the V_{max}/K_m values of Table 4.8 indicates that under non-saturating conditions ([S] < K_m) dihydroorotate is still a 23-fold better substrate than either **B** or **C**. Given that the V_{max}/K_m values for **B** and **C** are similar, under non-saturating conditions DHOase would act on **B** and **C** at about the same rate.

4.4.3 Molecular modeling of B and C in *E. coli* DHOase

The x-ray structure of homodimeric bacterial *E. coli* DHOase with dihydroorotate bound has recently been determined (Thoden et al., 2001). Each subunit contains a binuclear zinc center and dihydroorotate is bound to one subunit with the negatively charged carboxylate group of dihydroorotate forming a salt bridge with the positively charged guanidinium group of Arg20. The protein sequences of DHOase from *E. coli* and humans that code for the lysine residue, that functions as the bridging ligand for zinc, is well conserved. Thus it has been predicted that DHOase from mammalian CAD, like DHOase from *E. coli*, will also contain a binuclear metal center. Assuming mammalian DHOase has a similar structure to *E. coli* DHOase, the positively charged arginine in the active site is the probable reason that **B** and **C**, with their negatively charged carboxylate

groups, are substrates for DHOase, but neutral dexrazoxane is not. A mechanism was proposed in which a bridging hydroxide group attacks the *re*-face of dihydroorotate (Thoden et al., 2001). Given the structural similarity of dihydroorotate to **B** and **C**, a similar mechanism is likely. While the sequence identity homology of the hamster DHOase domain of CAD with that of *E. coli* DHOase is only 20%, there are clusters of highly conserved amino acids (Simmer et al., 1990). The Arg20 is, however, conserved in human DHOase (Thoden et al., 2001). The presence of the guanidinium salt bridge had been predicted earlier based on the homology of DHOase with carbonic anhydrase II (Williams et al., 1995).

The ability of furosemide, but not 4-chlorobenzenesulfonamide, to inhibit DHOase is probably due to the presence of a negatively charged carboxylate group on furosemide (Fig. 4.1c) allowing for stronger binding to the positively charged arginine in the active site of DHOase (Thoden et al., 2001; Williams et al., 1995). Furosemide is a diuretic widely used in the treatment of congestive heart failure. Given that only micromolar peak plasma levels of furosemide are achieved after a typical 40 mg dose (Straughn et al., 1986), it is unlikely that furosemide inhibition of DHOase has any significant pharmacological effects at clinically relevant diuretic doses.

4.4.4 DHOase-mediated hydrolysis of B and C: A basis for dexrazoxane protection against anthracycline-induced cardiotoxicity

DHOase is present in a variety of tissues including the heart, liver, and kidney (Kennedy, 1974) and in erythrocytes and leukocytes (Smith and A., 1959). The level of

DHOase activity in heart homogenate is 23% of that found in the liver (Kennedy, 1974). The presence of DHOase in the heart suggests that **B** and **C** may be enzymatically hydrolyzed by DHOase to ADR-925 in the heart tissue. Hydrolysis would likely be occurring in other tissues and in the blood as well. The presence of DHOase in the heart, in particular, may explain the cardioprotective effect of dexrazoxane. The ADR-925 thus formed may either remove iron from the iron-doxorubicin complex (Buss & Hasinoff, 1993), or bind free iron, thus preventing oxygen radical formation.

The rapid appearance of ADR-925 in preliminary pharmacokinetic studies in the rat (Schroeder & Hasinoff, 2002) and humans (Schroeder et al., 2003) is consistent with a DHOase-catalyzed conversion of **B** and **C** to ADR-925. It has been previously shown that **B** and **C** were present at relatively low steady state levels in a rat pharmacokinetic study (Hasinoff & Aoyama, 1999; Schroeder & Hasinoff, 2002). This result is consistent with the subsequent metabolism of **B** and **C** to ADR-925 by DHOase. We also previously showed that the zinc hydrolase DHPase, which is present in the liver and kidneys, but not in the heart (Hasinoff et al., 1991), converted dexrazoxane to **B** and **C,** but did not convert these intermediates to ADR-925 (Hasinoff, 1993). Previous studies have also shown that **B** and **C** were permeable enough to be taken up by attached neonatal rat myocytes suggesting that **B** and **C,** despite being negatively charged, may be permeable to cell membranes (Hasinoff et al., 2002). Thus, DHPase and DHOase, acting in succession on the parent drug and its metabolites **B** and **C,** provide a mechanism by which dexrazoxane may exert its cardioprotective effects.

4.5 References

Buss, J.L. & Hasinoff, B.B. (1993). The one-ring open hydrolysis product intermediates of the cardioprotective agent ICRF-187 (dexrazoxane) displace iron from iron-anthracycline complexes. *Agents Actions*, **40**, 86-95.

Carrey, E.A. (1993). Phosphorylation, allosteric effectors and inter-domain contacts in CAD; their role in regulation of early steps of pyrimidine biosynthesis. *Biochem Soc Trans*, **21**, 191-5.

Christopherson, R.I. & Jones, M.E. (1980). The effects of pH and inhibitors upon the catalytic activity of the dihydroorotase of multienzymatic protein pyr1-3 from mouse Ehrlich ascites carcinoma. *J Biol Chem*, **255**, 3358-70.

Christopherson, R.I., Schmalzl, K.J., Szabados, E., Goodridge, R.J., Harsanyi, M.C., Sant, M.E., Algar, E.M., Anderson, J.E., Armstrong, A., Sharma, S.C. & et al. (1989). Mercaptan and dicarboxylate inhibitors of hamster dihydroorotase. *Biochemistry*, **28**, 463-70.

Davidson, J.N., Chen, K.C., Jamison, R.S., Musmanno, L.A. & Kern, C.B. (1993). The evolutionary history of the first three enzymes in pyrimidine biosynthesis. *Bioessays*, **15**, 157-64.

Davidson, J.N., Rumsby, P.C. & Tamaren, J. (1981). Organization of a multifunctional protein in pyrimidine biosynthesis. Analyses of active, tryptic fragments. *J Biol Chem*, **256**, 5220-5.

Dawson, K.M. (1975). Studies on the stability and cellular distribution of dioxopiperazines in cultured BHK-21S cells. *Biochem Pharmacol*, **24**, 2249-53.

Earhart, R.H., Tutsch, K.D., Koeller, J.M., Rodriguez, R., Robins, H.I., Vogel, C.L., Davis, H.L. & Tormey, D.C. (1982). Pharmacokinetics of (+)-1,2-di(3,5-dioxopiperazin-1-yl)propane intravenous infusions in adult cancer patients. *Cancer Res*, **42**, 5255-61.

Evans, D.R., Bein, K., Guy, H.I., Liu, X., Molina, J.A. & Zimmermann, B.H. (1993). CAD gene sequence and the domain structure of the mammalian multifunctional protein CAD. *Biochem Soc Trans*, **21**, 186-91.

Hasinoff, B.B. (1993). Enzymatic ring-opening reactions of the chiral cardioprotective agent (+) (S)-ICRF-187 and its (-) (R)-enantiomer ICRF-186 by dihydropyrimidine amidohydrolase. *Drug Metab Dispos*, **21**, 883-8.

Hasinoff, B.B. (1994a). An HPLC and spectrophotometric study of the hydrolysis of ICRF-187 (dexrazoxane, (+)-1,2-bis(3,5-dioxopiperazinyl-1yl)propane and its one-ring opened intermediates. *Int. J. Pharm.*, **107**, 67-76.

Hasinoff, B.B. (1994b). Pharmacodynamics of the hydrolysis-activation of the cardioprotective agent (+)-1,2-bis(3,5-dioxopiperazinyl-1-yl)propane. *J Pharm Sci*, **83**, 64-7.

Hasinoff, B.B. & Aoyama, R.G. (1999). Relative plasma levels of the cardioprotective drug dexrazoxane and its two active ring-opened metabolites in the rat. *Drug Metab Dispos*, **27**, 265-8.

Hasinoff, B.B., Reinders, F.X. & Clark, V. (1991). The enzymatic hydrolysis-activation of the adriamycin cardioprotective agent (+)-1,2-bis(3,5-dioxopiperazinyl-1-yl)propane. *Drug Metab Dispos*, **19**, 74-80.

Hasinoff, B.B., Venkataram, S., Singh, M. & Kuschak, T.I. (1994). Metabolism of the cardioprotective agents dexrazoxane (ICRF-187) and levrazoxane (ICRF-186) by the isolated hepatocyte. *Xenobiotica*, **24**, 977-87.

Hochster, H., Liebes, L., Wadler, S., Oratz, R., Wernz, J.C., Meyers, M., Green, M., Blum, R.H. & Speyer, J.L. (1992). Pharmacokinetics of the cardioprotector ADR-529 (ICRF-187) in escalating doses combined with fixed-dose doxorubicin. *J Natl Cancer Inst*, **84**, 1725-30.

Huang, D.T., Thomas, M.A. & Christopherson, R.I. (1999). Divalent metal derivatives of the hamster dihydroorotase domain. *Biochemistry*, **38**, 9964-70.

Jakobsen, P., Sorensen, B., Bastholt, L., Mirza, M.R., Gjedde, S.B., Mouridsen, H.T. & Rose, C. (1994). The pharmacokinetics of high-dose epirubicin and of the cardioprotector ADR-529 given together with cyclophosphamide, 5-fluorouracil, and tamoxifen in metastatic breast-cancer patients. *Cancer Chemother Pharmacol*, **35**, 45-52.

Kelly, R.E., Mally, M.I. & Evans, D.R. (1986). The dihydroorotase domain of the multifunctional protein CAD. Subunit structure, zinc content, and kinetics. *J Biol Chem*, **261**, 6073-83.

Kennedy, J. (1974). Dihydroorotase from rat liver: purification, properties and regulatory role in pyrimidine biosynthesis. *Arch Biochem Biophys*, **160**, 358-65.

Pradhan, T.K. & Sander, E.G. (1973). Noncompetitive inhibition by substituted sulfonamides of dihydroorotase from Zymobacterium oroticum. *Life Sci*, **13**, 1747-52.

Qiu, Y. & Davidson, J.N. (2000). Substitutions in the aspartate transcarbamoylase domain of hamster CAD disrupt oligomeric structure. *Proc Natl Acad Sci U S A*, **97**, 97-102.

Schroeder, P.E., Davidson, J.N. & Hasinoff, B.B. (2002). Dihydroorotase catalyzes the ring opening of the hydrolysis intermediates of the cardioprotective drug dexrazoxane (ICRF-187). *Drug Metab Dispos*, **30**, 1431-5.

Schroeder, P.E. & Hasinoff, B.B. (2002). The doxorubicin-cardioprotective drug dexrazoxane undergoes metabolism in the rat to its metal ion-chelating form ADR-925. *Cancer Chemother Pharmacol*, **50**, 509-13.

Schroeder, P.E., Jensen, P.B., Sehested, M., Hofland, K.F., Langer, S.W. & Hasinoff, B.B. (2003). Metabolism of dexrazoxane (ICRF-187) used as a rescue agent in cancer patients treated with high-dose etoposide. *Cancer Chemother Pharmacol*, **52**, 167-74.

Simmer, J.P., Kelly, R.E., Rinker, A.G., Jr., Zimmermann, B.H., Scully, J.L., Kim, H. & Evans, D.R. (1990). Mammalian dihydroorotase: nucleotide sequence, peptide sequences, and evolution of the dihydroorotase domain of the multifunctional protein CAD. *Proc Natl Acad Sci U S A*, **87**, 174-8.

Smith LH, Jr. and Baker FA (1959) Pyrimidine metabolism in man. I. The biosynthesis of orotic acid. *J Clin Invest* 38:798-809.

Straughn, A.B., Wood, G.C., Raghow, G. & Meyer, M.C. (1986). Bioavailability of seven furosemide tablets in man. *Biopharm Drug Dispos*, **7**, 113-20.

Thoden, J.B., Phillips, G.N., Jr., Neal, T.M., Raushel, F.M. & Holden, H.M. (2001). Molecular structure of dihydroorotase: a paradigm for catalysis through the use of a binuclear metal center. *Biochemistry*, **40**, 6989-97.

Vogel, C.L., Gorowski, E., Davila, E., Eisenberger, M., Kosinski, J., Agarwal, R.P. & Savaraj, N. (1987). Phase I clinical trial and pharmacokinetics of weekly ICRF-187 (NSC 169780) infusion in patients with solid tumors. *Invest New Drugs*, **5**, 187-98.

Williams, N.K., Manthey, M.K., Hambley, T.W., O'Donoghue, S.I., Keegan, M., Chapman, B.E. & Christopherson, R.I. (1995). Catalysis by hamster dihydroorotase: zinc binding, site-directed mutagenesis, and interaction with inhibitors. *Biochemistry*, **34**, 11344-52.

Chapter 5: The effect of DHPase and DHOase inhibition on the metabolism of dexrazoxane and its one-ring open intermediates to ADR-925 in the rat

5.1   Introduction

Dexrazoxane (Figure 5.1) is clinically used to reduce doxorubicin-induced cardiotoxicity (Swain et al., 1997; Hasinoff, 1998; Hasinoff et al., 1998; Swain and Vici, 2004). The clinical use of doxorubicin, a highly effect antitumor agent (Gianni et al., 1983), is limited by its cumulative dose cardiotoxicity. Dexrazoxane attenuates anthracycline cardiotoxicity (Herman and Ferrans, 1987; Blum et al., 1990) and likely acts as a cardioprotective agent by diffusing into the cell and hydrolyzing to its one-ring open intermediates **B** and **C**, and then to it's fully rings-opened metal ion-chelating form ADR-925 (Figure 5.1). ADR-925, a structural analogue to EDTA, may act by chelating free iron or displacing iron bound to the iron-doxorubicin complex (Hasinoff, 1989; Buss and Hasinoff, 1993; Hasinoff, 1998; Hasinoff et al., 1998), thereby reducing iron-based oxygen radical formation.

Dihydropyrimidine amidohydrolase, EC 3.5.2.2, (DHPase) catalyzes the reversible hydrolysis of 5,6-dihydrouracil to N-carbamoyl-β-alanine and is the second enzyme in the pyrimidine synthesis pathway (Lee et al., 1986; Kikugawa et al., 1994). DHPase, which is present in the liver and the kidney, has been shown to efficiently hydrolyze dexrazoxane (Hasinoff et al., 1991; Hasinoff, 1993; Hasinoff, 1994c; Hasinoff and Aoyama, 1999b) and is likely the enzyme that is primarily responsible for the metabolism of dexrazoxane to **B** and **C**. While DHPase did not detectably hydrolyze **B** or **C** to ADR-925 (Hasinoff, 1993), **B** and **C** were shown to be enzymatically hydrolyzed

by dihydroorotase, EC 3.5.2.2 (DHOase), as described in Chapter 4 (Schroeder et al., 2002). DHOase catalyzes the reversible cyclization of N-carbamyl-L-aspartate to form L-5,6-dihydroorotate which is the third reaction in the *de novo* pyrimidine biosynthetic pathway (Christopherson and Jones, 1980; Carrey, 1993). Unlike DHPase (Hamajima et al., 1996), DHOase has been shown to have good activity in the heart (Kennedy, 1974).

An enzymatically mediated mechanism of cardioprotection from anthracycline-induced cardiotoxicity was hypothesized for dexrazoxane that included DHPase-mediated hydrolysis of dexrazoxane to **B** and **C**, and DHOase-mediated hydrolysis of **B** and **C** to ADR-925. A rat model was used to determine the contribution of DHPase and DHOase in the hydrolysis of dexrazoxane to ADR-925 *in vivo*. The DHPase and DHOase inhibitor furosemide (Schroeder et al., 2002) (Figure 5.2a) and the DHOase inhibitor 5-aminoorotic acid (Christopherson and Jones, 1980; Krungkrai et al., 1992; El Kolli et al., 1998) (Figure 5.2 b) were administered to the rat prior to dexrazoxane where the effect of DHPase and DHOase inhibition on ADR-925 plasma and tissue levels were determined. The effect of 5-aminoorotic acid mediated DHOase inhibition on plasma and tissue levels of ADR-925 following a **B/C** mixture bolus was also investigated. These *in vivo* studies further describe how the mechanism of dexrazoxane protection is linked to enzymatic activation.
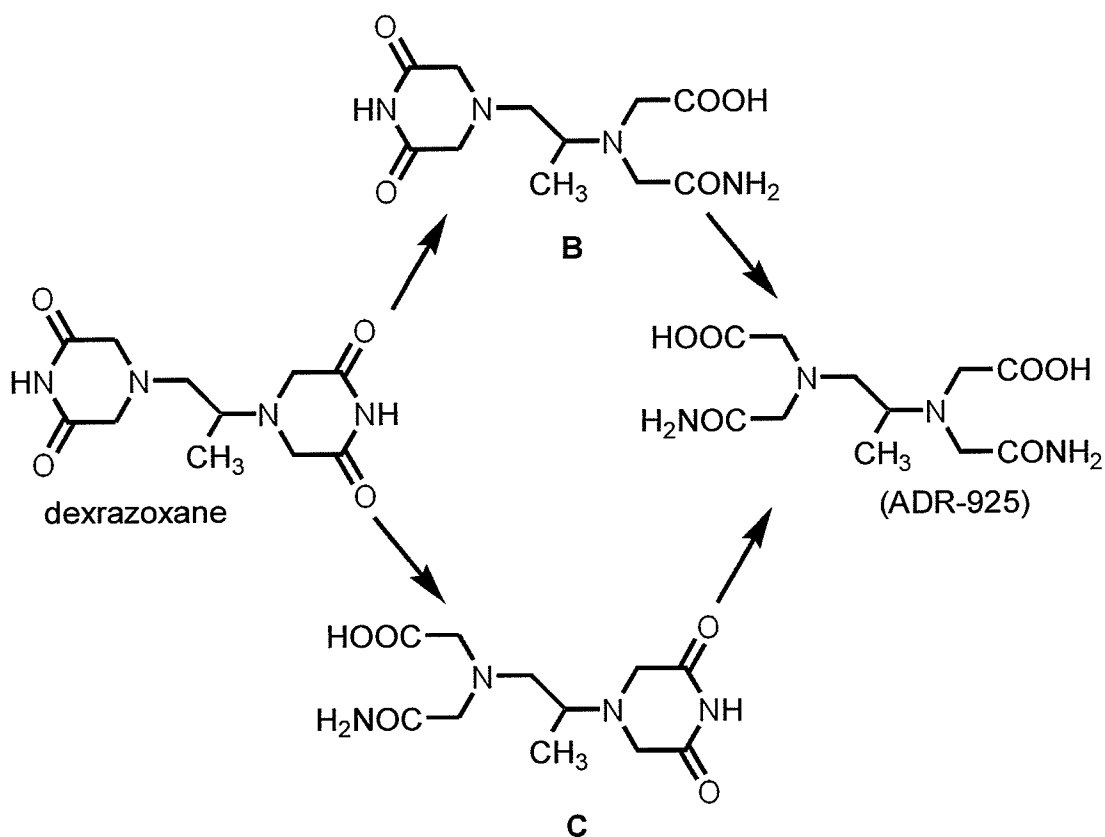
Figure 5.1. Reaction scheme for the hydrolysis of dexrazoxane to intermediates **B** and **C**, and its strongly metal ion-chelating form ADR-925.
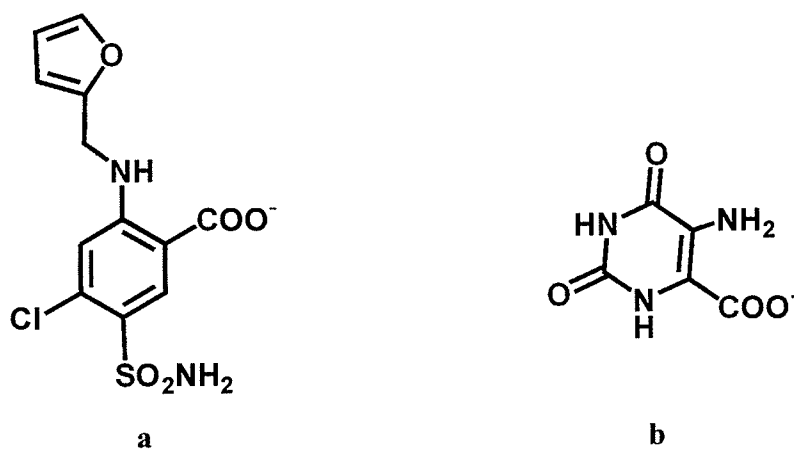
Figure 5.2 Structures of the DHPase and DHOase inhibitor furosemide (a) and the DHOase inhibitor 5-aminoorotic acid (b).

5.2 Materials and Methods

5.2.1 Materials

Dexrazoxane hydrochloride and ADR-925 were gifts from Adria Laboratories (Columbus, OH). Calcein ("high purity") was from Molecular Probes (Eugene, OR). HPLC-grade methanol and cobalt chloride hexahydrate were from Fisher (Nepean, Canada) and heparin, Tris, EDTA, furosemide, 5-aminoorotic acid, reagent grade catalase (Catalogue #: C-30), Coomassie Brilliant Blue Dye, and 1-heptanesulfonic acid sodium salt were from Sigma (St. Louis, MO).

5.2.2 Animal handling and surgery

The animals were handled and anaesthetized as described in Section 2.2.2 of Chapter 2 and the protocol was approved by the University of Manitoba Animal Care Committee.

5.2.3 Dosing and blood collection

A furosemide solution was prepared by slowly adding (1 µl/sec) 10 µl of 5 M NaOH to 1 ml of a freshly prepared 10 mg/ml furosemide solution in sterile saline (0.9 % NaCl, w/v) followed by rapid vortex until dissolved. The pH was titrated to 6-7 with 1 M HCl. The solution was kept in a 37 °C water bath until used. The furosemide solution was not filter sterilized to prevent furosemide loss due to precipitation. After the animal was anesthetized and the jugular vein cannulated (as described in Section 2.2.2) the rat was dosed with a 20 mg/kg furosemide bolus (2 ml/min) through the tail vein.

Dexrazoxane hydrochloride (freshly prepared, 10 mg/ml in sterile saline) was filtered using a Fisherbrand™ 0.22 μm syringe filter (Fisher, Canada) and administered at a dose of 40 mg/kg as an *i.v.* bolus infusion (2 ml/min) through the tail vein. Blood samples (300 μl) were removed from the left jugular vein from a group of 3 rats at times 5, 10, 30, 60, 90, and 120 min post-dexrazoxane infusion.

A 10 mg/ml 5-aminoorotic acid solution was prepared in sterile saline (0.9 % NaCl, w/v) by adding 10-20 μl of 5 M NaOH with rapid vortex. Once dissolved, the pH was titrated to the range of 6-7.5 with 1 M HCl and stored at 37 °C until use. As in the case of furosemide, 5-aminoorotic acid solution was not filter sterilized to avoid loss through precipitation. The rat was dosed with 20 mg/kg of 5-aminoorotic acid as an *i.v.* bolus infusion (2 ml/min) through the tail vein. Dexrazoxane hydrochloride (freshly prepared in 10 mg/ml sterile saline) was administered at a dose of 40 mg/kg as an *i.v.* bolus infusion (2 ml/min) through the tail vein. In the case where the **B/C** mixture was used (prepared as described in Section 2.2.4, with a **B/C** mole ratio of 4.2:1, determined by HPLC as described in Section 2.2.9), rats were dosed with 20 mg/kg of 5-aminoorotic acid as a 0.5 ml *i.v.* bolus infusion (2 ml/min) through the tail vein 5 min prior to a 20 mg/kg **B/C** mixture bolus (0.5 ml, also through the tail vein). Blood samples (300 μl) were removed from the left jugular vein from a group of 3 rats for both dexrazoxane and **B/C** mixture at times 2, 10, 20, 30, 45, 60, and 90 min. One 300 μl blood sample was drawn from each rat prior to the administration of dexrazoxane or **B/C** as a control.

The blood samples from all experiments were added to heparin (10 μl of 1000 units/ml) and centrifuged for 5 min at 500 *g*. The plasma was immediately removed,

acidified to a pH of 3 with 20 μl of 5 M HCl per ml of plasma, and stored at -80 °C to prevent further hydrolysis (Hasinoff, 1994a).

5.2.4 Precipitation of rat plasma proteins

Plasma proteins were precipitated with acetonitrile (2:1 (v/v)) as described in Section 2.2.6.

5.2.5 Quantitation of dexrazoxane, B, C, and ADR-925

Dexrazoxane, **B**, and **C**, were separated and quantified using HPLC as described in Chapter 2 Section 2.2.9. ADR-925 was determined in plasma and tissue homogenate supernatants using the calcein assay as described in Section 2.2.11.

5.2.6 Preparation of heart, liver, and brain tissue homogenates

In order to compare the effect of the DHPase and DHOase inhibition on ADR-925 accumulation in tissues, the heart and liver were removed immediately following the last acquired data point and treated as described in Section 2.2.7.

5.2.7 Data analysis

Pharmacokinetic parameters were obtained using the pharmacokinetic and pharmacodynamic modeling program WinNonlin (WinNonlin 4.0, Pharsight, Mountain View, CA) for an *i.v.* bolus. The effect of DHOase or DHPase inhibition on pharmacokinetic parameters for dexrazoxane, **B**, **C**, and ADR-925 were statistically compared by an independent-samples *t-test* where p is the probability of rejecting the null hypothesis (Jones, 2002).

200

5.3 Results

5.3.1 Pharmacokinetic analysis of the data

5.3.2.1 Determination of dexrazoxane distribution and ADR-925 formation by AUC_{5-120}

The dexrazoxane and ADR-925 concentration-time curve was compared in rats dosed with either 5-aminoorotic acid or furosemide prior to dexrazoxane relative to the concentration-time curve of rats dosed with dexrazoxane alone. The limited sampling in the alpha (or distribution) phase of the concentration-time curve made compartmental analysis of dexrazoxane (as described in Chapter 2 and Chapter 3) inappropriate. It was decided to compare the concentration-time curves for dexrazoxane for rats treated with DHOase or DHPase inhibitors prior to dexrazoxane relative to rats dosed with dexrazoxane alone through non-compartmental analysis of the area-under-the-curve AUC_{5-120} of the concentration-time data of dexrazoxane or ADR-925 from the first time point (5 min) to the last time point (120 min). Therefore, values for the maximum plasma concentration were obtained directly from the observed data, at 5 min. The area under the plasma concentration-time curve to the last observed concentration was calculated using the linear/log linear trapezoidal method (Winnonlin Model 201 for non-compartmental analysis) with the observed data.

5.3.2.2 Pharmacokinetics of B, C, and ADR-925 in rats dosed with a B/C mixture following a 5-aminoorotic acid bolus

The plasma pharmacokinetics for the *i.v.* bolus of a B/C mixture was fitted to an *i.v.* bolus one-compartment model (equation 5.1 and 5.2, WinNonlin Model 1) (WinNonlin 4.0, Pharsight, Mountain View, CA). The one-compartment model was used

to describe the entire plasma concentration (C) versus time (t) curve fitted by a single exponential term where C_B and C_C refer to the zero-time intercepts and k_b and k_c refer to the elimination rate constants of the concentration-time curve of **B** (equation 5.1) and **C**, (equation 5.2) respectively.

$$C_t = C_B \cdot e^{-k_b \cdot t} \qquad\qquad 5.1$$

$$C_t = C_C \cdot e^{-k_c \cdot t} \qquad\qquad 5.2$$

The elimination half life ($t_{\frac{1}{2}k}$) for **B** and **C** is defined by equations 5.3 and 5.4, respectively.

$$t_{\frac{1}{2}kb} = \frac{\ln 2}{k_b} \qquad\qquad 5.3$$

$$t_{\frac{1}{2}kc} = \frac{\ln 2}{k_c} \qquad\qquad 5.4$$

The apparent elimination rate of ADR-925 (k_{ADR}) was also determined by fitting the data to a two-parameter single-exponential decay function (equation 5.5) where the apparent elimination half life is estimated by equation 5.6.

$$C_t = C_{ADR} \cdot e^{-k_{ADR} \cdot t} \qquad\qquad 5.5$$

$$t_{\frac{1}{2}kADR} = \frac{\ln 2}{k_{ADR}} \qquad\qquad 5.6$$

The pharmacokinetic parameters for **B** and the apparent pharmacokinetic parameters for ADR-925 were determined from the concentration-time data for the first 30 min after the **B/C** bolus. The pharmacokinetic parameters for **C** were determined from the concentration-time data for the first 10 min after the **B/C** bolus.

5.3.2 Dexrazoxane metabolism to B, C, and ADR-925 after a 20 mg/kg i.v. bolus of the DHPase and DHOase inhibitor furosemide (20 mg/kg)

The results shown in Figures 5.3-5.5 show the individual rat concentration-time plasma levels (as shown in Tables 5.1-5.4) for dexrazoxane, **B**, **C**, and ADR-925. Figure 5.6 is the average dexrazoxane and metabolite concentration-time data for all three rats. As shown in Figure 5.7 the disposition kinetics of dexrazoxane is similar to that previously obtained for rats (Chapter 2, Section 2.3.6 (Schroeder and Hasinoff, 2002)) likewise dosed with 40 mg/kg of dexrazoxane hydrochloride (Hasinoff and Aoyama, 1999a; Schroeder and Hasinoff, 2002). The peak plasma concentration of dexrazoxane (observed data at 5 min) following an i.v. bolus of furosemide was found to be 603 ± 8.7 µM, which was consistent with the maximal dexrazoxane concentration of 529 ± 41 µM after a dexrazoxane bolus alone (as shown in Figure 5.7). Furthermore, the AUC_{5-120} of dexrazoxane in rats treated with furosemide 5 min prior to dexrazoxane was not significantly different from rats dosed with dexrazoxane alone ($p > 0.5$, Table 5.5). As in the case where dexrazoxane was given alone (as shown in Figure 5.7 and 5.8, data from Chapter 2, Section 2.3.6 (Schroeder and Hasinoff, 2002)), the intermediates **B** and **C** immediately appeared in plasma (5 min post dexrazoxane infusion) when furosemide was given 5 min prior to dexrazoxane. The peak concentrations for **B** and **C** were also found to be at a maximum 5 min post dexrazoxane infusion, with plasma concentrations of 12.4 ± 1.3 and 2.4 ± 1.1 µM, for **B** and **C** respectively. After dexrazoxane administration (5 min post furosemide infusion), the initial maximum of **B** and **C** levels was followed by a rapid decrease where, at 30 min, the low metabolite levels remained essentially constant or below the limit of detection (1.5 µM). As is the case when dexrazoxane is given alone, it can also be seen from the data in Figure 5.6 that the concentration of **B** was

typically larger than that of **C**. While peak **B** and **C** concentrations occurred immediately following the dexrazoxane bolus, the maximum concentrations of these metabolites (at 5 min post dexrazoxane infusion) were 5- and 3-fold less for **B** and **C** ($p < 0.05$), respectively, when furosemide was given prior to dexrazoxane relative to dexrazoxane alone. The initial concentration-time curve of ADR-925 plasma levels of rats dosed with furosemide and dexrazoxane mirrored those of rats dosed with dexrazoxane alone (as shown in Figure 5.7) however, after 45 min ADR-925 levels are less in rats dosed with furosemide prior to dexrazoxane versus rats dosed with dexrazoxane alone. The AUC_{5-120} of ADR-925 in rats dosed with furosemide 5 min prior to dexrazoxane was 1.8-fold lower ($p < 0.03$) relative to rats dosed with dexrazoxane alone.

Table 5.1 Plasma concentrations (μM) of dexrazoxane following a 40 mg/kg dexrazoxane hydrochloride bolus in male Sprague-Dawley rats pre-dosed with 20 mg/kg of the DHPase inhibitor furosemide

Time	Rat 1 Dexrazoxane, μM	Rat 2 Dexrazoxane, μM	Rat 3 Dexrazoxane, μM	Average Dexrazoxane, μM	SE ($\pm\mu$M)
5	590	619	600	603	8.7
10	440	384	458	427	22.7
30	140	75.7	105	110	18.9
60	75	65	62	67.3	4.0
90	57	57	40	51.3	5.8
120	41	38	34	37.7	2.1

Table 5.2 Plasma concentrations (μM) of **B** following a 40 mg/kg dexrazoxane hydrochloride bolus in male Sprague-Dawley rats pre-dosed with 20 mg/kg of the DHPase inhibitor furosemide

Time	Rat 1 B, μM	Rat 2 B, μM	Rat 3 B, μM	Average B, μM	SE ($\pm\mu$M)
5	11.5	10.8	15	12.4	1.3
10	7.9	3.9	7	6.3	1.2
30	<LOD	8	2.5	3.9	--
60	7.1	2.7	2	3.9	1.6
90	6.2	2.6	<LOD	4.4	--
120	2	<LOD	<LOD	<LOD	--

Table 5.3 Plasma concentrations (μM) of **C** following a 40 mg/kg dexrazoxane hydrochloride bolus in male Sprague-Dawley rats pre-dosed with 20 mg/kg of the DHPase inhibitor furosemide

Time	Rat 1 **C**, μM	Rat 2 **C**, μM	Rat 3 **C**, μM	Average **C**, μM	SE (±μM)
5	4.6	1	1.7	2.4	1.1
10	2.1	3.4	2	2.5	0.5
30	<LOD	<LOD	4.2	<LOD	--
60	<LOD	6.5	<LOD	<LOD	--
90	<LOD	7.1	<LOD	<LOD	--
120	<LOD	<LOD	<LOD	<LOD	--

Table 5.4 Plasma concentrations (μM) of ADR-925 following a 40 mg/kg dexrazoxane hydrochloride bolus in male Sprague-Dawley rats pre-dosed with 20 mg/kg of the DHPase inhibitor furosemide

Time	Rat 1 ADR-925, μM	Rat 2 ADR-925, μM	Rat 3 ADR-925, μM	Average ADR-925, μM	SE (±μM)
5	7.5	13.6	4.3	8.5	2.8
10	8.1	2.2	13.1	7.8	3.2
30	11.1	40.8	17.4	23.1	9.2
60	36.8	43.6	29.9	36.8	4.0
90	12.1	29.2	33.4	24.9	6.6
120	5.1	12.3	20.2	13.1	5.4

Table 5.5 Comparison of the AUC_{5-120} of dexrazoxane in rats dosed with the DHPase and DHOase inhibitor furosemide prior to dexrazoxane relative to rats dosed with dexrazoxane alone.

Rat Number	AUC_{5-120} of dexrazoxane	
	Dexrazoxane[a], (μM·min)	Furosemide + Dexrazoxane, (μM·min)
1	21,567	18,502
2	19,099	16,512
3	15,010	16,885
4	16,785	--
5	16,851	--
6	22,389	--
Average	18,617	17,300
SE	1,192	611
p	--	$p > 0.5$

[a] Reanalysis of data obtained from rats dosed with dexrazoxane alone (complete data set found in Chapter 2 Section 2.3.1)

Table 5.6 Comparison of the AUC_{5-120} of ADR-925 in rats dosed with the DHPase and DHOase inhibitor furosemide prior to dexrazoxane relative to dexrazoxane alone.

Rat Number	AUC_{5-120} of ADR-925	
	Dexrazoxane[a], (μM·min)	Furosemide + Dexrazoxane, (μM·min)
1	6602	1978
2	5344	3694
3	4863	2833
4	5299	--
5	3177	--
6	4609	--
Average	4982	2835
SE	457	496
p		$p < 0.03$

[a] Reanalysis of data obtained from rats dosed with dexrazoxane alone (complete data set found in Chapter 2 Section 2.3.1)
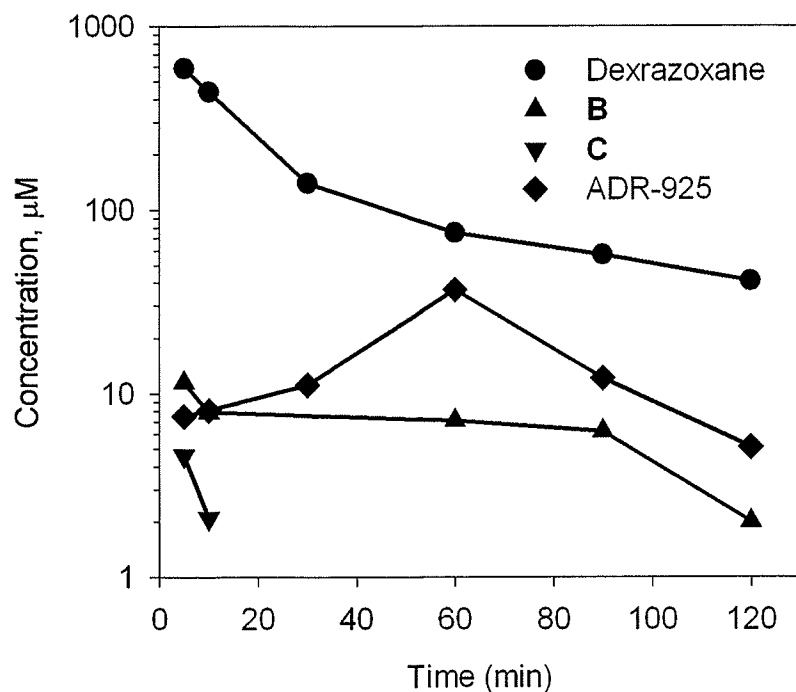
Figure 5.3 Plasma concentrations of dexrazoxane, **B**, **C**, and ADR-925 for rat 1 after an i.v. bolus of 40 mg/kg dexrazoxane hydrochloride 5 min after an i.v. bolus of the DHPase inhibitor furosemide (20 mg/kg).
After 10 min, **C** concentration-time data was below the limit of quantitation (LOQ).
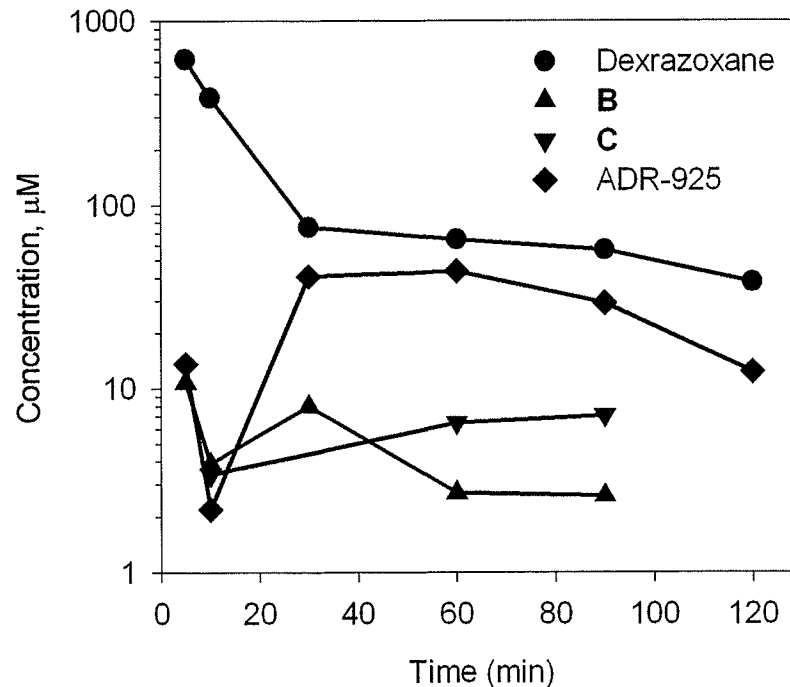
Figure 5.4 Plasma concentrations of dexrazoxane, **B**, **C**, and ADR-925 for rat 2 after an i.v. bolus of 40 mg/kg dexrazoxane hydrochloride 5 min after an i.v. bolus of the DHPase inhibitor furosemide (20 mg/kg).
After 90 min, **B** and **C** concentration-time data were below the limit of quantitation (LOQ).

207
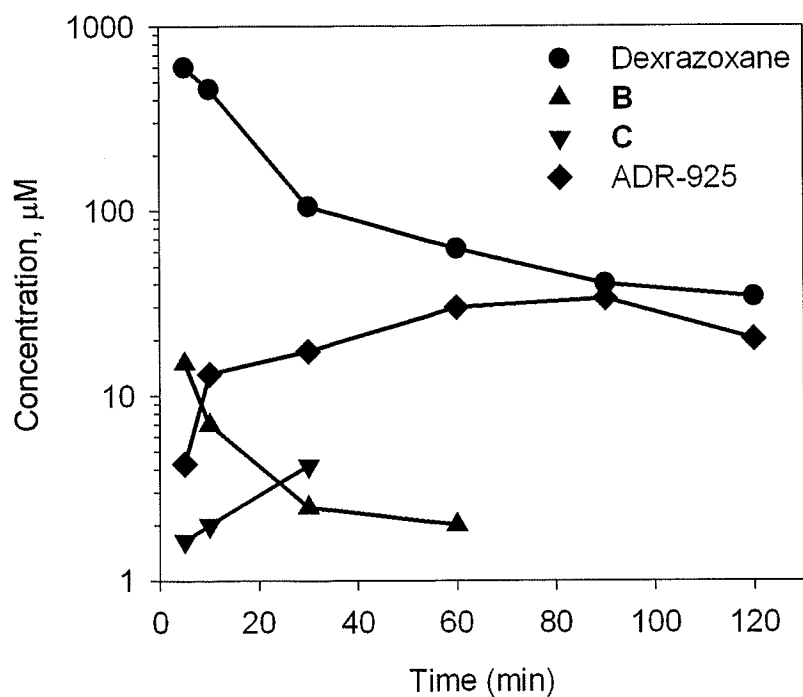
*Figure 5.5 Plasma concentrations of dexrazoxane, **B**, **C**, and ADR-925 for rat 3 after an i.v. bolus of 40 mg/kg dexrazoxane hydrochloride 5 min after an i.v. bolus of the DHPase inhibitor furosemide (20 mg/kg).*

After 60 and 30 min, the concentration-time data was below the limit of quantitation for **B** and **C**, respectively.
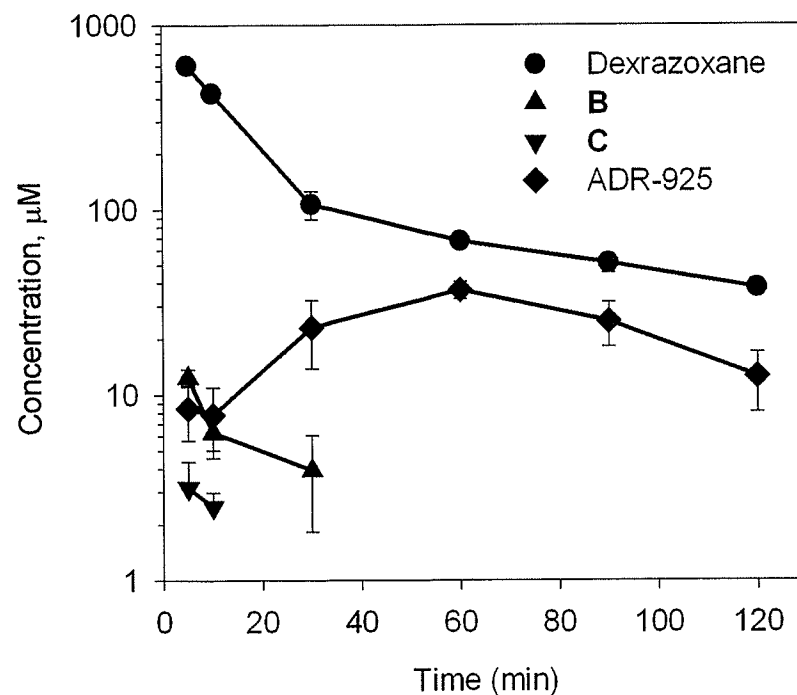
*Figure 5.6 Average rat plasma concentrations of dexrazoxane, **B**, **C**, and ADR-925 after an i.v. bolus of 40 mg/kg of dexrazoxane hydrochloride following an i.v. dose of the DHPase inhibitor furosemide (20 mg/kg).*

Error bars represent the SEMs from 3 rats per concentration-time point. After 30 and 10 min, the concentration-time data was below the limit of quantitation for **B** and **C**, respectively, in at least one rat.

208
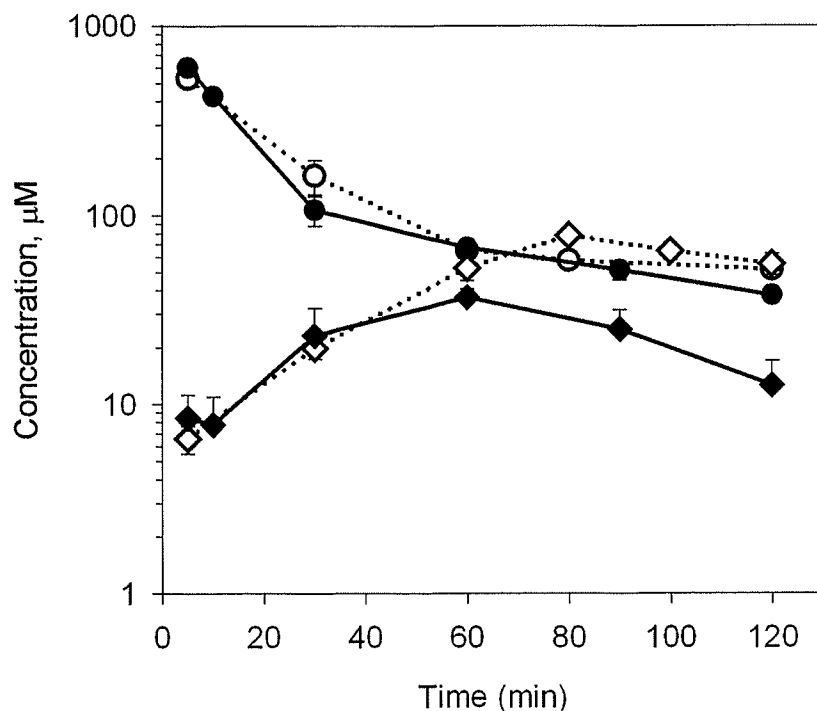
Figure 5.7 Average plasma concentrations of dexrazoxane (●) and ADR-925 (◆) for rats dosed with furosemide (20 mg/kg) 5 min prior to dexrazoxane hydrochloride (40 mg/kg) compared to average plasma concentrations of dexrazoxane (O) and ADR-925 (◇) from rats dosed with dexrazoxane (40 mg/kg) alone.
Error bars for solid symbols represent the SEMs from 3 rats per concentration-time point and error bars for outlined symbols represent the SEMs from 6 rats (data from Chapter 2 Section 2.3.1).
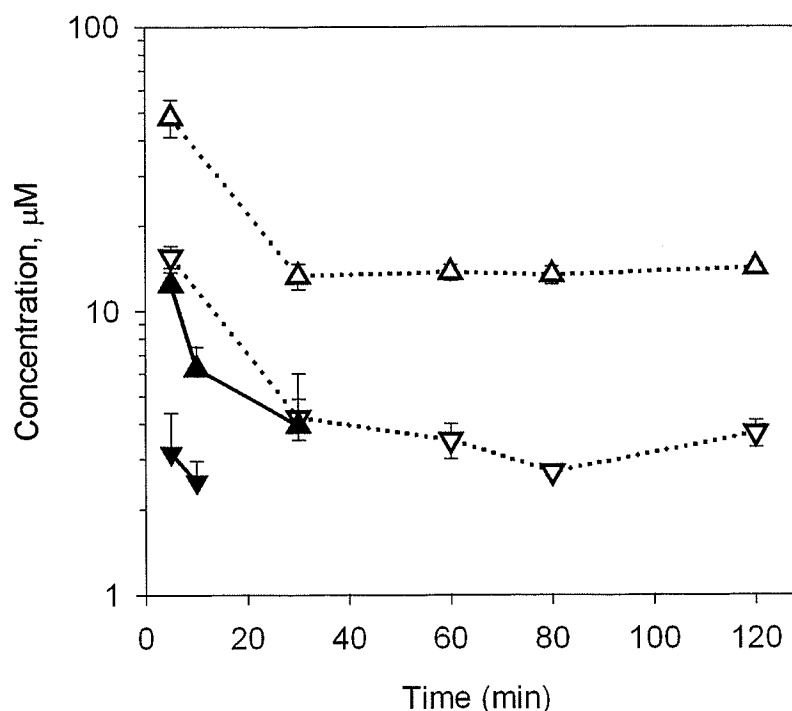
Figure 5.8 Average plasma concentrations of B (▲) and C (▼) for rats dosed with furosemide (20 mg/kg) 5 min prior to dexrazoxane (40 mg/kg) compared to average plasma concentrations of B (△) and C (▽) dosed with dexrazoxane (40 mg/kg) alone.
Error bars for solid symbols represent the SEMs from 3 rats per concentration-time point and error bars for outlined symbols represent the SEMs from 6 rats (data from Chapter 2). After 30 and 10 min, the concentration-time data was below the limit of quantitation for B and C, respectively, in at least one rat.

5.3.2.3 ADR-925 levels in tissues from rats dosed with 20 mg/kg furosemide 5 min prior to a 40 mg/kg dexrazoxane bolus

ADR-925 levels in heart and liver tissue homogenate supernatant of rats dosed with furosemide 5 min prior to the 40 mg/kg dexrazoxane hydrochloride bolus are shown in Table 5.7. ADR-925 levels found in the liver were approximately 3 fold greater than those found in the heart. Also, as shown in Table 5.8, ADR-925 levels in the heart were found to be 3-fold lower ($p < 0.02$) in rats dosed with furosemide 5 min prior to dexrazoxane relative to rats dosed with dexrazoxane alone. As shown in Table 5.8, no significant difference was found in liver homogenate supernatants between rats dosed with furosemide 5 min prior to dexrazoxane or dexrazoxane alone.

Table 5.7 Liver and heart tissue homogenate supernatant concentrations of ADR-925 as determined by the calcein assay from rats dosed with furosemide 5 min prior to dexrazoxane. Rat tissues were removed and treated as described in Section 2.2.7 at 120 min post-dexrazoxane infusion.

Rat Number	ADR-925 (μmol/g wet tissue)	
	Heart	Liver
1	0.0132	0.0648
2	0.0210	0.0728
3	0.0214	0.0507
Average	0.0185	0.0628
SE	0.0027	0.0066

Table 5.8 Comparison of mean ADR-925 tissue levels in rats dosed with furosemide prior to dexrazoxane relative to rats dosed with dexrazoxane alone.

Study	Heart homogenate		Liver homogenate	
	ADR-925, μmol/g wet tissue ($\pm$ SE)	p-Value	ADR-925, μmol/g wet tissue ($\pm$ SE)	p-Value
Dexrazoxane[a] (n=7)	0.0515 (0.0063)	--	0.0971 (0.0137)	--
Furosemide + Dexrazoxane (n=3)	0.0185 (0.0027)	$p < 0.02$	0.0628 (0.0066)	$p > 0.1$

[a] Obtained from rats dosed with dexrazoxane alone (complete data set found in Chapter 2 Section 2.3.1.1)

5.3.3 Metabolism of dexrazoxane to ADR-925 after a 20 mg/kg i.v. bolus of the DHOase inhibitor 5-aminoorotic acid

The results shown in Figures 5.9-5.11 show the individual rat concentration-time

plasma levels (as shown in Tables 5.9-5.12) for dexrazoxane, **B**, **C**, and ADR-925, where

Figure 5.12 is the average dexrazoxane and metabolite concentration-time data for all

three rats dosed with 5-aminoorotic acid 5 min prior to dexrazoxane. As shown in Figure

5.13 the concentration-time dexrazoxane plasma levels from rats dosed with 5-

aminoorotic acid 5 min prior to dexrazoxane is similar to that previously obtained for rats

(Chapter 2, (Schroeder and Hasinoff, 2002)) likewise dosed at 40 mg/kg of dexrazoxane

hydrochloride (Hasinoff and Aoyama, 1999a; Schroeder and Hasinoff, 2002). The peak

plasma concentration of dexrazoxane for rats dosed with 5-aminoorotic acid 5 min prior

to dexrazoxane was found to be 515 ± 38.5 μM (Table 5.9), which is consistent with the

initial dexrazoxane concentration of 529 ± 41 μM (Table 2.12) found immediately

following a dexrazoxane bolus alone (as shown in Figure 5.7). Also, the AUC_{5-120} of

dexrazoxane in rats dosed with 5-aminoorotic acid is not significantly different ($p > 0.5$)

than that of rats dosed with dexrazoxane alone as shown in Figure 5.16 and in Table 5.13.

As in the case where dexrazoxane was given alone (as shown in Figure 5.13), the

intermediates **B** and **C** immediately appeared in plasma (5 min post dexrazoxane

infusion) and also had apparent maximum concentrations at the earliest measured time

point (5 min). The initial maximum concentrations of **B** and **C** were not significantly

different ($p > 0.2$) in rats dosed with 5-aminoorotic acid prior to dexrazoxane, relative to

dexrazoxane alone. After dexrazoxane administration, the **B** and **C** levels rapidly fell

and, as shown in Figure 5.12, the concentration of **C** fell below the limit of quantitation.

As is the case when dexrazoxane is given alone, the data in Figure 5.12 shows the

concentration of **B** was always larger than that of **C** over the duration of the study. ADR-925 also immediately appeared in the plasma of rats dosed with 5-aminoorotic acid 5 min prior to dexrazoxane. As shown in Figure 5.13, plasma concentrations of ADR-925 were essentially maintained at low levels throughout the duration of the experiments when 5-aminoorotic acid was given prior to dexrazoxane. The formation of ADR-925 in rats treated with 5-aminoorotic acid was 5.3 fold lower ($p < 0.001$) than when dexrazoxane was given alone, as measured by their respective AUC_{5-120} (as shown in Table 5.14).

Table 5.9 Plasma concentrations (μM) of dexrazoxane following a 40 mg/kg dexrazoxane hydrochloride bolus in male Sprague-Dawley rats pre-dosed with 20 mg/kg of the DHOase inhibitor 5-aminoorotic acid

Time	Rat 1 Dexrazoxane, μM	Rat 2 Dexrazoxane, μM	Rat 3 Dexrazoxane, μM	Average Dexrazoxane, μM	SE $\pm\ \mu$M
5	493	589	464	515	38.5
15	332	346	156	278	62.3
30	147	148	89.6	128	19.7
45	75.6	74.7	67.0	72.4	2.8
60	46.1	57.5	58.8	54.1	4.1
90	31.8	35.1	57.5	41.5	8.2
120	26.1	29.7	40.9	35.3	4.7

Table 5.10 Plasma concentrations (μM) of **B** following a 40 mg/kg dexrazoxane hydrochloride bolus in male Sprague-Dawley rats pre-dosed with 20 mg/kg of the DHOase inhibitor 5-aminoorotic acid

Time	Rat 1 B, μM	Rat 2 B, μM	Rat 3 B, μM	Average B, μM	SE $\pm\ \mu$M
5	108.0	89.0	14.0	70.3	29.2
15	46.8	63.8	6.3	39.0	17.4
30	20.1	51.5	4.4	25.3	14.1
45	19.3	40.0	2.0	20.4	11.2
60	9.9	33.8	4.0	15.9	9.3
90	2.3	20.5	< LOD	11.4	--
120	< LOD	20.8	< LOD	--	--

Table 5.11 Plasma concentrations (μM) of **C** following a 40 mg/kg dexrazoxane hydrochloride bolus in male Sprague-Dawley rats pre-dosed with 20 mg/kg of the DHOase inhibitor 5-aminoorotic acid

Time	Rat 1 C, μM	Rat 2 C, μM	Rat 3 C, μM	Average C, μM	SE ± μM
5	15.0	34.9	2.2	17.4	9.7
15	9.6	5.7	1.6	5.6	2.4
30	< LOD	4.8	< LOD	--	--
45	< LOD	5.8	< LOD	--	--
60	< LOD	7.5	< LOD	--	--
90	< LOD	5.1	< LOD	--	--
120	< LOD	5.5	< LOD	--	--

Table 5.12 Plasma concentrations (μM) of ADR-925 following a 40 mg/kg dexrazoxane hydrochloride bolus in male Sprague-Dawley rats pre-dosed with 20 mg/kg of the DHOase inhibitor 5-aminoorotic acid

Time	Rat 1 ADR-925, μM	Rat 2 ADR-925, μM	Rat 3 ADR-925, μM	Average ADR-925, μM	SE ± μM
5	11.3	14.4	7.4	11.0	2.1
15	35.5	25.8	12.3	24.5	6.9
30	21.9	13.1	10.2	15.1	3.6
45	8.8	3.6	5.2	5.9	1.6
60	12.6	1.1	2.3	5.3	3.7
90	2.0	1.2	2.2	1.8	0.3
120	2.3	1.7	2.8	2.3	0.3

Table 5.13 Comparison of the AUC_{5-120} of dexrazoxane in rats dosed with the DHOase inhibitor 5-aminoorotic acid prior to dexrazoxane relative to rats dosed with dexrazoxane alone.

Rat Number	AUC_{5-120} of dexrazoxane	
	Dexrazoxane[a], (μM·min)	5-aminoorotic acid + Dexrazoxane, (μM·min)
1	21,567	15,071
2	19,099	16,796
3	15,010	13,441
4	16,785	--
5	16,851	--
6	22,389	--
Average	18,617	15,103
SE	1,192	970
p	--	$p > 0.5$

[a] Obtained from rats dosed with dexrazoxane alone (complete data set found in Chapter 2 Section 2.3.6)

Table 5.14 Comparison of the AUC_{5-120} of ADR-925 in rats dosed with the DHOase inhibitor 5-aminoorotic acid prior to dexrazoxane relative to rats dosed with dexrazoxane alone.

Rat Number	AUC_{5-120} of ADR-925	
	Dexrazoxane[a], (μM·min)	5-aminoorotic acid + Dexrazoxane (μM·min)
1	6602	1395
2	5344	803
3	4863	618
4	5299	--
5	3177	--
6	4609	--
Average	4982	939
SE	457	235
p	--	$p < 0.001$

[a] Obtained from rats dosed with dexrazoxane alone (complete data set found in Chapter 2 Section 2.3.6)
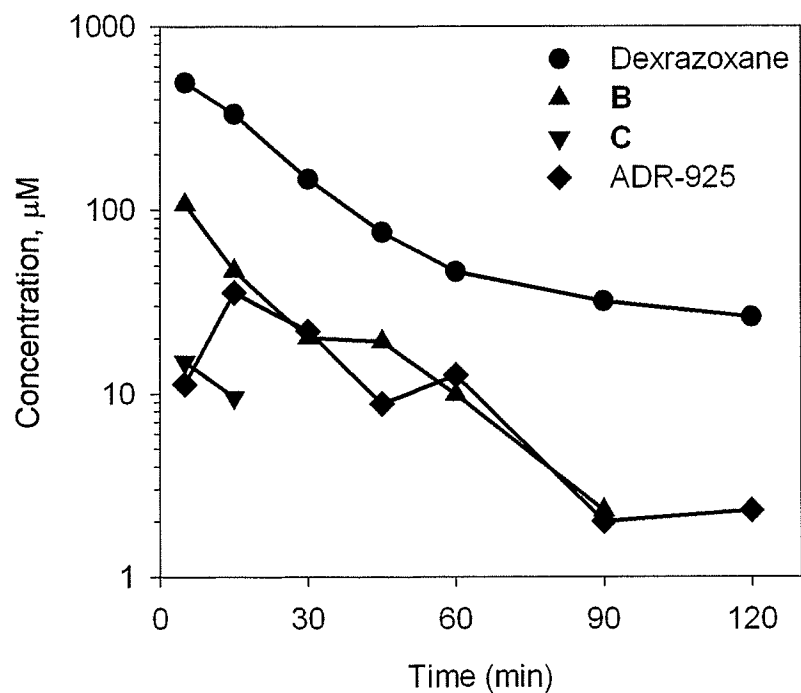
*Figure 5.9   Plasma concentrations of dexrazoxane, **B**, **C**, and ADR-925 for rat 1 after an i.v. dose of 40 mg/kg dexrazoxane hydrochloride following an i.v. dose of the DHOase inhibitor 5-aminoorotic acid (20 mg/kg) .*

After 90 and 15 min, the concentration-time data was below the limit of quantitation for **B** and **C**, respectively.
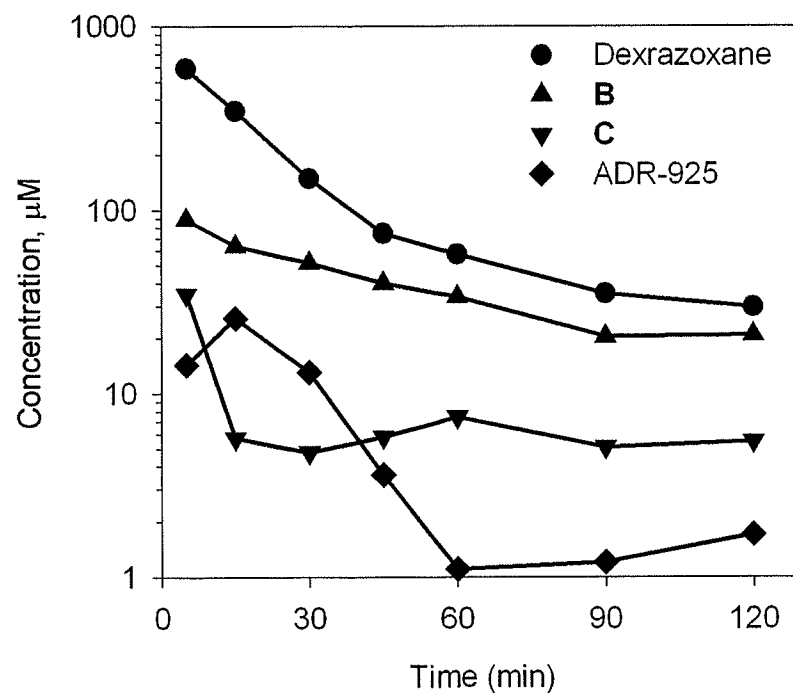
*Figure 5.10 Plasma concentrations of dexrazoxane, **B**, **C**, and ADR-925 for rat 2 after an i.v. dose of 40 mg/kg dexrazoxane hydrochloride following an i.v. dose of the DHOase inhibitor 5-aminoorotic acid (20 mg/kg) .*
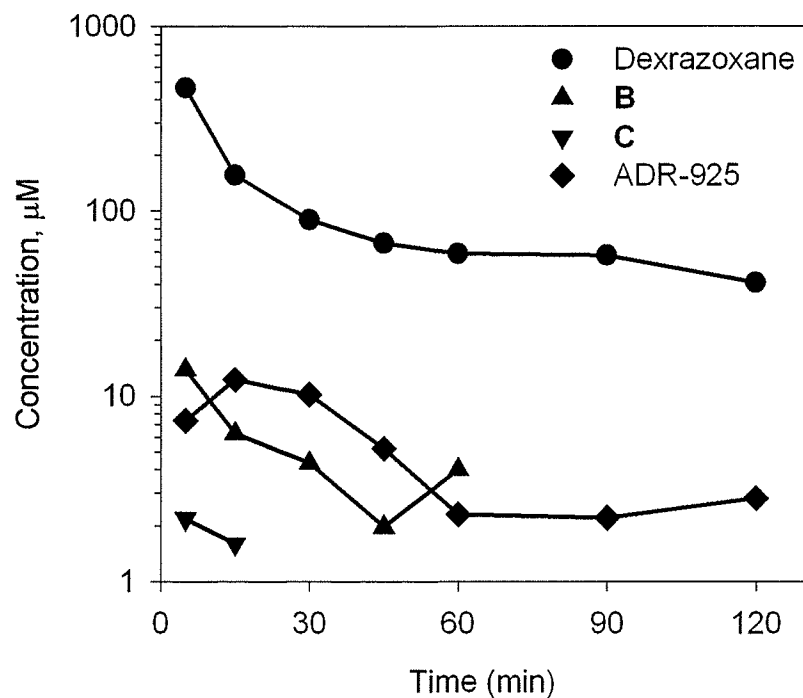
Figure 5.11 Plasma concentrations of dexrazoxane, **B**, **C**, and ADR-925 for rat 3 after an i.v. dose of 40 mg/kg dexrazoxane hydrochloride following an i.v. dose of the DHOase inhibitor 5-aminoorotic acid (20 mg/kg).

After 60 and 15 min, the concentration-time data was below the limit of quantitation for **B** and **C**, respectively.
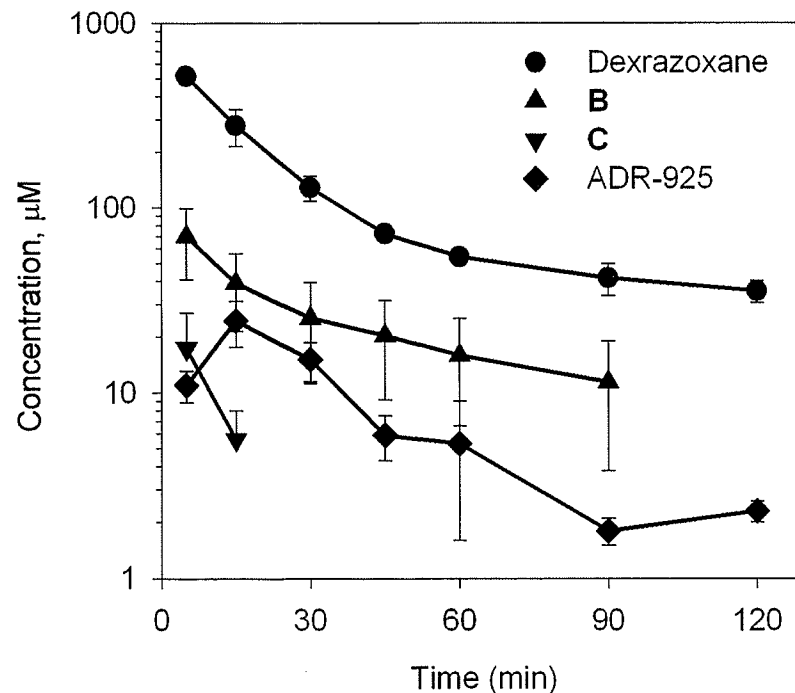
Figure 5.12 Average rat plasma concentrations of dexrazoxane, **B**, **C**, and ADR-925 after an i.v. dose of 40 mg/kg of dexrazoxane hydrochloride following an i.v. dose of the DHOase inhibitor 5-aminoorotic acid (20 mg/kg) .

Error bars represent the SEMs from 3 rats per concentration-time point After 90 and 15 min, the concentration-time data was below the limit of quantitation for **B** and **C**, respectively, in at least one rat.
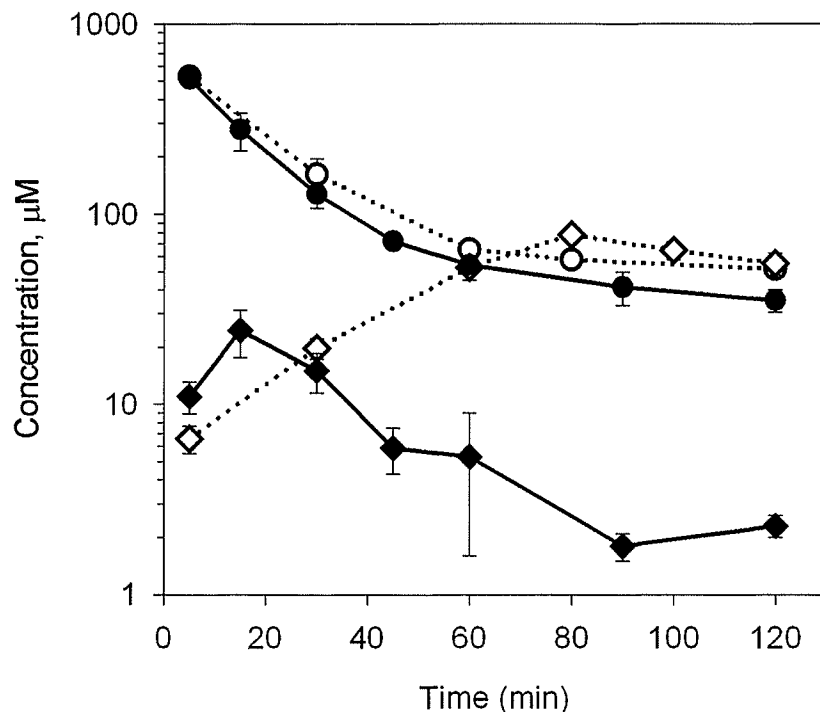
*Figure 5.13 Average plasma concentrations of dexrazoxane (●)
and ADR-925 (◆) for rats dosed with 5-aminoorotic acid
(20 mg/kg) 5 min prior to dexrazoxane (40 mg/kg) compared
to average plasma concentrations of dexrazoxane (○) and
ADR-925 (◇) dosed with dexrazoxane (40 mg/kg) alone.*
Error bars for solid symbols represent the SEMs from 3 rats per
concentration-time point and error bars for outlined symbols
represent the SEMs from 6 rats (data from Chapter 2).
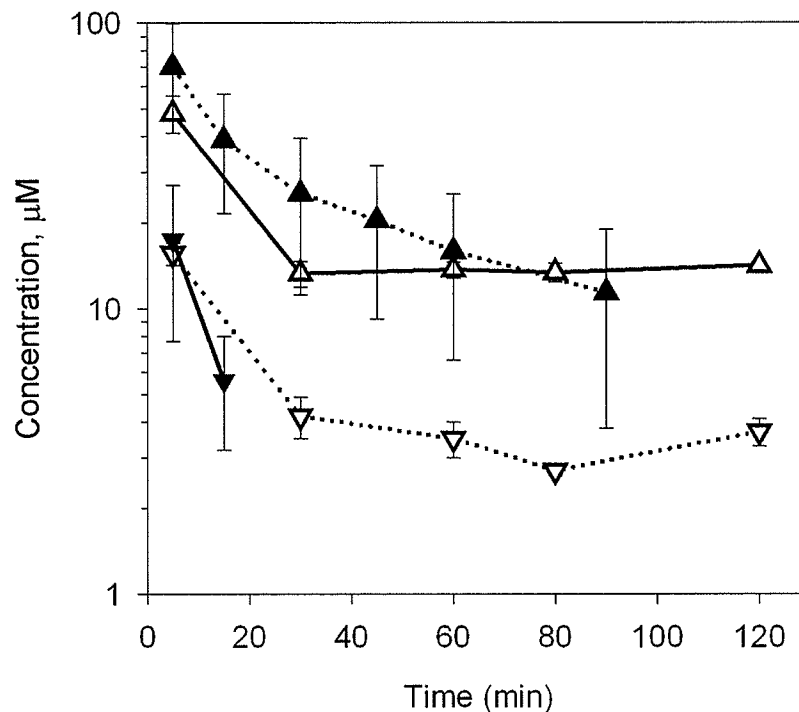
*Figure 5.14 Average plasma concentrations of B (▲) and C (▼)
for rats dosed with 5-aminoorotic acid (20 mg/kg) 5 min
prior to dexrazoxane (40 mg/kg) compared to average
plasma concentrations of B (△) and C (▽) dosed with
dexrazoxane (40 mg/kg) alone.*
Error bars for solid symbols represent the SEMs from 3 rats per
concentration-time point and error bars for outlined symbols
represent the SEMs from 6 rats (data from Chapter 2). After 90
and 15 min, the concentration-time data was below the limit of
quantitation for **B** and **C**, respectively, in at least one rat.

5.3.3.1 ADR-925 levels in tissues from rats dosed with 20 mg/kg 5-aminoorotic acid 5 min prior to a 40 mg/kg dexrazoxane bolus

ADR-925 levels in the heart and liver tissue homogenates of rats dosed with 5-aminoorotic acid 5 min prior to a 40 mg/kg dexrazoxane hydrochloride bolus are shown in Table 5.15. ADR-925 concentrations found in the heart and liver were not found to be significantly different ($p > 0.2$) with concentration of 0.0123 and 0.0122 μmol/g wet tissue, respectively. However, as shown in Table 5.16, ADR-925 levels in heart tissue homogenate supernatant of rats dosed with 5-aminoorotic acid 5 min prior to dexrazoxane were found to be 4.1 fold lower ($p < 0.005$) than heart tissue levels of rats dosed with dexrazoxane alone. The ADR-925 levels in liver tissue homogenate supernatant between rats dosed with 5-aminoorotic acid prior to dexrazoxane were also significantly less ($p < 0.005$) relative to rats dosed with dexrazoxane alone.

Table 5.15 Liver and heart tissue homogenate supernatant concentrations of ADR-925 from rats dosed with 5-aminoorotic acid 5 min prior to dexrazoxane as determined by the calcein assay. Rat tissues were removed and treated as described in Section 2.2.7 at 120 min post-dexrazoxane infusion.

Rat Number	ADR-925 (μmol/g wet tissue)	
	Heart	Liver
1	0.01385	0.01104
2	0.01323	0.01230
3	0.00978	0.01338
Average	0.01229	0.01224
SE	0.00129	0.00069

Table 5.16 Comparison of mean ADR-925 tissue levels in rats dosed 5-aminoorotic acid prior to dexrazoxane relative to rats dosed with dexrazoxane alone.

Study	Heart homogenate		Liver homogenate	
	ADR-925, μmol/g wet tissue (± SE)	p-Value	ADR-925, μmol/g wet tissue (± SE)	p-Value
Dexrazoxane[a]	0.0515 (± 0.0063)	--	0.0971 (± 0.0137)	--
5-aminoorotic acid + Dexrazoxane	0.0123 (± 0.0013)	$p < 0.005$	0.0122 (± 0.0069)	$p < 0.005$

[a] Obtained from rats dosed with dexrazoxane alone (complete data set found in Chapter 2 Section 2.3.6.1)

5.3.4 Metabolism of B/C to ADR-925 after a 20 mg/kg i.v. bolus of the DHOase inhibitor 5-aminoorotic acid

The results shown in Figures 5.15-5.17 show the individual rat concentration-time profiles (as shown in Tables 5.17-5.19) for **B**, **C**, and ADR-925 when rats are dosed with 5-aminoorotic acid 5 min prior to the **B/C** mixture, where Figure 5.18 is the average concentration-time data for all three rats. The results in Tables 5.20 and in Figures 5.15-5.18 show that when 5-aminoorotic acid is given 5 min prior to a **B/C** mixture bolus both metabolites are rapidly eliminated with half lives of 5.2 ± 0.8 and 3.0 ± 1.0 min for **B** and **C**, respectively. As seen in Figure 5.20 and in Table 5.20, the elimination of **B** and **C** in rats dosed with 5-aminoorotic acid is not significantly different from that obtained when the **B/C** mixture is given alone. In 5-aminoorotic acid treated rats, the C_0 for **B** and **C** was determined to be 414 ± 31.3 and 66.3 ± 13.4, respectively, as shown in Table 5.20 and the peak plasma concentration of ADR-925 of 48.7 ± 0.7 μM is shown in Figure 5.18. As in the case in rats dosed with the **B/C** mixture alone, ADR-925 appeared in the plasma very rapidly in rats treated with 5-aminoorotic and was found to be at a maximum

value at 2 min post **B/C** bolus, the first data collection time point. The C_{max} plasma concentration of ADR-925 was 2.4 fold lower in rats treated with 5-aminooroitc acid relative to rats dosed with the **B/C** mixture alone. Also, unlike the ADR-925 concentration-time profile after a **B/C** infusion, when **B/C** was infused following a 5-aminoorotic acid bolus, the ADR-925 plasma levels show a slower apparent elimination half life of 25.5 min relative to 8.5 min when the **B/C** mixture was administered alone.

Table 5.17 Plasma concentrations (μM) of **B** following a 20 mg/kg **B/C** bolus in male Sprague-Dawley rats pre-dosed with 20 mg/kg of the DHOase inhibitor 5-aminoorotic acid

Time	Rat 1 **B**, μM	Rat 2 **B**, μM	Rat 3 **B**, μM	Average **B**, μM	SE
2	349	323	285	319	19.0
10	56.7	130	114	100	22.6
20	15.7	15.9	77.9	36.5	21.1
30	4.5	5.9	57.9	22.8	17.9
45	2.0	2.0	33.3	12.4	10.6
60	3.7	< LOD	< LOD	--	--
90	2.0	< LOD	< LOD	--	--

Table 5.18 Plasma concentrations (μM) of **C** following a 20 mg/kg **B/C** bolus in male Sprague-Dawley rats pre-dosed with 20 mg/kg of the DHOase inhibitor 5-aminoorotic acid

Time	Rat 1 **C**, μM	Rat 2 **C**, μM	Rat 3 **C**, μM	Average **C**, μM	SE
2	46.9	46.7	31.8	41.8	5.1
10	5.1	12.7	2.0	6.6	3.2
20	5.2	2.6	< LOD	--	--
30	2.0	< LOD	< LOD	--	--
45	< LOD	< LOD	< LOD	--	--
60	< LOD	< LOD	< LOD	--	--
90	< LOD	< LOD	< LOD	--	--

Table 5.19 Plasma concentrations (μM) of ADR-925 following a 20 mg/kg **B/C** bolus in male Sprague-Dawley rats pre-dosed with 20 mg/kg of the DHOase inhibitor 5-aminoorotic acid

Time	Rat 1 ADR-925, μM	Rat 2 ADR-925, μM	Rat 3 ADR-925, μM	Average ADR-925, μM	SE
2	50.1	47.7	48.2	48.7	0.74
10	36.7	32.7	36.9	35.4	1.39
20	30.3	12.2	33.5	25.3	6.76
30	16.6	10.1	24.7	17.1	4.30
45	13.9	9.1	16.6	13.2	2.23
60	17.7	14.2	10.3	14.1	2.18
90	16.8	7.5	4.4	9.6	3.80

Table 5.20 One-compartment pharmacokinetic parameters for the first-order elimination of **B** and **C** and apparent elimination half lives of ADR-925 in the rat following a 20 mg/kg 5-aminoorotic acid bolus followed by a **B/C** bolus (20 mg/kg)

	B			**C**			ADR-925		
	n	$t_{\frac{1}{2}k10}$ (min)	C_0 (μM)	n	$t_{\frac{1}{2}k10}$ (min)	C_0 (μM)	n	$t_{\frac{1}{2}k10}$ (min)	C_0 (μM)
Average[a]	4	5.2	414	2	3.0	66.3	7	25.5	48.0
SE		0.8	33.1		1.0	13.4		3.6	3.4

n, is the number of plasma concentration-time points for each rat used to obtain the pharmacokinetic parameters.

[a] Pharmacokinetic parameters for the combined individual concentration-time data of **B**, **C**, and ADR-925 from rats 1-3 where errors were obtained from modeling data to equations 5.1, 5.2, and 5.5 (Section 5.3.2.2).
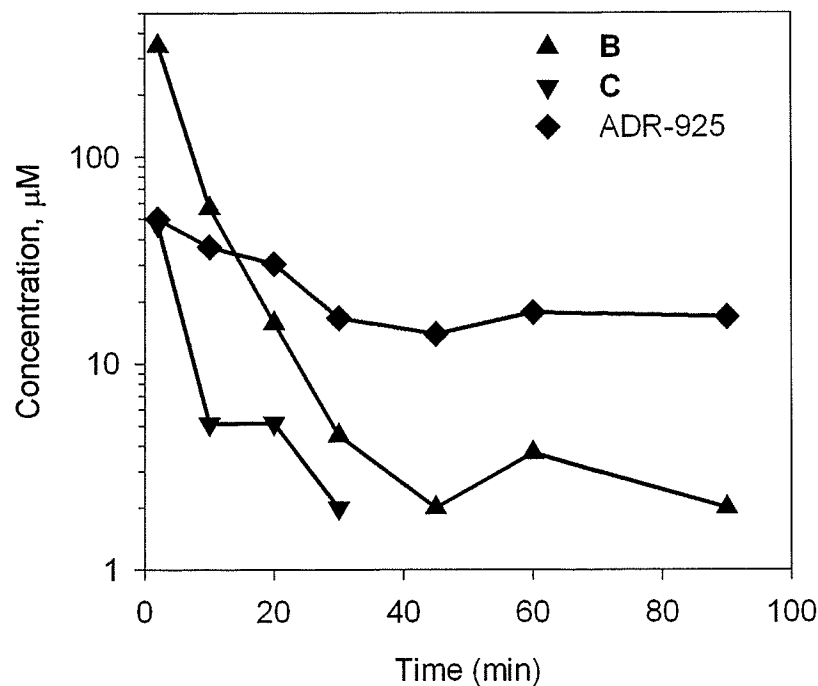
*Figure 5.15 Plasma concentrations of **B**, **C**, and ADR-925 for rat 1 after an i.v. dose of 20 mg/kg of the **B/C** mixture following an i.v. dose of the DHOase inhibitor 5-aminoorotic acid (20 mg/kg).*

After 30 min, **C** concentration-time data was below the limit of quantitation (LOQ).
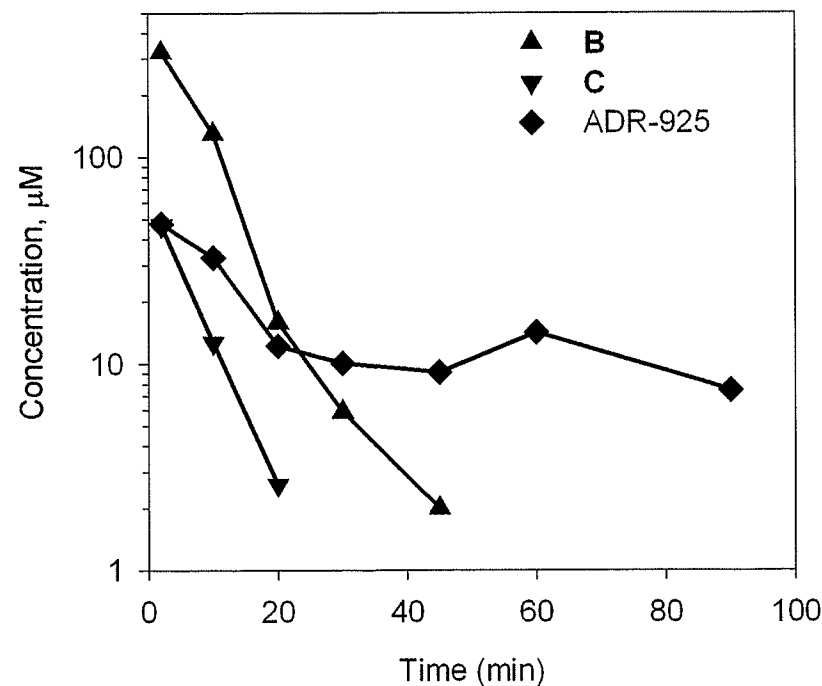
*Figure 5.16 Plasma concentrations of **B**, **C**, and ADR-925 for rat 2 after an i.v. dose of 20 mg/kg of the **B/C** mixture following an i.v. dose of the DHOase inhibitor 5-aminoorotic acid (20 mg/kg).*

After 60, 10, and 60 min, the concentration-time data was below the limit of quantitation for **B**, **C**, and ADR-925, respectively.

222
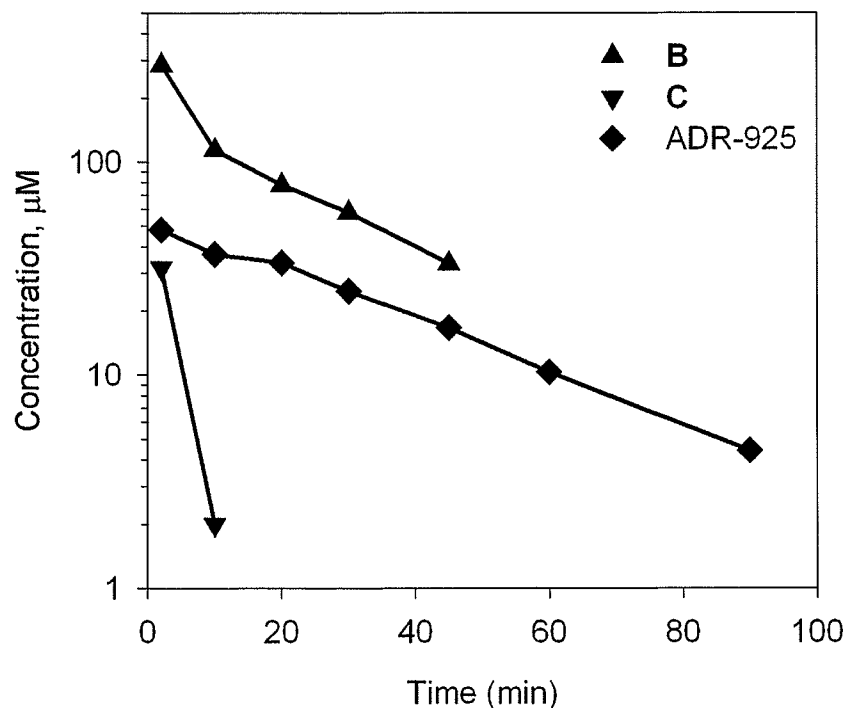
*Figure 5.17 Plasma concentrations of **B**, **C**, and ADR-925 for rat 3 after an i.v. dose of 20 mg/kg of the **B/C** mixture following an i.v. dose of the DHOase inhibitor 5-aminoorotic acid (20 mg/kg).*

After 45 and 20 min, the concentration-time data was below the limit of quantitation for **B** and **C**, respectively.
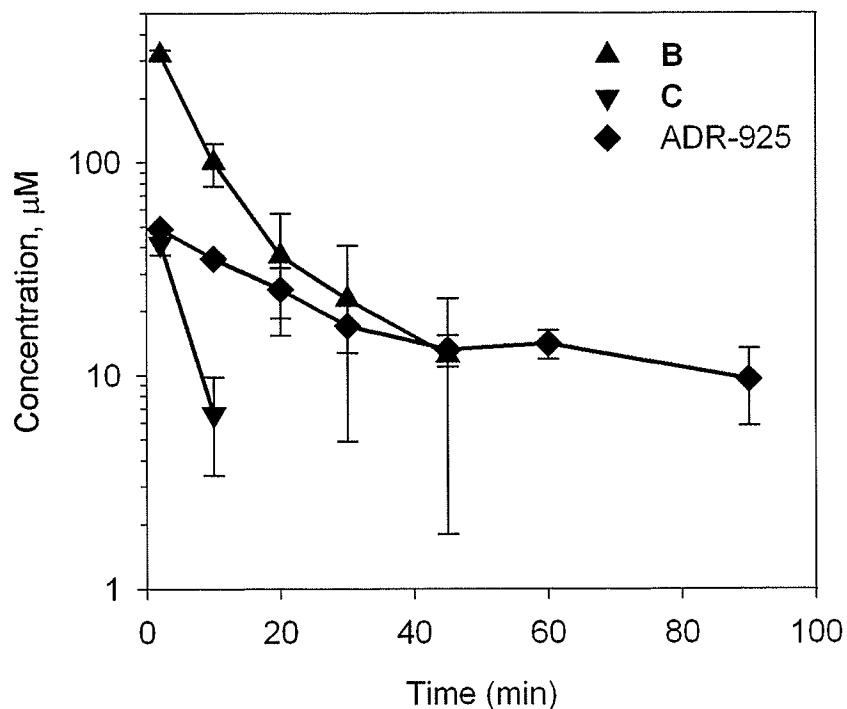
*Figure 5.18 Average plasma concentrations of **B**, **C**, and ADR-925 for 3 rats dosed with 20 mg/kg of the **B/C** mixture following an i.v. dose of the DHOase inhibitor 5-aminoorotic acid (20 mg/kg).*

Error bars for solid symbols represent the SE from 3 rats per concentration-time point and error bars for outlined symbols represent the SE from 6 rats (data from Chapter 2). After 45 and 20 min, the concentration-time data was below the limit of quantitation for **B** and **C**, respectively, in at least one rat.
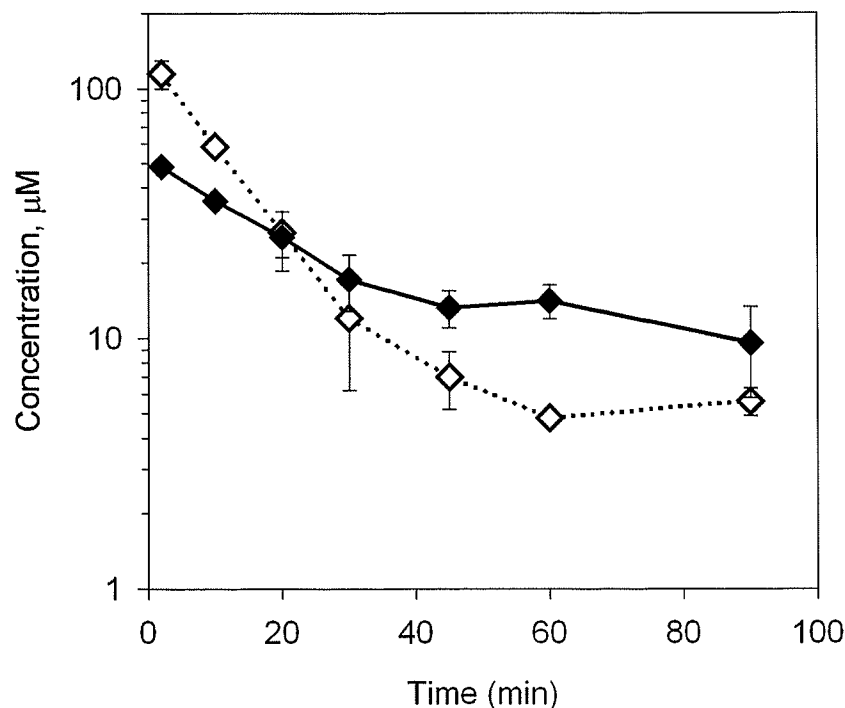
Figure 5.19 Average plasma concentrations of ADR-925 (◆) for rats dosed with 5-aminnoorotic acid (20 mg/kg) 5 min prior to the B/C mixture (20 mg/kg) compared to average plasma concentrations of ADR-925 (◇) dosed with the B/C mixture (20 mg/kg) alone.

Error bars for solid symbols represent the SEMs from 3 rats per concentration-time point and error bars for outlined symbols represent the SEMs from 6 rats (data from Chapter 2).
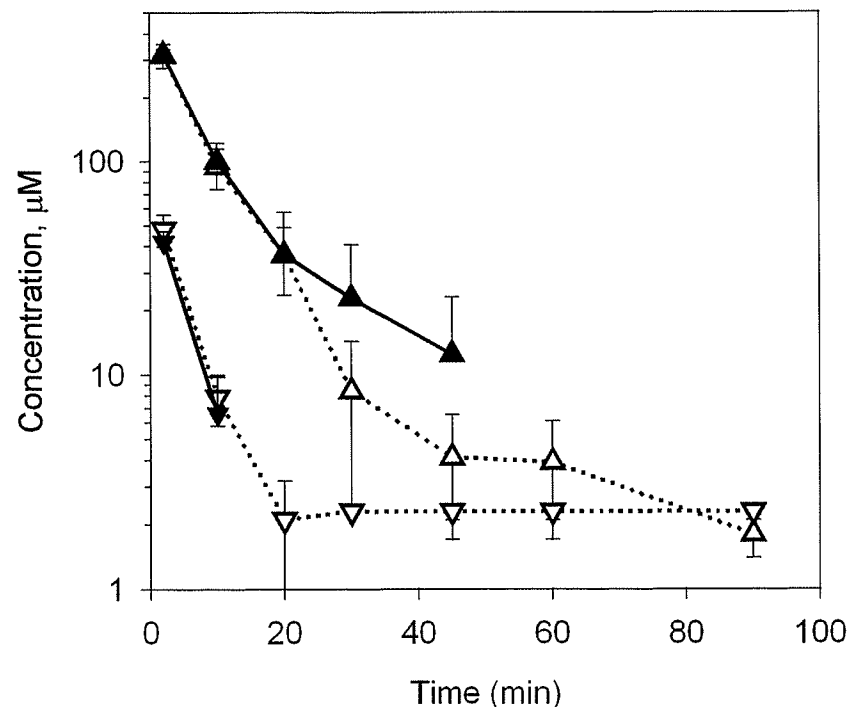
Figure 5.20 Average plasma concentrations of B (▲) and C (▼) for rats dosed with 5-aminoorotic acid (20 mg/kg) 5 min prior B/C mixture (20 mg/kg) compared to average plasma concentrations of B (△) and C (▽) dosed with B/C mixture (20 mg/kg) alone.

Error bars for solid symbols represent the SEMs from 3 rats per concentration-time point and error bars for outlined symbols represent the SEMs from 6 rats (data from Chapter 2). Concentration-time data that is not shown identifies concentrations below the limit of quantitation (1.5 μM).

224

5.3.4.1 ADR-925 detection in tissues from rats dosed with 20 mg/kg 5-aminoorotic acid 5 min prior to a 20 mg/kg B/C mixture bolus

ADR-925 levels in the heart and liver tissue homogenates of rats dosed with 5-aminoorotic acid 5 min prior to the 20 mg/kg B/C mixture bolus are shown in Table 5.21. As in the case when rats were dosed with B/C mixture alone, ADR-925 concentrations found in the liver were approximately 2-fold greater than those found in the heart for rats dosed with B/C. 5-aminoorotic acid did not appear to have an effect on the tissue accumulation of ADR-925 in the rat as no significant difference was noted in ADR-925 levels in heart and liver tissue of rats dosed with 5-aminoorotic acid relative to rats dosed with the B/C mixture alone.

Table 5.21 Liver and heart tissue homogenate supernatant concentrations of ADR-925 as determined by the calcein assay from rats dosed with 5-aminoorotic acid 5 min prior to the B/C mixture. Rat tissues were removed and treated as described in Section 2.2.7 at 120 min post-B/C mixture bolus.

Rat Number	ADR-925 (μmol/g wet tissue)	
	Heart	Liver
1	0.02862	0.04481
2	0.03011	0.04013
3	0.02765	0.05418
Average	0.02880	0.04638
SE	0.000726	0.00421

Table 5.22 Comparison of mean ADR-925 tissue levels in rats dosed with 5-aminoorotic acid prior to the **B/C** mixture relative to rats dosed with the **B/C** mixture alone.

	Heart homogenate		Liver homogenate	
Study	ADR-925, μmol/g wet tissue (± SE)	p-Value	ADR-925, μmol/g wet tissue (± SE)	p-Value
B/C mixture[a]	0.0275 (± 0.0062)	--	0.0395 (± 0.015)	--
5-aminoorotic acid + **B/C** mixture	0.0288 (± 0.00073)	$p > 0.5$	0.0464 (± 0.0042)	$p > 0.5$

[a] Obtained from rats dosed with the **B/C** mixture alone (complete data set found in Chapter 2 Section 2.3.7.1)

5.4 Discussion

5.4.1 The effect of DHPase/DHOase inhibitor furosemide on dexrazoxane metabolism in the rat

Under physiological conditions (37 °C and pH 7.4) dexrazoxane undergoes slow base-catalyzed hydrolysis *in vitro* to **B** and **C** ($t_{1/2}$ 9.3 h) and then to ADR-925 ($t_{1/2}$ 23 h) (Hasinoff, 1994b; Hasinoff, 1994a). Dexrazoxane pharmacokinetics have been studied in a variety of preclinical animal models (Herman and Ferrans, 1998) as well as clinical studies (Earhart et al., 1982; Vogel et al., 1987; Hochster et al., 1992; Jakobsen et al., 1994), where the elimination of dexrazoxane was found to be rapid (β phase $t_{1/2}$ 4.16 ± 2.94 h, (Hochster et al., 1992)). Given the slow rate of the *in vitro* dexrazoxane hydrolysis to ADR-925, the question arises how significant quantities of ADR-925 can be formed in the heart to prevent doxorubicin-induced iron mediated cardiotoxicity. DHPase, which is present in the liver and the kidney (Hamajima et al., 1996), has been shown to efficiently hydrolyze dexrazoxane (Hasinoff et al., 1991; Hasinoff, 1993;

Hasinoff, 1994c; Hasinoff and Aoyama, 1999b) and is likely the enzyme that is primarily responsible for the metabolism of dexrazoxane to **B** and **C** *in vivo*. Furthermore, dexrazoxane hydrolysis to **B** and **C** in the presence of isolated hepatocytes has been previously shown to be enzymatically mediated by DHPase (Hasinoff et al., 1994). However, a purified DHPase study showed that while dexrazoxane was a substrate for DHPase, its one-ring open hydrolysis products **B** and **C** were not (Hasinoff et al., 1991).

Furosemide, a DHPase and DHOase inhibitor, is clinically used as an adjunct therapy in the treatment of chronic heart failure due to its diuretic properties that were found to be effective in relieving symptoms and improving cardiovascular hemodynamics (Dikshit et al., 1973; Benet, 1979; Silke, 1994; Kramer et al., 1999). Furosemide is one of the most powerful diuretics available and works by inhibiting the active reabsorption of chloride in the diluting segment of the loop of Henle, thereby preventing the reabsorption of sodium (Benet, 1979). The pharmacokinetics of furosemide have been well studied in humans (Benet, 1979; Straughn et al., 1986; Yagi et al., 1996; Vree and van der Ven, 1999) as well as in rats (Lambert et al., 1982; Christensen et al., 1987). When furosemide was give 5 min prior to dexrazoxane the plasma concentration of furosemide was not monitored. However, the pharmacokinetics of an *i.v.* bolus of furosemide were investigated in male Sprague Dawley rats (at two doses of 10 and 40 mg/kg) where the best fit to the data was a three-compartment open model (tri-exponential decay) (Hammarlund and Paalzow, 1982). This study also found a dose-dependent decrease in metabolic clearance and an increase in the terminal half-life of furosemide (from 29 min to 49 min for the 10 mg/kg dose and 40 mg/kg dose, respectively), suggesting saturable metabolism of furosemide (Hammarlund and Paalzow, 1982). Considering the data from

Hammarlund and Paalzow, it may be postulated that furosemide tissue levels reach sufficient concentrations (142 μM, Hasinoff unpublished result) to inhibit DHPase and DHOase activity, at least for the first 60 min of the study where the greatest effects on **B** and **C** formation are seen.

ADR-925 plasma levels, as measured by AUC_{5-120}, in rats dosed with furosemide prior to dexrazoxane was significantly ($p < 0.03$) less by 1.4 fold relative to rats dosed with dexrazoxane alone as shown in Table 5.6. Furosemide's diuretic mechanism is not associated with inhibition of DHPase. One potential concern in using an inhibitor with diuretic properties is the potential influence on the disposition kinetics of dexrazoxane and its metabolites. The disposition kinetics (as measured by the non-compartmental AUC_{5-120}) of dexrazoxane were not found to be significantly different ($p > 0.5$) in rats dosed with furosemide 5 min prior to dexrazoxane relative to rats dosed with dexrazoxane alone. While furosemide diuretic properties cannot be ruled out completely for being responsible for the change in ADR-925 formation and disposition kinetics, the dexrazoxane disposition kinetics were not detectably affected, indicating that the effect of furosemide on ADR-925 formation and disposition kinetics is most likely DHPase-mediated.

ADR-925 levels measured in heart tissue homogenate supernatants (as shown in Table 5.7) of rats dosed with furosemide 5 min prior to dexrazoxane were 2.7 fold less ($p < 0.05$) relative to ADR-925 heart tissue levels of rats dosed with dexrazoxane alone. ADR-925 levels in the liver tissue homogenate supernatants were not found to be significantly different ($p > 0.2$) in rats dosed with furosemide 5 min prior to dexrazoxane relative to rats dosed with dexrazoxane alone. Inhibition of DHPase by furosemide was

228

unlikely the reason for decreased ADR-925 levels in the heart as DHPase is not found in the heart (Dudley et al., 1974; Hamajima et al., 1996) and dexrazoxane has been shown not to be detectably hydrolyzed in porcine heart homogenate supernatant (Hasinoff et al., 1991). However, **B** and **C** have been shown to be permeable to heart cells (Hasinoff et al., 2003). Thus, the decrease in circulating **B** and **C** could result in less metabolite uptake into the heart. Furosemide, shown to inhibit DHOase-mediated hydrolysis of **C** in a purified enzyme model (Chapter 4, (Schroeder et al., 2002)), could further inhibit the hydrolysis of **B** and **C** to ADR-925 in the heart.

Furosemide is approximately 99 % protein-bound in the rat (Hammarlund and Paalzow, 1982) and studies with human patients has shown that human serum albumin (HSA) was the only blood protein responsible for furosemide binding (Prandota and Pruitt, 1975). *In vitro* studies (fully described in Chapter 6) show that serum albumin significantly hydrolyzes **C**. Thus, furosemide-bound albumin may prevent albumin mediated hydrolysis of **B** or **C** to ADR-925 in the blood and may, therefore, also be partially responsible for decreased ADR-925 levels in plasma (Figure 5.7).

5.4.2 The effect of DHOase inhibition on dexrazoxane metabolism in the rat

5-Aminoorotic acid is a strong inhibitor of DHOase (Krungkrai et al., 1992; El Kolli et al., 1998) with a K_i of 6 µM (Christopherson and Jones, 1980) and in a purified DHOase enzyme study (Schroeder et al., 2002), 5-aminoorotic acid was also found to inhibit the DHOase mediated hydrolysis of **C**. The AUC_{5-120} of ADR-925 in rats dosed with 5-aminoorotic acid 5 min prior to dexrazoxane was found to be 5.3 fold lower ($p < 0.001$) than that of rats dosed with dexrazoxane alone. ADR-925 tissue levels in the heart were found to be 4.1 fold lower ($p < 0.005$) in rats dosed with 5-aminoorotic acid 5 min

prior to dexrazoxane relative to rats dosed with dexrazoxane alone. The ADR-925 plasma levels found at the end of the study (120 min) were 12.9 fold lower in rats dosed with 5-aminoorotic acid prior to dexrazoxane relative to rats dosed with dexrazoxane alone, a result consistent with the 4.1 fold lower ADR-925 levels in the heart tissue. The AUC_{5-120} of dexrazoxane in rats dosed with 5-aminoorotic acid 5 min prior to dexrazoxane and rats dosed with dexrazoxane alone was not found to be significantly different ($p > 0.5$), indicating that 5-aminoorotic acid does not change the disposition kinetics of dexrazoxane. Thus, the significant decrease in ADR-925 plasma and tissue levels in rats dosed with 5-aminoorotic acid 5 min prior to dexrazoxane relative to rats dosed with dexrazoxane alone are most likely due to 5-aminoorotic acid mediated DHOase inhibition.

It has previously been determined that dexrazoxane is not metabolized in plasma ((Hasinoff and Aoyama, 1999b) and Chapter 6) and is, therefore, most likely metabolized to **B** or **C** extravascularly. Dexrazoxane is a small, neutral molecule that is permeable to cells (Dawson, 1975), and should be easily taken up by tissue. The rapid appearance of **B** and **C** in the plasma of rats dosed with 5-aminoorotic acid prior to dexrazoxane strongly indicates that 5-aminoorotic acid is not significantly interfering with the enzymatic conversion of dexrazoxane to **B** and **C** by DHPase (or another dexrazoxane hydrolyzing enzyme). The results of this study clearly show that when 5-aminoorotic acid is given to rats prior to dexrazoxane, the formation of ADR-925 in plasma is significantly reduced (p <0.001) by 5.3 fold as shown in Table 5.14. It has been previously shown that DHOase, which is present in the liver, kidney, and heart (Kennedy, 1974), can hydrolyze both **B** and **C** (as detailed in Chapter 4 (Schroeder et al., 2002)). The decrease in ADR-925

230

formation, as found in the plasma (Figure 5.13) and in tissues (Table 5.16) is most likely due to 5-aminoorotic acid mediated inhibition of DHOase. These results are also consistent with the hypothesis of **B** and **C** *in vivo* metabolism mediated, at least in part, by DHOase.

5.4.3 The effect of DHOase inhibition on B/C metabolism to ADR-925

The maximum plasma concentration and elimination rate constant, C_0 and k_{10}, of **B** and **C** were found to be unchanged between rats dosed with 5-aminoorotic acid prior to **B/C** mixture and rats dosed with the **B/C** mixture alone. With C_0 of 414 ± 31.1 and 66.3 ± 13.4 μM for **B** and **C**, respectively (Table 5.20), for rats were dosed with 5-aminoorotic acid 5 min prior to **B/C** mixture relative to 416 ± 14.8 and 74.6 μM ± 3.6 for **B** and **C**, respectively (Table 2.20), for rats dosed with **B/C** mixture alone. Also, the elimination rate half life for **B** and **C** were essentially unchanged, 5.2 and 3.0 min respectively for rats dosed with 5-aminoorotic acid 5 min prior to the **B/C** mixture (as shown in Table 5.20) relative to 4.9 and 3.1 min for rats dosed with the **B/C** mixture alone (Table 2.20). It was found that the initial plasma levels (apparent C_0) of ADR-925 in rats dosed with 5-aminoorotic acid prior to **B/C** mixture were 2.8 fold less ($p < 0.01$) than those in rats dosed with **B/C** mixture alone. The apparent half life of elimination was found to be greater in rats treated with 5-aminoorotic acid prior to dexrazoxane (25.5 min, Table 5.20)) relative to rats dosed with the **B/C** mixture alone (8.5 min, Table 2.19). Despite the change in the apparent elimination of ADR-925 in rats dosed with 5-aminoorotic acid prior to the **B/C** mixture, there was no significant change ($p > 0.2$) in the amount of ADR-925 found in heart and liver tissue of relative to rats dosed with the **B/C** mixture alone. This is not entirely inconsistent upon closer examination of the ADR-925

231

concentration-time plasma data. Figure 5.19 shows that, at the end of the experiment (90 min) the ADR-925 plasma levels of in rats dosed with 5-aminoorotic acid prior to the B/C mixture and rats dosed with the B/C mixture alone were approximately the same. At 90 min post B/C bolus, there is no significant difference ($p > 0.3$) in the ADR-925 plasma levels of rats dosed with 5-aminoorotic acid 5 min prior to the B/C mixture relative to the rats dosed with the B/C mixture alone. This correlates well with the tissue homogenate data which indicate no significant difference in ADR-925 levels in either the heart ($p > 0.5$) or liver tissues ($p > 0.5$) of rats dosed with 5-aminoorotic acid prior to B/C mixture or rats dosed with the B/C mixture alone.

The greatest inhibition of *in vivo* ADR-925 formation resulted when 5-aminoorotic acid was given prior to dexrazoxane as opposed to the B/C mixture. While the hydrolysis of dexrazoxane is not accelerated in the presence of Ca^{2+} and Mg^{2+}, the hydrolysis of B and C are (Buss and Hasinoff, 1997). A major contribution for the hydrolysis of C to ADR-925 in blood plasma was determined to be the high concentrations of Ca^{2+} and Mg^{2+} (as described in Chapter 6). Both Ca^{2+} and Mg^{2+} have been found to increase the hydrolysis of C between 2.5 and 18 fold, respectively (Buss and Hasinoff, 1997). Blood typically contains millimolar concentrations of both calcium and magnesium (Luquita et al., 2001) and these metal ions are a potential contributor to the rapid hydrolysis of B and C to ADR-925 *in vivo*. Thus, dexrazoxane, being essentially stable in blood, can diffuse into the cell (Dawson, 1975) where it is enzymatically hydrolyzed to ADR-925 (Doroshow et al., 1991). When the B/C mixture is given alone, peak ADR-925 plasma levels are seen immediately following the infusion. This is most likely due to a combination of metal ion-catalyzed hydrolysis in the blood

and **B** and **C** uptake by cells followed by DHOase-mediated enzymatic hydrolysis in tissue. In the case where rats were dosed with 5-aminoorotic acid prior to **B/C** initial apparent C_0 plasma levels of ADR-925 were 2.8 fold lower than when **B/C** was given alone. While inhibition of ADR-925 formation was not as great as when 5-aminoorotic acid was give 5 min prior to dexrazoxane, the changes in ADR-925 disposition when 5-aminoorotic acid was given prior to the **B/C** mixture is still a significant result. Metal ion catalysis of **B** and **C** is independent of 5-aminoorotic acid mediated DHOase inhibition, thus the changes in ADR-925 disposition kinetics are most likely DHOase mediated. So while **B** and **C** are distributed into the tissues, they are not enzymatically hydrolyzed to ADR-925 which will slow the rate of ADR-925 formation, possibly explaining the lower apparent C_0 of ADR-925.

Rats treated with 5-aminoorotic acid resulted in an extended elimination half life (3 fold greater, Table 5.20) relative to rats dosed with the **B/C** mixture alone. Typically, the rate of elimination of a drug should not be dose-dependent or, in the case of a metabolite, formation dependent. This indicates that there are other contributing metabolic and pharmacokinetic processes involved. It is difficult to fully describe the increase in the elimination half life with the data provided other then to recognize that 5-aminoorotic acid may influence other physiological processes resulting in an extended apparent half life of elimination. Despite this, the non-DHOase mediated hydrolysis of **B** and **C**, by either plasma metal ions or other proteins, can begin to explain the concentration-time curve ADR-925 formation after a **B/C** mixture bolus in rats dosed with the DHOase inhibitor 5-aminoorotic acid. The rapid appearance of ADR-925 in rats dosed with 5-aminoorotic acid prior to the **B/C** mixture also indicates that metal ion

catalysis in the blood may be a lead contributor to the formation of ADR-925 in rats

dosed with a **B/C** mixture.

5.5 References

Benet LZ (1979) Pharmacokinetics/pharmacodynamics of furosemide in man: a review. *J Pharmacokinet Biopharm* **7**:1-27.

Blum RH, Walsh C, Green MD and Speyer JL (1990) Modulation of the effect of anthracycline efficacy and toxicity by ICRF-187. *Cancer Invest* **8**:267-268.

Buss JL and Hasinoff BB (1993) The one-ring open hydrolysis product intermediates of the cardioprotective agent ICRF-187 (dexrazoxane) displace iron from iron-anthracycline complexes. *Agents Actions* **40**:86-95.

Buss JL and Hasinoff BB (1997) Metal ion-promoted hydrolysis of the antioxidant cardioprotective agent dexrazoxane (ICRF-187) and its one-ring open hydrolysis products to its metal-chelating active form. *J Inorg Biochem* **68**:101-108.

Carrey EA (1993) Phosphorylation, allosteric effectors and inter-domain contacts in CAD; their role in regulation of early steps of pyrimidine biosynthesis. *Biochem Soc Trans* **21**:191-195.

Christensen S, Petersen JS, Steiness E and Andreasen F (1987) Dose dependence of proximal and distal tubular effects of furosemide in conscious rats. *J Pharmacol Exp Ther* **241**:987-993.

Christopherson RI and Jones ME (1980) The effects of pH and inhibitors upon the catalytic activity of the dihydroorotase of multienzymatic protein pyr1-3 from mouse Ehrlich ascites carcinoma. *J Biol Chem* **255**:3358-3370.

Dawson KM (1975) Studies on the stability and cellular distribution of dioxopiperazines in cultured BHK-21S cells. *Biochem Pharmacol* **24**:2249-2253.

Dikshit K, Vyden JK, Forrester JS, Chatterjee K, Prakash R and Swan HJ (1973) Renal and extrarenal hemodynamic effects of furosemide in congestive heart failure after acute myocardial infarction. *N Engl J Med* **288**:1087-1090.

Doroshow J, Burke TG, VanBalgooy J, Akman S, and Verhoef V (1991) Cellular pharmacology of ICRF-187 in adult rat heart myocytes (M). *Proc Am Assoc Cancer Res* **32**:332.

Dudley KH, Butler TC and Bius DL (1974) The role of dihydropyrimidinase in the metabolism of some hydantoin and succinimide drugs. *Drug Metab Dispos* **2**:103-112.

Earhart RH, Tutsch KD, Koeller JM, Rodriguez R, Robins HI, Vogel CL, Davis HL and Tormey DC (1982) Pharmacokinetics of (+)-1,2-di(3,5-dioxopiperazin-1-yl)propane intravenous infusions in adult cancer patients. *Cancer Res* **42:**5255-5261.

El Kolli M, Coulibaly A, Chevalier J, Barbe J and Cremieux A (1998) Antibacterial activity of 5-aminoorotic acid derivatives. *Curr Microbiol* **36:**245-247.

Gianni L, Corden BJ and Myers C (1983) The biochemical basis of anthracycline toxicity and anti-tumor activity. *Rev. Biochem. Toxicol.* **5:**1-83.

Hamajima N, Matsuda K, Sakata S, Tamaki N, Sasaki M and Nonaka M (1996) A novel gene family defined by human dihydropyrimidinase and three related proteins with differential tissue distribution. *Gene* **180:**157-163.

Hammarlund MM and Paalzow LK (1982) Dose-dependent pharmacokinetics of furosemide in the rat. *Biopharm Drug Dispos* **3:**345-359.

Hasinoff BB (1989) The interaction of the cardioprotective agent ICRF-187 [+)-1,2-bis(3,5-dioxopiperazinyl-1-yL)propane); its hydrolysis product (ICRF-198); and other chelating agents with the Fe(III) and Cu(II) complexes of adriamycin. *Agents Actions* **26:**378-385.

Hasinoff BB (1993) Enzymatic ring-opening reactions of the chiral cardioprotective agent (+) (S)-ICRF-187 and its (-) (R)-enantiomer ICRF-186 by dihydropyrimidine amidohydrolase. *Drug Metab Dispos* **21:**883-888.

Hasinoff BB (1994a) An HPLC and spectrophotometric study of the hydrolysis of ICRF-187 (dexrazoxane, (+)-1,2-bis(3,5-dioxopiperazinyl-1yl)propane and its one-ring opened intermediates. *Int. J. Pharm.* **107:**67-76.

Hasinoff BB (1994b) Pharmacodynamics of the hydrolysis-activation of the cardioprotective agent (+)-1,2-bis(3,5-dioxopiperazinyl-1-yl)propane. *J Pharm Sci* **83:**64-67.

Hasinoff BB (1994c) Stereoselective hydrolysis of ICRF-187 (dexrazoxane) and ICRF-186 by dihydropyrimidine amidohydrolase. *Chirality* **6:**213-215.

Hasinoff BB (1998) Chemistry of dexrazoxane and analogues. *Semin Oncol* **25:**3-9.

Hasinoff BB and Aoyama RG (1999a) Relative plasma levels of the cardioprotective drug dexrazoxane and its two active ring-opened metabolites in the rat. *Drug Metab Dispos* **27:**265-268.

236

Hasinoff BB and Aoyama RG (1999b) Stereoselective metabolism of dexrazoxane (ICRF-187) and levrazoxane (ICRF-186). *Chirality* **11**:286-290.

Hasinoff BB, Hellmann K, Herman EH and Ferrans VJ (1998) Chemical, biological and clinical aspects of dexrazoxane and other bisdioxopiperazines. *Curr Med Chem* **5**:1-28.

Hasinoff BB, Reinders FX and Clark V (1991) The enzymatic hydrolysis-activation of the adriamycin cardioprotective agent (+)-1,2-bis(3,5-dioxopiperazinyl-1-yl)propane. *Drug Metab Dispos* **19**:74-80.

Hasinoff BB, Schroeder PE and Patel D (2003) The metabolites of the cardioprotective drug dexrazoxane do not protect myocytes from doxorubicin-induced cytotoxicity. *Mol Pharmacol* **64**:670-678.

Hasinoff BB, Venkataram S, Singh M and Kuschak TI (1994) Metabolism of the cardioprotective agents dexrazoxane (ICRF-187) and levrazoxane (ICRF-186) by the isolated hepatocyte. *Xenobiotica* **24**:977-987.

Herman EH and Ferrans VJ (1987) Amelioration of chronic anthracycline cardiotoxicity by ICRF-187 and other compounds. *Cancer Treat Rev* **14**:225-229.

Herman EH and Ferrans VJ (1998) Preclinical animal models of cardiac protection from anthracycline-induced cardiotoxicity. *Semin Oncol* **25**:15-21.

Hochster H, Liebes L, Wadler S, Oratz R, Wernz JC, Meyers M, Green M, Blum RH and Speyer JL (1992) Pharmacokinetics of the cardioprotector ADR-529 (ICRF-187) in escalating doses combined with fixed-dose doxorubicin. *J Natl Cancer Inst* **84**:1725-1730.

Jakobsen P, Sorensen B, Bastholt L, Mirza MR, Gjedde SB, Mouridsen HT and Rose C (1994) The pharmacokinetics of high-dose epirubicin and of the cardioprotector ADR-529 given together with cyclophosphamide, 5-fluorouracil, and tamoxifen in metastatic breast-cancer patients. *Cancer Chemother Pharmacol* **35**:45-52.

Jones D (2002) *Pharmaceutical Statistics*. Pharmaceutical Press, London.

Kennedy J (1974) Dihydroorotase from rat liver: purification, properties and regulatory role in pyrimidine biosynthesis. *Arch Biochem Biophys* **160**:358-365.

Kikugawa M, Kaneko M, Fujimoto-Sakata S, Maeda M, Kawasaki K, Takagi T and Tamaki N (1994) Purification, characterization and inhibition of dihydropyrimidinase from rat liver. *Eur J Biochem* **219**:393-399.

Kramer BK, Schweda F and Riegger GA (1999) Diuretic treatment and diuretic resistance in heart failure. *Am J Med* **106**:90-96.

Krungkrai J, Krungkrai SR and Phakanont K (1992) Antimalarial activity of orotate analogs that inhibit dihydroorotase and dihydroorotate dehydrogenase. *Biochem Pharmacol* **43:**1295-1301.

Lambert C, Caille G and du Souich P (1982) Nonrenal clearance of furosemide as a cause of diuretic response variability in the rat. *J Pharmacol Exp Ther* **222:**232-236.

Lee M, Cowling R, Sander E and Pettigrew D (1986) Bovine liver dihydropyrimidine amidohydrolase: pH dependencies of inactivation by chelators and steady-state kinetic properties. *Arch Biochem Biophys.* **248:**368-378.

Luquita A, Gennaro AM and Rasia M (2001) Influence of adsorbed plasma proteins on erythrocyte rheological properties: in vitro and ex vivo studies. *Pflugers Arch* **443:**78-83.

Prandota J and Pruitt AW (1975) Furosemide binding to human albumin and plasma of nephrotic children. *Clin Pharmacol Ther* **17:**159-165.

Schroeder PE and Hasinoff BB (2002) The doxorubicin-cardioprotective drug dexrazoxane undergoes metabolism in the rat to its metal ion-chelating form ADR-925. *Cancer Chemother Pharmacol* **50:**509-513.

Schroeder PE, Davidson JN and Hasinoff BB (2002) Dihydroorotase catalyzes the ring opening of the hydrolysis intermediates of the cardioprotective drug dexrazoxane (ICRF-187). *Drug Metab Dispos* **30:**1431-1435.

Silke B (1994) Haemodynamic impact of diuretic therapy in chronic heart failure. *Cardiology* **84 Suppl 2:**115-123.

Straughn AB, Wood GC, Raghow G and Meyer MC (1986) Bioavailability of seven furosemide tablets in man. *Biopharm Drug Dispos* **7:**113-120.

Swain SM and Vici P (2004) The current and future role of dexrazoxane as a cardioprotectant in anthracycline treatment: expert panel review. *J Cancer Res Clin Oncol* **130:**1-7.

Swain SM, Whaley FS, Gerber MC, Weisberg S, York M, Spicer D, Jones SE, Wadler S, Desai A, Vogel C, Speyer J, Mittelman A, Reddy S, Pendergrass K, Velez-Garcia E, Ewer MS, Bianchine JR and Gams RA (1997) Cardioprotection with dexrazoxane for doxorubicin-containing therapy in advanced breast cancer. *J Clin Oncol* **15:**1318-1332.

Vogel CL, Gorowski E, Davila E, Eisenberger M, Kosinski J, Agarwal RP and Savaraj N (1987) Phase I clinical trial and pharmacokinetics of weekly ICRF-187 (NSC 169780) infusion in patients with solid tumors. *Invest New Drugs* **5:**187-198.

Vree TB and van der Ven AJ (1999) Clinical consequences of the biphasic elimination kinetics for the diuretic effect of furosemide and its acyl glucuronide in humans. *J Pharm Pharmacol* **51**:239-248.

Yagi N, Kiuchi T, Satoh H, Terashima Y, Kenmotsu H, Sekikawa H and Takada M (1996) Bioavailability and diuretic effect of furosemide following administration of tablets and retarded capsules to human subjects. *Biol Pharm Bull* **19**:616-622.

6.0 Chapter 6: Metabolism of dexrazoxane and its one-ring opened intermediates by the isolated neonatal rat myocytes and adult rat hepatocytes

6.1 Introduction

Dexrazoxane likely acts as a cardioprotective agent by diffusing into the cell and hydrolyzing to its one-ring open intermediates **B** and **C**, and then to it's fully rings-opened metal ion-chelating form, ADR-925 (Figure 6.1). Dihydropyrimidine amidohydrolase, EC 3.5.2.2, (DHPase) catalyzes the reversible hydrolysis of 5,6-dihydrouracil to N-carbamoyl-β-alanine and is the second enzyme in the pyrimidine synthesis pathway (Kikugawa et al., 1994). DHPase, which is present in the liver and the kidney, has been shown to hydrolyze dexrazoxane (Hasinoff et al., 1991; Hasinoff, 1993; Hasinoff, 1994b; Hasinoff and Aoyama, 1999b) and is likely the primary enzyme responsible for the metabolism of dexrazoxane to **B** and **C**. It has been previously determined that dexrazoxane underwent an enzymatic ring-opening hydrolysis by the 105,000 _g_ soluble supernatant fraction of homogenates of porcine liver and kidney, but not of heart (Hasinoff et al., 1991). DHPase, present in the supernatant, was shown to be responsible for this enzymatic hydrolysis (Hasinoff et al., 1991).

However, a purified DHPase study showed that while dexrazoxane was a substrate for DHPase, its one-ring open hydrolysis products **B** and **C** were not (Hasinoff et al., 1991). Dexrazoxane metabolites **B** and **C** were, however, shown to be enzymatically hydrolyzed by dihydroorotase EC 3.5.2.2 (DHOase) as described in Chapter 4 (Schroeder et al., 2002). DHOase catalyzes the reversible cyclization of N-carbamyl-L-aspartate to form L-5,6-dihydroorotate which is the third reaction in the _de_

novo pyrimidine biosynthetic pathway (Carrey, 1993; Evans et al., 1993). Unlike DHPase which is not present in heart tissue, DHOase has shown to have good activity in the heart (Kennedy, 1974). Thus, although dexrazoxane may not be detectably hydrolyzed in the heart, the enzyme DHOase could contribute to the hydrolysis of **B** and **C** to ADR-925, thereby lending an enzymatic mediated mechanism of protection by dexrazoxane in the heart.

To further investigate the role of DHOase-mediated metabolism of **C**, primary cells from both neonatal rat myocyte and adult rat hepatocyte isolations were used. In addition, the DHOase inhibitors 5-aminoorotic acid (Figure 6.2 a) and furosemide (Figure 6.2 b) and the DHPase inhibitor 4-chlorobenzenesulfonamide (Figure 6.2 c) were chosen to further define the contribution of DHPase and DHOase in the metabolism of dexrazoxane and **C** in primary cell suspensions. The hydrolysis of **C** in blood was also examined where the metal ion chelator diethylenetriaminepentaacetic acid (DTPA, Figure 6.2.d) was used to investigate the role of metal ions in the hydrolysis of **C** in an *in vitro* blood model.
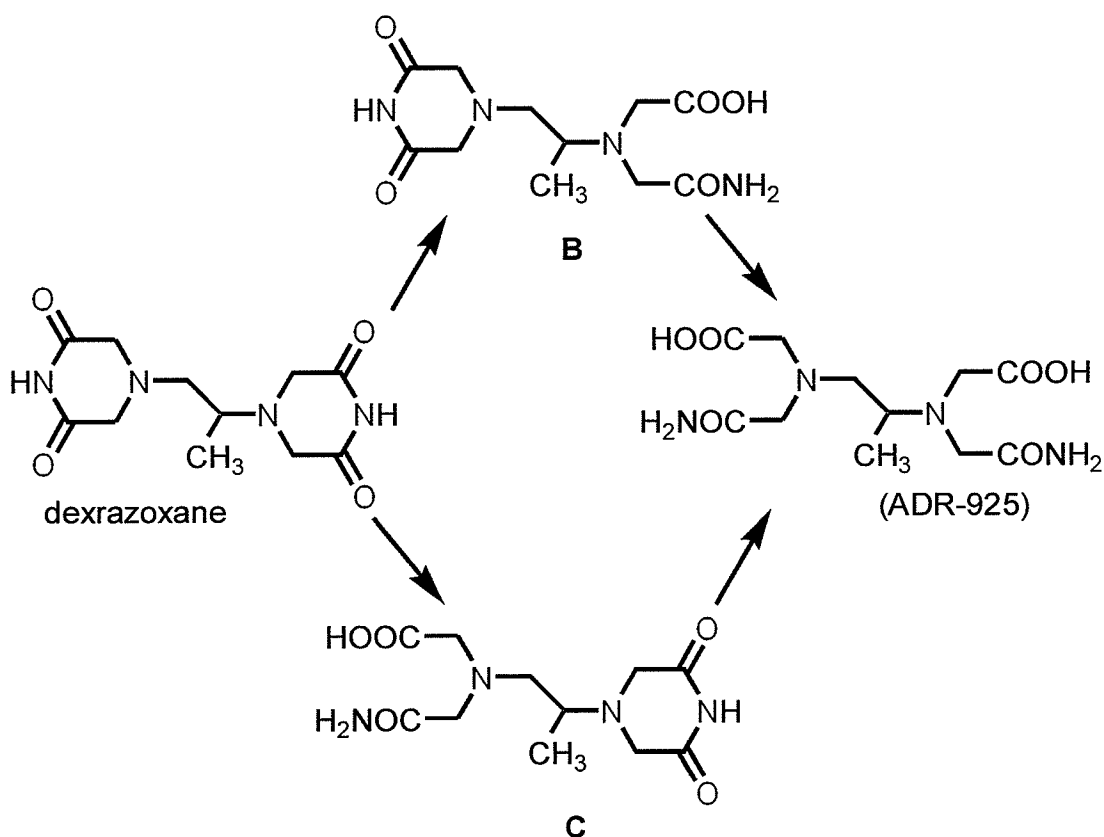
*Figure 6.1. Reaction scheme for the hydrolysis of dexrazoxane to intermediates **B** and **C**, and its strongly metal ion-chelating form ADR-925.*
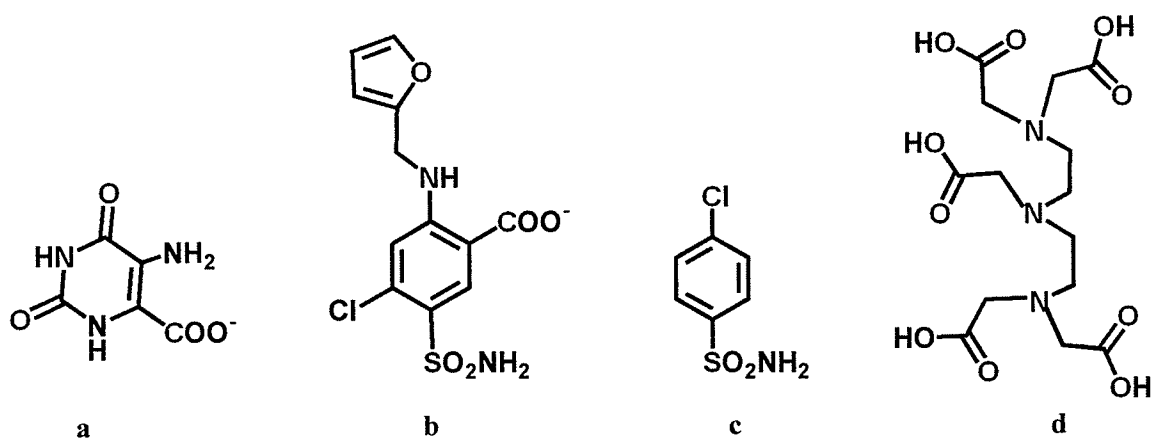
Figure 6.2 Structures of DHOase inhibitors 5-aminoorotic acid, 6.2a and furosemide 6.2b, the DHPase inhibitor 4-chlorobenzenesulfonamide 6.2.c., and the metal ion chelator diethylenetriaminepentaacetic acid (DTPA) 6.2.d.

6.2 Materials and Methods

6.2.1 Materials

Dexrazoxane hydrochloride and ADR-925 were gifts from Adria Laboratories (Columbus, OH). HPLC-grade methanol, $NaHCO_3$, KH_2PO_4, Na_2SO_4, NaCl, $CaCl_2$ and HEPES were from Fisher (Fair Lawn, NJ). $MgCl_2$ was from Mallinckrodt (Paris, Kentucky) and KCl was from Anachemia (Montreal, Canada). 1-Heptanesulfonic acid sodium salt, Chelex, EDTA, DTPA, Tris, and human serum albumin (~99 % fatty acid free, Cat # A3782, Lot # 120K7603) were obtained from Sigma (St. Louis, MO). PBS-glucose, D-MEM, α-MEM, fetal bovine and horse serum, penicillin, streptomycin, and fungizone and antibiotic-antimycotic were from Invitrogen (Burlington, ON, Canada). Trypsin, collagenase, and DNAase were from Worthington Biochemicals (Lakewood NJ, USA). Calcein was from Molecular Probes (Eugene, OR). Metabolite C was prepared from NaOH-hydrolyzed dexrazoxane and isolated as described in Chapter 4 Section 4.2.2.

6.2.2 Neonatal rat cardiac myocytes isolation

Neonatal rat pups (2-3 days old) were obtained from University of Manitoba Animal Holding Facility (UMAHF) and transported to the Faculty of Pharmacy immediately prior to surgery. Ventricular myocytes were isolated using a modified procedure as previously described (Kirshenbaum and Schneider, 1995). The rat pups were placed on a sterilized surface and a cervical dislocation was performed with forceps to instantly euthanize the animal. The hearts were immediately removed and placed in a sterile 50 ml tube of PBS-glucose and kept on ice. Typically, 12 − 16 rat pups were

sacrificed per isolation. The hearts were washed twice with 40 ml of cold PBS-glucose after which they were minced in 5 ml of cold PBS-glucose. The minced heart pieces were washed twice with 40 ml of cold PBS-glucose upon which the volume was decanted to 5 ml. The minced heart pieces were transferred with a sterile, cut-opened end pipette tip in 3-4 ml of warm (37 °C) PBS-glucose to a sterile digestion flask.

The digestion process consisted of adding PBS-glucose, 200 μl Trypsin (2 % w/v), 100 μl Collagenase (2 % w/v in PBS-glucose), and 40-80 μl DNAse (1 % w/v in PBS-glucose) to a sterile digestion flask for approximately 8.5 min. After each 8.5 min digestion period, the supernatant containing isolated heart cells was removed and placed in cold plating media. Once the digestions were complete (typically 6-8 digestions) the isolated cells were centrifuged for 10 min at 150 g and re-suspended in 20 ml of cold plating media (DF-12 with 7.5 % horse serum and 7.5 % fetal bovine serum). The cells were then filtered using a 0.4 μm cell strainers obtained by Becton Dickenson (Lincoln Park, NJ) into 50 ml sterile centrifuge tubes. Cells were centrifuged again for 10 min at 150 g upon which media was decanted to 12 ml. To separate myocytes from fibroblasts, the cells were plated into a Falcon 3025 tissue plate and incubated at 37 °C (5% CO_2) for 1 hour. Within 1 h the majority of the fibroblasts attached to the plate and the myocytes that remained suspended in plating media were collected into a sterile 50 ml centrifuge tube, centrifuged for 10 minutes at 150 g and re-suspended in 20 ml of plating media, which was filtered using a 40 μm filter basket. The preparation typically resulted in a viability of greater than 90 % by trypan blue exclusion.

6.2.3 Collagenase liver perfusion of adult rat hepatocytes

Studies were performed in accordance with the principles and guidelines of the

Canadian Council on Animal Care and the University of Manitoba Animal Care Committee. Hepatocytes were isolated by Guqi Wang and were a gift from the laboratory of Dr. Frank Burczynski (University of Manitoba, Faculty of Pharmacy). Female Sprague-Dawley rats (200-250 g), purchased from University of Manitoba breeding stock, were housed in a temperature-light controlled room and allowed food and water *ad libitum*. Hepatocyte suspensions were prepared by the collagenase perfusion described previously (Burczynski and Cai, 1994). Briefly, animals were anaesthetized with an intraperitoneal injection of pentobarbital (50 mg/kg). A midline incision was made upon which the portal vein was isolated and cannulated. Livers were perfused *in situ* at 20 ml/min with oxygenated Swim's S-77 medium containing 5 mM EDTA for the first 8 min, and thereafter with Swim's S-77 medium containing 25 mg/dl collagenase and 5 mM $CaCl_2$ for approximately 10 min. Perfused livers were excised, combed free of connective tissue, and filtered through 150 mesh followed by 50-mesh stainless steel filters (Sigma Chemical Company, St. Louis, MO). Parenchymal cells were separated from nonparenchymal cells by centrifugation at 55 g for 3 min. The isolated hepatocytes, which comprised greater than 95% of the isolated cell population, were stored at room temperature and used within 1 h of the completed perfusion. Cell viability was visually assessed to be greater than 90% by the trypan blue exclusion method.

6.2.4 Blood collection from adult rats for *in vitro* dexrazoxane and dexrazoxane metabolite hydrolysis studies

Animal handling and surgery for blood collection is described in Section 2.2.2 of Chapter 2. As in the case with the *in vivo* metabolism studies described in Chapters 2 and 5, the animals were euthanized with Euthanol after the blood collection. Typically, 15 ml

of blood was removed per adult rat (300-350 g) from the jugular vein following cannulation. The blood was collected in two 15 ml sterile centrifuge tubes containing 100 µl heparin (1000 units/ml) and centrifuged at 500 g for 5 min. The plasma was removed and used for a metabolism experiment within one hour of collection.

6.2.5 Blood collection from human volunteer for *in vitro* dexrazoxane and dexrazoxane metabolite hydrolysis studies

Blood was withdrawn from a 27 year old female at the Victoria General Hospital (Winnipeg, MB) into standard 5 ml heparinized tubes (Fisher, Canada). Two 5 ml samples were taken per visit. All *in vitro* human whole blood and blood plasma experiments began less than one hour after collection. This protocol was approved by the University of Manitoba Health Research Ethics Board.

6.2.6 Preparation of cell suspension media and physiological buffers

Cells were incubated in α-MEM suspension buffer for hepatocyte and myocyte suspension studies where the loss of dexrazoxane or C was measured. One package of α-MEM was dissolved in 1 l of distilled water buffered with 40 mM HEPES, titrated to pH of 7.2 with 5 M HCl/NaOH, and filter sterilized using a 20 µm bottle top filter (Sarstedt, St. Leonard, PQ). 10 ml of antibiotic (penicillin and streptomycin) was aseptically added after sterilization. α-MEM was stored at 4 °C for no longer then 30 days after preparation.

For cell suspension studies where ADR-925 was measured by the calcein assay, a physiological hepatocyte suspension buffer was prepared as α-MEM interfered with the calcein assay. The hepatocyte suspension buffer, in which dexrazoxane metabolism to ADR-925 was studied, was prepared as previously described (Hasinoff et al., 1994) and

contained 137 mM NaCl, 5.4 mM KCl, 1.2 mM $CaCl_2$, 0.64 mM $MgCl_2$, 1.1 mM KH_2PO_4, 0.7 mM Na_2SO_4, 34 mM HEPES, and titrated to a pH of 7.4 with 5 M NaOH.

Artificial plasma was made as previously described (Luquita et al., 2001) and contained 130 mM NaCl, 4.9 mM KCl, 2.5 mM $CaCl_2$, 1.2 mM $MgCl_2$, 5 mM KH_2PO_4, 34 mM HEPES, and titrated to a pH of 7.4 with 5 M NaOH. The Tris/saline buffer was used in blood, plasma, and HSA studies. 2 M Tris was dissolved in water, titrated to a pH of 7.4 (at 37 °C) and stirred with 2 g Chelex resin per 100 ml for 24 h prior to use. To buffer blood and plasma, 50 μl of 2 M Tris was added per 950 μl such that the final Tris concentration was 100 mM. Likewise, the control Tris/saline buffer was made by added 50 μl of 2 M Tris to 950 μl of saline (0.9 % NaCl w/v).

6.2.7 Hydrolysis of dexrazoxane, C or dihydroorotate in the presence of neonatal rat myocytes and adult rat hepatocytes

Immediately following the primary cell isolation (for both neonatal rat myocytes and adult rat hepatocytes) cell densities were determined using a hemocytometer and cell viability was determined using the trypan blue exclusion method (Haugland, 1996). The cells were then centrifuged at 400 g for 5 min and re-suspended in α–MEM such that the cell density was 2 x 10^6 cells/ml (with the exception of the hepatocyte metabolism of dexrazoxane study where the cell densities were 7 x 10^6 cells/ml and cells were re-suspended in the hepatocyte suspension buffer). Cells were then added to a 6-well plate for suspension cells (Sarstedt, St. Leonard, PQ) and placed in an incubator (37 °C, 5 % CO_2) for 15 min to allow media to equilibrate. For the entire duration of the experiment, the 6-well plates were placed on a Thermolyne Slow Speed Roto Mix (obtained from Fisher) where they were very gently agitated on the lowest setting.

Dexrazoxane, C, or dihydroorotate was dissolved in α-MEM, and added to

247

suspension cells in a total volume of 2 – 4 ml. In the case where inhibitors were used, cells were pre-incubated with the inhibitor (dissolved in sterile saline, 0.9 % NaCl (w/v)) for 30 min prior to the addition of substrate (dexrazoxane, C, or dihydroorotate). As shown in Table 6.1, the combined volume of drug and saline/inhibitor was consistently 4.5 % of the total suspension volume. Aliquots (100-150 µl) of the cell suspension were removed at timed intervals and centrifuged at 500 g for 5 min. The supernatant was removed and acidified to pH 3.0 with 10 µl of 50 mM HCl and stored at -80 °C until analyzed, to prevent further hydrolysis (Hasinoff, 1994a). Aliquots were also removed at various intervals during the experiment in order to monitor cell viability by the trypan blue exclusion method. Only myocytes from cell isolation preparations that had an initial viability of greater than 90 % and a viability of greater than 80 % at the end of the metabolism study were considered for analysis in this chapter. Likewise, only hepatocytes with an initial viability of greater than 80 % and an end of experiment viability of greater than 70 % were considered.

Table 6.1 Typical volumes of drug and inhibitors/saline for neonatal rat myocyte and adult rat hepatocyte cell suspension studies.

Experiment	Volume of cell suspension in α-MEM (µl)	Volume of drug (µl)	Volume inhibitor or saline (µl)
Drug Control	3820	80	100 (saline)
Drug + Cell suspension	3820	80	100 (saline)
Inhibitor + cell suspension	3820	80	100 (inhibitor)

6.2.8 Dexrazoxane hydrolysis in hepatocyte suspension buffer supernatant

248

An experiment was done to determine whether non-viable hepatocytes, that may have leaked dexrazoxane metabolizing enzymes, were facilitating extra-cellular dexrazoxane hydrolysis over the duration of the experiment. In order to test this, hepatocytes were incubated for 3 h in suspension buffer, upon which the cell suspension was centrifuged at 500 g for 5 min and the supernatant was collected. Dexrazoxane was added to the supernatant (free of hepatocytes) and samples were removed and acidified at timed intervals. Samples were acidified to pH 3 and stored at -80 °C until analyzed.

6.2.9 Hydrolysis of dexrazoxane, C or dihydroorotate in blood, blood plasma, and 45 mg/ml HSA

Experiments were also carried out to determine whether whole blood or plasma could facilitate the hydrolysis of dexrazoxane, C, or dihydroorotate. In these experiments, whole blood and plasma were buffered with Tris to a pH of 7.4 such that the final Tris concentration was 100 mM. Tris buffer was treated with Chelex (2 g/100 ml) for 24 hr prior to use to chelate any heavy metal ion that could facilitate the hydrolysis of dexrazoxane or C as described in Section 6.2.6 (Buss and Hasinoff, 1995; Buss and Hasinoff, 1997). Blood and blood plasma were incubated with Tris at 37 °C with 5 % CO_2 for 30 min in a 6-well plate prior to the addition of substrate. After the substrate was added, aliquots were removed at timed intervals. Plates were gently agitated by hand every 15 min throughout the duration of the experiment. In the case where whole blood was used, aliquots were removed, centrifuged at 500 g, upon which the plasma was collected. Samples were acidified to a pH of 3 with 5 M HCl and stored at -80 °C until analyzed (Hasinoff, 1994a).

In the case were dexrazoxane, C, or dihydroorotate was incubated with 45 mg/ml

human serum albumin (HSA). HSA (fatty acid free) was dissolved in 100 mM Tris/saline (0.9 % NaCl w/v) buffer (Chelex treated (2 g/100 ml) for 24 h prior to use). Prior to the addition of substrate, the Tris buffered HSA solution was placed in a 37 °C 5 % CO_2 incubator for 30 min. Samples were removed at timed intervals and acidified to a pH of 3 with 5 M HCl and shored at -80 °C until analyzed.

6.2.10 HPLC separation of dexrazoxane, C, and dihydroorotate from α-MEM

The HPLC instrumentation for the analysis of dexrazoxane and C on a reversed phase C_{18}-column (detection wavelength 205 nm) has been described in Chapter 2 Section 2.2.9. Briefly, dexrazoxane was separated using 500 μM Na_2EDTA/2 mM heptanesulfonic acid (pH 4.5) isocratically pumped through a 10 mm μBondapak 3.9 x 300 mm reversed phase C_{18}-column (Waters, Mississauga, Canada) at a rate of 1 ml/min for 3 min. From 3 to 4 min, the methanol concentration was linearly increased to 15 % and maintained for 10 min to elute dexrazoxane (t_r 7.8 min, as shown in Figure 6.3) and to remove any late eluting peaks. The initial mobile phase was isocratically pumped through the column for 30 min prior to the next injection. C was separated using 500 μM Na_2EDTA (pH 4.5) that was isocratically pumped through the column at a rate of 1 ml/min for 5 min. From 5 to 6 min methanol was linearly increased from 0 to 50% and maintained for 10 minutes to remove any late eluting peaks. Under these conditions C eluted with a retention time of 6.1 min (as shown in Figure 6.4). HPLC analysis of dihydroorotate has been described in detail in Chapter 4 (Section 4.2.10). Briefly, dihydroorotate was separated (t_r 2.9 min, Figure 6.5) on a 10 mm μBondapak 3.9 x 300 mm reversed phase C_{18}-column with an elution profile of 10 mM 1-octanesulfonic acid (pH 2.5, 1 ml/min) for 5 min after which the methanol concentration was linearly

increased over 1 min from 0 to 40% (v/v) and maintained for 20 min. The column was re-equilibrated with 10 mM 1-octanesulfonic acid (pH 2.5, 1 ml/min) for 30 min before the next injection. All samples were analyzed in duplicate.

6.2.11 HPLC calibration plots: quantitation of dexrazoxane, C, and dihydroorotate in α-MEM

The HPLC calibration curves (5 to 100 μM dexrazoxane, 5 to 200 μM C, and 10 to 75 μM dihydroorotate) were prepared by adding standards containing known amounts of dexrazoxane, C (prepared as previously described (Hasinoff, 1994a)), and dihydroorotate to α-MEM. The calibration plots for dexrazoxane, C, and dihydroorotate were constructed by plotting integration peak areas (as shown in Tables 6.2 – 6.4) as a function of concentration as shown in Figures 6.6 through 6.8. Calibration curves were prepared prior to each series of samples to be analyzed where each concentration point is an average of two injections.

6.2.12 Data Analysis

6.2.12.1 Determination of statistical significance between substrate hydrolysis rates

The rate of hydrolysis (or disappearance) of substrate in the presence of cells, blood, plasma, or buffer can be described mathematically using a linear regression model of the independent variable (time) and the dependent variable (substrate concentration). The regression parameter of slope was used as a means to compare the effect of substrate loss in cells, blood, or plasma with the substrate loss of the control under the same experimental conditions and design. Thus, the slopes of the best fit lines associated with treatment versus control can be statistically compared by an independent-samples *t-test* (Jones, 2002) where p is the statistical significance obtained from linear least squares fit.

251

6.2.12.2   Determination of the degree of inhibition

In the case where inhibitors were used the degree of inhibition was expressed as a percentage value relative to the control hydrolysis rate in suspension buffer. The percent inhibition was described using the following equation.

$$\% \text{ inhibition} = \left[1 - \frac{\text{net rate hydrolysis (inhibitor)}}{\text{net rate hydrolysis}} \right] \times 100$$

The *net rate of hydrolysis (inhibitor)* refers to the rate of hydrolysis of the substrate in the presence of an inhibitor and the experimental conditions (cells, blood, or plasma). The *net rate of hydrolysis* refers to the hydrolysis of the substrate in the presence of experimental control conditions (cells, blood, or plasma without an inhibitor present). The background hydrolysis of C (Hasinoff, 1994a) was corrected for by subtracting the rate of substrate loss (-slope) of the C control from the slope of the hydrolysis in the presence of cells, blood, or plasma with and without inhibitors.

6.3   Results

6.3.1   HPLC separation of dexrazoxane, C, and dihydroorotate from α-MEM

Dexrazoxane, C, and dihydroorotate were separated using a 10 mm μBondapak 3.9 x 300 mm reversed phase C_{18}-column with column conditions described in Section 6.2.10. Under these conditions, dexrazoxane, C, and dihydroorotate were separated with retention times of 7.8, 6.1, and 2.9 min, respectively (as seen in Figures 6.3 – 6.5). Also, as seen in Figures 6.3 – 6.5, dexrazoxane, C, and dihydroorotate were well resolved and separated from α-MEM peaks. The limit of quantitation in α-MEM, estimated from three times the limit of detection, of dexrazoxane, C, and dihydroorotate was 0.5, 1.0, and

2 μM, respectively. The limit of detection was made through an estimate of drug/metabolite peak heights that exceeded the background noise of α-MEM control three-fold.

6.3.2 HPLC calibration plots: quantitation of dexrazoxane, C, and dihydroorotate in α-MEM

The calibration plots for dexrazoxane, C, and dihydroorotate were constructed by plotting integration peak areas (as shown in Tables 6.2 – 6.4) as a function of concentration as shown in Figures 6.6 through 6.8. Calibration curves were prepared prior to each series of samples to be analyzed where each concentration point is an average of two injections. The day-to-day variation of the slopes was small and is expressed as a percent difference at the end of Tables 6.2-6.4.
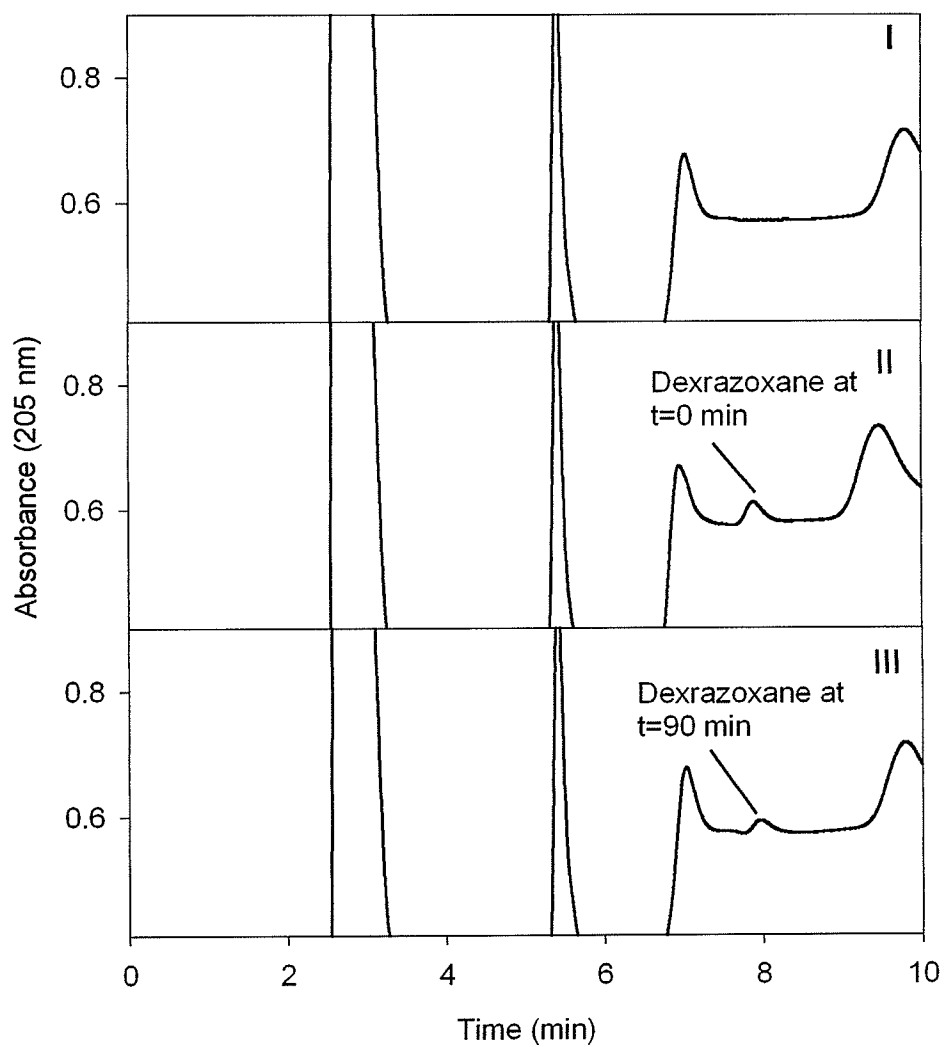
Figure 6.3 HPLC chromatograms of the separation of dexrazoxane from α-MEM
components for myocytes dosed with 10 μM dexrazoxane.

Dexrazoxane was separated on a C_{18} reverse-phase column. Blank α-MEM is shown in
chromatogram I. HPLC chromatograms II and III were obtained after 0 and 90 min after
dexrazoxane was added to the myocyte cell suspension.
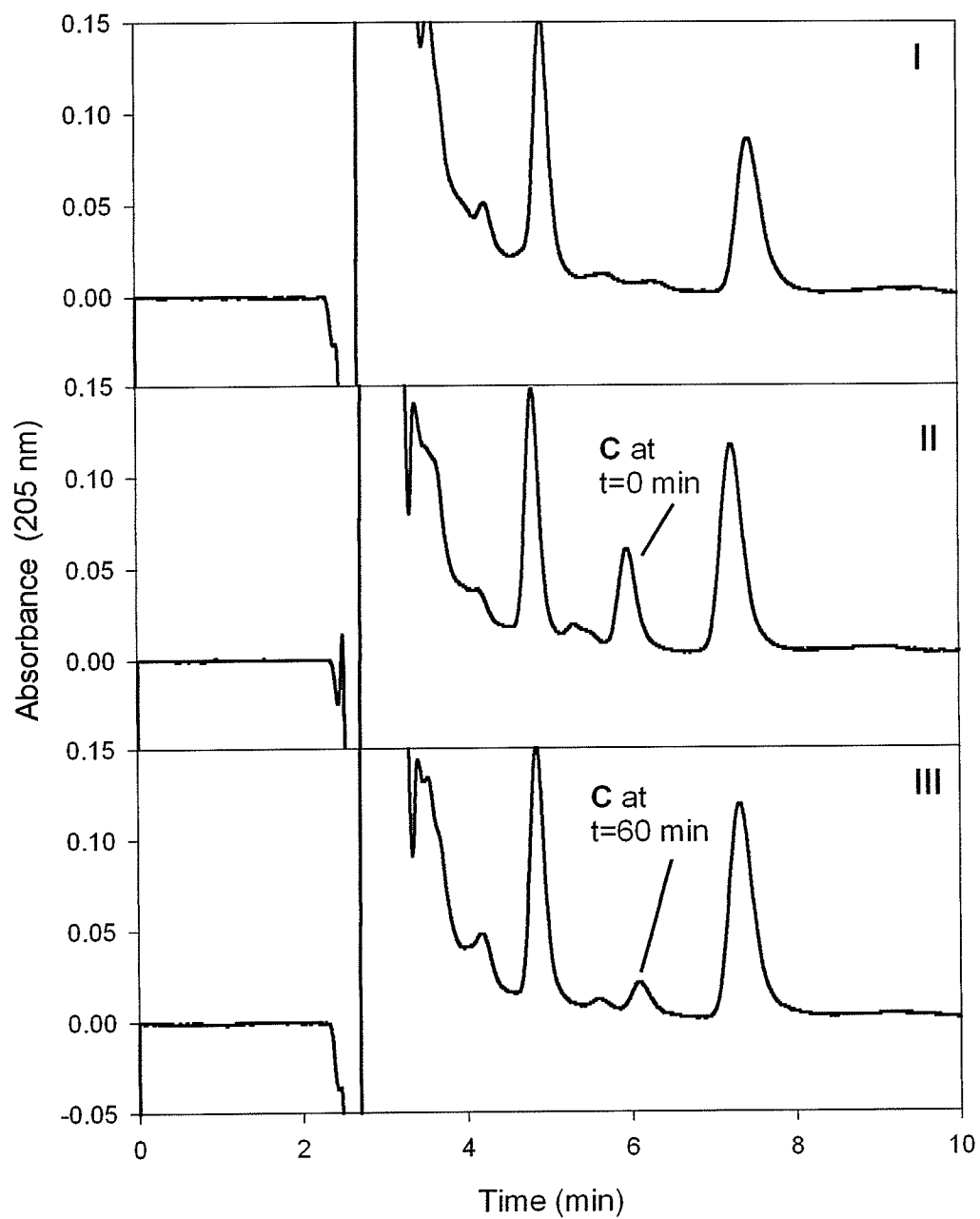
Figure 6.4 HPLC chromatograms of the separation of C from α-MEM components for myocytes dosed with 50 μM C.

C was separated on a C_{18} reverse-phase column. Blank α-MEM is shown in chromatogram I. HPLC chromatograms II and III were obtained after 0 and 60 min after C was added to the myocyte cell suspension.
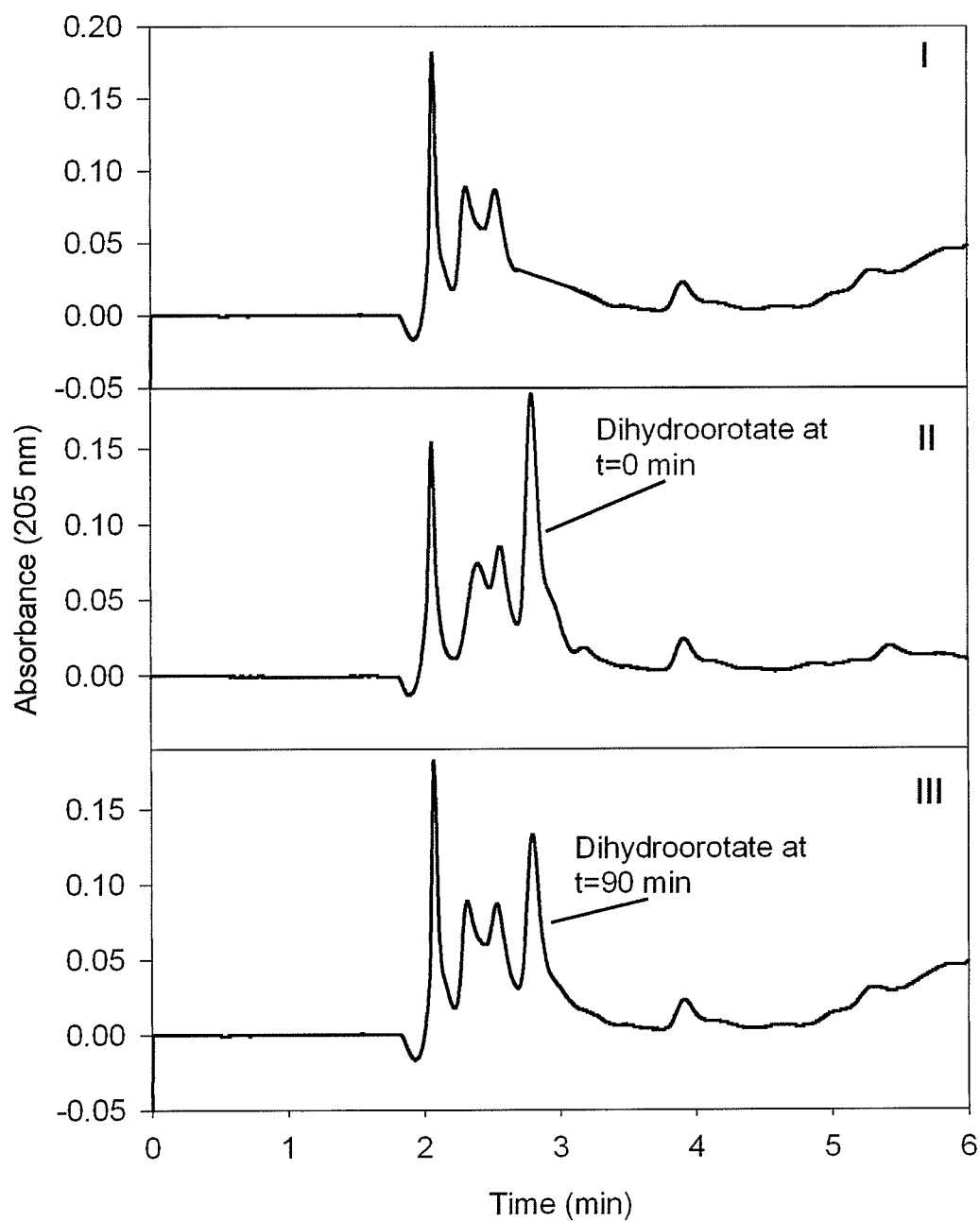
Figure 6.5   HPLC chromatograms of the separation of dihydroorotate from α-MEM components for myocytes dosed with 50 μM dihydroorotate.

Dihydroorotate was separated on a C_{18} reverse-phase column. Blank α-MEM is shown in chromatogram I.   HPLC chromatograms II and III were obtained after 0 and 90 min after dihydroorotate was added to the myocyte cell suspension.

Table 6.2 HPLC calibration curve of **C** (UV absorbance at 205 nm) in α-MEM for **C** metabolism studies in neonatal rat myocytes and adult rat hepatocytes.

Concentration (μM)	Average Peak Area (Arbitrary Units)
200	306521
100	152421
60	91991
40	59951
30	49164
20	28788
10	15264
5	7728
Slope[a]	1535
Y-intercept	-75
r^2	0.995

[a] Between-day variation in the slopes of the calibration plots was 2%.

Table 6.3 HPLC calibration curve of dexrazoxane (UV absorbance at 205 nm) in α-MEM for metabolism studies in neonatal rat myocytes and adult rat hepatocytes.

Concentration (μM)	Average Peak Area (Arbitrary Units)
100	354023
75	272180
50	182218
25	98624
15	50899
5	25395
Slope[a]	3508
Y-intercept	6012
r^2	0.998

[a] Between-day variation in the slopes of the calibration plots was 3%.

Table 6.4 HPLC calibration curve of dihydroorotate (UV absorbance at 205 nm) in α-MEM for dihydroorotate metabolism studies in neonatal rat myocytes.

Concentration (μM)	Average Peak Area (Arbitrary Units)
10	15893
20	25543
30	46864
50	73254
75	112048
Slope [a]	1499
Y-intercept	-761
r^2	0.996

[a] Between-day variation in the slopes of the calibration plots was 1%.
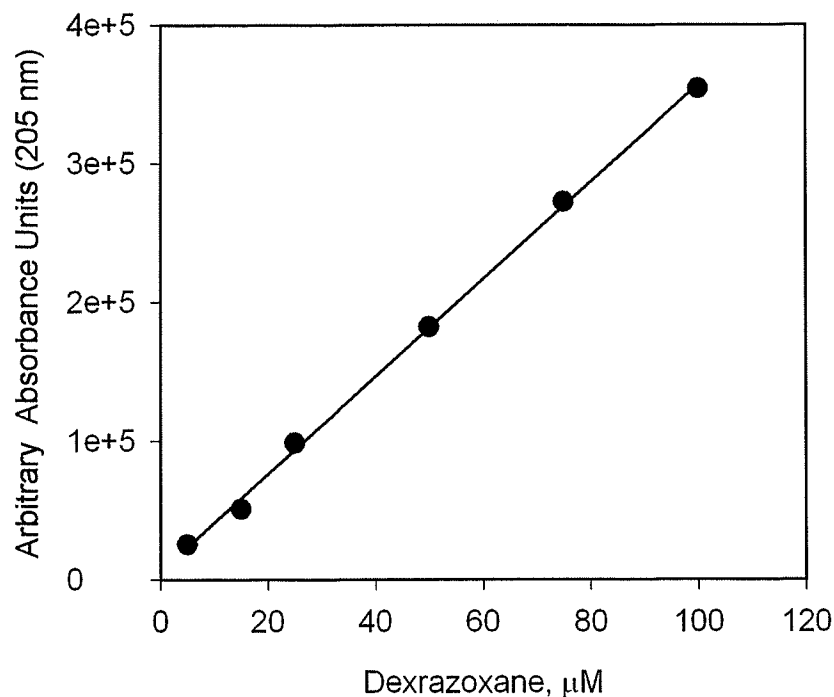
Figure 6.6 HPLC calibration curve of dexrazoxane in α-MEM
HPLC calibration plots using integrated peak areas were prepared by adding standards containing known amounts of dexrazoxane to α-MEM. A mobile phase of 500 μM $Na_2EDTA/2$ mM heptanesulfonic acid and methanol (85/15, v/v) (as described in Section 6.2.10) was used to separate dexrazoxane (t_r 7.8 min).
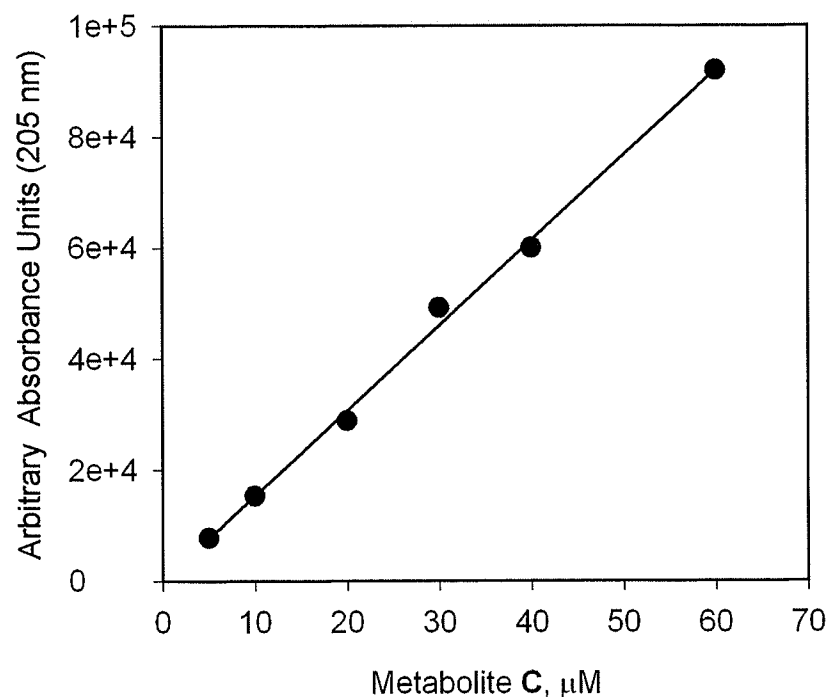
Figure 6.7 HPLC calibration curve of C in α-MEM
HPLC calibration plots using integrated peak areas were prepared by adding standards containing known amounts of C to α-MEM. A mobile phase of 500 μM Na_2EDTA (pH 4.5) (as described in Section 6.2.10) was used to separate C (t_r 5.8 min).

259
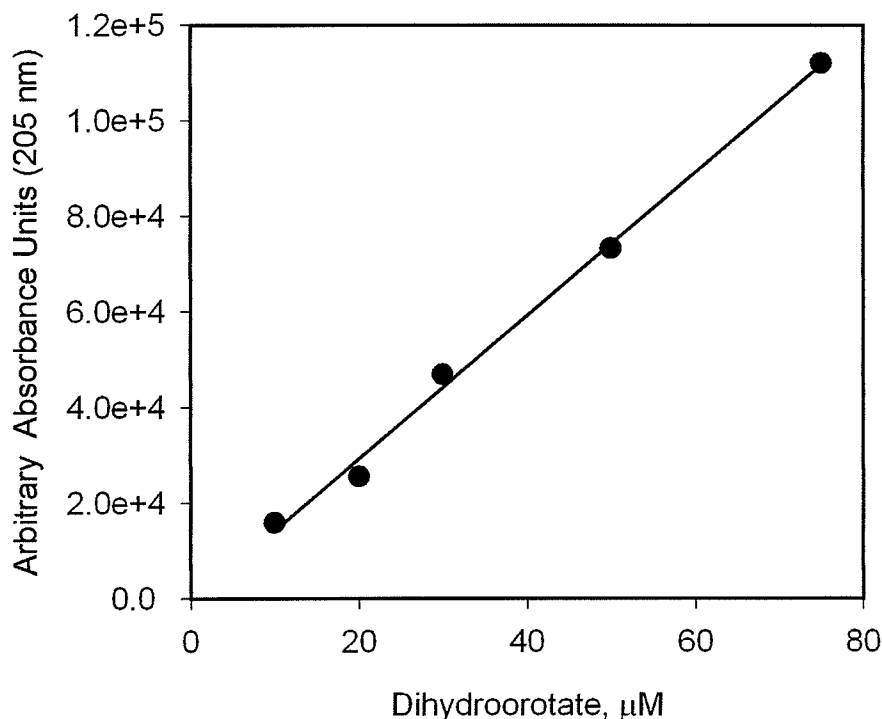
Figure 6.8 HPLC calibration curve of dihydroorotate in α-MEM
HPLC calibration plots using integrated peak areas were prepared by
adding standards containing known amounts of dihydroorotate to α-MEM.
A mobile phase of 10 mM 1-octanesulfonic acid (pH 2.5, 1 ml/min) was
used to separate dihydroorotate (t_r 2.9 min, Figure 6.5).

6.3.3 Dexrazoxane metabolism in neonatal rat myocyte suspensions

Figure 6.9 – 6.11 show the concentration-time profile after myocytes are dosed

with 10 μM dexrazoxane. Figure 6.12 shows the average of the three studies of the

disappearance of dexrazoxane from α-MEM (suspension buffer) both in the presence and

absence of neonatal rat myocytes. The loss of dexrazoxane from the α-MEM buffer

control experiment is consistent with the base-catalyzed hydrolysis of dexrazoxane to **B**

and **C** under physiological conditions (Buss and Hasinoff, 1997; Hasinoff, 1994a).

Dexrazoxane incubated in the presence of myocytes shows a greater overall loss of

dexrazoxane relative to the α-MEM control (where myocytes are not present) at 90 min. The disappearance of dexrazoxane in the presence of myocytes had two distinct phases. For the first 20 min incubation period, as shown in Figure 6.12 the rate of loss of dexrazoxane was 7.6-fold greater ($p < 0.001$) in the presence of myocytes then the control (absence of myocytes), as measured by their respective slopes. Also, after 30 min, the rate of dexrazoxane loss in the presence of myocytes is not significantly different than that of the control experiment (as measured by their respective slopes, $p > 0.2$).

Table 6.5 Dexrazoxane hydrolysis in the presence of 2×10^6 myocytes/ml in α-MEM suspension buffer

Time (min)	Experiment number			Average, μM	SE, ± μM
	1	2	3		
0	9.9	10.0	9.8	9.9	0.06
2.5	9.5	9.4	9.6	9.5	0.06
5	8.8	9.1	9.3	9.1	0.14
7.5	8.3	9.2	9.3	8.9	0.31
15	8.2	8.7	9.2	8.7	0.28
20	8.0	8.4	9.1	8.5	0.34
30	8.3	8.0	8.6	8.3	0.16
45	7.3	7.8	7.7	7.6	0.17
60	7.1	7.8	7.6	7.5	0.21
90	6.6	7.5	7.8	7.3	0.38
120	5.9	7.2	7.5	6.9	0.49

Table 6 6 Dexrazoxane hydrolysis control (in the myocyte suspension buffer, α-MEM)

Time (min)	Experiment number			Average, μM	SE, ± μM
	1	2	3		
0	10.0	9.9	9.8	9.9	0.02
30	9.7	9.6	9.5	9.6	0.05
60	9.4	9.3	9.5	9.4	0.04
90	9.1	9.2	9.1	9.1	0.03
120	8.8	9.0	9.1	9.0	0.08
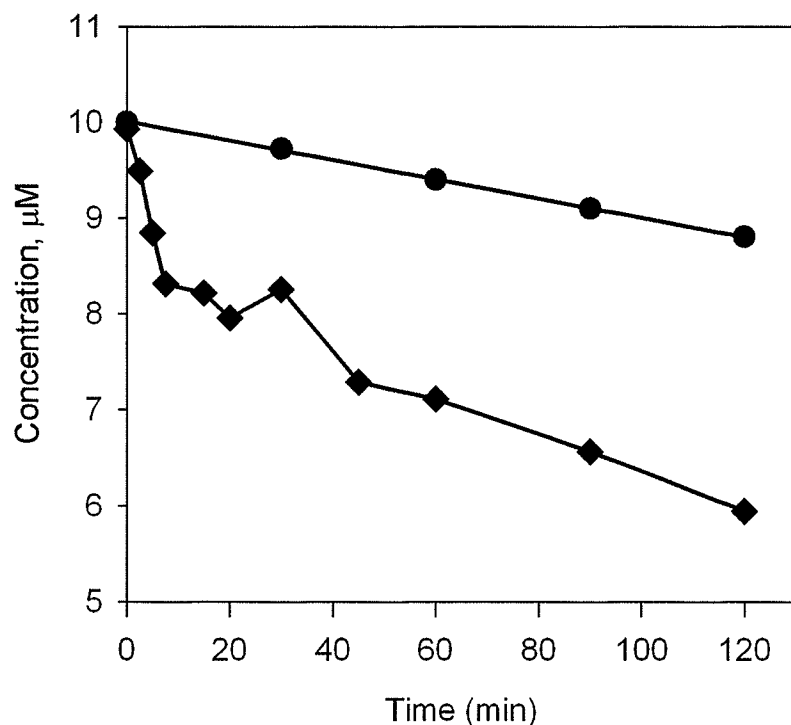
Figure 6.9 Dexrazoxane loss from the myocyte suspension buffer (α-MEM) of experiment 1
Loss of 10 μM dexrazoxane in the presence of myocytes (2 x 10⁶ myocytes/ml) in α-MEM suspension buffer; ●, dexrazoxane loss in α-MEM suspension buffer alone; ♦, dexrazoxane loss in the presence of myocytes. The loss of dexrazoxane was determined by HPLC as described in Section 6.2.10
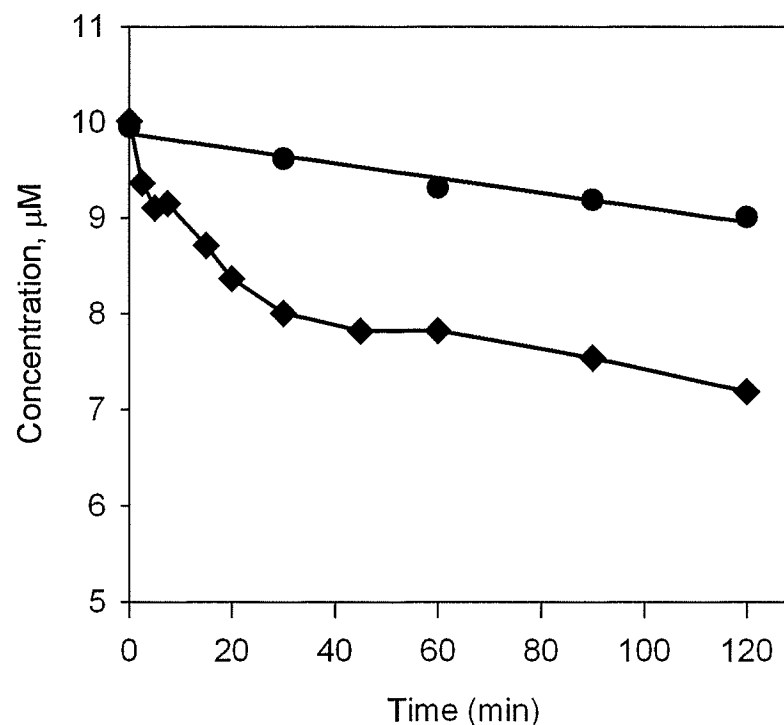
Figure 6.10 Dexrazoxane loss from the myocyte suspension buffer (α-MEM) of experiment 2
Loss of 10 μM dexrazoxane in the presence of myocytes (2 x 10⁶ myocytes/ml) in α-MEM suspension buffer; ●, dexrazoxane loss in α-MEM suspension buffer alone; ♦, dexrazoxane loss in the presence of myocytes. The loss of dexrazoxane was determined by HPLC as described in Section 6.2.10
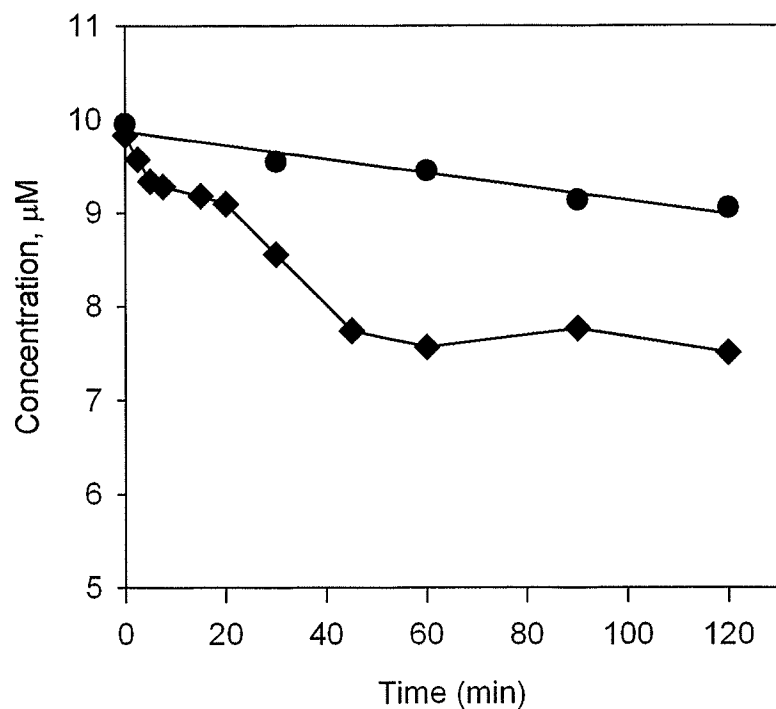
Figure 6.11 Dexrazoxane loss from the myocyte suspension buffer (α-MEM) of experiment 3

Loss of 10 μM dexrazoxane in the presence of myocytes (2 x 10^{6} myocytes/ml) in α-MEM suspension buffer; ●, dexrazoxane loss in α-MEM suspension buffer alone; ◆, dexrazoxane loss in the presence of myocytes. The loss of dexrazoxane was determined by HPLC as described in Section 6.2.10.
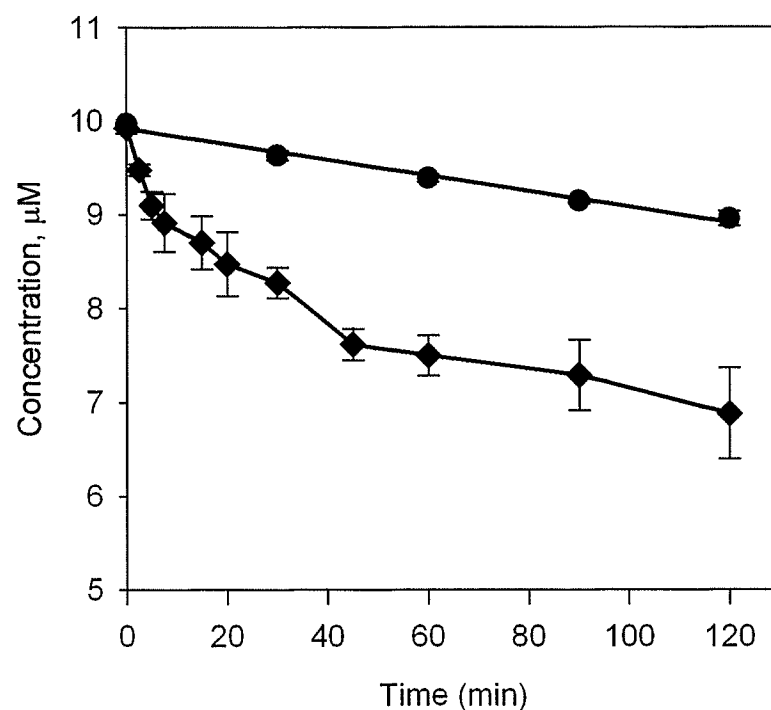
Figure 6.12 Average dexrazoxane loss from the myocyte suspension buffer of experiments 1-3

Loss of 10 μM dexrazoxane in the presence of myocytes (2 x 10^{6} myocytes/ml) in α-MEM suspension buffer; ●, dexrazoxane loss in α-MEM suspension buffer alone; ◆, dexrazoxane loss in the presence of myocytes. The loss of dexrazoxane was determined by HPLC as described in Section 6.2.10.

6.3.4 Dexrazoxane metabolism to ADR-925 in an adult rat hepatocyte suspensions

The results in Figure 6.13-15 clearly show that dexrazoxane rapidly disappeared from hepatocyte suspension buffer in the presence of adult rat hepatocytes relative to the suspension buffer control. ADR-925 is also rapidly formed in the presence of hepatocytes and was found at detectable levels in the hepatocyte suspension buffer within seconds of adding dexrazoxane. At 5 h, ADR-925 levels were responsible for approximately one third of all dexrazoxane and dexrazoxane metabolites present in the suspension buffer, as shown in Figure 6.16 and Table 6.9. Dexrazoxane hydrolysis to ADR-925 in control experiments (in suspension buffer alone) found that at 5 h, ADR-925 was responsible for less then 5 % of the total dexrazoxane and dexrazoxane metabolites in the suspension buffer.

Table 6.7 Dexrazoxane loss in the presence of 7×10^6 hepatocytes/ml in hepatocyte suspension buffer dosed with 100 μM dexrazoxane

Time (min)	Experiment number			Average, μM	SE, ± μM
	1	2	3		
	Dexrazoxane, μM	Dexrazoxane, μM	Dexrazoxane, μM		
0	100	103	99.6	101	1.0
15	89.1	90.8	ND	89.9	0.7
30	83.6	83.7	83.5	83.6	0.1
60	60.1	60.5	60.8	60.5	0.2
120	31.3	33.0	32.0	32.1	0.5
180	15.3	15.8	15.5	15.5	0.1
240	8.7	9.2	8.9	8.9	0.2
300	6.0	6.5	6.2	6.2	0.1

ND, Data point not determined.

Table 6.8 Dexrazoxane loss in suspension buffer dosed with 100 µM dexrazoxane.

Time (min)	Experiment number			Average, µM	SE, ± µM
	1	2	3		
	Dexrazoxane, µM	Dexrazoxane, µM	Dexrazoxane, µM		
0	100	103	102	102	0.8
15	99.5	98.8		99.1	0.3
30	97.1	96.7	96.5	96.8	0.2
60	97.5	97.5	94.8	96.6	0.9
120	92.9	96.0	93.0	94.0	1.0
180	86.1	92.8	85.5	88.1	2.4
240	84.0	89.2	78.9	84.1	3.0
300	83.1	86.5	76.2	81.9	3.1

Table 6.9 ADR-925 formation in the presence of 7×10^6 hepatocytes/ml dosed with 100 µM dexrazoxane.

Time (min)	Experiment number		Average, µM	Average deviation, ± µM
	1	2		
	ADR-925, µM	ADR-925, µM		
0	5.5	2.0	3.7	2.4
15	13.1	11.2	12.1	1.3
30	16.0	10.2	13.1	4.1
60	17.3	15.5	16.4	1.2
120	19.7	18.5	19.1	0.8
180	24.2	22.4	23.3	1.2
240	29.8	24.9	27.3	3.5
300	33.4	27.8	30.6	3.9

Table 6.10 ADR-925 formation in suspension buffer dosed with 100 µM dexrazoxane.

Time (min)	Experiment number		Average, µM	Average deviation, ± µM
	1	2		
	ADR-925, µM	ADR-925, µM		
0	0.0	0.0	0.0	0.0
15	0.0	0.0	0.0	0.0
30	0.7	0.0	0.4	0.5
60	1.4	1.1	1.3	0.2
120	1.2	1.5	1.4	0.2
180	3.2	2.0	2.6	0.8
240	5.7	4.0	4.8	1.2
300	8.0	7.1	7.6	0.6
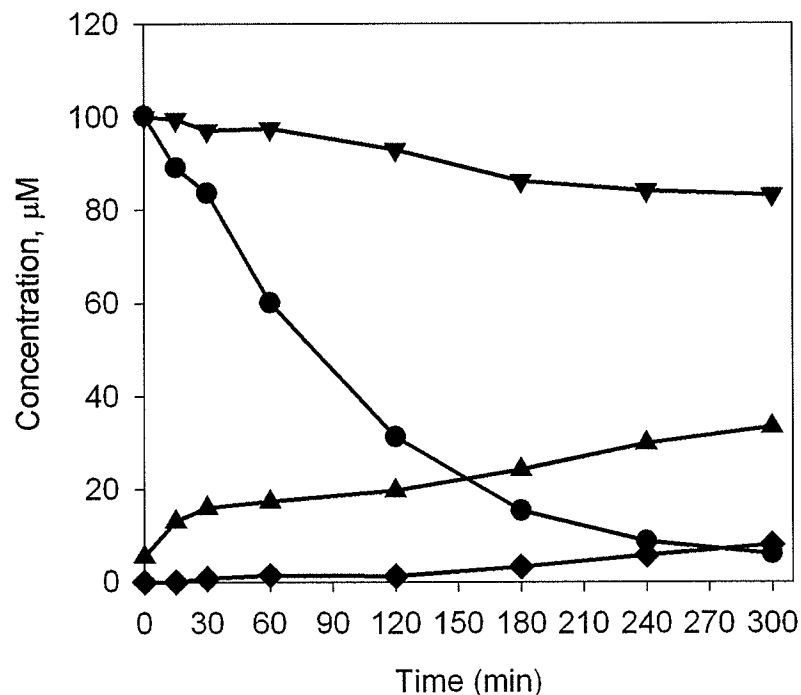
Figure 6.13 Hydrolysis of 100 µM dexrazoxane to ADR-925 in a hepatocyte suspension, study 1

Hydrolysis of 100 µM dexrazoxane in the presence of hepatocytes (7 x 10^6 hepatocytes/ml) in hepatocyte suspension buffer; ●, dexrazoxane loss in the presence of hepatocytes; ▲, ADR-925 formation in the presence of hepatocytes;▼, dexrazoxane loss in suspension buffer alone; ◆, ADR-925 formation in suspension buffer alone. The loss of dexrazoxane was measured by HPLC as described in Section 6.2.10. ADR-925 formation was measured by the calcein assay as described in Section 2.2.11.
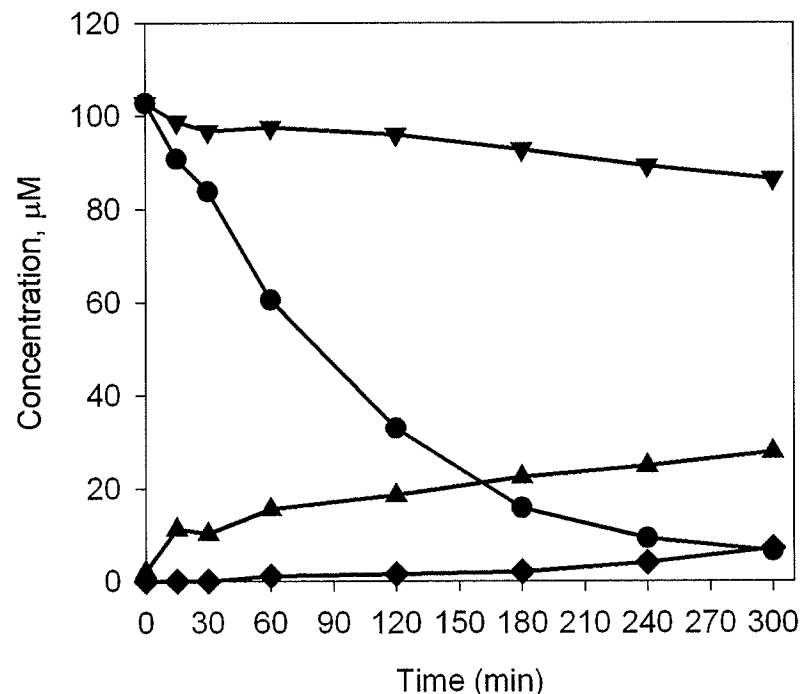
Figure 6.14 Hydrolysis of 100 µM dexrazoxane to ADR-925 in a hepatocyte suspension, study 2

Hydrolysis of 100 µM dexrazoxane in the presence of hepatocytes (7 x 10^6 hepatocytes/ml) in hepatocyte suspension buffer; ●, dexrazoxane loss in the presence of hepatocytes; ▲, ADR-925 formation in the presence of hepatocytes;▼, dexrazoxane loss in suspension buffer alone; ◆, ADR-925 formation in suspension buffer alone. The loss of dexrazoxane was measured by HPLC as described in Section 6.2.10. ADR-925 formation was measured by the calcein assay as described in Section 2.2.11.

266
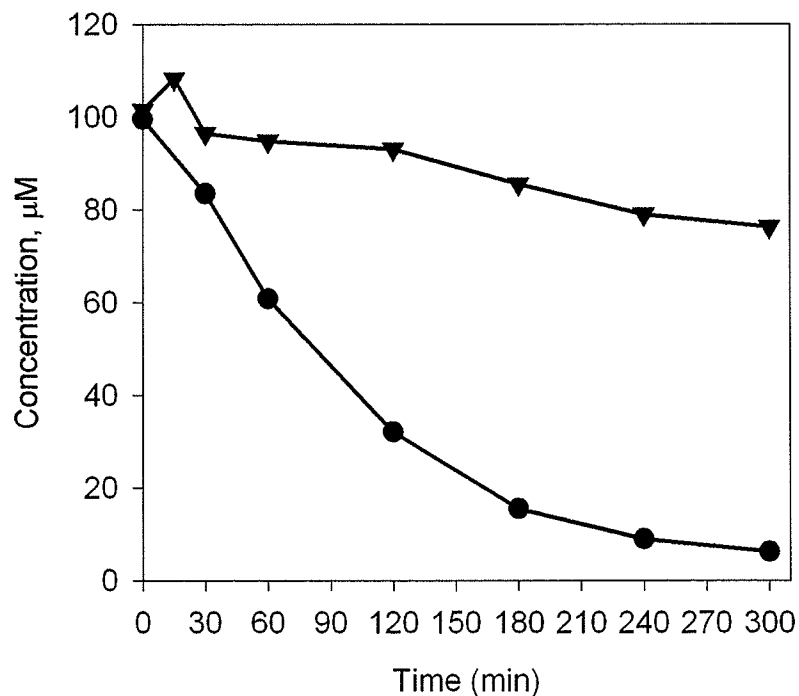
Figure 6.15 Hydrolysis of 100 μM dexrazoxane in a hepatocyte suspension (7 x 10^6 hepatocytes/ml), study 3

Hydrolysis of 100 μM dexrazoxane in the presence of hepatocytes (7 x 10^6 hepatocytes/ml) in hepatocyte suspension buffer;●, dexrazoxane loss in the presence of hepatocytes; ▼, dexrazoxane loss in suspension buffer alone. The loss of dexrazoxane was measured by HPLC as described in Section 6.2.10.
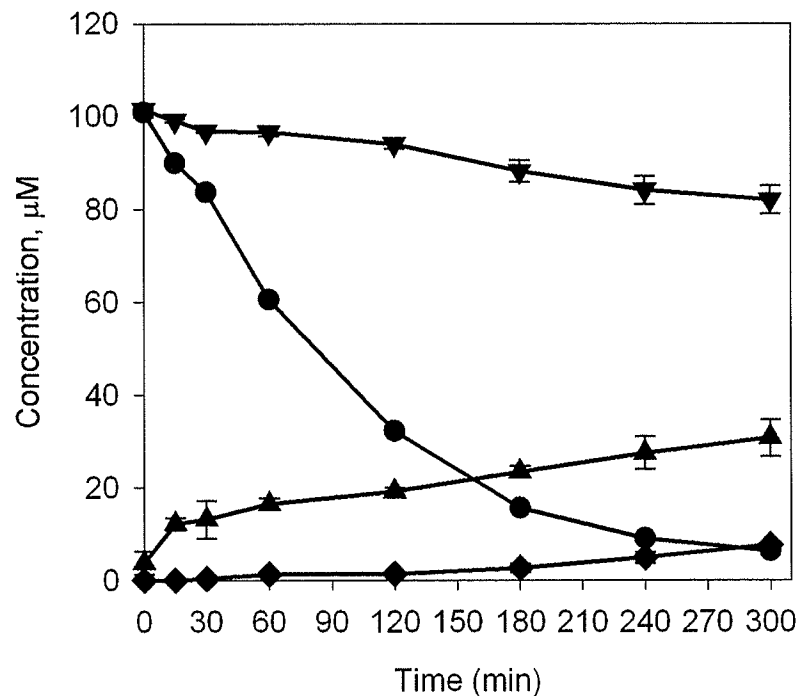
Figure 6.16 Average hydrolysis of 100 μM dexrazoxane to ADR-925 in a hepatocyte suspension for studies 1-3.

Hydrolysis of 100 μM dexrazoxane in the presence of hepatocytes (7 x 10^6 hepatocytes/ml) in hepatocyte suspension buffer;●, dexrazoxane loss in the presence of hepatocytes; ▲, ADR-925 formation with hepatocytes;▼, dexrazoxane loss suspension buffer alone; ◆, ADR-925 formation in suspension buffer alone.

267

6.3.5 Dexrazoxane hydrolysis in hepatocyte supernatant suspension buffer

In order to determine whether dexrazoxane hydrolysis was facilitated by components/enzymes released from non-viable hepatocytes, an experiment was done using hepatocyte suspension buffer supernatant after a 3 h hepatocyte incubation period as described in Section 6.2.8. As shown in Figure 6.17 ADR-925 levels at 5 h, as measured by the calcein assay, were also not notably different from those of the control at 5 hours, with ADR-925 concentrations of 8 and 12 μM, for the control and hepatocyte supernatant respectively. Compared to ADR-925 levels found in the presence of hepatocytes, found to be 30 μM, the hydrolysis of dexrazoxane, **B**, and **C**, from extra-cellular components was, thus, not considered to be the primary contributor of ADR-925 appearance in the presence of hepatocytes. As shown in Figure 6.18, dexrazoxane hydrolysis in the hepatocyte supernatant suspension buffer was not significantly different ($p > 0.1$) then that of the dexrazoxane control (as measured by their respective slopes).
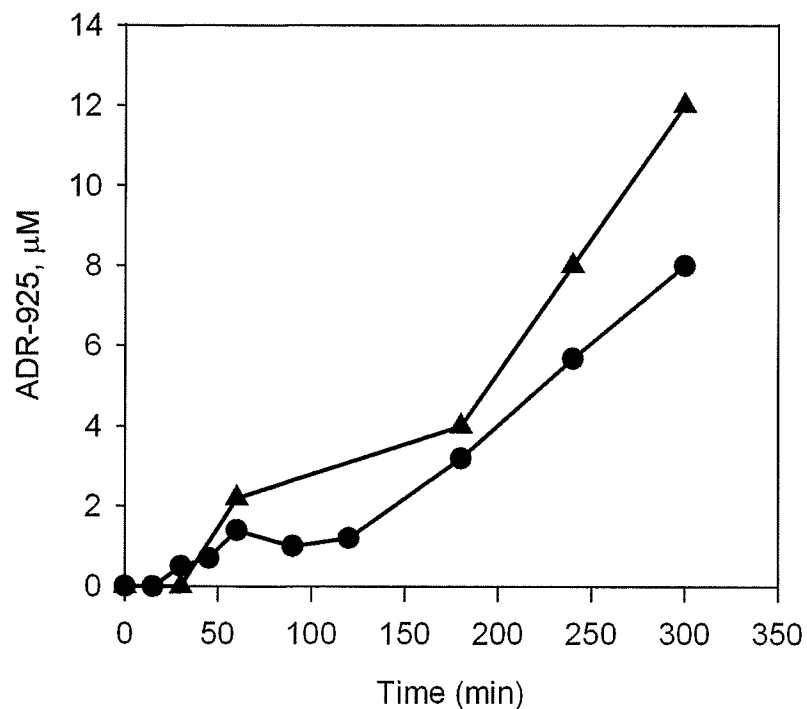
Figure 6.17 Formation of ADR-925 from dexrazoxane incubated with hepatocyte buffer supernatant

Hydrolysis of 100 μM dexrazoxane to ADR-925 in the presence of the hepatocyte suspension buffer supernatant; ●, ADR-925 formation from dexrazoxane in suspension buffer;▲, ADR-925 formation from dexrazoxane in the presence of hepatocyte suspension buffer supernatant. The formation of ADR-925 was measured by the calcein assay as described in Section 2.2.11.
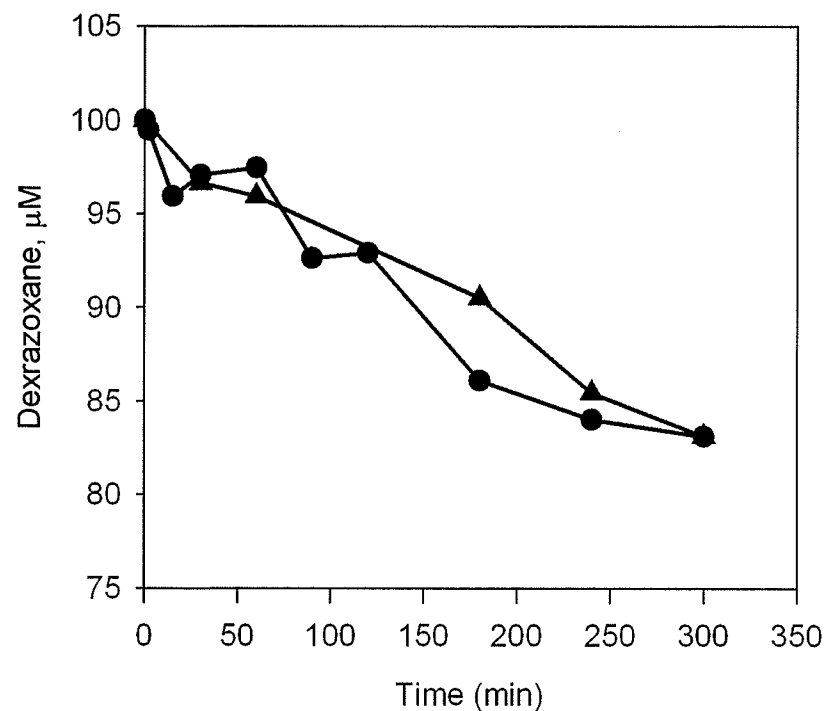
Figure 6.18 Disappearance of dexrazoxane in hepatocyte suspension buffer supernatant

Disappearance of 100 μM dexrazoxane in the presence of the hepatocyte suspension buffer supernatant; ●, dexrazoxane disappearance in the presence of hepatocyte suspension buffer; ▲, dexrazoxane disappearance in the presence of hepatocyte suspension buffer supernatant. The loss of dexrazoxane was determined by HPLC as described in Section 6.2.10.

269

6.3.6 The effect of DHOase inhibition on C metabolism in neonatal rat myocyte suspensions

The rate of loss of C in the presence of myocytes was found to be 2.1-fold greater ($p < 0.001$) than the control experiment in α-MEM alone, as measured by their respective slopes, shown in Figures 6.19-21. It was also determined that the loss of C was inhibited by DHOase inhibitors 5-aminoorotic acid (Krungkrai et al., 1992) and furosemide, both of which were shown to inhibit the DHOase-mediated hydrolysis of C in an enzyme kinetic model described in Chapter 4 (Schroeder et al., 2002). 5-aminoorotic acid and furosemide were found to inhibit the loss of C by 81 and 92 %, respectively relative to the control (Figure 6.22). Also, as noted in Table 6.11, there was no statistical difference between the hydrolysis rate of C in the presence of myocytes when either 5-aminoorotic acid or furosemide were present relative to the control (in the absence of myocytes). Myocytes incubated in the presence of 4-chlorobenzesulfonamide also showed a decrease in the hydrolysis rate of C of approximately 50%, however, the degree of inhibition was found to be significantly less ($p < 0.01$) than the inhibition seen when either 5-aminoorotic acid or furosemide were used, as detailed in Table 6.11.

270

Table 6.11   The effect of DHOase inhibition on **C** hydrolysis in neonatal rat
myocyte suspensions

Experiment	n	Rate of loss ($\mu M \cdot min^{-1}$)	$p^{\,a}$	% inhibition [b]
C Buffer Control	3	0.179	--	--
Myocyte Control	3	0.378	$p < 0.001$	--
5-Aminoorotic Acid	3	0.216	$p > 0.2$	81.4
4-Chlorobenzenesulfonamide	3	0.277	$p < 0.01$	50.8
Furosemide	3	0.194	$p > 0.5$	92.5

[a] The slope (rate of loss) of the **C** buffer control was compared to that of the rate
of loss of **C** in the presence of myocytes or myocytes and inhibitors.
[b] % inhibition is relative to the background hydrolysis (**C** Buffer Control) as
detailed in Section 6.2.12.2.

Table 6.12   Metabolite **C** hydrolysis in α-MEM suspension buffer alone

Time (min)	Experiment number			Average, μM	SE, $\pm \mu M$
	1	2	3		
	C, μM	**C**, μM	**C**, μM		
0	50.1	50.0	50.2	50.1	0.07
15	47.4	46.8	47.8	47.4	0.31
30	43.3	45.0	46.7	45.0	1.00
45	36.9	42.1	43.7	40.9	2.07
60	31.9	39.8	41.5	37.8	3.02
90	28.0	38.1	38.2	34.8	3.44

Table 6.13   Metabolite **C** hydrolysis in the presence of myocytes (2×10^6 cells/ml)
in α-MEM suspension buffer

Time (min)	Experiment number			Average, μM	SE, $\pm \mu M$
	1	2	3		
	C, μM	**C**, μM	**C**, μM		
0	48.6	50.0	49.1	49.2	0.41
15	40.5	38.8	42.9	40.8	1.21
30	32.1	33.0	40.4	35.2	2.66
45	26.3	26.1	34.7	29.0	2.87
60	19.4	22.3	28.9	23.5	2.86
90	7.8	18.2	18.2	14.8	3.52

Table 6.14 Metabolite **C** hydrolysis in myocytes (2×10^6 cells/ml) in the presence of 1 mM 5-aminoorotic acid in α-MEM suspension buffer

Time (min)	Experiment number			Average, μM	SE, $\pm \mu$M
	1	2	3		
	C, μM	**C**, μM	**C**, μM		
0	50.8	49.7	50.2	50.2	0.31
15	47.5	47.9	47.0	47.5	0.26
30	41.3	44.7	43.0	43.0	1.01
45	35.9	43.9	40.2	40.0	2.37
60	32.8	34.9	37.6	35.1	1.40
90	26.9	33.0	35.6	31.8	2.60

Table 6.15 Metabolite **C** hydrolysis in myocytes (2×10^6 cells/ml) in the presence of 1 mM 4-chlorobenzenesufonamide in α-MEM suspension buffer

Time (min)	Experiment number			Average, μM	SE, $\pm \mu$M
	1	2	3		
	C, μM	**C**, μM	**C**, μM		
0	50.8	50.9	49.6	50.4	0.40
15	47.0	55.1	48.2	50.1	2.55
30	43.8	49.0	42.5	45.1	2.03
45	34.4	42.1	40.1	38.8	2.33
60	31.5	37.1	35.4	34.7	1.67
90	24.1	29.1	29.3	27.5	1.74

Table 6.16 Metabolite **C** hydrolysis in myocytes (2×10^6 cells/ml) in the presence of 1 mM furosemide in α-MEM suspension buffer

Time (min)	Experiment number			Average, μM	SE, $\pm \mu$M
	1	2	3		
	C, μM	**C**, μM	**C**, μM		
0	49.7	50.1	49.0	49.6	0.33
15	43.3	49.3	48.9	47.2	1.98
30	36.0	46.6	47.5	43.4	3.74
45	32.7	42.3	44.4	39.8	3.68
60	29.4	40.2	44.0	37.9	4.47
90	21.7	37.7	37.8	32.4	5.45
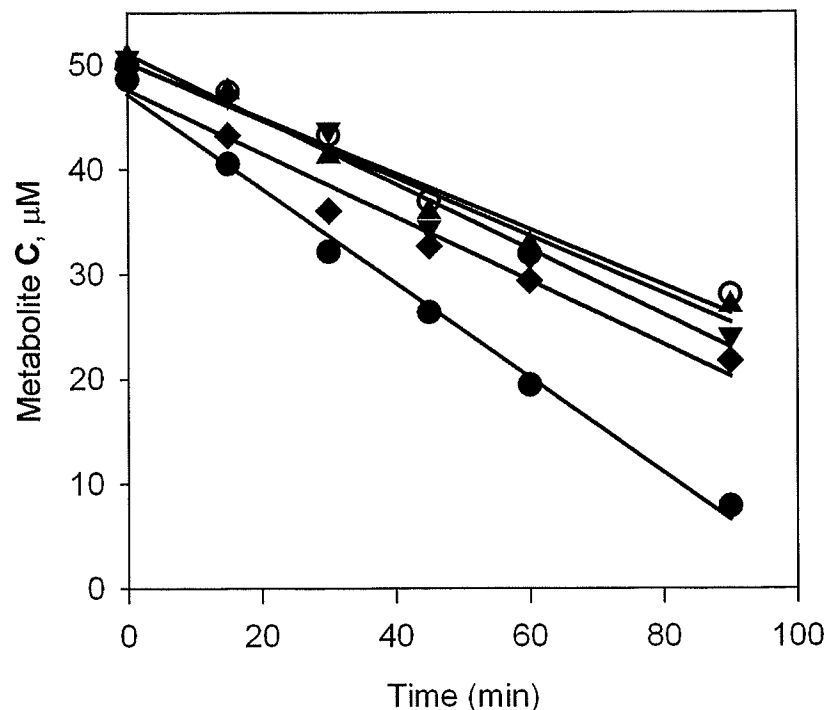
Figure 6.19 The effect of DHOase inhibitors on the loss of C in a myocyte suspension for study 1

Hydrolysis of 50 μM C in the presence of a myocyte suspension (2 x 10⁶ myocytes/ml); O, C in α-MEM alone; ●, C with myocytes; ▲, C with 1 mM of the DHOase inhibitor 5-aminoorotic acid; ▼, C with 1 mM of the DHPase inhibitor 4-chlorobenzene-sulfonamide and; ♦, furosemide. The loss of C was determined by HPLC as described in Section 6.2.10.
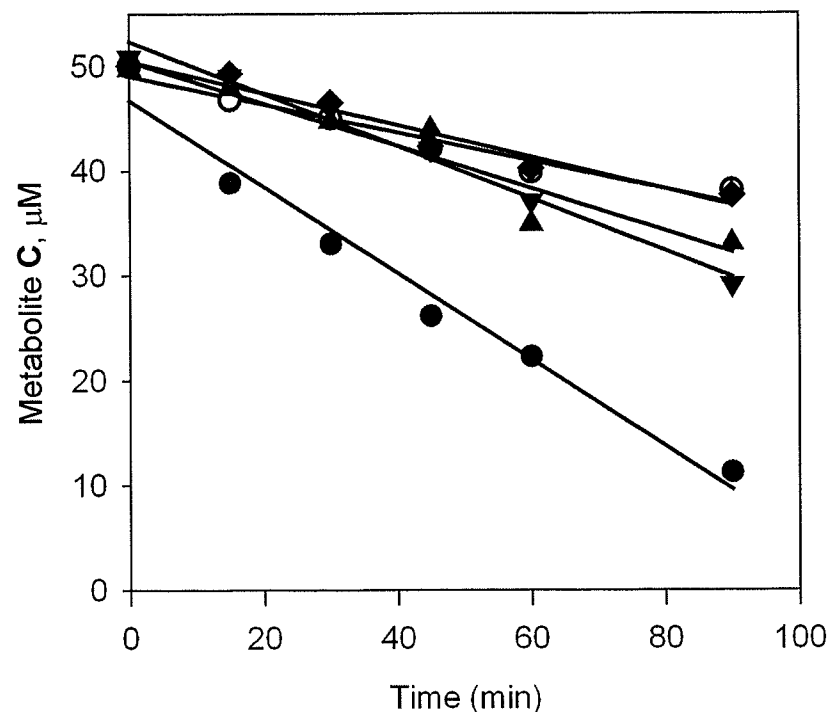
Figure 6.20 The effect of DHOase inhibitors on the loss of C in a myocyte suspension for study 2

Hydrolysis of 50 μM C in the presence of a myocyte suspension (2 x 10⁶ myocytes/ml); O, C in α-MEM alone; ●, C with myocytes; ▲, C with 1 mM of the DHOase inhibitor 5-aminoorotic acid; ▼, C with 1 mM of the DHPase inhibitor 4-chlorobenzene-sulfonamide and; ♦, furosemide. The loss of C was determined by HPLC as described in Section 6.2.10.

273

Figure 6.21 The effect of DHOase inhibitors on the loss of C in a myocyte suspension for study 3

Hydrolysis of 50 μM **C** in the presence of a myocyte suspension (2 x 10^6 myocytes/ml); O, **C** in α-MEM alone; ●, **C** with myocytes; ▲, **C** with 1 mM of the DHOase inhibitor 5-aminoorotic acid; ▼, **C** with 1 mM of the DHPase inhibitor 4-chlorobenzene-sulfonamide and; ♦, furosemide. The loss of **C** was determined by HPLC as described in Section 6.2.10.

Figure 6.22 The average effect of DHOase inhibitors on the loss of C in myocyte suspension studies 1-3

Hydrolysis of 50 μM **C** in the presence of the myocyte suspension (2 x 10^6 myocytes/ml); O, **C** in α-MEM alone; ●, **C** with myocytes; ▲, **C** with 1 mM of the DHOase inhibitor 5-aminoorotic acid; ▼, **C** with 1 mM of the DHPase inhibitor 4-chlorobenzene-sulfonamide and; ♦, furosemide. The loss of **C** was determined by HPLC as described in Section 6.2.10.

274

6.3.7 Dihydroorotate metabolism in neonatal rat myocyte suspensions

Dihydroorotate, the endogenous substrate of DHOase (Christopherson and Jones, 1980; Brown and Collins, 1991; Davidson et al., 1993), was incubated with neonatal rat myocytes to determine whether dihydroorotate is metabolized in a neonatal rat myocyte suspension. Dihydroorotate is very stable under physiological conditions and does not hydrolyze (Kelly et al., 1986), as confirmed by control experiments where dihydroorotate was incubated with α-MEM alone. However, in the presence of myocytes, there is a significant loss ($p < 0.001$) in concentration of dihydroorotate relative to the dihydroorotate control (shown in Table 6.17), as measured by their respective slopes. Also, in the presence of the dihydroorotase inhibitor 5-aminoorotic acid, there was 88 % inhibition of dihydroorotate hydrolysis, relative to the dihydroorotate control. 4-chlorobenzenesulfonamide and furosemide were also found to significantly inhibit dihydroorotate metabolism, with a percent inhibition of 62 and 41 %, respectively.

Table 6.17 The effect of DHOase inhibition of dihydroorotate hydrolysis in the presence of myocytes

Experiment	n	Rate of loss ($\mu M \cdot min^{-1}$)	$p^{\,a}$	% inhibition [b]
Dihydroorotate control	3	0	--	--
Myocyte control	3	0.201	$p < 0.001$	--
5-aminoorotic acid	3	0.024	$p > 0.1$	88.1
4-chlorobenzenesulfonamide	3	0.076	$p < 0.001$	62.2
Furosemide	3	0.118	$p < 0.001$	41.3

[a] The slopes (rate of loss) of the *dihydroorotate control* was compared to that of the rate of loss of dihydroorotate in the presence of myocytes or myocytes and inhibitors.
[b] % inhibition is relative to the background hydrolysis (dihydroorotate control) as detailed in Section 6.2.12.2.

Table 6.18 Dihydroorotate loss in α-MEM suspension buffer alone

| Time (min) | Experiment number | | | Average, μM | SE, ± μM |
| | 1 | 2 | 3 | | |
	dihydroorotate, μM	dihydroorotate, μM	dihydroorotate, μM		
0	51.4	50.4	49.6	50.5	0.54
15	49.5	49.2	50.5	49.8	0.34
30	49.1	49.7	48.6	49.2	0.34
45	49.3	49.8	48.6	49.2	0.37
60	49.6	49.3	49.6	49.5	0.11
90	50.3	50.5	48.5	49.7	0.63

Table 6.19 Dihydroorotate hydrolysis in the presence of myocytes (2×10^6 cells/ml) in α-MEM suspension buffer

| Time (min) | Experiment number | | | Average, μM | SE, ± μM |
| | 1 | 2 | 3 | | |
	dihydroorotate, μM	dihydroorotate, μM	dihydroorotate, μM		
0	51.4	50.2	49.4	50.3	0.59
15	48.7	47.6	45.8	47.4	0.85
30	46.3	45.6	41.4	44.4	1.56
45	42.7	42.2	37.9	40.9	1.55
60	39.3	39.6	35.0	37.9	1.52
90	35.8	30.3	31.4	32.5	1.71

Table 6.20 Dihydroorotate hydrolysis in myocytes (2×10^6 cells/ml) in the presence of 1 mM 5-aminoorotic acid in α-MEM suspension buffer

| Time (min) | Experiment number | | | Average, μM | SE, ± μM |
| | 1 | 2 | 3 | | |
	dihydroorotate, μM	dihydroorotate, μM	dihydroorotate, μM		
0	51.1	49.6	50.2	50.3	0.45
15	51.6	50.7	49.2	50.5	0.71
30	50.9	48.7	49.9	49.8	0.66
45	50.0	48.0	48.5	48.8	0.60
60	50.7	47.3	48.2	48.7	1.04
90	49.8	47.1	48.8	48.5	0.80

Table 6.21   Dihydroorotate hydrolysis in myocytes (2×10^6 cells/ml) in the presence of 1 mM 4-chlorobenzenesufonamide in α-MEM suspension buffer

Time (min)	Experiment number		Average, μM	Average deviation, ± μM
	1	2		
	dihydroorotate, μM	dihydroorotate, μM		
0	49.1	50.2	49.6	0.75
15	48.3	49.6	48.9	0.86
30	47.6	48.6	48.1	0.65
45	46.2	48.1	47.1	1.34
60	44.8	46.6	45.7	1.27
90	42.1	43.6	42.8	1.05

Table 6.22   Dihydroorotate hydrolysis in myocytes (2×10^6 cells/ml) in the presence of 1 mM furosemide in α-MEM suspension buffer

Time (min)	Experiment number		Average, μM	Average deviation, ± μM
	1	2		
	dihydroorotate, μM	dihydroorotate, μM		
0	49.3	49.6	49.4	0.21
15	46.1	46.6	46.3	0.34
30	44.1	43.6	43.8	0.34
45	42.7	41.9	42.3	0.58
60	40.1	41.7	40.9	1.13
90	36.5	40.6	38.6	2.88
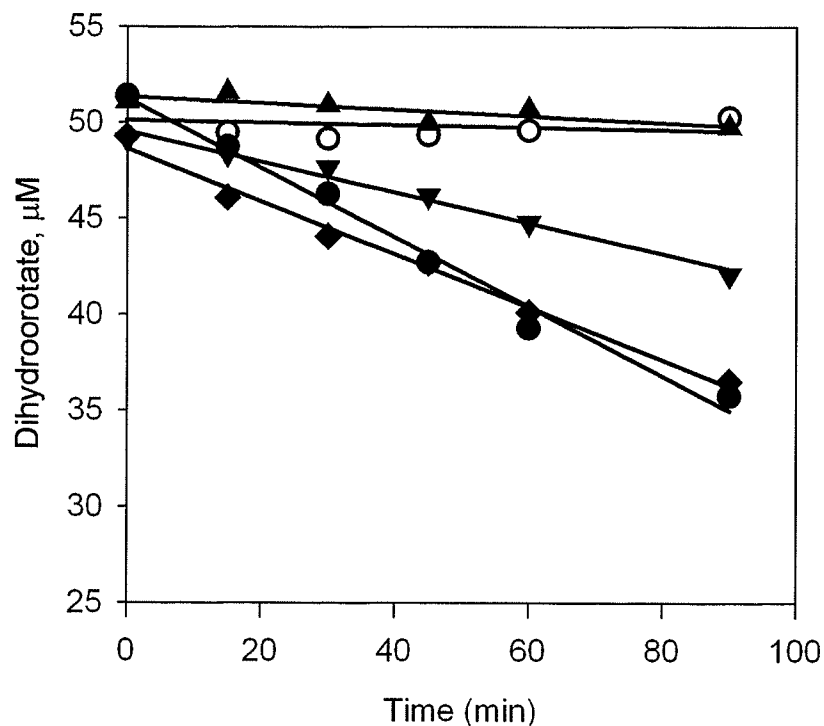
Figure 6.23. The effect of DHOase inhibitors on dihydroorotate loss in a myocyte suspension, experiment 1

Hydrolysis of 50 μM dihydroorotate in the presence of a myocyte suspension (2 x 10^6 myocytes/ml); O, dihydroorotate in α-MEM alone; ●, dihydroorotate in the presence of myocytes; ▲, dihydroorotate with 1 mM of the DHOase inhibitor 5-aminoorotic acid; ▼, dihydroorotate with 1 mM of the DHPase inhibitor 4-chlorobenzene-sulfonamide and; ◆, furosemide. The loss of dihydroorotate was determined by HPLC as described in Section 6.2.10.
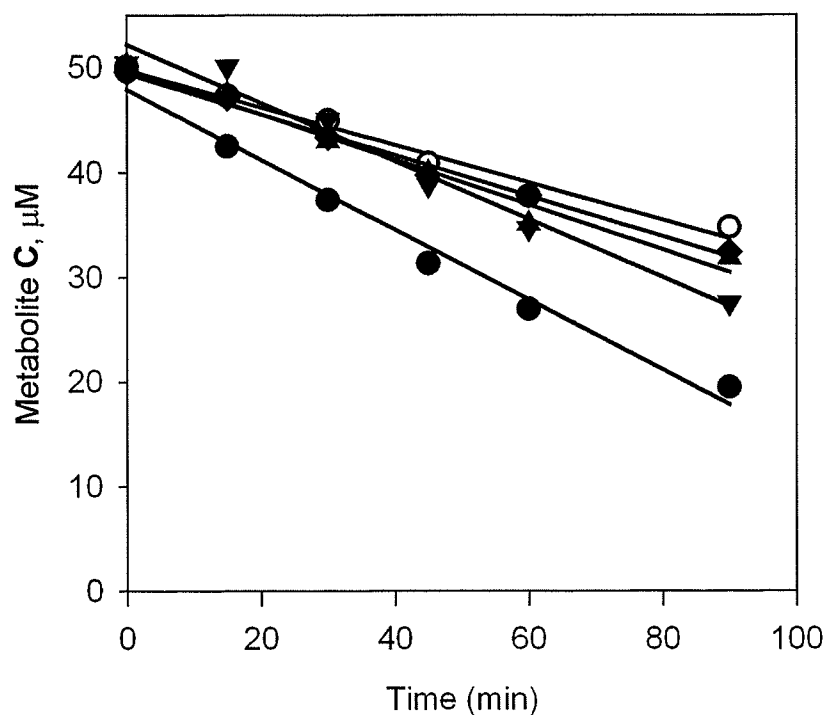
Figure 6.24 The effect of DHOase inhibitors on dihydroorotate loss in a myocyte suspension, experiment 2

Hydrolysis of 50 μM dihydroorotate in the presence of a myocyte suspension (2 x 10^6 myocytes/ml); O, dihydroorotate in α-MEM alone; ●, dihydroorotate in the presence of myocytes; ▲, dihydroorotate with 1 mM of the DHOase inhibitor 5-aminoorotic acid; ▼, dihydroorotate with 1 mM of the DHPase inhibitor 4-chlorobenzene-sulfonamide and; ◆, furosemide. The loss of dihydroorotate was determined by HPLC as described in Section 6.2.10.
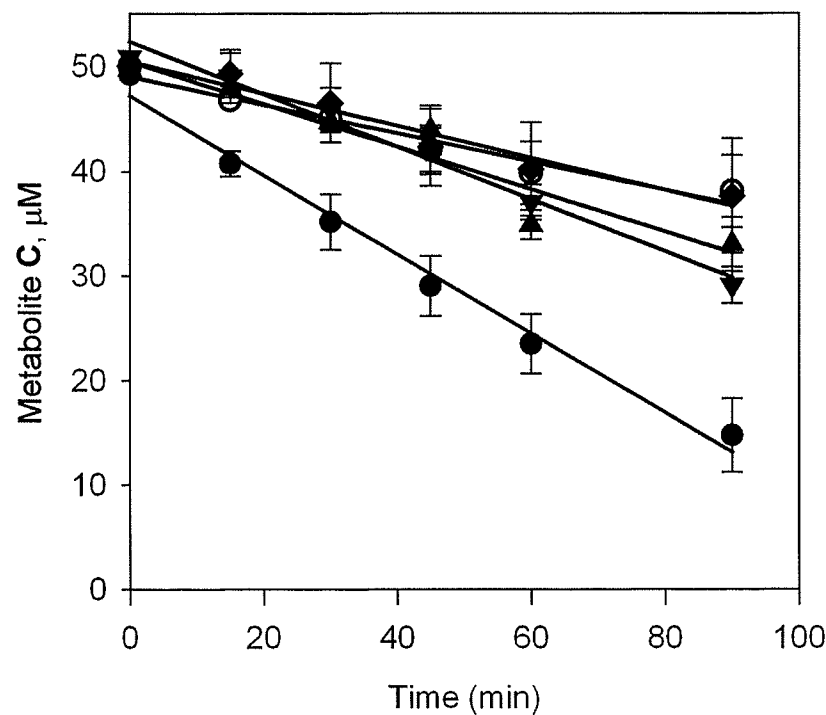
Figure 6.25 The effect of DHOase inhibitors on dihydroorotate loss in a myocyte suspension, experiment 3
Hydrolysis of 50 μM dihydroorotate in the presence of a myocyte suspension (2 x 10^6 myocytes/ml); O, dihydroorotate in α-MEM alone; ●, dihydroorotate in the presence of myocytes; ▲, dihydroorotate with 1 mM of the DHOase inhibitor 5-aminoorotic acid. The loss of dihydroorotate was determined by HPLC as described in Section 6.2.10.
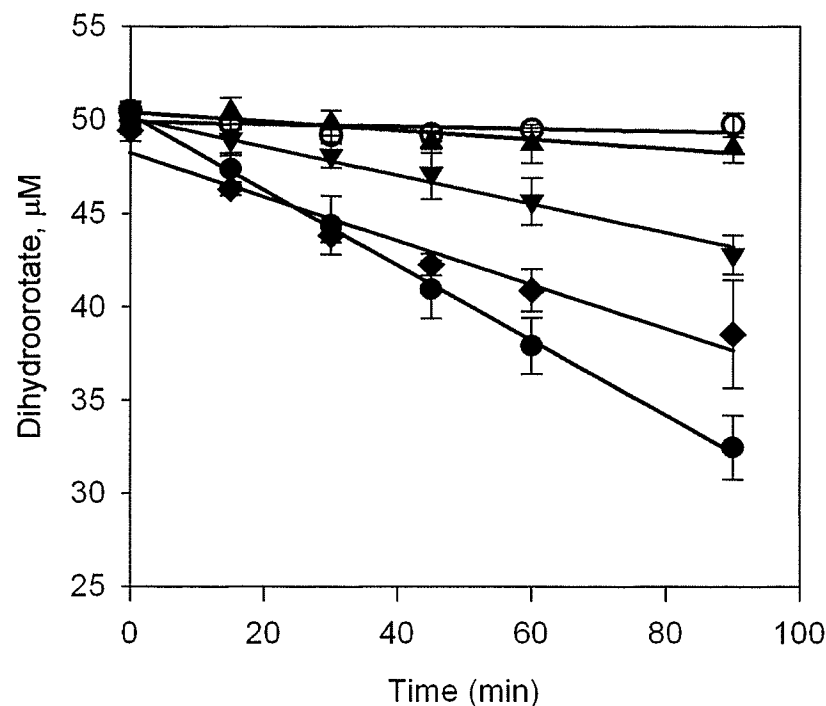
Figure 6.26 The average effect of DHOase inhibition on dihydroorotate loss in myocyte suspension experiments 1-3
Hydrolysis of 50 μM dihydroorotate in the presence of a myocyte suspension (2 x 10^6 myocytes/ml); O, dihydroorotate in α-MEM alone; ●, dihydroorotate in the presence of myocytes; ▲, dihydroorotate with 1 mM of the DHOase inhibitor 5-aminoorotic acid; ▼, dihydroorotate with 1 mM of the DHPase inhibitor 4-chlorobenzene-sulfonamide and; ◆, furosemide.

6.3.8 The effect of DHOase inhibition on the metabolism of C in a suspension of primary adult rat hepatocytes

The hydrolysis of C in the presence of hepatocytes was found to be significantly greater than the hydrolysis of C in α-MEM alone, as shown in Figure 6.30. The rate of loss of C in the presence of hepatocytes was found to be 3 fold greater ($p < 0.001$) then the hydrolysis of C in α-MEM alone, as measured by their respective slopes. As in the case with suspension neonatal rat myocytes, the DHOase inhibitor 5-aminoorotic acid (Krungkrai et al., 1992) was found to be a strong inhibitor of C hydrolysis in hepatocytes and decreased the rate of hydrolysis by 68 % (shown in Table 6.23). 4-chlorobenzesulfonamide, was also found to inhibit the hydrolysis of C by 52 %. Neither 5-aminoorotic acid nor 4-chlorobenzenesulfonamide inhibited the loss of C completely, as shown in Table 6.23. As in the case with neonatal rat myocytes, 4-chlorobenzenesulfonamide was the weakest inhibitor.

Table 6.23   The effect of DHOase inhibition on C hydrolysis in an adult rat hepatocyte suspension (2×10^6 cells/ml).

Experiment	n	Rate of loss ($\mu M \cdot min^{-1}$)	p [a]	% inhibition [b]
C buffer control	3	0.217	--	--
hepatocyte control	3	0.525	$p < 0.001$	--
5-aminoorotic acid	3	0.315	$p > 0.2$	68.2
4-chlorobenzenesulfonamide	2	0.364	$p > 0.2$	52.3

[a] The slopes (rate of loss) of the C buffer control (α-MEM) was compared to that of the rate of loss of C in the presence of hepatocyte or hepatocyte and inhibitors.
[b] % inhibition is relative to the background hydrolysis (C Buffer Control) as detailed in Section 6.2.12.2.

280

Table 6.24 Metabolite **C** hydrolysis in the presence of α-MEM alone dosed with 50 μM **C**.

Time (min)	Experiment number			Average, μM	SE, ± μM
	1	2	3		
	C, μM	**C,** μM	**C,** μM		
0	51.5	50.0	50.0	50.5	0.51
15	48.0	47.4	48.4	48.3	0.12
30	45.6	42.7	41.7	43.7	0.98
60	40.6	38.3	38.5	39.1	0.73
90	37.3	32.1	34.3	34.5	1.51

Table 6.25 Metabolite **C** hydrolysis in the presence of hepatocytes (2×10^6 cells/ml) dosed with 50 μM **C**.

Time (min)	Experiment number			Average, μM	SE, ± μM
	1	2	3		
	C, μM	**C,** μM	**C,** μM		
0	51.5	49.2	49.1	50.0	0.78
15	40.3	38.9	33.8	37.7	1.98
30	33.9	27.6	25.6	29.0	2.53
45	25.1	18.3	14.3	19.2	3.19
60	12.7	11.7	7.7	10.7	1.57
90	7.9	2.1	<LOD	3.3	

Table 6.26 Metabolite **C** hydrolysis in hepatocytes (2×10^6 cells/ml) in the presence of 1 mM 5-aminoorotic acid dosed with 50 μM **C**.

Time (min)	Experiment number			Average, μM	SE, ± μM
	1	2	3		
	C, μM	**C,** μM	**C,** μM		
0	51.5	50.0	50.0	50.5	0.51
15	47.1	40.6	46.6	44.8	2.12
30	42.3	35.3	41.3	39.6	2.23
45	37.4	27.2	35.3	33.3	3.18
60	33.0	19.1	29.6	27.3	4.26
90	28.7	15.0	26.7	23.4	4.34

281

Table 6.27 Metabolite **C** hydrolysis in hepatocytes (2×10^6 cells/ml) in the presence of 1 mM 4-chlorobenzenesufonamide dosed with 50 µM **C**.

Time (min)	Experiment number			Average, µM	SE, ± µM
	1	2	3		
	C, µM	**C**, µM	**C**, µM		
0	51.5	50.4	50.4	50.8	0.36
15	47.1	41.8	39.8	42.9	2.23
30	43.6	39.6	29.6	37.6	4.25
45	40.3	24.2	25.6	30.0	5.24
60	38.7	19.2	20.7	26.2	6.39
90	30.4	7.6	15.6	17.8	6.82
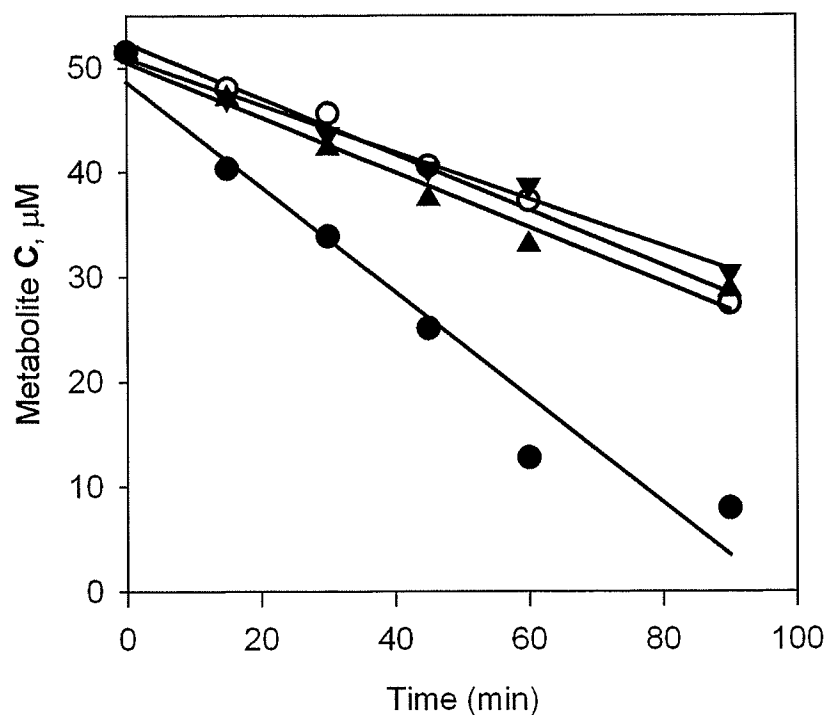
Figure 6.27 The effect of DHOase inhibition on the loss of C in the hepatocyte suspension of study 1

Hydrolysis of 50 μM **C** in the presence of the hepatocyte suspension (2 x 10⁶ hepatocytes/ml); O, **C** in α-MEM alone; ●, **C** with hepatocytes; ▲, **C** with 1 mM of the DHOase inhibitor 5-aminoorotic acid; ▼, **C** with 1 mM of the DHPase inhibitor 4-chlorobenzene-sulfonamide. The loss of **C** was determined by HPLC as described in Section 6.2.10.
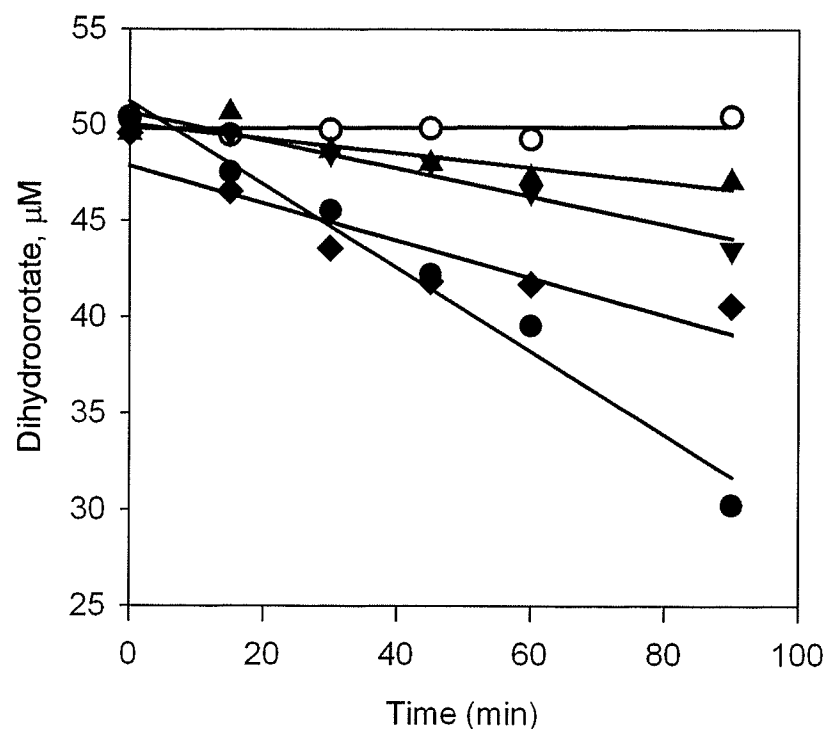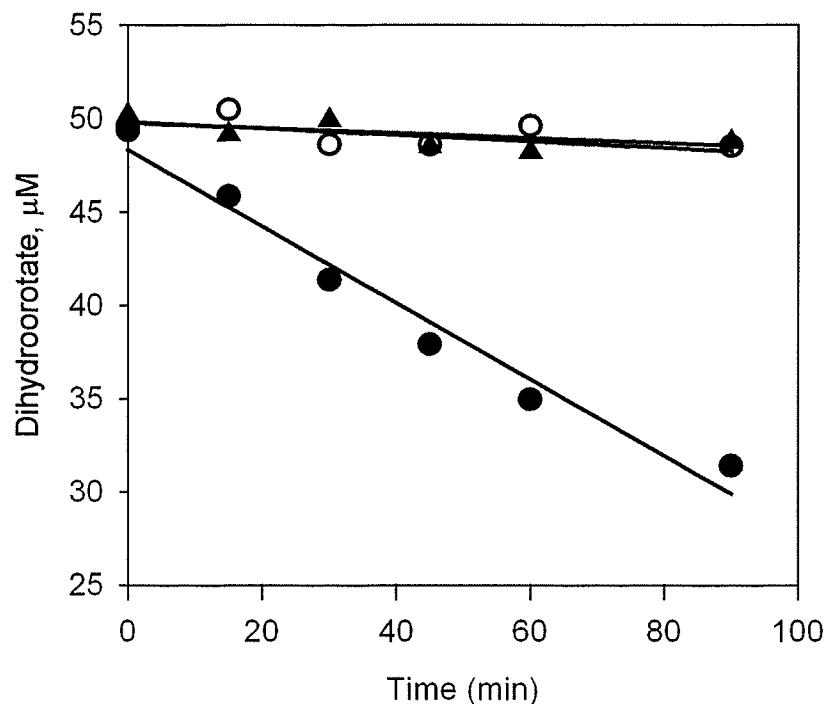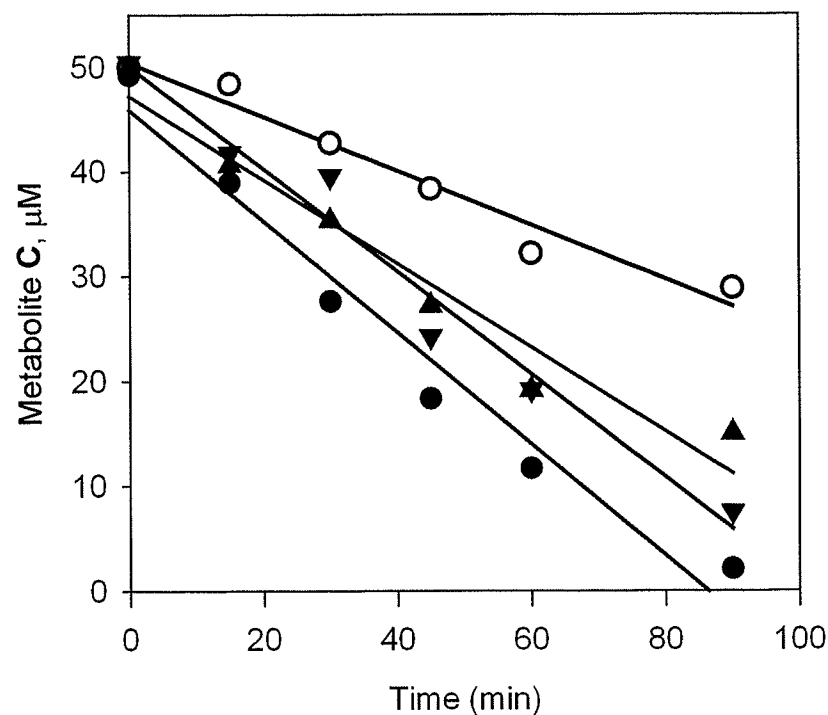
Figure 6.28 The effect of DHOase inhibition of the loss on C in the hepatocyte suspension of study 2

Hydrolysis of 50 μM **C** in the presence of the hepatocyte suspension (2 x 10⁶ hepatocytes/ml); O, **C** in α-MEM alone; ●, **C** with hepatocytes; ▲, **C** with 1 mM of the DHOase inhibitor 5-aminoorotic acid; ▼, **C** with 1 mM of the DHPase inhibitor 4-chlorobenzene-sulfonamide. The loss of **C** was determined by HPLC as described in Section 6.2.10.

283
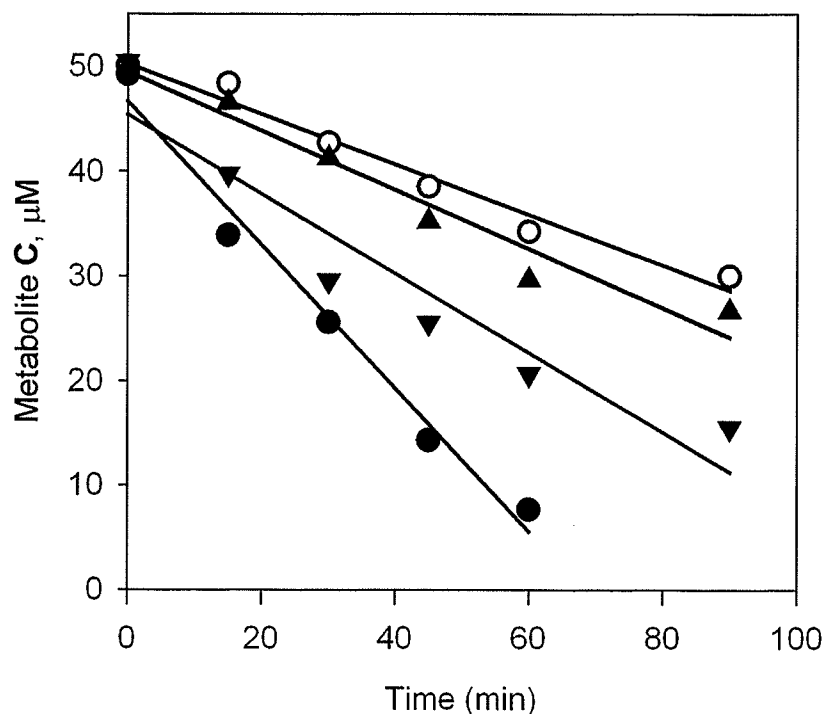
Figure 6.29 The effect of DHOase inhibition on the loss of C in the hepatocyte suspension of study 3
Hydrolysis of 50 µM **C** in the presence of the hepatocyte suspension (2 x 10^6 hepatocytes/ml); O, **C** in α-MEM alone; ●, **C** with hepatocytes; ▲, **C** with 1 mM of the DHOase inhibitor 5-aminoorotic acid; ▼, **C** with 1 mM of the DHPase inhibitor 4-chlorobenzene-sulfonamide. The loss of **C** was determined by HPLC as described in Section 6.2.10.
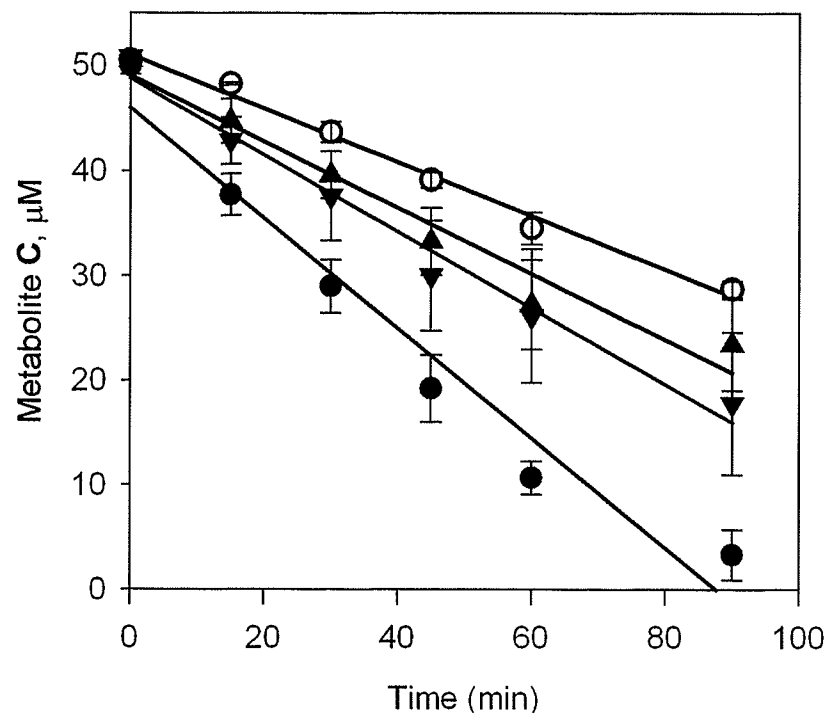
Figure 6.30 The average effect of DHOase inhibition on the loss of C in a hepatocyte suspension for studies 1-3
Hydrolysis of 50 µM **C** in the presence of the hepatocyte suspension (2 x 10^6 hepatocytes/ml); O, **C** in α-MEM alone; ●, **C** with hepatocytes; ▲, **C** with 1 mM of the DHOase inhibitor 5-aminoorotic acid; ▼, **C** with 1 mM of the DHPase inhibitor 4-chlorobenzene-sulfonamide. The loss of **C** was determined by HPLC as described in Section 6.2.10.

284

6.3.9 Incubation of dexrazoxane, C, and dihydroorotate in rat and human blood/ and plasma

Experiments were also done to determine if either whole blood or blood plasma could promote the hydrolysis of dexrazoxane, dihydroorotate, or C. As shown in Figure 6.31-6.32 neither plasma nor whole blood of either humans or rats significantly promoted the hydrolysis of dexrazoxane over 4 h compared to Tris/artificial plasma buffer controls (as prepared in Section 6.2.6), a result consistent with previously published results (Hasinoff and Aoyama, 1999a). It was found that in the presence of the blood and plasma of both the human and rat, as shown in Figure 6.35-6.36, the hydrolysis of C was significantly greater then in Tris/Saline buffer (Section 6.2.6) by nearly 4-fold ($p < 0.001$). Also, for both the rat and human, there was no significant difference ($p > 0.5$) in the hydrolysis rate of C in whole blood or plasma. DHOase is found in the blood (Fairbanks et al., 1995). Thus, it was decided to determine whether either rat or human blood could hydrolyze the endogenous substrate of DHOase, dihydroorotate, at a fast enough rate to explain the hydrolysis of C. Dihydroorotate, as shown in Figures 6.33-34, was not significantly hydrolyzed in either human ($p > 0.5$) or rat blood ($p > 0.5$) (as shown in Table 6.30).

Table 6.28 Dexrazoxane hydrolysis in human blood and plasma under physiological conditions.

Time (min)	Dexrazoxane loss in Tris/saline buffer		Dexrazoxane loss in whole human blood buffered in 100 mM Tris/Saline		Dexrazoxane loss in human plasma buffered in 100 mM Tris/Saline	
	Average (µM)	Average deviation, ± µM	Average (µM)	Average deviation, ± µM	Average (µM)	Average deviation, ± µM)
0	207	12.4	207	3.0	201	6.7
15	203	10.5	206	3.6	197	5.5
30	202	13.3	203	4.3	195	9.7
45	200	13.1	197	4.2	195	6.1
60	198	14.5	193	4.3	194	6.7
90	194	11.4	188	3.0	188	5.8
120	187	15.4	183	2.9	183	7.7
180	171	14.4	178	3.9	167	5.9
240	166	16.4	164	6.7	161	8.6

Table 6.29 Dexrazoxane hydrolysis in rat blood and plasma under physiological conditions.

Time (min)	Dexrazoxane loss in Tris/saline		Dexrazoxane loss in rat plasma buffered in 100 mM Tris/saline		Dexrazoxane loss in rat blood buffered in 100 mM Tris/saline	
	Average (µM)	Average deviation, ± µM	Average (µM)	Average deviation, ± µM	Average (µM)	Average deviation, ± µM
0	201	3.39	199	9.06	201	4.95
60	194	2.48	190	4.91	192	4.95
120	183	2.29	180	6.58	186	1.41
180	176	7.99	172	2.39	174	4.24
240	171	12.26	167	0.73	163	0.71

Table 6.30 Comparisons of dexrazoxane loss in the presence of plasma and blood of the rat and human

Human	n	Rate of loss ($\mu M \cdot min^{-1}$)	p^{a}
Physiological buffer control	2	0.180	--
Human plasma	2	0.170	$p > 0.5$
Human blood	2	0.174	$p > 0.5$
Rat	n	Rate of loss ($\mu M \cdot min^{-1}$)	p^{a}
Physiological buffer control	2	0.134	--
Rat plasma	2	0.156	$p > 0.2$
Rat blood	2	0.142	$p > 0.5$

[a] The slopes (rate of loss) of the *physiological buffer control* was compared to that of the rate of loss of dexrazoxane in the presence of blood or plasma.

Table 6.31 Dihydroorotate hydrolysis in human blood and plasma under physiological conditions.

Time (min)	Plasma		Blood	
	Human (μM)	Rat (μM)	Human (μM)	Rat (μM)
0	210	206	202	209
15	213	211	201	205
30	208	207	198	202
45	213	208	201	200
60	206	204	202	204
90	208	204	199	209
120	210	206	202	209
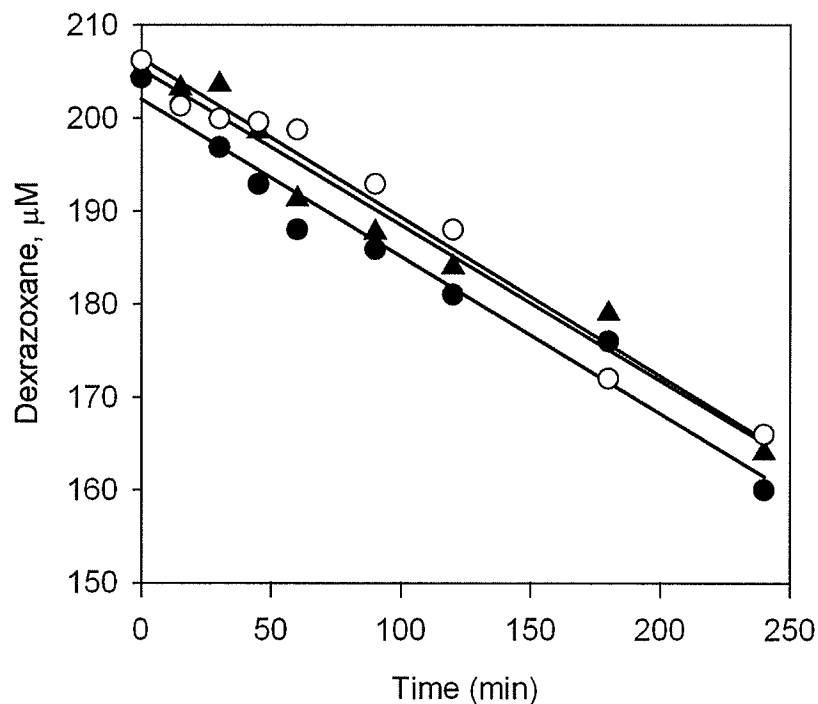
Figure 6.31 Hydrolysis of dexrazoxane in human plasma and blood under physiological conditions

Hydrolysis of 200 μM dexrazoxane in the presence of human blood and blood plasma (buffered with 100 mM Tris to a pH 7.4 at 37 °C); O, dexrazoxane hydrolysis in the presence of physiological buffer (100 mM Tris, pH 7.4 at 37 °C) alone; ●, dexrazoxane hydrolysis in the presence of human blood; ▲, dexrazoxane hydrolysis in human blood plasma. No significant ($p > 0.5$) hydrolysis was found in human blood or plasma relative to the control. The loss of dexrazoxane was determined by HPLC as described in Section 6.2.10.
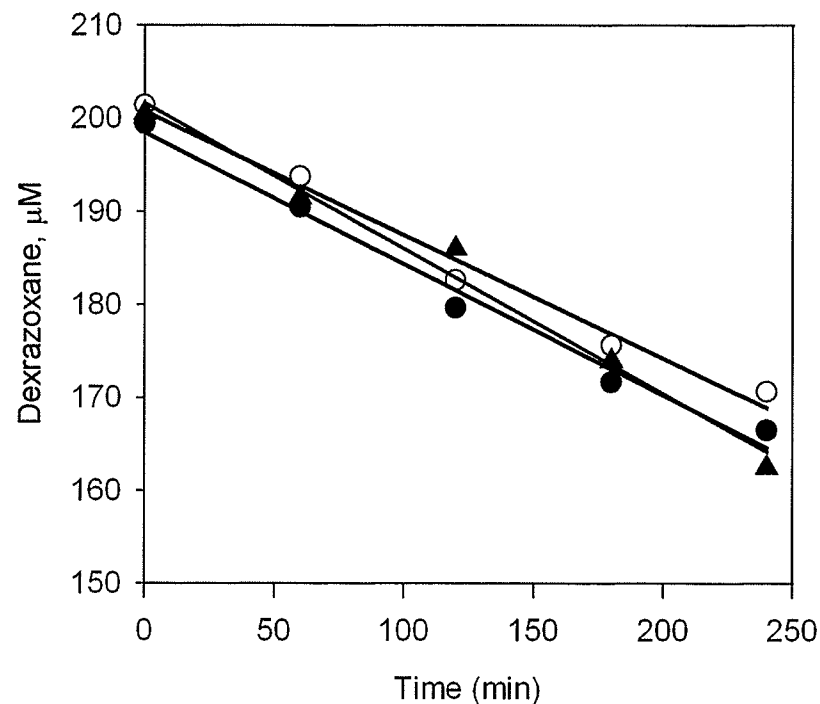
Figure 6.32 Hydrolysis of dexrazoxane in rat plasma and blood under physiological conditions

Hydrolysis of 200 μM dexrazoxane in the presence of rat blood and blood plasma (buffered with 100 mM Tris to a pH 7.4 at 37 °C); O, dexrazoxane hydrolysis in the presence of physiological buffer (100 mM Tris, pH 7.4 at 37 °C) alone; ●, dexrazoxane hydrolysis in the presence of rat blood; ▲, dexrazoxane hydrolysis in rat blood plasma. No significant ($p > 0.5$) hydrolysis was found in rat blood or plasma relative to the control. The loss of dexrazoxane was determined by HPLC as described in Section 6.2.10.

288
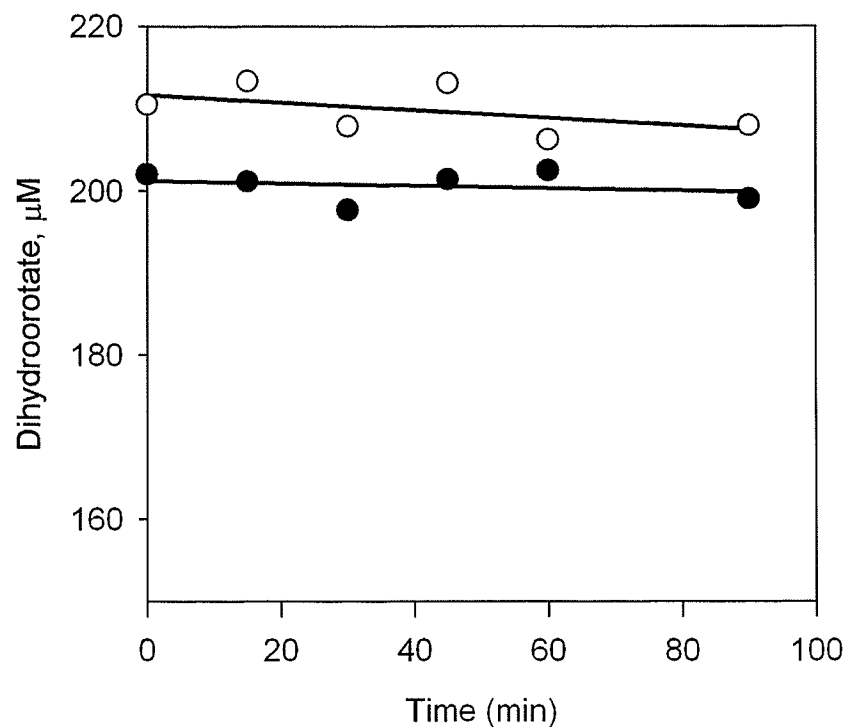
Figure 6.33 Dihydroorotate stability in human plasma and blood under physiological conditions
200 µM dihydroorotate in the presence of human blood and blood plasma (buffered with 100 mM Tris to a pH 7.4 at 37 °C); O, dihydroorotate in the presence of human blood; ●, dihydroorotate hydrolysis in the presence of human plasma.
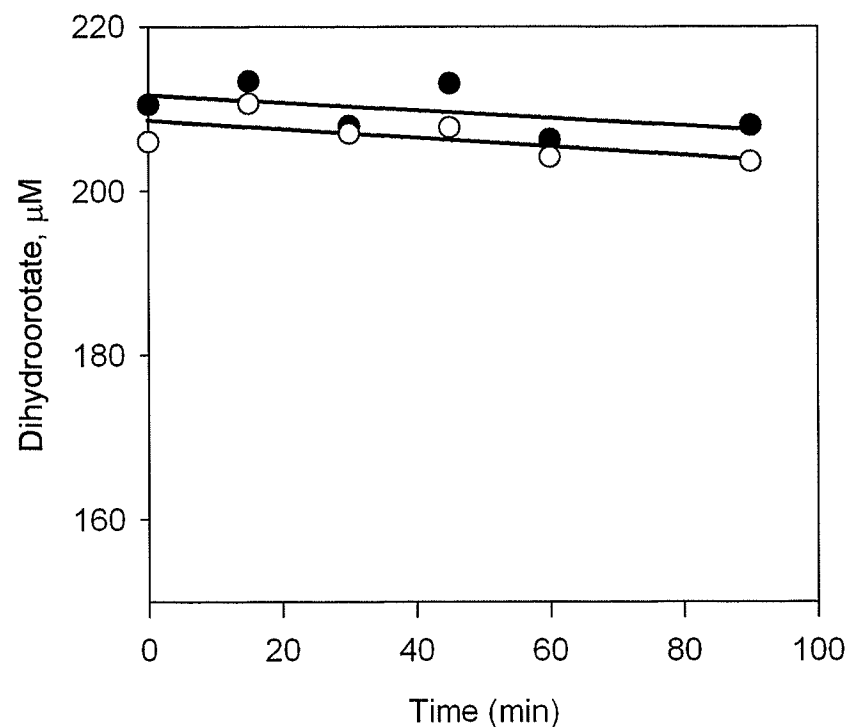
Figure 6.34 Dihydroorotate stability in rat plasma and blood under physiological conditions
200 µM dihydroorotate in the presence of rat blood and blood plasma (buffered with 100 mM Tris to a pH 7.4 at 37 °C); O, dihydroorotate in the presence of rat blood; ●, dihydroorotate hydrolysis in the presence of rat plasma.

289

Table 6.32 Metabolite **C** hydrolysis in rat blood and plasma under physiological conditions

Time (min)	**C** loss in 100 mM Tris/saline		**C** loss in rat plasma buffered in 100 mM Tris/saline		**C** loss in rat blood buffered in 100 mM Tris/saline	
	Average (μM)	SE ($\pm$ μM)	Average (μM)	SE ($\pm$ μM)	Average (μM)	Average deviation ($\pm$ μM)
0	204	1.30	198	3.20	202	2.42
15	197	1.12	152	10.64	169	9.80
30	190	2.52	116	12.22	134	0.50
45	183	3.51	83	14.35	106	2.99
60	179	5.98	54	13.79	77.1	6.20
90	168	4.79	21	7.08	33.5	3.54

Table 6.33 Metabolite **C** hydrolysis in human blood and plasma under physiological conditions.

Time (min)	**C** loss in 100 mM Tris/saline		**C** loss in human plasma buffered in 100 mM Tris/saline		**C** loss in human blood buffered in 100 mM Tris/saline	
	Average (μM)	Average deviation ($\pm$ μM)	Average (μM)	Average deviation, ($\pm$ μM)	Average (μM)	Average deviation, ($\pm$ μM)
0	197	1.3	194	3.0	198	2.6
15	186	0.4	123	0.5	135	8.9
30	175	2.4	94	0.2	103	1.3
45	162	4.0	76	1.6	84	2.1
60	155	1.3	49	0.9	55	5.3
90	151	1.2	20	0.7	23	1.2

Table 6.34 Comparisons of **C** loss in the presence of plasma and blood of the rat and human

Human	n^b	Rate of loss ($\mu M \cdot min^{-1}$)	$p^{\,a}$
Tris/saline buffer	2	0.537	--
Human plasma	2	1.79	$p < 0.002$
Human blood	2	1.84	$p < 0.002$
Rat	n^b	**Rate of loss** ($\mu M \cdot min^{-1}$)	$p^{\,a}$
Tris buffer	3	0.394	--
Rat plasma	3	1.96	$p < 0.001$
Rat blood	3	1.89	$p < 0.001$

[a] The slopes (rate of loss) of the Tris/saline buffer was compared to that of the rate of loss of **C** in the presence of plasma or blood.

[b] n, blood drawn on separate dates
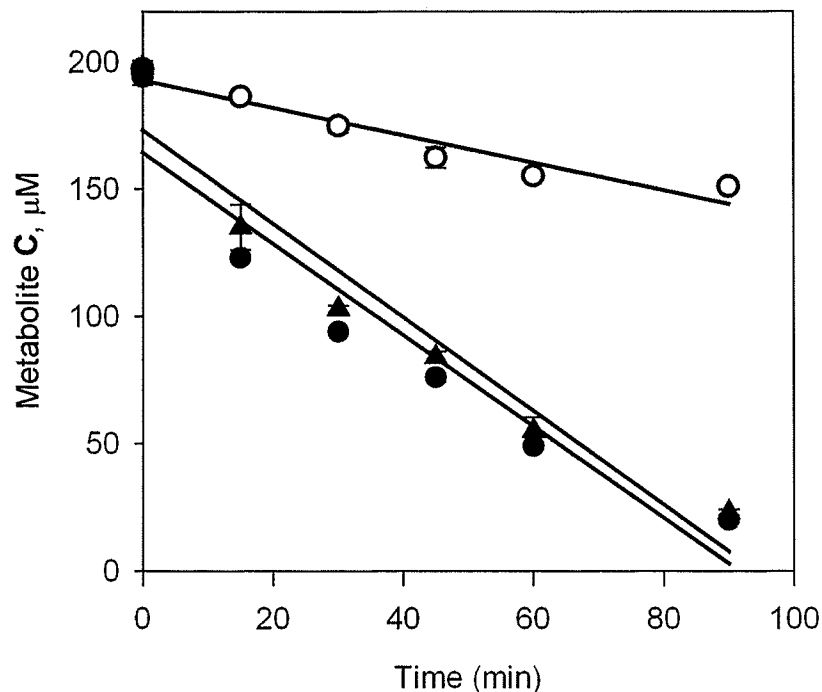
Figure 6.35 Hydrolysis of C in human blood and plasma under physiological conditions

Hydrolysis of 200 μM **C** in the presence of human blood and plasma (pH 7.4 at 37 °C); O, **C** hydrolysis in the presence of 100 mM Tris in saline (0.9 % NaCl, w/v) alone; ●, **C** hydrolysis in the presence of human plasma (buffered with 100 mM Tris in saline (0.9 % NaCl, w/v); ▲, **C** hydrolysis in the presence of human blood (buffered with 100 mM Tris in saline (0.9 % NaCl, w/v).
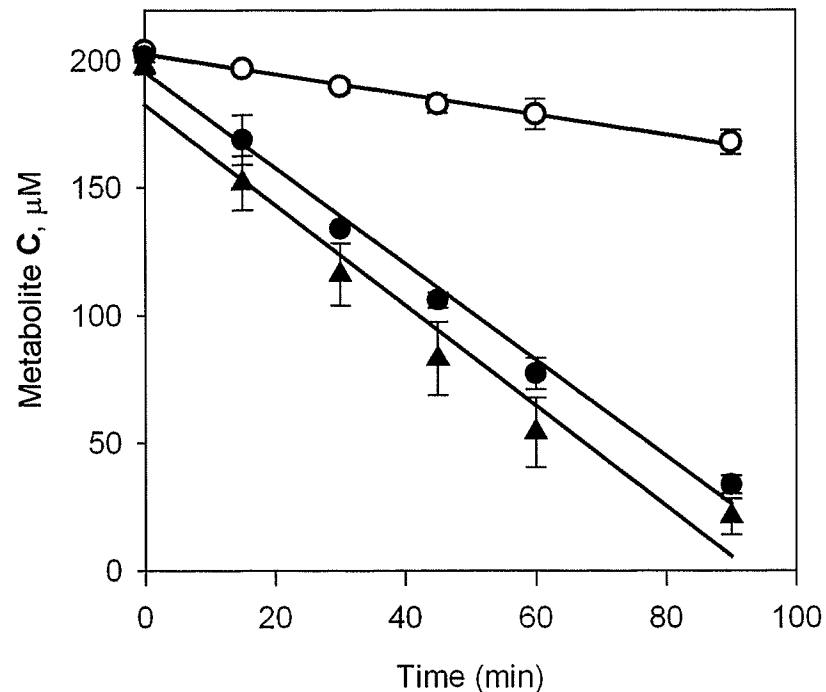
Figure 6.36 Hydrolysis of C in rat blood and plasma under physiological conditions

Hydrolysis of 200 μM **C** in the presence of rat blood and plasma (pH 7.4 at 37 °C); O, **C** hydrolysis in the presence of 100 mM Tris in saline (0.9 % NaCl, w/v) alone; ●, **C** hydrolysis in the presence of rat plasma (buffered with 100 mM Tris in saline (0.9 % NaCl, w/v); ▲, **C** hydrolysis in the presence of rat blood (buffered with 100 mM Tris in saline (0.9 % NaCl, w/v).

6.3.10 The effect of metal ion chelation by DTPA on C hydrolysis in rat plasma

Experiments were done to determine whether the hydrolysis of C in plasma and blood were enzymatically mediated or metal ion mediated. The hydrolysis of C in the presence of Tris buffered artificial plasma (prepared as described in Section 6.2.6) shown in Figure 6.38 was significantly ($p < 0.001$) greater then the background hydrolysis of C in 100 mM Tris saline (0.9 % NaCl, w/v) pH of 7.4 at 37 °C, as measured by their respective slopes. In plasma, a 30 min pre-incubation with the metal ion chelator DTPA (5 mM), decreased the hydrolysis rate of C by 97 % as shown in Table 6.37. Also, as noted in Table 6.37, there was no significant difference ($p > 0.5$) between the hydrolysis of C in plasma with 5 mM DTPA to that of physiological buffer suggesting that metal ions contribute greatly to C hydrolysis in blood and plasma. In the case where artificial plasma (prepared as described in Section 6.2.6) was incubated with 5 mM DTPA, there was also no significant difference ($p > 0.5$) between the hydrolysis of C Tris saline (0.9 % NaCl, w/v) and that of artificial plasma containing 5 mM DTPA. Also, there was no significant difference between the hydrolysis of C in the presence of 5 mM DTPA in either rat plasma or artificial plasma.

Table 6.35 **C** hydrolysis in rat plasma under physiological conditions in the presence of metal ion chelator DTPA

Time (min)	C loss in rat plasma buffered in 100 mM Tris/saline		C loss 100 mM Tris/saline		C loss in rat plasma with 100 μM DTPA buffered in 100 mM Tris/saline		C loss in rat plasma with 5 mM DTPA buffered in 100 mM Tris/saline	
	Average (μM)	Average deviation (±μM)	Average (μM)	Average deviation (±μM)	Average (μM)	Average deviation (±μM)	Average (μM)	Average deviation (±μM)
0	201	3.86	203	2.12	206	5.66	199	0.94
15	173	4.31	198	0.71	176	7.07	197	17.5
30	140	8.05	191	1.41	169	4.95	188	17.7
45	102	9.14	184	0.71	149	2.12	181	21.1
60	76	7.90	179	2.12	118	2.83	170	14.4
90	27	11.4	171	1.41	59	9.90	157	4.24

Table 6.36 **C** hydrolysis in artificial plasma under physiological conditions in the presence of metal ion chelator DTPA

Time (min)	C loss in artificial plasma buffered in 100 mM Tris/saline		C loss in artificial plasma with 5 mM DTPA buffered in 100 mM Tris/saline	
	Average (μM)	Average deviation (± μM)	Average (μM)	Average deviation (± μM)
0	203	6.43	206	0.30
15	180	10.03	201	0.80
30	168	10.88	195	1.08
45	157	11.29	192	1.17
60	146	7.35	186	5.02
90	123	4.24	183	2.96

Table 6.37 Comparisons of C loss in the presence of plasma and blood of the rat and human

Rat Plasma	n	Rate of loss ($\mu M \cdot min^{-1}$)	$p^{\,a}$	% inhibition
Tris/saline buffer	2	0.36	--	--
Plasma control	2	1.98	$p < 0.001$	--
Plasma with 100 μM DTPA	2	1.58	$p < 0.001$	27
Plasma with 5 mM DTPA	2	0.50	$p > 0.2$	97
Artificial plasma	n	Rate of loss ($\mu M \cdot min^{-1}$)	$p^{\,a}$	% inhibition
Artificial plasma control	2	0.85	--	--
Artificial plasma with 5 mM DTPA	2	0.26	$p < 0.001$	--

[a] The slopes (rate of loss) of the Tris/saline buffer was compared to that of the rate of loss of C in the presence of blood or plasma.

[b] % inhibition is relative to the background hydrolysis (physiological buffer) as detailed in Section 6.2.12.2.
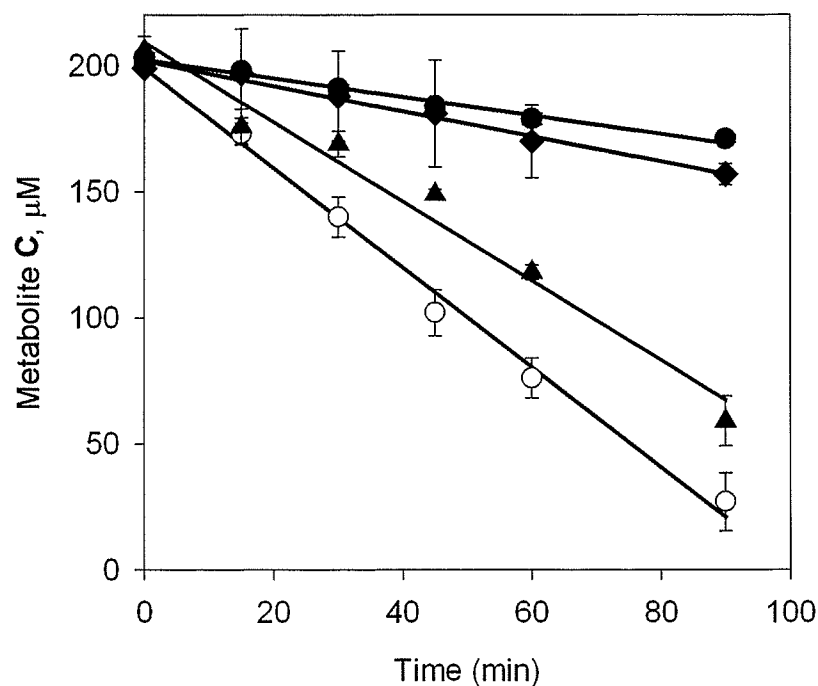
Figure 6.37 The effect of the metal ion chelator DTPA on the loss of C in rat plasma

Hydrolysis of 200 μM **C** in rat plasma (buffered with 100 mM Tris at 37 °C) in the presence of DTPA; ○, **C** hydrolysis in the presence of rat plasma alone; ●, **C** hydrolysis in physiological buffer; ▲, **C** hydrolysis in the presence of plasma and 100 μM DTPA; ♦, **C** hydrolysis in the presence of plasma and 5 mM DTPA. The loss of **C** was determined by HPLC as described in Section 6.2.10.
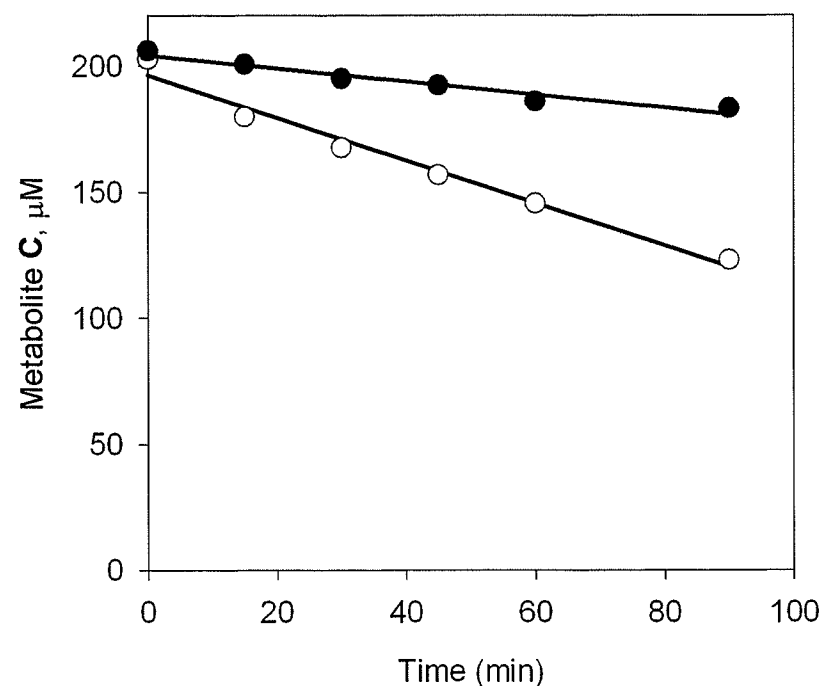
Figure 6.38 The effect of the metal ion chelator DTPA on the loss of C in artificial plasma

Hydrolysis of 200 μM **C** in rat plasma (buffered with 100 mM Tris at 37 °C) in the presence of DTPA and artificial plasma (as prepared in Section 6.2.6); ○, **C** hydrolysis in artificial plasma alone; ●, **C** hydrolysis in artificial plasma and 5 mM DTPA. The loss of **C** was determined by HPLC as described in Section 6.2.10

6.3.11 Hydrolysis of dexrazoxane and C by human serum albumin (HSA)

Experiments were done to determine whether the hydrolysis of dexrazoxane and C could be mediated by human serum albumin (HSA). HSA is the most abundant protein in the blood and is found in human blood at concentrations of 45 mg/ml (Kragh-Hansen et al., 2002; Kratochwil et al., 2002). As shown in Figure 6.39, under physiological conditions (pH 7.4 at 37 °C) HSA did not detectably hydrolyze dexrazoxane relative to the Tris/saline buffer control ($p > 0.5$). However HSA did significantly ($p < 0.001$) increase the hydrolysis rate of C, relative to Tris/saline buffer, by over 2 fold, as shown in Figure 6.40. In order to determine the possibility that HSA-mediated C hydrolysis was metal ion based, further studies were done including incubating the metal ion chelator DTPA (5 mM) with HSA in Tris/saline buffer for 30 min prior to the addition of C. As shown in Figure 6.40, DTPA significantly decreased the rate of loss of C by nearly 2 fold ($p < 0.001$) resulting, in 75 % decrease in the loss of C.

Table 6.38   Dexrazoxane and C hydrolysis in human serum albumin (HSA) under physiological conditions in the presence of metal ion chelator DTPA

Time (min)	Hydrolysis in 100 mM Tris/saline buffer		Hydrolysis in 45 mg/ml HSA in 100 mM Tris/saline buffer		C hydrolysis in 45 mg/ml HSA with 5 mM DTPA in 100 mM Tris/saline buffer
	Dexrazoxane (μM)	C (μM)	Dexrazoxane (μM)	C (μM)	C (μM)
0	198	197	204	198	205
15	199	196	203	189	199
30	198	194	204	180	187
45	198	189	200	168	180
60	200	186	204	155	170
90	202	170	199	138	168
120	198	166	197	128	161

Table 6.39 Comparisons of dexrazoxane and C loss in the presence of 45 mg/ml human serum albumin

Dexrazoxane	n	Rate of loss (μM·min^{-1})	p [a]	% inhibition [b]
Tris/saline buffer control	1	0.05	--	--
45 mg/ml HSA	1	0.03	$p > 0.5$	--
C	n	Rate of loss (μM·min^{-1})	p [a]	% inhibition [b]
Tris/saline buffer control	1	0.290	--	--
45 mg/ml HSA	1	0.613	$p < 0.001$	--
45 mg/ml HSA and 5 mM DTPA	1	0.371	$p > 0.2$	75

[a] The slopes (rate of loss) of the Tris/saline buffer control was compared to that of the rate of loss of dexrazoxane or C in the presence of human serum albumin.

[b] % inhibition is expressed relative to the background hydrolysis (physiological buffer) as detailed in Section 6.2.12.2.
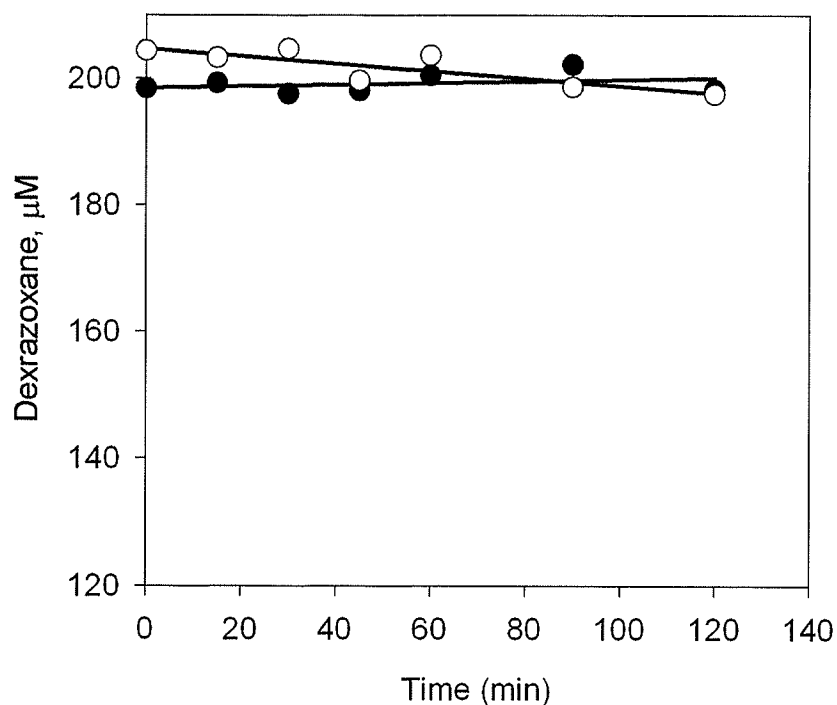
Figure 6.39 The effect of HSA (45 mg/ml) on dexrazoxane loss under physiological conditions
Hydrolysis of 200 μM dexrazoxane in the presence of 45 mg/ml HSA under physiological conditions (100 mM Tris/saline, pH 7.4 at 37 °C); O, dexrazoxane hydrolysis in the presence of 100 mM Tris/saline (pH 7.4 at 37 °C) alone; ●, dexrazoxane hydrolysis in the presence of 45 mg/l HSA in 100 mM Tris/saline (pH 7.4 at 37 °C). The loss of dexrazoxane was determined by HPLC as described in Section 6.2.10
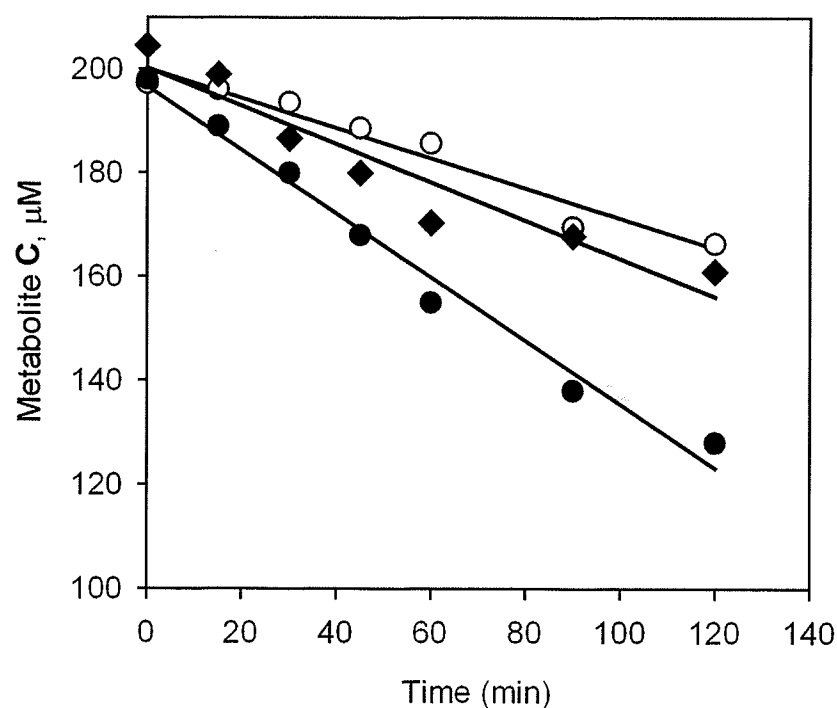
Figure 6.40 The effect the metal ion chelator DTPA on HSA (45 mg/ml) mediated hydrolysis of C under physiological conditions
Hydrolysis of 200 μM **C** in the presence of HSA (45 mg/l) under physiological conditions; O, **C** hydrolysis in the presence of 100 mM Tris/saline buffer (pH 7.4 at 37 °C) alone; ●, **C** hydrolysis in the presence of 45 mg/l HSA in 100 mM Tris/saline (pH 7.4 at 37 °C); ◆, **C** hydrolysis in 45 mg/l HSA with 5 mM DTPA in 100 mM Tris/saline buffer. The loss of **C** was measured by HPLC as described in Section 6.2.10

6.4 Discussion

6.4.1 Dexrazoxane metabolism in neonatal rat myocyte and adult rat hepatocyte suspensions

A substantial body of evidence suggests that anthracycline-dependent free radical generation resulting in DNA or membrane damage is the most probable cause for anthracycline-induced cardiotoxicity (Myers, 1998; Singal and Iliskovic, 1998). Strong evidence exists from isolated primary adult and neonatal rat myocyte models that dexrazoxane's mechanism of protection involves inhibition of doxorubicin-dependant hydroxyl radical production (Rajagopalan et al., 1988) and inhibition of lipid peroxidation and thiol oxidation (Thomas et al., 1993). In an *in vitro* heart microsomal model, Fe^{3+} mediated oxidative damage was significantly reduced by ADR-925 (Vile and Winterbourn, 1990) relative to dexrazoxane, suggesting that the hydrolysis of dexrazoxane to ADR-925, the metal ion chelating form, is necessary to limit the role of iron in doxorubicin-mediated free radical production. *In vitro* primary culture of neonatal rat myocytes has also shown that, depending on concentration, doxorubicin caused both apoptotic and necrotic damage (Hasinoff et al., 2003a), suggesting that doxorubicin toxicity may be caused by mitochondrial damage and dexrazoxane may be protective by preventing iron-based oxidative damage. Dexrazoxane was also shown to prevent the anthracycline daunorubicin-induced apoptosis in primary cultures of neonatal and adult rat myocytes (Sawyer et al., 1999). Dexrazoxane pharmacokinetics have been studied in a variety of preclinical animal models (Herman and Ferrans, 1998) as well as clinical studies (Earhart et al., 1982; Vogel et al., 1987; Hochster et al., 1992; Jakobsen et al., 1994), where dexrazoxane's elimination was found to be rapid (β $t_{1/2}$ 4.16 ± 2.94 h,

(Hochster et al., 1992)) thereby eliminating base catalyzed hydrolysis of dexrazoxane (Hasinoff, 1994a) as a mechanism for dexrazoxane's *in vivo* activation. In Chapters 2 and 3, it was discovered that significant ADR-925 plasma levels were rapidly achieved and sustained following an i.v. bolus dose of dexrazoxane, lending a pharmacodynamic explanation of dexrazoxane cardioprotective action through its fully hydrolyzed metal ion chelating form ADR-925.

In order to fully describe dexrazoxane's mechanism of action through enzymatic activation, a series of *in vitro* studies were performed using tissue homogenate supernatants (Hasinoff, 1990), purified enzyme kinetic studies (Hasinoff, 1993; Hasinoff, 1994b), and adult rat hepatocytes (Hasinoff et al., 1994). It has previously been determined that while DHPase can hydrolyze dexrazoxane to **B** and **C**, it is not active toward the conversion of **B** or **C** to ADR-925 (Hasinoff et al., 1991; Hasinoff, 1993). Furthermore, dexrazoxane hydrolysis to **B** and **C** in the presence of isolated hepatocytes has been previously shown to be enzymatically mediated by DHPase (Hasinoff et al., 1994). In the same experiment, it was also found that DHPase inhibitor 4-chlorobenzenesulfonamide strongly inhibited the hydrolysis of dexrazoxane to **B** and **C** by 82 %, which indicated that DHPase was primarily responsible for the hydrolysis of dexrazoxane in the liver (Hasinoff et al., 1994). The above mentioned study, however, did not address if the third active metal-ion chelating metabolite, ADR-925, was formed in hepatocytes. The results in Figure 6.16 show that ADR-925 is formed almost immediately after dexrazoxane is administered. Figure 6.16 also shows that ADR-925 levels increase rapidly over the entire 300 min duration of the study relative to control experiment. Thus, the rapid appearance of ADR-925 suggests that **B** and **C** are being

enzymatically hydrolyzed to ADR-925 in adult rat hepatocytes. Also, the data shown in Figure 6.16 are ADR-925 levels measured from the hepatocyte supernatant, which indicate that ADR-925 can be released from viable hepatocyte cells. ADR-925 release from viable cells may begin to explain the plasma levels of ADR-925 following an *i.v.* bolus in a rat model (Schroeder and Hasinoff, 2002) and human patients (Schroeder et al., 2003). A control study (described in Section 6.2.8) confirmed that dexrazoxane hydrolysis in the presence of suspension hepatocytes was not the primary result of dexrazoxane, **B**, or **C** hydrolyzing enzymes or components that leaked from non-viable cells.

The ADR-925 produced from hepatocytes, as shown in Figure 6.16, could be the result of ADR-925 that was released from the hepatocytes after the enzymatic conversion of **B** and **C** to ADR-925. However, while the hydrolysis of dexrazoxane is not greatly accelerated in the presence of Ca^{2+} and Mg^{2+}, the hydrolysis of **B** and **C** are (Buss and Hasinoff, 1997). Therefore, the ADR-925 found in the hepatocyte supernatant suspension buffer is most probably the combined result of the metal ion mediated hydrolysis of intermediates **B** and **C**, and the cellular release of ADR-925 preformed in hepatocyte cells. Thus, it is unclear as to how much of the ADR-925 is enzymatically formed and released, and how much is formed by Ca^{2+} and Mg^{2+} mediated hydrolysis in the suspension buffer.

Dexrazoxane was found to be enzymatically hydrolyzed in liver and kidney supernatant, but not that of the heart (Hasinoff et al., 1991). The results of suspension neonatal rat myocytes exposed to dexrazoxane (Figure 6.12) are generally consistent with the observation that dexrazoxane is not detectably hydrolyzed in the heart. However

there is an initial significant rate of loss of dexrazoxane from the suspension buffer which is 7.6-fold greater then the suspension buffer control for the first 20 min. The total loss of dexrazoxane is small, with an average net dexrazoxane loss of approximately 3 μM greater then that of the control at 90 min, a result that was likewise observed at dexrazoxane doses of 100 μM. It is therefore most likely that dexrazoxane is not being enzymatically hydrolyzed to **B** or **C** once it diffuses into the myocyte. No detectable amounts of **B** or **C** were found for any time point of the experiment which is most likely because **B** and **C** levels never exceeded the detection limit (1.5 μM). Dexrazoxane, which is permeable to cells (Dawson, 1975), may be diffusing into the myocyte and hydrolyzing to **B** and **C** not only by enzymatic means but, also by base-catalyzed hydrolysis (Hasinoff, 1990) and metal ion catalysis (Buss and Hasinoff, 1993; Buss and Hasinoff, 1995). Also, this experiment quantifies the loss of dexrazoxane in myocyte suspension buffer and, therefore, cannot directly comment whether metabolism, if any, occurs in the myocyte cell itself where metabolites are not being released into the α-MEM suspension buffer at detectable amounts.

6.4.2 The effect of DHOase inhibition on the hydrolysis of C in neonatal rat myocyte and adult rat hepatocyte suspensions

The hydrolysis of **C** was found to be significantly increased in the presence of neonatal rat myocytes. Unlike DHPase, DHOase has been found to have very good activity in the heart (Kennedy, 1974). In an enzymatic study, as detailed in Chapter 4 (Schroeder et al., 2002), DHOase was found to hydrolyze **C**. Dihydroorotate, the endogenous substrate of DHOase (Mori et al., 1975; Kelly et al., 1986; Musmanno et al., 1992), was also hydrolyzed in the presence of myocytes (Figure 6.26). DHOase activity

in primary neonatal rat myocytes was further confirmed when pre-incubation with the DHOase inhibitor 5-aminoorotic acid resulted in a 88 % inhibition of dihydroorotate loss, as shown in Table 6.17. Also, the degree of inhibition by 5-aminoorotic acid in myocytes is similar for **C** and dihydroorotate, 82 and 88 %, respectively. Interestingly, while furosemide was found to inhibit **C** hydrolysis in myocytes by 92%, furosemide showed only moderate inhibition (41 %) of dihydroorotate hydrolysis in myocytes. While 5-aminoorotic acid has been found to be a relatively strong and specific inhibitor of DHOase, with a K_i of 8 μM (Christopherson and Jones, 1980) the inhibitory nature of furosemide toward DHOase has not been closely examined. In Chapter 4 (Schroeder et al., 2002), it was determined that DHOase-mediated hydrolysis of **C** was inhibited by 90 and 80 % in the presence of 1 mM 5-aminoorotic acid and furosemide, respectively. The hydrolysis of **C** in the presence of neonatal rat myocytes is shown in Figure 6.22. A previous result indicated that **B** and **C**, and ADR-925 are permeable to attached rat myocytes (Hasinoff et al., 2003b). The results of Figure 6.22 clearly show that **C** is rapidly metabolized by myocytes, and is thus permeable to neonatal rat myocytes in a suspension model, as well.

DHOase inhibitors 5-aminoorotic acid and furosemide inhibit the hydrolysis of **C** to ADR-925 in both myocyte and hepatocyte models (Figure 6.22 and 6.30), confirming that this hydrolysis is, at least in part, enzymatically mediated by DHOase. Previous studies of DHOase content and activity in rat tissue found DHOase activity in the liver is approximately twice that of the heart (Kennedy, 1974). This correlates well with the hydrolysis of **C** in hepatocytes and neonatal myocytes, where the net hydrolysis in hepatocytes was 1.5 fold greater then that of myocytes, providing further evidence that

the hydrolysis of **C** is likely mediated by DHOase. Also, the hydrolysis of **C** in both myocytes and hepatocytes were strongly inhibited in the presence of 1 mM 5-aminoorotic acid, a strong DHOase inhibitor (Christopherson and Jones, 1980; Krungkrai et al., 1992). 5-aminoorotic acid has also been shown to inhibit DHOase mediated hydrolysis of **C** in the presence of purified enzyme (Schroeder et al., 2002). Thus, these results suggest that the hydrolysis of **C** to ADR-925 in adult rat hepatocytes and neonatal rat myocytes is most likely mediated by DHOase.

6.4.3 Hydrolysis of dexrazoxane and C in rat and human blood plasma

Dexrazoxane was not hydrolyzed at a faster rate in blood or plasma then the saline control (Figure 6.31-6.32). However, **C** was found to hydrolyze rapidly in the presence of both human and animal plasma as shown in Figures 6.35-6.36. A major contribution for the hydrolysis of **C** to ADR-925 in blood plasma was determined to be the high concentrations of Ca^{2+} and Mg^{2+}. Both Ca^{2+} and Mg^{2+} have been found to hydrolyze **C** with a rate of 0.0043 and 0.0089 min^{-1}, respectively (Buss and Hasinoff, 1997) relative to a hydrolysis rate of 0.00174 min^{-1} without Ca^{2+} and Mg^{2+}. Blood and blood plasma typically contains concentrations of approximately 2.5 and 1.2 mM for Ca^{2+} and Mg^{2+}, respectively (Luquita et al., 2001), and these metal ions are a potential contributor to the rapid hydrolysis of **B** and **C** to ADR-925 *in vivo*. Dexrazoxane, on the other hand, is very stable in the presence of Ca^{2+} and Mg^{2+}, with a hydrolysis rate constant of 0.0442 and 0.0410 h^{-1}, respectively (Buss and Hasinoff, 1997) relative to a hydrolysis rate of 0.0411 h^{-1} without Ca^{2+} and Mg^{2+}. The hydrolysis of **C** in plasma is not completely accounted for by the calcium or magnesium mediated hydrolysis of **C**. The Ca^{2+} and Mg^{2+} – mediated hydrolysis of **C** only accounts for approximately 40 % of the plasma hydrolysis

of C relative to the saline (0.9% NaCl, pH 7.4) control.

Human serum albumin, found at high concentrations in the blood (45 mg/ml, (Kratochwil et al., 2002)) was found to facilitate the hydrolysis of C (Figure 6.40), but not dexrazoxane (Figure 6.39). The HSA mediated hydrolysis of C was significant ($p <$ 0.001, Table 6.39) relative to the Tris/saline buffer and suggests that HSA does contribute towards the hydrolysis of C in blood. Zinc(II) and copper(II) both bind to HSA, at different sites, with specific high affinity sites $10^{7.53}$ and $10^{11.18}$, respectively (Masuoka et al., 1993). Also, it has been determined that 5 mM of the metal chelator DTPA effectively reduces the HSA-mediated hydrolysis of C to that of the control, as shown in Table 6.39. It has also been previously determined that both zinc and copper rapidly facilitate the hydrolysis of C (Buss and Hasinoff, 1997). Thus, it is possible that HSA-mediated hydrolysis of C is due to interaction with either the zinc or copper bound to HSA. Although DHOase has been found in blood cells such as leukocytes (Smith and Baker, 1959; Smith, 1960; Fairbanks et al., 1995), incubation of dihydroorotate (the endogenous substrate of DHOase (Simmer et al., 1990)) did not result in any measurable metabolism of dihydroorotate as seen in Figure 6.33 and 6.34. At physiological pH, dihydroorotate is negatively charged which may hinder its entrance into blood cells. This suggests that DHOase does not detectably contribute to ADR-925 formation in the case of B and C hydrolysis in the blood.

6.5 References

Brown DC and Collins KD (1991) Dihydroorotase from Escherichia coli. Substitution of Co(II) for the active site Zn(II). *J Biol Chem* **266:**1597-1604.

Burczynski FJ and Cai Z (1994) Palmitate uptake by hepatocyte suspensions: Effect of albumin. **267:**G371-G379.

Buss JL and Hasinoff BB (1993) The one-ring open hydrolysis product intermediates of the cardioprotective agent ICRF-187 (dexrazoxane) displace iron from iron-anthracycline complexes. *Agents Actions* **40:**86-95.

Buss JL and Hasinoff BB (1995) Ferrous ion strongly promotes the ring opening of the hydrolysis intermediates of the antioxidant cardioprotective agent dexrazoxane (ICRF-187). *Arch Biochem Biophys* **317:**121-127.

Buss JL and Hasinoff BB (1997) Metal ion-promoted hydrolysis of the antioxidant cardioprotective agent dexrazoxane (ICRF-187) and its one-ring open hydrolysis products to its metal-chelating active form. *J Inorg Biochem* **68:**101-108.

Carrey EA (1993) Phosphorylation, allosteric effectors and inter-domain contacts in CAD; their role in regulation of early steps of pyrimidine biosynthesis. *Biochem Soc Trans* **21:**191-195.

Christopherson RI and Jones ME (1980) The effects of pH and inhibitors upon the catalytic activity of the dihydroorotase of multienzymatic protein pyr1-3 from mouse Ehrlich ascites carcinoma. *J Biol Chem* **255:**3358-3370.

Davidson JN, Chen KC, Jamison RS, Musmanno LA and Kern CB (1993) The evolutionary history of the first three enzymes in pyrimidine biosynthesis. *Bioessays* **15:**157-164.

Dawson KM (1975) Studies on the stability and cellular distribution of dioxopiperazines in cultured BHK-21S cells. *Biochem Pharmacol* **24:**2249-2253.

Earhart RH, Tutsch KD, Koeller JM, Rodriguez R, Robins HI, Vogel CL, Davis HL and Tormey DC (1982) Pharmacokinetics of (+)-1,2-di(3,5-dioxopiperazin-1-yl)propane intravenous infusions in adult cancer patients. *Cancer Res* **42:**5255-5261.

Evans DR, Bein K, Guy HI, Liu X, Molina JA and Zimmermann BH (1993) CAD gene sequence and the domain structure of the mammalian multifunctional protein CAD. *Biochem Soc Trans* **21:**186-191.

Fairbanks LD, Bofill M, Ruckemann K and Simmonds HA (1995) Importance of ribonucleotide availability to proliferating T-lymphocytes from healthy humans. Disproportionate expansion of pyrimidine pools and contrasting effects of de novo synthesis inhibitors. *J Biol Chem* **270**:29682-29689.

Hasinoff BB (1989) Self-reduction of the iron(III)-doxorubicin complex. *Free Radic Biol Med* **7**:583-593.

Hasinoff BB (1990) The hydrolysis activation of the doxorubicin cardioprotective agent ICRF-187 [+)-1,2-bis(3,5-dioxopiperazinyl-1-yl)propane). *Drug Metab Dispos* **18**:344-349.

Hasinoff BB (1993) Enzymatic ring-opening reactions of the chiral cardioprotective agent (+) (S)-ICRF-187 and its (-) (R)-enantiomer ICRF-186 by dihydropyrimidine amidohydrolase. *Drug Metab Dispos* **21**:883-888.

Hasinoff BB (1994a) Pharmacodynamics of the hydrolysis-activation of the cardioprotective agent (+)-1,2-bis(3,5-dioxopiperazinyl-1-yl)propane. *J Pharm Sci* **83**:64-67.

Hasinoff BB (1994b) Stereoselective hydrolysis of ICRF-187 (dexrazoxane) and ICRF-186 by dihydropyrimidine amidohydrolase. *Chirality* **6**:213-215.

Hasinoff BB (1998) Chemistry of dexrazoxane and analogues. *Semin Oncol* **25**:3-9.

Hasinoff BB and Aoyama RG (1999a) Relative plasma levels of the cardioprotective drug dexrazoxane and its two active ring-opened metabolites in the rat. *Drug Metab Dispos* **27**:265-268.

Hasinoff BB and Aoyama RG (1999b) Stereoselective metabolism of dexrazoxane (ICRF-187) and levrazoxane (ICRF-186). *Chirality* **11**:286-290.

Hasinoff BB, Hellmann K, Herman EH and Ferrans VJ (1998) Chemical, biological and clinical aspects of dexrazoxane and other bisdioxopiperazines. *Curr Med Chem* **5**:1-28.

Hasinoff BB, Reinders FX and Clark V (1991) The enzymatic hydrolysis-activation of the adriamycin cardioprotective agent (+)-1,2-bis(3,5-dioxopiperazinyl-1-yl)propane. *Drug Metab Dispos* **19**:74-80.

Hasinoff BB, Schnabl KL, Marusak RA, Patel D and Huebner E (2003a) Dexrazoxane (ICRF-187) protects cardiac myocytes against doxorubicin by preventing damage to mitochondria. *Cardiovasc Toxicol* **3**:89-99.

Hasinoff BB, Schroeder PE and Patel D (2003b) The metabolites of the cardioprotective drug dexrazoxane do not protect myocytes from doxorubicin-induced cytotoxicity. *Mol Pharmacol* **64:**670-678.

Hasinoff BB, Venkataram S, Singh M and Kuschak TI (1994) Metabolism of the cardioprotective agents dexrazoxane (ICRF-187) and levrazoxane (ICRF-186) by the isolated hepatocyte. *Xenobiotica* **24:**977-987.

Haugland R (1996) *Handbook of Fluorescent Probes and Research Chemicals.* Molecular Probes, Eugene, Oregon.

Herman EH and Ferrans VJ (1998) Preclinical animal models of cardiac protection from anthracycline-induced cardiotoxicity. *Semin Oncol* **25:**15-21.

Hochster H, Liebes L, Wadler S, Oratz R, Wernz JC, Meyers M, Green M, Blum RH and Speyer JL (1992) Pharmacokinetics of the cardioprotector ADR-529 (ICRF-187) in escalating doses combined with fixed-dose doxorubicin. *J Natl Cancer Inst* **84:**1725-1730.

Jakobsen P, Sorensen B, Bastholt L, Mirza MR, Gjedde SB, Mouridsen HT and Rose C (1994) The pharmacokinetics of high-dose epirubicin and of the cardioprotector ADR-529 given together with cyclophosphamide, 5-fluorouracil, and tamoxifen in metastatic breast-cancer patients. *Cancer Chemother Pharmacol* **35:**45-52.

Jones D (2002) *Pharmaceutical Statistics.* Pharmaceutical Press, London.

Kelly RE, Mally MI and Evans DR (1986) The dihydroorotase domain of the multifunctional protein CAD. Subunit structure, zinc content, and kinetics. *J Biol Chem* **261:**6073-6083.

Kennedy J (1974) Dihydroorotase from rat liver: purification, properties and regulatory role in pyrimidine biosynthesis. *Arch Biochem Biophys* **160:**358-365.

Kikugawa M, Kaneko M, Fujimoto-Sakata S, Maeda M, Kawasaki K, Takagi T and Tamaki N (1994) Purification, characterization and inhibition of dihydropyrimidinase from rat liver. *Eur J Biochem* **219:**393-399.

Kirshenbaum LA and Schneider MD (1995) Adenovirus E1A Represses Cardiac Gene Transcription and Reactivates DNA Synthesis in Ventricular Myocytes, via Alternative Pocket Protein- and p300-binding Domains. *J. Biol. Chem.* **270:**7791-7794.

Kratochwil NA, Huber W, Muller F, Kansy M and Gerber PR (2002) Predicting plasma protein binding of drugs: a new approach. *Biochem Pharmacol* **64:**1355-1374.

Kragh-Hansen U, Chuang VT and Otagiri M (2002) Practical aspects of the ligand-binding and enzymatic properties of human serum albumin. *Biol Pharm Bull* **25**:695-704.

Krungkrai J, Krungkrai SR and Phakanont K (1992) Antimalarial activity of orotate analogs that inhibit dihydroorotase and dihydroorotate dehydrogenase. *Biochem Pharmacol* **43**:1295-1301.

Luquita A, Gennaro AM and Rasia M (2001) Influence of adsorbed plasma proteins on erythrocyte rheological properties: *in vitro* and ex vivo studies. *Pflugers Arch* **443**:78-83.

Masuoka J, Hegenauer J, Van Dyke B and Saltman P (1993) Intrinsic stoichiometric equilibrium constants for the binding of zinc(II) and copper(II) to the high affinity site of serum albumin. *J. Biol. Chem.* **268**:21533-21537.

Mori M, Ishida H and Tatibana M (1975) Aggregation states and catalytic properties of the multienzyme complex catalyzing the initial steps of pyrimidine biosynthesis in rat liver. *Biochemistry* **14**:2622-2630.

Musmanno LA, Jamison RS, Barnett RS, Buford E and Davidson JN (1992) Complete hamster CAD protein and the carbamylphosphate synthetase domain of CAD complement mammalian cell mutants defective in de novo pyrimidine biosynthesis. *Somat Cell Mol Genet* **18**:309-318.

Myers C (1998) The role of iron in doxorubicin-induced cardiomyopathy. *Semin Oncol* **25**:10-14.

Pradhan TK and Sander EG (1973) Noncompetitive inhibition by substituted sulfonamides of dihydroorotase from Zymobacterium oroticum. *Life Sci* **13**:1747-1752.

Rajagopalan S, Politi PM, Sinha BK and Myers CE (1988) Adriamycin-induced free radical formation in the perfused rat heart: implications for cardiotoxicity. *Cancer Res* **48**:4766-4769.

Sawyer DB, Fukazawa R, Arstall MA and Kelly RA (1999) Daunorubicin-induced apoptosis in rat cardiac myocytes is inhibited by dexrazoxane. *Circ Res* **84**:257-265.

Schroeder PE, Davidson JN and Hasinoff BB (2002) Dihydroorotase catalyzes the ring opening of the hydrolysis intermediates of the cardioprotective drug dexrazoxane (ICRF-187). *Drug Metab Dispos* **30**:1431-1435.

Schroeder PE and Hasinoff BB (2002) The doxorubicin-cardioprotective drug dexrazoxane undergoes metabolism in the rat to its metal ion-chelating form ADR-925. *Cancer Chemother Pharmacol* **50:**509-513.

Schroeder PE, Jensen PB, Sehested M, Hofland KF, Langer SW and Hasinoff BB (2003) Metabolism of dexrazoxane (ICRF-187) used as a rescue agent in cancer patients treated with high-dose etoposide. *Cancer Chemother Pharmacol* **52:**167-174.

Simmer JP, Kelly RE, Rinker AG, Jr., Zimmermann BH, Scully JL, Kim H and Evans DR (1990) Mammalian dihydroorotase: nucleotide sequence, peptide sequences, and evolution of the dihydroorotase domain of the multifunctional protein CAD. *Proc Natl Acad Sci U S A* **87:**174-178.

Singal PK and Iliskovic N (1998) Doxorubicin-induced cardiomyopathy. *N Engl J Med* **339:**900-905.

Smith LH, Jr. and Baker FA (1959) Pyrimidine metabolism in man. I. The biosynthesis of orotic acid. *J Clin Invest* **38:**798-809.

Smith LH, Jr., Sullivan M, Baker, F, Frederick E (1960) Inhibition of Dihydroorotase in Pyrimidine Biosynthesis. *Cancer Res* **20:**1059-1065.

Swain SM, Whaley FS, Gerber MC, Ewer MS, Bianchine JR and Gams RA (1997a) Delayed administration of dexrazoxane provides cardioprotection for patients with advanced breast cancer treated with doxorubicin-containing therapy. *J Clin Oncol* **15:**1333-1340.

Swain SM, Whaley FS, Gerber MC, Weisberg S, York M, Spicer D, Jones SE, Wadler S, Desai A, Vogel C, Speyer J, Mittelman A, Reddy S, Pendergrass K, Velez-Garcia E, Ewer MS, Bianchine JR and Gams RA (1997b) Cardioprotection with dexrazoxane for doxorubicin-containing therapy in advanced breast cancer. *J Clin Oncol* **15:**1318-1332.

Thomas C, Vile GF and Winterbourn CC (1993) The hydrolysis product of ICRF-187 promotes iron-catalyzed hydroxyl radical production via the Fenton reaction. *Biochem Pharmacol* **45:**1967-1972.

Vile GF and Winterbourn CC (1990) dl-N,N'-dicarboxamidomethyl-N,N'-dicarboxymethyl-1,2-diaminopropane (ICRF-198) and d-1,2-bis(3,5-dioxopiperazine-1-yl)propane (ICRF-187) inhibition of Fe3+ reduction, lipid peroxidation, and CaATPase inactivation in heart microsomes exposed to adriamycin. *Cancer Res* **50:**2307-2310.

Vogel CL, Gorowski E, Davila E, Eisenberger M, Kosinski J, Agarwal RP and Savaraj N (1987) Phase I clinical trial and pharmacokinetics of weekly ICRF-187 (NSC 169780) infusion in patients with solid tumors. *Invest New Drugs* **5:**187-198.

311